IDENTIFICATION, MODELLING AND MODIFICATION

OF MECHANICAL STRUCTURES FROM MODAL

ANALYSIS TESTING

by

© FATHY M. M. ISMAIL, B.Sc.(Eng.), M.Sc.

A Thesis

Submitted to the School of Graduate Studies

in Partial Fulfilment of the Requirements

for the Degree

Doctor of Philosophy

McMaster University

December 1982

IDENTIFICATION, MODELLING, MODIFICATION

OF MECHANICAL STRUCTURES

TO MY FAMILY

DOCTOR OF PHILOSOPHY (1982)   McMASTER UNIVERSITY
(Mechanical Engineering)   Hamilton, Ontario

TITLE: Identification, Modelling and Modification
          of Mechanical Structures from Modal Analysis
          Testing

AUTHOR   Fathy Mohamed M. Ismail, B.Sc. (Hons.)
                                    (Alexandria University)

                                    M.Sc.
                                    (Alexandria University)

SUPERVISOR: Professor J. Tlusty

NUMBER OF PAGES: (xviii), 286

ABSTRACT

One important field of "Structural Dynamics" is "Modal Analysis Testing". This field, concerns the modes of vibration which constitute the link between experimental and analytical methods, like Finite Elements.

The present work deals with the use of the experimental data obtained from Modal Analysis Testing; in building a mathematical model of the structure, identifying its parameters and predicting the effects of possible design changes on its dynamics. It also deals with the use of these experimental data in predicting the behaviour of the structure according to a certain criterion. In this work, in particular, machine tool structures are considered.

A systematic formulation of identifying the structural parameters from the Modal Analysis Testing is presented. It depends basically on the accessibility of the relevant coordinates for measurement. If all these coordinates are accessible then the formulation based on the equation of motion of the system and on the orthogonality relationships leads to linear equations. On the other hand if some of the relevant coordinates are missing, like coordinates on the bearings inside a headstock, then nonlinear optimization is used to minimize the errors between experimental and estimated

modal parameters. These identification formulations are applied here to theoretical structures as well as actual machine tools.

As a special exercise a procedure is suggested to be used in predicting the dynamics of a lathe with different workpieces using the modal data measured on a single workpiece. Such a procedure can help estimate the limit of stability against machining chatter beforehand and consequently could be implemented in the postprocessors of Numerically Controlled Turning Centers.

The thesis deals also with further development of the theory of machining chatter. For the first time digital simulation in the time domain of the cutting process including chatter is carried out using mathematical models of machine tools established through Modal Analysis Testing. Cutting tests carried out in this work have shown that the digital simulation approach to machining chatter represents the reality very closely. Thus it could be used in formulating acceptance test procedures of machine tools as well as in designing the cutters to achieve higher metal removal rates.

ACKNOWLEDGEMENTS

TABLE OF CONTENTS

LIST OF FIGURES

FIGURE

(xiv)

LIST OF TABLES

NOMENCLATURE

Symbol	Description
$\{\ \}$	Vector
$< \ >^T$	Transpose of a vector
$[\ ]_{mxn}$	Matrix of m rows and n columns
$[\ ]^T$	Transpose of a matrix
$[\ ]^{-1}$	Inverse of a matrix
$[\ ]^{-T}$	Inverse of the transpose of a matrix
$[\ ]^{+}$	Pseudo-inverse of a matrix
$\ulcorner \ \lrcorner$	Diagonal matrix
$\ulcorner I \lrcorner$	Identity matrix
Ω^2	Eigenvalue of undamped system
$\{\phi\}$	Eigenvector of undamped or proportionally viscous damped system
λ	Eigenvalue of damped system
$\{\psi\}$	Eigenvector of a system with non proportional viscous damping
$*$	Conjugate

CHAPTER 1

INTRODUCTION

With the advancement in the measuring equipment and techniques in the last two decades "Structural Dynamic Testing", is becoming more and more an essential part of all integrated activities of the design cycle of mechanical structures.

One important field of "Structural Dynamic Testing" is "Modal Analysis Testing". This field concerns the modes of vibration which are the link between testing and analytical methods.

The area of "Modal Analysis Testing" has developed to a great extent in the last decade basically due to the advent of the minicomputer based Fourier Analyzers and the implementation of the FFT (Fast Fourier Transform). Several "Modal Analysis Testing" systems are now commercially available which provide animated displays of the structure as it deforms in its natural modes of vibration. With the animated displays Modal Analysis Testing has gained great popularity in the last few years. However its main potential as a powerful tool to be used in establishing mathematical models of the structures under test for further analysis has not yet been fully utilized. The work presented here is an effort in this direction.

This thesis deals with the use of the experimental

1

data obtained from Modal Analysis Testing in building a
mathematical model of the structure, identifying its para-
meters and predicting the effects of possible design changes
on its dynamics. It also deals with the use of these experi-
mental data in predicting the behaviour of the structure
according to a certain criterion. The main focus here,
although not necessarily limited to, is on machine tool
structures.

The contents of this thesis are summarized below.

In Chapter 2 the basic concepts and notations used
throughout the work are included. The theoretical background
of Modal Analysis is presented for vibratory systems with
either proportional or nonproportional viscous damping. The
previous work in the field of identifying the structure's
parameters from the test data is surveyed. Also included is
a survey of the previous work in the field of machining
instability.

In Chapter 3 an attempt is made to formulate in a
systematic way different procedures whereby the unknown
structural parameters could be identified from the experimental
modal data. These procedures depend basically on the
accessibility of the coordinates for measurement as well as
the amount of available data. Theoretical examples are used
to illustrate the applications of these procedures.

Chapter 4 presents practical applications of the
procedures formulated in Chapter 3. Mathematical models of

two actual machine tool structures are derived from experimentally established modal parameters.

In Chapter 5 a procedure is developed whereby the Modal Analysis Testing is used to obtain the dynamic characteristics of a substructure by subtracting another known substructure from the assembly. It is developed with the aim that it could be applied to lathe structures.

In Chapter 6 the use of Modal Analysis Testing in establishing simple vibratory models of a milling machine to be used in predicting the limits of machining instability (chatter) is presented. The prediction is based on the digital simulation in the time domain. Experimental verification involving cutting tests of steel and aluminium, is given.

Chapter 7 gives the conclusions of this work and presents some ideas about possible future research.

CHAPTER 2

BACKGROUND AND
LITERATURE SURVEY

2.1 Dynamic Behaviour of a Structure

Understanding the dynamic behaviour of structures and structural components is becoming an increasingly important part of the design process for any mechanical system. Economic and environmental considerations have advanced to the state where over-design and less than optimum performance and reliability are not readily tolerated.

The understanding of the dynamic behaviour of the structure means the response of the structure to varying load conditions can be predicted, e.g. the response of a machine tool subject to varying cutting forces. These varying load conditions may lead to fatigue failures, problems of noise and comfort. One more problem with the machine tools is dynamic instability, namely the appearance of self-excited vibrations (chatter).

2.2 Structural Dynamics Testing Versus Finite Elements Analysis

Building a mathematical model for dynamic analysis from the drawings using the finite elements technique has proven successful in the case of integrated structures. It has the great advantage of allowing the engineer to predict the dynamic performance at the drawing board stage so that potential weaknesses

4

can be pinpointed before the actual structure is built. How-ever, it has two distinct disadvantages:

a). The formulation of an adequate computer model and com-puting time can be significantly expensive and time consuming.

b) Neither discontinuities such as screwed joints or guide-ways nor damping can be simulated effectively so far [1 - 5]. This can lead to significant deviations between dynamic response of the model and that of the actual structure.

Because of these disadvantages, structural dynamics testing technique is becoming more and more an essential part of the development cycle of the product especially in the fields of; aerospace, ship and automotive industries and machine tools. Its uses can be classified as:

a) checking and refining a finite element model

b) identifying natural frequencies and mode shapes

c) troubleshooting

d) formulating a mathematical model of the test structure for the purpose of further analysis.

The fourth item in this classification is the main concern in the present work.

2.3 Modal Analysis

One area of structural dynamics testing is referred to as "Modal Analysis". Simply stated, modal analysis is the pro-

cess of characterizing the dynamic properties of an elastic structure by identifying its modes of vibration. That is, each mode has a specific natural frequency and damping factor which can be identified from practically any point on the structure. In addition, it has a characteristic "mode shape" which defines the mode spatially over the entire structure. Moreover, associated with each mode there is a stiffness, its value depends on the mode shape itself as well as where it is being normalized.

It is important, first to illustrate how the modal parameters are obtained using the mass, stiffness and damping matrices of the structure derived from the drawings using, e.g. finite elements, and how the transfer functions at the different locations on the structure are expressed in terms of these parameters. Secondly, to show that in modal analysis testing, starting with measured transfer functions, how the modal parameters are extracted.

The modal characteristics or, as we will call them here, modal parameters provide a great analytical tool for further prediction of the dynamic behaviour of the structure under different loading conditions or when performing any design changes.

Before proceeding it is necessary to mention some concepts, notations and coordinate transformations used throughout the present work.

2.3.1 Transformations of Coordinates. Basic Concepts and Notations

All structures we will be dealing with are assumed to be linear and have lumped parameters.

In ref. [6] the concepts of design, local and modal parameters were presented in some detail. Here they are recapitulated.

A computation starts usually with the <u>design</u> data and the formulation of the mass, stiffness and damping matrices $[m_x]$, $[k_x]$ and $[c_x]$ in a system of local coordinates x. These are connected with selected local points of the structure and their deflections. The equation of motion of the system in these local coordinates, and for the time being assume that there is no damping, is:

$$[m_x] \{\ddot{x}\} + [k_x] \{x\} = \{F\} \tag{2.1}$$

and for natural vibrations it is:

$$[m_x] \{\ddot{x}\} + k_x \{x\} = 0 \tag{2.2}$$

The relationship between the elements m_{ij} and k_{ij}; i=1 to n and j=1 to n of $[m_x]$ and $[k_x]$ respectively, and the lumped or "design" parameters of the system m_i and k_i is:

$$\begin{Bmatrix} m_{11} \\ m_{12} \\ \cdot \\ \cdot \\ \cdot \\ \cdot \\ m_{nn} \end{Bmatrix}_{nnx1} = [T_m]_{nnxnm} \begin{Bmatrix} m_1 \\ m_2 \\ \cdot \\ \cdot \\ \cdot \\ m_{nm} \end{Bmatrix}_{nmx1} \tag{2.3}$$

where:

n = is the number of degrees of freedom in the system.

nn = $\frac{n(n+1)}{2}$ is the total number of independent elements in $[m_x]$ taking into account that $[m_x]$ is symmetric.

nm = is the number of lumped "design" masses in the system.

A similar expression to Eq. (2.3) can be written for the stiffness elements, e.g. for a two degrees of freedom system in Fig. 2.1a) it is

$$\begin{Bmatrix} m_{11} \\ m_{12} \\ m_{22} \end{Bmatrix} = \begin{bmatrix} 1 & 0 \\ 0 & 0 \\ 0 & 1 \end{bmatrix} \begin{Bmatrix} m_1 \\ m_2 \end{Bmatrix} \tag{2.4}$$

and, similarly for the stiffness elements k_{ij}

$$\begin{Bmatrix} k_{11} \\ k_{12} \\ k_{22} \end{Bmatrix} = \begin{bmatrix} 1 & 1 \\ 0 & -1 \\ 0 & 1 \end{bmatrix} \begin{Bmatrix} k_1 \\ k_2 \end{Bmatrix} \tag{2.5}$$

Solving the eigenvalue problem for Eq.(2.2) leads to n eigenvalues (natural frequencies) Ω_i^2 and n eigenvectors (mode shapes) $\{\phi_i\}$ in the coordinates $\{x\}$. Both Ω_i^2 and $\{\phi_i\}$ are real. The mode shapes being real implies that the displacements of the different points of the structure in a particular mode, e.g. $\{\phi_i\}$, occur either in phase or 180° out of phase with

respect to each other. The eigenvectors fill the modal matrix [P]

$$[P] = [\phi_1 \cdot \cdot \phi_i \cdot \cdot {}_n]_{nxn} = \begin{bmatrix} p_{11} & p_{1i} & p_{1n} \\ \cdot & \cdot & \cdot \\ \cdot & \cdot & \cdot \\ \cdot & \cdot & \cdot \\ 1 \cdot \cdot \cdot \cdot \cdot & 1 \cdot \cdot \cdot \cdot \cdot & 1 \\ \cdot & \cdot & \cdot \\ \cdot & \cdot & \cdot \\ \cdot & \cdot & \cdot \\ \cdot & \cdot & \cdot \\ \cdot & \cdot & \cdot \end{bmatrix} -x_r \qquad (2.6)$$

where one row was chosen filled with 1's and the corresponding local coordinate will be the reference coordinate x_r.

The modal matrix transforms the local coordinates $\{x\}$ into modal coordinates $\{q\}$, local forces $\{F\}$ into modal forces $\{R\}$ and it diagonalizes the mass and stiffness matrices.

$$\{x\}_n = [P]\{q\}_n, \quad \{R\} = [P]^T\{F\}, \quad K^r = [P]^T[k_x][P],$$

$$M^r = [P]^T[m_x][P] \qquad \qquad (2.7)$$

And in particular it is $\Omega_i^2 = \dfrac{K_i^r}{M_i^r}$

The diagonal matrices K^r and M^r carry the superscript r to indicate that they have been obtained using [P] normalized to x_r. If a force f is assumed to act on x_r the force vector $\{R\}$ is obtained as:

$$\{R\} = [P]^T\{F\} = \begin{bmatrix} \ldots\ldots 1 \ldots \\ \ldots\ldots 1 \ldots \\ \ldots\ldots 1 \ldots \\ \ldots\ldots 1 \ldots \end{bmatrix} \begin{Bmatrix} 0 \\ 0 \\ f \\ 0 \\ 0 \end{Bmatrix} = \begin{Bmatrix} f \\ f \\ f \\ f \\ f \end{Bmatrix} \qquad (2.8)$$

If f is harmonic with frequency ω, it is

$$\lfloor -\omega^2 \, M^r + K^r \rfloor \, \{q\} = \{R\} \qquad (2.9)$$

and

$$q_i = \frac{f}{K_i^r - \omega^2 M_i^r} \qquad (2.10)$$

where K_i^r and M_i^r are the elements of the matrices $\lceil K^r \rfloor$ and $\lceil M^r \rfloor$ associated with the mode i. The response at the reference coordinate x_r is the "direct" Transfer Function (TF).

$$\frac{x_r}{f} = \sum_{i=1}^{n} q_i \qquad (2.11)$$

and the response at any other local coordinate x_k is the "cross" TF:

$$\frac{x_k}{f} = \sum_{i=1}^{n} p_{ki} \, q_i \qquad (2.12)$$

Considering the simple example of two degrees of freedom in Fig. 2.1.a), there will be two mode shapes associated with two natural frequencies. Fig. 2.1.b) shows how the two masses move in the two modes, while Fig. 2.1.c) shows the two mode

shapes with the displacements drawn in the direction perpendicular
to the actual axis of freedom. The mode shapes were normalized
at x_2.

2.3.2 Modal Representation of a Mechanical Structure with Linear Viscous Damping

In a mechanical structure several damping mechanisms
may be considered: dry friction, viscous and material (struct-
ural, internal). For the special case of machine tool structures,
the sources of damping can be classified into three groups:

- Structural damping of the material itself.
- damping in joints, slideways, bearings, etc.
- possibly installed active or passive dampers.

Material damping in metals is quite low, especially for steel,
and seldom has a significant effect on overall damping character-
istics relative to the damping effect of the last two sources
which arise at discrete points within the structure [7].
Koenigsberger and Tlusty [8] state: "The use of viscous damping
for the description of vibration of machines is an idealization.
In the vibration of actual machine tools energy is dissipated
in several ways which differ in the various parts of the
structure. In fixed joints partially dry friction occurs, in
guideways semi-dry or viscous damping occurs, in the material
of the parts of the structures there are internal energy
losses. The nature of the individual damping sources is complex
and not sufficiently understood. The distribution of the

damping over the structure depends also on the distribution of stresses and therefore on the modes of vibration as well as on the design and the manufacturing deviations of the structure. It would be, therefore, very difficult to introduce in a unified and sufficiently simple manner, into calculations damping that would exactly express reality". However, since in machine tool structures the damping is relatively small and we will be dealing with linear vibratory models the assumption of viscous damping becomes acceptable [2, 9-11].

Introducing the viscous damping into the equation of motion (2.1), it is written as

$$[m_x] \{\ddot{x}\} + [c_x] \{\dot{x}\} + [k_x] \{x\} = \{F\} . \qquad (2.13)$$

and for natural vibrations it is

$$[m_x]\{\ddot{x}\} + [c_x] \{\dot{x}\} + [k_x]\{x\} = 0 \qquad (2.14)$$

where the matrix $[c_x]$ includes constant real numbers assembled from the values of the lumped "design" dampers in the system, in a similar way to $[m_x]$ and $[k_x]$. Here, the damping force is linearly proportional and opposing the velocity. Two cases of linear viscous damping are considered:

2.3.2.1 Proportional Viscous Damping

As we saw in Section 2.3.1 for a system with no damping, solving the eigenvalue problem of Eq. (2.2) leads to n real eigenvalues Ω_i^2 and n real eigenvectors $\{\phi_i\}$ which make up the modal matrix [P]. This matrix diagonalizes both the mass and

stiffness matrices $[m_x]$ and $[k_x]$ respectively. If the matrix [P] also diagonalizes the damping matrix $[c_x]$, then the system is said to have proportional damping. Hurty and Rubenstein [12] state that the condition under which the damping matrix be diagonalized is that $[c_x]$ can be expressed as a linear combination of the $[m_x]$ and $[k_x]$ matrices:

$$[c_x] = \alpha[m_x] + \beta[k_x] \qquad (2.15)$$

where both α and β are real constants. This condition is, however sufficient but not necessary [2]. A necessary and sufficient condition was derived by Caughey [13] as:

$$[c_x][m_x]^{-1}[k_x] = [k_x][m_x]^{-1}[c_x] \qquad (2.16)$$

Therefore, for a vibratory system which satisfies Eq. (2.16), the modal representation is obtained as follows:

- solve the eigenvalue problem for Eq. (2.14) neglecting the damping term $([c_x]\{\dot{x}\})$. This leads to n real undamped n atural frequencies Ω_i^2 and n real mode shapes $\{\phi_i\}$; i=1 to n. Form the modal matrix [P] and obtain the modal masses, stiffnesses and forces using Eq. (2.7).

- Obtain the modal damping matrix $\ulcorner C \lrcorner^r$ similar to $\ulcorner M \lrcorner^r$ and $\ulcorner K \lrcorner^r$;

$$\ulcorner C \lrcorner^r = [P]^T [c_x][P] \qquad (2.17)$$

The damping ratio in mode i is defined as $\zeta_i = \dfrac{C_i^r}{2\sqrt{K_i^r M_i^r}}$. The actual eigenvalues of the damped

system will be denoted λ_i, i=1 to n. They are complex and obtained from ζ and Ω as follows;

$$\lambda_i = \Omega_i(\zeta_i + j\sqrt{1-\zeta_i^2}) = \mu_i + j\nu_i; \quad i=1 \text{ to } n; \text{ where } \mu_i \text{ is the}$$

damping coefficient and ν_i is the damped natural frequency of mode i.

Introducing C_i^r into Eq. (2.9) it is

$$\left[-\omega^2 M^r + j\omega C^r + K^r\right] \{q\} = \{R\} \qquad (2.18)$$

and the modal displacement at the ith mode becomes

$$q_i = \frac{f}{-\omega^2 M_i^r + j\omega C_i^r + K_i^r} \qquad (2.19)$$

assuming that a sinusoidal force f with frequency ω is acting at x_r.

The direct TF and cross TF's are obtained according to Eq.'s (2.11) and (2.12), respectively.

2.3.2.2 Non-proprotional Linear Viscous Damping

If the vibratory system does not satisfy Eq. (2.16) it is said that the system has non-proportional damping. Actually, this is the most common situation and represents the general case of linear viscous damping. Although it has been known for a long time, its use was limited, partially due to the complex mode shapes associated with it and due to the measurement techniques available at that time. However, in the last 12 years with the advancements of both computational and experimental facilities, it became the most popular damping representation among almost all authors working in the field of modal analysis, e.g. [2, 14-17].

Frazer et al. [18] have developed a method of obtaining the complex eigenvalues and eigenvectors for a system with non-proportional damping in which the following matrix identity is added to Eq. (2.13)

$$[m_x]\{\dot{x}\} - [m_x]\{\dot{x}\} = 0$$

Hence the following matrix equation of order 2n is obtained

$$\begin{bmatrix} [c_x] & [m_x] \\ [m_x] & [\,0\,] \end{bmatrix} \begin{Bmatrix} \{\dot{x}\} \\ \{\ddot{x}\} \end{Bmatrix} + \begin{bmatrix} [k_x] & [0] \\ [\,0\,] & [m_x] \end{bmatrix} \begin{Bmatrix} \{x\} \\ \{\dot{x}\} \end{Bmatrix} = \begin{Bmatrix} \{F\} \\ \{0\} \end{Bmatrix} \qquad (2.20)$$

or

$$[A]\{\dot{z}\} + [B]\{z\} = \{Q\} \qquad (2.21)$$

where

$$[A] = \begin{bmatrix} [c_x] & [m_x] \\ [m_x] & [\,0\,] \end{bmatrix} \quad , \quad [B] = \begin{bmatrix} [k_x] & [\,0\,] \\ [\,0\,] & [m_x] \end{bmatrix}$$

$$, \{z\} = \begin{Bmatrix} \{x\} \\ \{\dot{x}\} \end{Bmatrix} \quad \{Q\} = \begin{Bmatrix} \{F\} \\ \{0\} \end{Bmatrix} \qquad (2.22)$$

To get the eigenvalues and eigenvectors of the system put $\{Q\} = \{0\}$ and seek a solution in the form $\{z\} = \{Z\} e^{\lambda t}$, Eq. (2.21) becomes

$$\lambda[A]\{Z\} + [B]\{Z\} = 0 \qquad (2.23)$$

$$\therefore \quad [\lambda\,^rI + [A]^{-1}\,[B]]\,\{Z\} = 0 \qquad (2.24)$$

Eq. (2.24) represents the eigenvalue problem of the system, when solved it leads to n pairs of conjugate complex eigenvalues;

$$\lambda_i = \mu_i + j\,\nu_i$$
$$\lambda_i^* = \mu_i - j\,\nu_i \qquad ; \ i=1,n$$

and n pairs of conjugate complex eigenvectors $\{\psi\}$ each with 2n elements. The mode shapes being complex implies that the displacements of the different points of the structure in a particular mode, e.g. $\{\psi_i\}$, would have phase differences between them which might take any value. These eigenvectors fill the modal matrix [P] which transforms the local displacements $\{x\}$ and velocities $\{\dot{x}\}$ into modal coordinates $\{q\}$;

$$\{Z\} = \begin{Bmatrix} \{x\} \\ \vdots \\ \\ \{\dot{x}\} \end{Bmatrix} = \begin{bmatrix} \begin{Bmatrix} \{\psi_1\} \\ \vdots \\ \lambda_1\psi_1 \end{Bmatrix} & \begin{Bmatrix} \{\psi_1\}^* \\ \vdots \\ \lambda_1^*\{\psi_1\}^* \end{Bmatrix} & \cdots & \begin{Bmatrix} \{\psi_n\} \\ \vdots \\ \lambda_n\{\psi_n\} \end{Bmatrix} & \begin{Bmatrix} \{\psi_n\}^* \\ \vdots \\ \lambda_n^*\{\psi_n\}^* \end{Bmatrix} \end{bmatrix} \begin{Bmatrix} q_1 \\ q_2 \\ \vdots \\ q_{2n} \end{Bmatrix}$$

$$\underbrace{\hspace{8cm}}_{[P]}$$

$$(2.25)$$

The eigenvectors are orthogonal to [A] and [B] and hence the modal matrix [P] diagonalizes them;

$$\ulcorner a_\lrcorner^r = [P]^T [A][P], \qquad \ulcorner b_\lrcorner^r = [P]^T [B][P] \qquad (2.26)$$

where $\ulcorner a_\lrcorner^r$ and $\ulcorner b_\lrcorner^r$ are complex and they contain pairs of conjugate values, and for mode i it is:

$$\lambda_i = -\frac{b_i}{a_i} \qquad (2.27)$$

Assuming that a sinusoidal force f is acting at x_r, the direct TF was obtained in [2] as

$$\frac{x_r}{f} = \sum_{i=1}^{n} [\frac{1}{a_i(j\omega - \lambda_i)} + \frac{1}{a_i^*(j\omega - \lambda_i^*)}]$$

(2.28)

and the cross TF at any other coordinate x_k as

$$\frac{x_k}{f} = \sum_{i=1}^{n} [\frac{p_{ki}}{a(j\omega - \lambda)} + \frac{p_{ki}^*}{a^*(j\omega - \lambda^*)}]$$

(2.29)

Eq.'s (2.28) and (2.29) were also expressed in [2] in different forms.

Summarizing:

- For a system with no damping, the modal parameters are: the eigenvalues Ω_i^2, eigenvectors $\{\phi_i\}$ and the modal stiffnesses K_i^r. All of them are real.

- For a system with proportional viscous damping the modal parameters are: the eigenvalues λ_i, eigenvectors $\{\phi_i\}$ and the modal stiffnesses K_i^r. Both K_i^r and $\{\phi_i\}$ are real while the λ_i's are complex.

- For a system with non-proportional damping the modal parameters are: the eigenvalues λ_i, eigenvectors $\{\psi_i\}$ and the parameters a_i^r. All of them are complex.

2.3.3 Extracting Modal Parameters from Modal Analysis Testing

In Section 2.3.2 it has been shown how the transfer functions, direct and crosses, are expressed in terms of the

modal parameters. The direct TF is obtained at that local
coordinate where the force is applied, while the cross TF's
are obtained at the other locations. In modal analysis testing,
we start by measuring these transfer functions, and by decom-
posing them into the individual modes, the modal parameters
are obtained. To do so, Fig. 2.2 illustrates the steps to
be followed which are:

i) Exciting the structure and measuring the input force:
Several excitation instruments, e.g. using a shaker
or a hammer, and techniques, e.g. sinusoidal, swept-
sine, random, impulse, are now available for exciting
the structure. Their applications depend on the mass
and flexibility of the structure, existence of non-
linearity as well as the frequency range to be covered
[8, 19-29]. The force sensing element is usually a
piezoelectric load cell.

ii) Simultaneously measuring the vibrations at the different
points on the structure, usually at one point at a
time.

iii) Conditioning the individual signals to reduce aliasing,
leakage and noise problems [2, 25, 30-31].

iv) Processing the signals (force and vibration) to obtain
the transfer function: By definition, the transfer
function is the Fourier Transform of the output divided
by the Fourier Transform of the input. Mathematically
speaking it is;

$$TF = \frac{S_o}{S_i} \qquad (2.30)$$

or equivalently;

$$TF = \frac{S_o \cdot S_i^*}{S_i \cdot S_i^*} \qquad (2.31)$$

where; S_i^* is the conjugate of S_i

$S_o \cdot S_i^*$ is the cross power spectrum of the input and

output

$S_i \cdot S_i^*$ is the autopower spectrum of the input.

In the case of structural dynamic testing, the output is the vibration while the input is the exciting force. With the advent of the Fourier Analyzers and incorporating the FFT (Fast Fourier Transform) this process takes only few seconds. To reduce the effect of noise and non-linearities several TF measurements, typically 10 [30], are usually averaged out.

In order to improve the frequency resolution in a certain frequency range McKinny [32] has incorporated the band selectable Fourier analysis into the FFT. The TF's are to be measured at all selected points on the structure.

The different terminology of TF are:

Dynamic compliance   = Displacement/Force.

Mobility   = Velocity/Force.

Inertance   = Acceleration/Force.

There are several ways of presenting TF [33]. In the present work the real and imaginary parts plotted in linear scales will be, mostly, used.

v)   Curve fitting:

This is the process of extracting the modal data
from the measured transfer functions by approximating them
to the modal representation of the vibratory system, e.g.
Eq. (2.29). A simple intuitive method [8] may prove effective
in the case of lightly damped uncoupled modes, while a non-linear
least square estimation algorithms [2, 9, 34] becomes unavoidable
in the case of highly damped strongly coupled modes.

An important aspect in curve fitting the transfer
functions is that, the measurements are done over a limited
frequency range, consequently the contributions of the modes
outside that range must be considered. This is accomplished
[2,9] by modifying, e.g. Eq. (2.29) into:

$$\frac{x_r}{f} = \frac{1}{-\omega^2 m_r} + \sum_{i=1}^{p} \left[\frac{1}{a_i(j\omega - \lambda_i)} + \frac{1}{a_i^*(j\omega - \lambda_i^*)} \right] + S_r \quad (2.32)$$

where;

p is the number of modes in the measured frequency range.

$\dfrac{1}{\omega^2 m_r}$ a term representing the missing lower modes.
$\omega^2 m_r$ is called the residual inertia

S_r a term representing the contribution of the missing
        higher modes. It is designated residual flexibility.
        Both m_r and S_r are real.

2.4   Modal Analysis Testing Applications

2.4.1 Visual Inspection of the Weak Points of the Structure

Commercial systems, e.g. a based mini-computer Fourier

analyzers, are now available which provide an animated display
of the structure as it moves in its individual modes. By
visually inspecting these displays it is possible to indicate
the "weak links" in the structure [35, 36]. Subsequently, design
changes through trial and error may be proposed.

2.4.2 Performing Design Changes

There are, fundamentally, two distinct ways to try
and solve the problem of quantitatively predicting design
changes of an existing structure which has been subject to
experimental modal analysis [37].

One way consists of Identifying the structure as a
lumped mass, spring and damping model by determining, in
general, its mass, stiffness and damping matrices in local
coordinates associated with the individual points of the model
and, further, to determine the individual springs, masses and
dampers of the model.

Another approach consists of identifying the properties
of the structure at those points only where a Modification
is intended by means of adding a mass or a stiffness beam or
adding another whole structural part.

These two approaches will be discussed in the two
sections, 2.5 and 2.6.

2.4.3 Predicting the Structure Response Under. Various Loading Conditions

Once the modal parameters of the structure have been

found, through modal analysis testing, the decoupled equations of the system can be written, e.g. for proportional viscous damping, as:

$$M_i^r \ddot{q}_i(t) + C_i^r \dot{q}_i(t) + K_i^r q(t) = <\phi_i>^T \{F(t)\}; \quad i=1,n$$

(2.33)

where:

q$_i$(t) is the modal displacement of the mode i.

M_i^r, C_i^r, K_i^r are the modal mass, stiffness and damping parameters of the mode i, obtained through modal analysis testing.

$<\phi_i>^T$ is the transpose of the mode shape i.

$\{F(t)\}$ is the loading vector.

Eq. (2.33) represents a single degree of freedom system which can be solved to get the modal displacement q_i(t) for any loading condition. At any time instant t the displacements at the different points on the structure can be obtained from:

$$\{x(t)\} = [P] \{q(t)\}$$

(2.34)

where;

[P] is the measured modal matrix.

To incorporate the initial conditions, e.g. the initial displacements $\{x(0)\}$, into Eq. (2.33) we also use Eq. (2.34), i.e.

$$\{q(0)\} = [P]^{-1} \{x(0)\}$$

(2.35)

In the special case of machine tools, which are the main concern in the present work, the cutting forces represent

the varying loading conditions on the structure. They may
lead to "chatter" problems. This will be discussed in Section
2.7.

2.5 Identification of Mechanical Structures from Experimental Data

The objective of the identification/process of a
mechanical structure is to find the constants or coefficients
in the equation of motion of the system in local coordinates
from the experimentally measured data. This is a typical
inverse problem in the classification of Bekey [38] of engineer-
ing problems.

Two approaches of identification are to be considered:
"non-modal" where the modal data are not used, and "modal" where
the modal parameters are directly utilized. Although our
concern here is the applications of modal analysis and consequently
the modal approach, the non-modal approach will be briefly
discussed for the sake of completeness.

2.5.1 Non-modal Approach

Kozin et al. [39-40] have developed a scheme for
identifying the coefficients in the equation of motion in which
the time history of the input forcing function and response
time histories for displacements, velocities, and accelerations
in all the degrees of freedom are required. The approach is
based on a simple application of classical regression analysis.
To illustrate its use, consider the equation of a single degree

of freedom system.

$$m \ddot{x}(t) + c \dot{x}(t) + k x(t) = F(t) \qquad (2.36)$$

Multiply this equation successively by $\ddot{x}(t)$, $\dot{x}(t)$ and $x(t)$ we get,

$$m \ddot{x}^2(t) + c \dot{x}(t) \ddot{x}(t) + k x(t) \ddot{x}(t) = F(t) \ddot{x}(t)$$

$$m \ddot{x}(t) \dot{x}(t) + c \dot{x}^2(t) + k x(t) \dot{x}(t) = F(t) \dot{x}(t)$$

$$m \ddot{x}(t) x(t) + c \dot{x}(t) x(t) + k x^2(t) = F(t) x(t)$$

$$(2.37)$$

By integrating the equations in (2.37) over the time sampling interval t, we obtain 3 linear equations in the unknown coefficients m, c and k.

Although this procedure looks straightforward [41], its application necessitates the use of all displacements, velocities and accelerations, which implies, either to measure all of them, or measure only, e.g. the accelerations and determine numerically the velocities and displacements. The procedure worked well with error-free computer experiments on a simulated five mass chain. However, its application with corrupted data has not been reported.

Distefano et al. [42] have identified the coefficients in the equation of motion of a single degree of freedom system with nonlinear damping and stiffness respectively. The identification was done by minimizing the difference between the analytical acceleration time response and the measured acceleration time history. The application was limited to a

single-degree of freedom system due to the complexity involved.

Dale and Cohen [43] identified the coefficients in the partial differential equation of motion for linear simple continuous structures (such as rods or beams) by converting the equation into a set of n ordinary first order differential equations. They reported good results from computer experiments with simulated errors, e.g. by truncating the actual eigenvalues to the fourth decimal. Nevertheless, the theory was not applied to actual structures.

Mains and Noonan [44] used directly the equation of motion to identify the matrices $[m_x]$, $[c_x]$ and $[k_x]$. Their procedure is as follows:

for a sinusoidal excitation it is

$$[[k_x] - \omega^2 [m_x] + i\omega [c_x]] [y] = F_0 \tag{2.38}$$

where $[y]$ is a complex displacement matrix, F_0 is real, then

$$[y] = [y_R] + [y_I] \tag{2.39}$$

wherein $[y_R]$ and $[y_I]$ are the real and imaginary parts respectively. By substituting Eq. (2.39) in (2.38) and after some manipulation $[m_x]$, $[c_x]$ and $[k_x]$ can be obtained from

$$[m_x] = [[Y_{R1}] - [Y_{R2}]]/(\omega_2^2 - \omega_1^2)$$

$$[c_x] = [[Y_{I1}] + [Y_{I2}]]/(\omega_1 + \omega_2) \tag{2.40}$$

$$[k_x] = [\omega_2^2 [Y_{R1}] - \omega_1^2 [Y_{R2}]]/(\omega_2^2 - \omega_1^2)$$

where $[Y_{R1}] = [[y_{R1}]^2 + [y_{I1}]^2]]^{-1} F_o [y_{R1}]$

$\quad\quad [Y_{I1}] = - [[y_{R1}]^2 + [y_{I1}]^2]^{-1} F_o [y_{I1}]$ (2.41)

obtained when exciting the structure with frequency ω_1, and similarly for $[Y_{R2}]$ and $[Y_{I2}]$ when exciting with ω_2.

The two frequencies ω_1 and ω_2 were chosen such that they are far apart and antiresonances, where as claimed by the authors the errors in measuring $[y]$ are in the order of $\pm$ 5%. The method did not work very well neither with computer experiments with simulated errors, nor on actual experimental data. The authors have concluded that conditioning the measuring data is essential before utilizing them in the identification process.

Caravani and Thomson [45] identified the values of discrete dampers in a chain like structure from error-free computer experiments using gradient search. The sensitivity of the technique to noisy data has yet to be examined.

2.5.2 Modal Approach

In this approach the modal parameters as measured are available, and it is required to find the mass, stiffness and damping matrices of the structure in local coordinates. For example for a system with proportional viscous damping, the available modal parameters are λ_i, $\{\phi_i\}$ and K_i^r; $i=1,p$, where p is the number of modes in the measured frequency range. Find $[m_x]$, $[k_x]$ and $[c_x]$ which are square of size nxn, where n is the order of the system.

If the number of measured modes equals the order of the system matrices, i.e. p=n, and if the measured modes were exact, then $[m_x]$, $[c_x]$ and $[k_x]$ could be obtained directly by back transformation from modal to local coordinates, i.e.

$$[m_x] = [P]^{-T} \lceil M^r \rfloor [P]^{-1}$$

$$[c_x] = [P]^{-T} \lceil C^r \rfloor [P]^{-1} \qquad (2.36)$$

$$[k_x] = [P]^{-T} \lceil K^r \rfloor [P]^{-1}$$

However, this is not the case;

i) usually the number of measured modes is much less than the order of the system matrices; $p < n$.

ii) not all the local coordinates of the system are accessible, i.e. some of the elements of the mode shape vectors are missing.

iii) the measured data are inaccurate which is common to both identification approaches. These inaccuracies could be due to [46] errors of various types such as errors in calibration, errors due to capacitive reactance of loads, errors resulting from mismatching of equipments, errors due to extraneous signals or errors due to random noise. Some inaccuracies may be attributed to the assumption of linearity of the system which is basically non-linear. Moreover, these inaccuracies will depend on the stiffness of the mode itself and the locations at which the measurements were

taken.

Therefore, the inverse of the modal matrix [P] either does not exist in the case it is not complete, or will lead to extremely unrealistic results, e.g. negative masses [44].

Consequently, the works in the field of identifying the system matrices of the structure from experimental data were directed towards circumventing these problems.

Ibanetz [47], Raney and Hewlett [48], Flannelly et al. [46], Thoren [49] have concentrated on a low order model where the number of degrees-of-freedom of the system must be equal to the number of measured modes, i.e. n=p. In this case matrices $[m_x]$, $[c_x]$ and $[k_x]$ will be of size pxp, whose elements might not have direct physical meaning, nevertheless they are capable of representing the dynamics of the system in the frequency range covered by the measured p modes, and at these p local coordinates at which the measurements were done. The need for dealing with low order models in the works of these authors stems from their realization of the importance of using the orthogonality relationship between the measured eigenvectors and the matrices $[m_x]$, $[c_x]$ and $[k_x]$ of the system as a mean of conditioning the measured data. Having introduced this relationship, they obtained good results in terms of reproducing the measured data for both computer experiments with simulated errors [46] and actual structures [47-49]. They assumed the vibratory system to have proportional damping.

Berman and Flannelly [50] have introduced the concept of incomplete model whereby given the mass matrix $[m_x]$ of size

nxn, and p mode shapes it is possible to formulate a truncated stiffness matrix as follows.

$$[k_x]_{nxn} = \sum_{i=1}^{p} \frac{\Omega_i^2}{M_i^r} [m_x]\{\phi_i\} < \phi_i >^T [m_x]; \quad p<n \qquad (2.37)$$

where,

Ω_i^2 is the natural undamped frequency of mode i

M_i^r is the corresponding modal mass

$\{\phi_i\}$ is the measured eigenvector.

The matrix $[k_x]$ is of the order n and rank p and cannot be inverted. Its elements, due to the use of the lower modes, could be several orders of magnitude different from the actual ones. However, they showed that with computer experiments it has the potential of predicting design changes. Proportional structural damping was assumed.

Hall et al. [51], Ross [52], Berman and Flannelly [50], Collins et al. [53, 54], Inamura and Sata [55] have identified the unknown elements in the matrices $[m_x]$, $[c_x]$ and $[k_x]$ of size nxn using limited modal data.

Hall et al. [51] assumed the knowledge of $[m_x]$ for a computer simulated undamped beam having three different cross sections, and identified $[k_x]$. They used the gradient search to minimize the difference between the analytical and experimental mode shapes and frequencies in the least square sense. The method gave the exact values of the unknown parameters in $[k_x]$ when exact, but not complete, data were used. However, the convergence was relatively slower and some of the identified

parameters were off by more than 20% when simulated errors were introduced.

Ross [52] suggests a method in which one calculates the eigenvectors of known but unreliable mass and stiffness matrices, and then adds the top eigenvectors of the mass matrix and/or the lower eigenvectors of the stiffness matrix columnwise to the measured mode shapes to obtain a square modal matrix. Such a modal matrix may then be inverted and the formulation of more reliable mass and stiffness matrices follows directly. This method has never been put to a test neither on computer experiments nor on actual structures.

Berman and Flannelly [50] in a computer experiment on a beam with simulated errors in measuring the eigenvectors, have identified the unknown elements in the mass matrix $[m_x]_{nxn}$, using the orthogonality relationship. The pseudo-inverse method [56] was used to find these elements in the least square sense.

Inamura and Sata [55] suggested a method of introducing slope informations, which are not measured, in the mode shape vectors. The slopes are deduced from the measured displacements using shape functions in a way similar to that used in finite elements formulations. They used these filled mode shape vectors directly (without further conditioning) to identify the stiffness and damping coefficients of a bolted joint between two beams. The success was limited, e.g. the differences between the second measured natural frequency and the predicted using the identified coefficients was more than 30%.

Collins et al. [53-54] developed a method, similar to that of Hall [51] in which the gradient search is used to minimize the difference between the estimated and measured eigenvalues and eigenvectors. Moreover, in their development they treated the uncertainties of both the measurements and the prior estimates of the unknown parameters statistically. The method worked well with computer experiments on chain like structures. However when it was applied on an actual structure (model of Saturn) the success was limited.

Gravitz [57], McGrew [58] and Torgoff [59] have developed different methods by which the measured mode shapes are corrected to be orthogonal to a known mass matrix.

Gravitz [57], first obtains the truncated flexibility matrix $[h_x]$ of order n and rank p as follows.

$$[h_x] = [P] \ulcorner \Omega^2 \lrcorner^{-1} [[P]^T [m_x][P]]^{-1} [P]^T \tag{2.38}$$

If the mode shapes are inaccurate, $[h_x]$ will not be symmetrical. To make it so, the average of $[h_x]$ and its transpose is taken:

$$[h_x]_{mod.} = 1/2 [[h_x] + [h_x]^T] \tag{2.39}$$

This modified flexibility matrix is used with the known mass matrix to obtain the modified mode shapes by solving the eigenvalue problem.

McGrew [58] assumes that the measured higher mode contains the actual mode plus linear combination of the lower modes. Consequently, he derived a correction matrix, based on the known mass matrix and the lower modes; which when multiplied

by the measured higher mode yields the actual one. Assuming the first mode to be correct, the next modes are corrected in succession.

Targoff [59] through an iterative procedure corrects the measured mode shapes by minimizing the off-diagonal terms in the modal mass matrix. His method proceeds as follows:

The orthogonality relationship dictates,

$$[P]^T [m_x] [P] = {}^{\ulcorner}M_{\lrcorner}$$

Let the mode shapes be normalized such that

$$[V]^T [V] = {}^{\ulcorner}I_{\lrcorner}$$

where [V] contains the new normalized mode shapes.

Due to experimental errors the product $[V]^T [V]$ will yield the matrix [OR] instead of the identity matrix. The measured mode shapes could be thought of as being the product of the exact mode shapes $[V_e]$ multiplied by a corruption matrix [C], then

$$[C]^T [V_e]^T [V_e] [C] = [OR]$$

or $\quad [C]^T [C] = [OR]$

If only symmetrical errors exist, then $[C]^T [C] = [C]^2$ and the orthogonalization process reduces to that of finding the square root of $[C]^2$ which can be obtained through iterations.

2.6 Modification of Mechanical Structures from Experimental Data

In the modification approach as mentioned in Section 2.4.2, the dynamic characteristics of the structure at those points where other structures will be connected have to be identified. Moreover, the dynamic characteristics at other points on any of the subsystems may also be included if they are of special interest, e.g. points at which the forces will be acting or where the response is desired.

The modification of a structure could be performed by connecting other structures to it, or restraining some of its coordinates. Fig. 2.3 reproduced from [70] depicts the different connecting elements between two substructures.

By identifying the dynamic characteristics at some points on a structure it is meant that, either the transfer functions TF's or the modal parameters at those points are to be obtained. These characteristics will be used in the synthesis process.

Synthesis of substructures using their modal components to obtain the response of the total system, has been extensively studied by many authors, e.g. Hurtz [60, 61], Gladwell [62], Craig and Bampton [63], Banfield and Hruda [64] and Tolani and Rocke [65]. They, mostly, used computer experiments to prove the effectiveness of the method. Klosterman [9, 66-69] extended the synthesis technique to include the experimental data and applied it on actual structures.

The technique of synthesizing substructures using their mode components, or as Klosterman calls it "Building Blocks" appears to be the most practical approach for complex structures. Whereby the structure is divided into small components, each of which is analyzed separately using either available digital computer routines or experimental tests depending on the complexity of the component. Then the response of the structure is predicted by the proper coupling of these components.

To illustrate the synthesis procedure e.g. for sub-structures having no damping let;

$$\ulcorner K \lrcorner_i \ , \ \ulcorner M \lrcorner_i \ , \ [P]_i$$

be the measured or calculated modal parameters of substructure i. The matrices $\ulcorner K \lrcorner_i$ and $\ulcorner M \lrcorner_i$ are of size $p_i \times p_i$ and the modal matrix $[P]_i$ is of the size $n_i \times p_i$; where n_i is the number of coordinates on the substructure i which include both the connection points and any other points of interest and p is the number of available modes. Similar modal parameters are available for the other substructures. For all the sub-structures in a decoupled form we can write;

$$
\begin{bmatrix} \ulcorner M \lrcorner_1 & & 0 \\ & \ulcorner M \lrcorner_2 & \\ 0 & & \ddots \\ & & & \ulcorner M \lrcorner_N \end{bmatrix}
\begin{Bmatrix} \{\ddot{q}\}_1 \\ \{\ddot{q}\}_2 \\ \vdots \\ \{\ddot{q}\}_N \end{Bmatrix}
+
\begin{bmatrix} \ulcorner K \lrcorner_1 & & 0 \\ & \ulcorner K \lrcorner_2 & \\ 0 & & \ddots \\ & & & \ulcorner K \lrcorner_N \end{bmatrix}
\begin{Bmatrix} \{q\}_1 \\ \{q\}_2 \\ \vdots \\ \{q\}_N \end{Bmatrix}
= [\phi]^T
\begin{Bmatrix} \{F\}_1 \\ \{F\}_2 \\ \vdots \\ \{F\}_N \end{Bmatrix}
$$

$$(2.40)$$

where;

$\{q\}_i$ is the modal displacement vector of substructure i of length p_i. -

$\{F\}_i$ is the loading vector on substructure i of length n_i

$$[\phi] = \begin{bmatrix} [P]_1 & & & 0 \\ & [P]_2 & & \\ 0 & & \ddots & \\ & & & [P]_N \end{bmatrix} \qquad (2.41)$$

N is the total number of substructures.

$$\begin{Bmatrix} \{x\}_1 \\ \{x\}_2 \\ \vdots \\ \{x\}_N \end{Bmatrix} = [\phi] \begin{Bmatrix} \{q\}_1 \\ \{q\}_2 \\ \vdots \\ \{q\}_N \end{Bmatrix} \qquad (2.42)$$

where $\{x\}_i$ is the vector of local coordinates of the substructure i.

When the substructures are connected, constraint equations are necessary to relate the local coordinates. They can be written as;

$$[D] \begin{Bmatrix} \{x\}_1 \\ \vdots \\ \{x\}_N \end{Bmatrix} = [D][\phi] \begin{Bmatrix} \{q\}_1 \\ \vdots \\ \{q\}_N \end{Bmatrix} = [DD] \begin{Bmatrix} \{q\}_1 \\ \vdots \\ \{q\}_N \end{Bmatrix} = 0$$

$$\qquad (2.43)$$

Eq. (2.43) will relate the modal displacements of the substructures to each other, and then they can be expressed as;

$$\left\{ \begin{array}{c} \{q\}_1 \\ \vdots \\ \vdots \\ \{q\}_N \end{array} \right\} = [G] \{q_I\} \qquad (2.44)$$

where $\{q_I\}$ is the vector of independent modal displacements. Substituting Eq. (2.44) in Eqs. (2.40) and postmultiplying by $[G]^T$ we get,

$$[M]_T \{\ddot{q}_I\} + [K]_T \{q_I\} = [G]^T [\Phi]^T \left\{ \begin{array}{c} \{F\}_1 \\ \vdots \\ \vdots \\ \{F\}_N \end{array} \right\} \qquad (2.45)$$

Eqs. (2.45) can then be solved to determine the natural frequencies, mode shapes and the frequency response for the total structure.

Another approach of synthesizing substructures using directly the measured transfer functions was also described by Klosterman [69], Van Loon [2] and Vanhonacher [71]. It is best illustrated by an example. Consider the two sub-structures b and c in Fig. 2.4, when connected at point s to form the total system as it is required to determine the transfer function H_{ii}^a at point i.

For substructure b, and taking into account that it is linear,

$$x_i^b = H_{ii}^b \, F_i^b + H_{is}^b \, F_s^b \tag{2.46}$$

$$x_s^b = H_{is}^b \, F_i^b + H_{ss}^b \, F_s^b \tag{2.47}$$

where x   is the displacement

H_{is} is the measured transfer function. The first subscript indicates where the displacement is measured, while the second subscript represents the location at which the force is applied.

For substructure c

$$x_s^c = H_{ss}^c \, F_{sc} \tag{2.48}$$

When the two substructures are connected it is:

$$F_s^c = - F_s^b, \; x_s^b = x_s^c, \; F_i^b = F_i^a \text{ and } x_i^b = x_i^a \tag{2.49}$$

Substituting Eqs. (2.49) into (2.46), (2.47) and (2.48), we obtain H_{ii}^a in terms of the measured TF's of the substructures b and c when they stand alone as;

$$H_{ii}^a = H_{ii}^b - \frac{H_{is}^b \cdot H_{is}^b}{H_{ss}^b + H_{ss}^c} \tag{2.50}$$

Although the mathematical operations involved in Eq. (2.50) can be easily performed in a Fourier Analyzer, the direct use of the measured TF's may lead to erroneous results. A better way as suggested by Van Loon [2] is, first to curve fit these TF's and then use the analytical

expressions into Eq. (2.50).

2.7 Chatter in Machining

The specific type of self excited vibrations which occurs in machining of metals and which is generally called "chatter" has been the subject of extensive research in the past thirty years.

At an early stage of research into the problem of chatter in machining the existence of negative damping generated in the cutting process was considered a necessary condition, and the only source for chatter to occur [72, 73]. This attitude prevailed with many authors through the years, and with some almost until today [74, 75].

However, it was recognized rather early that the most powerful sources of self excitation, those of "mode coupling" and of "regeneration" are not associated with the chip formation mechanics but with the structural dynamics of the machine tool and the feedback between subsequent cuts. It was shown that chatter can occur without the participation of a negative damping in the cutting process [76-81].

Thus, in dealing with chatter problems we might distinguish, from the practical point of view, three items as it is diagrammatically indicated in Fig. 2.5. They are, the machine tool, the cutting process and the mutual orienta-tions between the resultant cutting forces, and the directions of the different modes of the structure. These mutual orientations depend on the geometry of the cut. The machine

tool represents a three-dimensional multi-degree-of-freedom system carrying the tools at one point and the workpiece at the opposite point. The vibration z of the machine tool influences the cutting process and produces the forces F at certain directions which in turn act on the structure and excite vibrations z, and thus close the loop. Eventually the stability of this loop depends on the three items.

The dynamics of the cutting process is represented quantitatively by the dynamic cutting force coefficient (DCFC). Several authors have developed different techniques for measuring the different components of this coefficient, e.g. [82-85]. Tlusty [86] in his critical survey of the research activities in the area of cutting dynamics, indicated the significance of the different components of the DCFC with respect to the process instability. Moreover, he presented the results of the DCFC measurements carried out in different laboratories around the world using the same tools and materials and identical test rigs. The comparison showed that the discrepancy was largest for the imaginary part of the direct inner modulation component, which actually represents the damping in the cutting process. Consequently, Tlusty and Heczko [87] devised a rig whose damping could be regulated such that the damping in the cutting process could be calculated more reliably. The work of these authors showed very clearly that the damping in the cutting process could be positive or negative depending, among other things, on the

cutting speed, tool wear and the frequency of the rig.

The instability of the closed loop in Fig. 2.5 was first studied by Tlusty et al. [76-78]. They recognized the two separate mechanisms, "regeneration" and "mode coupling", and accordingly they derived the limit of stability. This limit of stability was defined as the width of cut after which the vibrations, assuming among other things that the system is linear, would grow indefinitely, and it was denoted b_{lim} It was derived as,

$$b_{lim} = \frac{1}{2r \ G_{min}} \qquad (2.51)$$

where;

   r = dynamic cutting force coefficient which is assumed to be a real positive number.

   G_{min} = the minimum of the real part of the oriented relative transfer function between the tool and the workpiece.

Eq. (2.51) gives an important insight into the inter-action between machine tool structural dynamics and the cutting process dynamics. A further analysis was also presented [8] in which r was considered to be a complex number and in which the geometrical constraints were taken into account. With r being complex, the damping generated in the cutting comes into effect in determining the instability of the closed loop. Moreover, by incorporating the geometrical constraints, the phase angle between the undulations on the

surface being cut and that machined in the previous pass is not free to adjust itself but is rather determined by the length between subsequent cuts and the number of waves in this length as shown in Fig. 2.6. The length between subsequent cuts in turning is the circumference of the workpiece, while in milling it is the distance between two successive teeth.

In deriving the stability limit [76-81], it was assumed that the resulting cutting forces act in a direction which remains always constant during cutting. While this assumption is true in the case of turning, it represents an oversimplification of reality in the case of milling operations.

CHAPTER 3

CLASSIFICATION OF IDENTIFICA-
TION SCHEMES USING THE MODAL
ANALYSIS APPROACH

3.1   Introduction

This chapter deals with the problem of identifying

the parameters of a lumped spring-mass-damper model of a

structure from measured modal data. The structure is assumed

to be linear. The problems arise mainly because the measured

data are inaccurate and, often they are also, in a sense,   -

incomplete. The purpose of such modeling is to enable us to

estimate the effect of design changes by computing the effects

of corresponding changes of the model.

This general task may be subdivided into several groups

of problems depending, on one hand, on the range of the intended

design changes and, on the other hand, on the range of measured

data available. From the first point of view it is often so

that the intended change consists of adding a known system

(known by computation or by measurement: as an example

consider adding a tuned damper) to the structure at selected

points and the effect is required at the same or other selected

points only. In such a case identification is necessary at

the selected joints and at the selected points of interest

For this purpose a Partial Identification is necessary. In

other instances it is required to establish as complete model

as possible and by analyzing it to select and test various design changes. For this purpose a Complete Identification is required. The word complete has to be taken conditionally as is explained further.

From the point of view of the range of measured data, or still better, of input data some of which might have been measured and some computed, it is important to separate first, experiments in which we have access and measure at all relevant coordinates. The measured mode shapes are complete for the given purpose. These cases lead to a system of linear equations in the unknown stiffnesses, masses and damping coefficients. It is not decisive whether measurement was obtained of all mode shapes, i.e. on as many mode shapes as there are degrees of freedom, i.e. as there are independent coordinates. The other group will be experiments where some relevant points have not been measured. This group will be called measurements of incomplete mode shapes and they lead to a system of nonlinear equations.

It is obvious that in any case we need at least as many independent equations as is the number of unknown parameters to be identified. It is preferable, with respect to the inaccuracies of the inputs, to have more equations than the number of unknowns, to have a redundant system of input data. If the number of input data is insufficient it is only possible to select from the infinite number of results such

which are closest to some estimate which establishes prefer-
ence.

In the following, the above mentioned groups of
methods are presented and illustrated on simulated examples.
In the next chapter they will be applied on actual machines.

Before proceeding any further let us define first,
what is to be considered a good identified model of the
structure. It is that model which not only reproduces the
data from which it has been identified, but also helps predict
the effect of design changes more accurately. To illustrate
the importance of the second characteristic of a good model,
consider the very simple example of a two degrees of freedom,
Fig. 3.1. Assume that a measurement has been done at co-
ordinate x_1 or coordinate x_2 in which only the two natural
frequencies are determined. Moreover, assume that the two
masses m_1 and m_2 are known and it is required to identify the
two springs k_1 and k_2. The formulation of the system natural
vibrations

$$[-\Omega_1^2[m_x] + [k_x]]\{\phi_x\} = 0 \qquad (3.1)$$

leads to the characteristic equation

$$|-\Omega_1^2[m_x] + [k_x]| = 0 \qquad (3.2)$$

In general, assuming $[m_x]$ and Ω_i^2 are known, Eq. (3.2)
represents a system of n simultaneous equations of degree n
in the elements k_{ij} of $[k_x]$, n being the order of the system.

In the present case n=2. Therefore, Eq. (3.2) will yield two solutions:

$$\begin{Bmatrix} k_1 \\ k_2 \end{Bmatrix} = \begin{Bmatrix} 1 \\ 2 \end{Bmatrix} \quad \text{or} \quad \begin{Bmatrix} 3.325 \\ 0.603 \end{Bmatrix}$$

Each of these solutions leads to the same natural frequencies. However, if we change either of the masses m_1 or m_2, remeasure the natural frequencies and solve Eq. (3.2) for Ω_i's by plugging in one of the identified stiffness matrices at a time, it will be clear that the solution ($k_1 = 1$, $k_2 = 2$), not only reproduced the data but also predicted the design change accurately, and consequently it is the correct one.

This important feature of a good identified model suggests that, it would be actually advantageous to use both the modal data of the structure as measured before and after performing some artificial design change, in the identification process. This design change might be merely adding a mass at one of the coordinates. For instance in the simple cited example of two degrees of freedom system, if we had used simultaneously the data from both measurements, we could have arrived at the following two linear equations,

$$(\Omega_2^4 - \Omega_1^4) \, m_1 m_2 - (\Omega_2^2 - \Omega_1^2)[(m_1 + m_2) \, k_2 + m_2 \, k_1] = 0$$

$$(\Omega_4^4 - \Omega_3^4) \, m_1 \bar{m}_2 - (\Omega_4^2 - \Omega_2^2)[(m_1 + \bar{m}_2) \, k_2 + \bar{m}_2 \, k_1] = 0$$

(3.3)

where:

Ω_1^2 and Ω_2^2:   are the natural frequencies in the first

measurement.

Ω_3^2 and Ω_4^2:   are the natural frequencies in the second

measurement where the mass m_2 has been

changed into $\bar{m}_2$.

Solving Eqs. (3.3) gives directly the unique solution $k_1 = 1$ and $k_2 = 2$.

3.2   Complete Mode Shapes: Methods Based on Linear Equations

In the course of this discussion and from the cited examples it will become understandable what is meant by "complete" mode shapes: such which are measured on all the "relevant" coordinates (relevant for the identification process).

3.2.1   Full Length Mode Shapes

3.2.1.1   Procedure

Full length mode shapes are those measured on all n chosen local coordinates, n being the number of freedoms. The system is assumed, for simplicity, to have no damping.

The identification procedure is based on the equations of motion written separately for each mode i:

$$[-\Omega_i^2 \, [m_x] + [k_x]] \, \{\phi_i\} = 0 \tag{3.4}$$

The elements of matrices $[m_x]$ and $[k_x]$ contain the local stiffnesses k_i and masses m_i, some or all of which may be unknown. Let the number of such unknown parameters be d. Eqs. (3.4) are linear in these unknowns. If they are written using as many as $p \leq n$ modes they represent

$$n_1 = p \times n \tag{3.5}$$

linear equations.

So far, the measured frequencies and mode shapes were used. Adding the knowledge of the modal stiffnesses K_i^r and masses M_i^r the orthogonality relationships can be written as,

$$[P]_{pxn}^T [m_x]_{nxn} = \ulcorner M^r \lrcorner_{pxp} \tag{3.6}$$

and similarly

$$[P]_{pxn}^T [k_x]_{nxn} [P]_{nxp} = \ulcorner K^r \lrcorner_{pxp} \tag{3.7}$$

Eqch of Eqs. (3.6) and (3.7) represent

$$n_2 = \frac{p(p+1)}{2} \tag{3.8}$$

linear equations in the unknowns k_i and m_i. Either of them can be added to the n_1 equations (3.4).

Any other additional information about the system which leads to linear equations can be further added if it is not equivalent to some of the data used already, e.g. the total mass of the structure $m_T = \Sigma m_i$. This additional information may represent n_3 independent equations.

Moreover, if another one or more sets of modal parameters obtained when performing some known design changes are also available, they may represent additional n_4 linear independent equations.

Thus we may have available

$$n_T = n_1 + n_2 + n_3 + n_4 \qquad (3.9)$$

independent linear equations in the unknown parameters.

All these available equations may be assembled as

$$[D]_{n_T \times d} \begin{Bmatrix} k_i \\ m_i \end{Bmatrix}_d = \{g\}_{n \times 1} \qquad (3.10)$$

Let us first assume $n_T > d$

This is the preferable case. The experimental input is redundant, though inaccurate. The solution of Eq. (3.1), representing the best fit to all the inputs in the least square sense, may be obtained by using the pseudo-inverse of [D]:

$$\begin{Bmatrix} k_i \\ m_i \end{Bmatrix}_d = [[D]^T [D]]^{-1}_{d \times d} [D]^T_{d \times n_T} \{g\}_{n_T} \qquad (3.11)$$

If initial estimates of the unknowns $\{ {k_e \atop m_e} \}_d$ are available, then Eq. (3.10) can be modified as:

$$[D] \{\{ {k_i \atop m_i} \} - \{ {k_e \atop m_e} \}\} = \{g\} - [D] \{ {k_e \atop m_e} \} \qquad (3.12)$$

A weighted diagonal matrix $[W]_{d \times d}$ may be introduced to represent the analyst confidence in the corresponding estimates.

$$[[D] \ulcorner W \lrcorner^{-1}][\ulcorner W \lrcorner \{\{m_i^{k_i}\} - \{m_e^{k_e}\}\}] = \{g\} - [D]\{m_e^{k_e}\} \tag{3.13}$$

Then the solution for $\{m_i^{k_i}\}$ is;

$$\{m_i^{k_i}\} = [X]\{g\} - [Y]\{m_e^{k_e}\} \tag{3.14}$$

where;

$$[X] = \ulcorner W \lrcorner^{-1} \quad [[D] \ulcorner W \lrcorner^{-1}]^+ \tag{3.15}$$

$$[Y] = \ulcorner I \lrcorner - [X][D] \tag{3.16}$$

$[[D] \ulcorner W \lrcorner^{-1}]^+$ is the pseudo-inverse of $[[D] \ulcorner W \lrcorner^{-1}]$

$$= [[[D] \ulcorner W \lrcorner^{-1}]^T [D] \ulcorner W \lrcorner^{-1}]]^{-1} [[D] \ulcorner W \lrcorner^{-1}] \tag{3.17}$$

In this way the solution obtained will be the closest to the estimated one in the least square sense. If $n_T < d$.

The solution for $\{m_i^{k_i}\}$ is, again, obtained from Eq. (3.14), however the pseudo-inverse $[[D] \ulcorner W \lrcorner^{-1}]^+$ is now defined as;

$$[[D] \ulcorner W \lrcorner^{-1}]^+ = \ulcorner W \lrcorner^{-1} [D]^T [[D] \ulcorner W \lrcorner^{-2} [D]^T]^{-1} \tag{3.18}$$

In the case that the whole matrix $[m_x]$ is reliably known, it is also possible to use some of the techniques [57], [58], [59] to improve the mode shapes by orthogonalizing them with respect to $[m_x]$. Then these improved mode shapes will be used to identify the unknown springs from the equations of motion.

In the special case where the number of complete measured mode shapes equals the number of degrees of freedom, i.e. $p = n$, and only the modal masses are known, a method is presented by Tlusty and Ismail in [91] for improving these mode shapes before using them in the identification process.

3.2.1.2 Examples on Using Full Length Mode Shapes

i) Number of available equations is larger than
   the number of unknowns:

Fig. 3.2 shows a five degrees of freedom undamped system. The eigenvalue problem of this system was first solved to yield the eigenvalues $\Omega_1^2 - \Omega_5^2$, the mode shapes $\{\phi_1\} - \{\phi_5\}$, and the modal stiffnesses $K_1^5 - K_5^5$. These data are listed in Table 3.1. Then to simulate experimental errors, the individual elements of the mode shapes were corrupted by adding random errors to them. No errors were added to the natural frequencies because in practice, they are usually the most accurately measured modal parameters.

The identification exercise is as follows:

Given; i)   The known exact mass matrix $[m_x]_{5x5}$

    ii) The measured natural frequencies $\Omega_1 - \Omega_p$; $p \leq n$

    iii) The measured full length mode shapes $\{\phi_1\} - \{\phi_p\}$; $p \leq n$.

Identify the values of the five springs $k_1 - k_5$, assuming that no initial estimates are available.

For one single mode, the equation of motion is written as;

Table 3.1 Exact Modal Data of the Five Degrees of Freedom System in Figure 3.2

	Mode 1	Mode 2	Mode 3	Mode 4	Mode 5
Frequency (Hz)	.04530	.13223	.20845	.26778	.30542
Modal Stiffness at x_5 N/m	.22739	2.29417	8.25914	26.63350	127.58600
Mode Shape					
x_1	.28463	-.83083	1.30972	-1.68251	1.91899
x_2	.54620	-1.08846	.37279	1.39788	-3.22871
x_3	.76352	-.59435	-1.20362	.52111	3.51334
x_4	.91897	.30972	-.71537	-1.83083	-2.68251
x_5	1.0000	1.0000	1.0000	1.0000	1.0000

$$[[k_x] - \Omega_i^2 [m_x]] \{\phi_i\} = 0$$

or

$$[k_x] \{\phi_i\} = \Omega_i^2 [m_x] \{\phi_i\} \qquad (3.19)$$

The stiffness matrix $[k_x]$ can be written as

$$[k_x] = [T]^T \ulcorner k_y \lrcorner [T] \qquad (3.20)$$

where, the elements on the diagonal of $\ulcorner k_y \lrcorner$ are the unknown springs k_1-k_5.

[T] is a transformation matrix between the absolute displacements x's and the relative displacements y's, i.e. $\{y\} = [T] \{x\}$.

Subsituting Eq. (3.20) into Eq. (3.19) we get

$$[T]^T \ulcorner k_y \lrcorner [T] \{\phi_i\} = \Omega_i^2 [m_x] \{\phi_i\} \qquad (3.21)$$

let $[T] \{\phi_i\} = \{c_i\}$, then;

$$[T]^T \ulcorner k_y \lrcorner \{c_i\} = \Omega_i^2 [m_x] \{\phi_i\} \qquad (3.22)$$

The diagonal matrix $\ulcorner k_y \lrcorner$ and the vector $\{c_i\}$ can be interchanged by assembling the diagonal elements of $\ulcorner k_y \lrcorner$ into the vector $\{k_s\}$ and putting the elements of the vector $\{c_i\}$ on the diagonal of a matrix $\ulcorner C_i \lrcorner$. Hence Eq. (3.22) becomes,

$$[T]^T \ulcorner C_i \lrcorner \{k_s\} = \Omega_i^2 [m_x] \{\phi_i\} \qquad (3.23)$$

Let $[D_i] = [T]^T \ulcorner C_i \lrcorner$ and $\{g_i\} = \Omega_i^2 [m_x] \{\omega_i\}$, subsequently Eq. (3.23) is written for one mode as;

$$[D_i] \{k_s\} = \{g_i\} \tag{3.24}$$

Eq. (3.24) represents 5 simultaneous equations in the unknown springs k_1-k_5. Therefore, in the present example one single mode is sufficient to determine uniquely the five springs. For the available p modes, we can write

$$\begin{bmatrix} [D_1] \\ \vdots \\ \vdots \\ \vdots \\ [D_p] \end{bmatrix}_{npx5} \begin{Bmatrix} k_1 \\ \cdot \\ k_5 \end{Bmatrix} = \begin{Bmatrix} \{g_1\} \\ \vdots \\ \vdots \\ \{g_p\} \end{Bmatrix}_{npx1}$$

or

$$[D]_{npx5} \{k_s\} = \{g\}_{npx1} \tag{3.25}$$

$$\{k_s\} = [[D]^T [D]]^{-1} [D]^T \{g\} \tag{3.26}$$

Eq. (3.26) is actually the same as Eq. (3.11) but taking into account only the unknown springs.

The identification process was carried out for the following cases:

A. Using the mode shapes directly.

B. Using additional data obtained by introducing some design changes.

C. Using the mode shapes after orthogonalizing them with respect to the known mass matrix.

In every case the exact mode shapes were multiplied by a corruption matrix $[C_o]$ to simulate experimental errors.

The matrix $[C_o]$ was generated in the way shown below.

$$[C_o] \begin{bmatrix} 1 & & & & \\ 0 & 1 & & \text{Symm.} & \\ 0 & 0 & 1 & & \\ 0 & 0 & 0 & 1 & \\ 0 & 0 & 0 & 0 & 1 \end{bmatrix} \begin{bmatrix} \pm.1 & & & & \\ \pm.08 & \pm 0.1 & & \text{Symm.} & \\ \pm.06 & \pm.08 & \pm.01 & & \\ \pm.04 & \pm.05 & \pm.08 & \pm 0.1 & \\ \pm.02 & \pm.04 & \pm.06 & \pm.08 & \pm 0.1 \end{bmatrix}$$

$$(3.27)$$

where $\pm.1$ means a generated random number between -0.1 and +0.1. Correspondingly the elements of the corrupted mode shape vectors were obtained as;

$$p_{i,j}^c = p_{i,j}(1 + \pm.1) + p_{i,j\pm1} \times \pm.08 + p_{i,j\pm2} \times \pm 0.06 + \ldots$$

$$(3.28)$$

where $p_{i,j}$, $p_{i,j+1} \ldots$ are the exact values. In this way the elements of the mode vector j are affected by both the errors associated with the mode j and those associated with the rest of the modes. The error contribution of these modes decreases as they get further from the mode j.

The random errors in the matrix $[C_o]$ were generated, the mode shapes were corrupted and subsequently the five springs $k_1 - k_5$ were identified. This process was carried out one hundred times to yield the averages and standard deviations associated with the five springs.

The results are presented in the following:

A. Using the mode shapes directly:

The corrupted mode shapes were used directly in Eq. (3.26). The identification process was carried out using from one to five modes. The averages and the limits corresponding to 90% confidence are listed in Table 3.2.

Table 3.2 shows that the average values of the identified springs are very close to the exact ones as one would expect. The 90% confidence limits get narrower as the number of modes used increases. It is interesting to notice the remarkable improvement in identifying the spring k_5 when the equations associated with the second mode were added to those of the first mode. The standard deviation dropped from 1.2676, which means that the identified value using only the first mode was totally unreliable, to only 0.1042.

B. Using additional data obtained by introducing some design changes:

The design changes were introduced by changing the element m_5 of the mass matrix into $2 m_5$, $3 m_5$ and $4 m_5$. In every case the eigenvalue problem was solved to yield the exact modal parameters. Then the mode shapes were corrupted in the way described above.

Therefore, we have altogether four sets of modal parameters, one for the original structure and three additional ones obtained by introducing the artificial design changes. All these data were assembled in Eq. (3.26) and the identification process of the five springs was carried out using from one to five modes.

Table 3.2 Identified Springs, Mode Shapes Used Directly
Average ± 90% Confidence Limits

No. of Modes	k_1	k_2	k_3	k_4	k_5
1	$1.1039 \pm .2826$	$.9893 \pm .3597$	$1.0066 \pm .3823$	$1.1592 \pm .6851$	1.3460 ± 2.0915
2	$.9867 \pm .2300$	$.9765 \pm .2564$	$1.0159 \pm .2024$	$1.0107 \pm .1696$	$.9771 \pm .1719$
3	$.9900 \pm .0895$	$.9856 \pm .0970$	$1.0122 \pm .0906$	$1.0223 \pm .1624$	$.9888 \pm .0715$
4	$.9974 \pm .0343$	$.9930 \pm .0286$	$1.0088 \pm .0811$	$1.0037 \pm .0396$	$.9968 \pm .0297$
5	$1.0010 \pm .0096$	$.9975 \pm .0045$	$1.0002 \pm .0028$	$.9973 \pm .0048$	$.9994 \pm .0034$

In all cases the average values of the identification springs were almost identical to the exact ones. Figs. 3.3.a)-e) show the standard deviations of the springs k_1-k_5. It is clearly visible from these figures that, in general, including the additional data associated with the first two modifications has reduced the standard deviations, (which can be considered as measures of the errors in estimating k_1-k_5), quite significantly. This is especially true when the number of modes used is small. The inclusion of the data associated with the third modifications did not lead to any appreciable improvement.

The degree of improvement in estimating the five springs due to including the additional data decreased from k_5 to k_4... to k_1. This is due to the fact that the design changes were performed at coordinate x_5. The trend of improvement in these estimates was reversed, i.e. from k_1 to k_2... to k_5 when the modifications were performed at coordinate x_1 instead of x_5.

C. Using the mode shapes after orthogonalization:

In this case the same corrupted mode shapes used in A) above were first orthogonalized with respect to the mass matrix $[m_x]$ before using them in Eq. (3.26). The Targoff [50] orthogonalization algorithm was used. The number of modes to be orthogonalized and subsequently used in identifying the five springs was from two to five modes.

Examples of the corrupted modes before and after

the orthogonalization process are presented in Tables 3.3
and 3.4. Table 3.3 corresponds to the case of five modes
being orthogonalized, while Table 3.4 corresponds to the
case of only two modes being orthogonalized. As we can
see in Table 3.3 the orthogonalization process returns the
five modes almost identical to the exact ones, see Table 3.1.
On the other hand, in the case that the number of the
available modes is less than the order of the system, the
returned modes, though perfectly orthogonal to the mass
matrix, could be significantly different from the exact ones
as can be seen in Table 3.4. This is because the orthogonaliza-
tion process does not correct for the missing modes.

The results of the identification process using the
modified modes are listed in Table 3.5. Comparing these
results with those in Table 3.2 obtained when the modes were
used directly, one can only say that, in the case of the five
modes available, the orthogonalization process yields better
estimates of the five springs. For a number of modes less
than five, (which is the order of the system), the orthogonaliza-
tion process does not offer a distinct advantage in terms
of identifying the unknown springs.

ii) Number of available equations is less than the
    number of unknowns

Fig. 3.4 shows a three degrees of freedom undamped
system. It contains six springs k_1-k_6. Assume that the
data available about this system are:

Table 3.3 Orthogonalization of 5 Mode Shape
Vectors with Respect to $[m_x]$

Modes Before Orthogonalization				
1	2	3	4	5
.27989	-.78263	1.02900	-1.39580	2.24463
.63446	-1.07670	.32739	1.33160	-4.10240
.77738	-.65770	-1.07000	.30766	4.03850
.89340	.22133	-.68019	-1.50980	-3.02520
1.00000	1.00000	1.00000	1.00000	1.00000
Modes After Orthogonalization				
.28620	-.83906	1.29320	-1.68260	1.93030
.54293	-1.0947	.36756	1.39400	-3.25290
.76511	-.59403	-1.19580	.52864	3.52700
.92126	.31366	-.71070	-1.82330	-2.6973
1.00000	1.00000	1.00000	1.00000	1.00000

Table 3.4   Orthogonalization of 2 Mode Shape
Vectors with Respect to $[m_x]$

Before Orthogonalization		After Orthogonalization	
1	2	3	4
.27989	-0.78263	.245975	-.74427
.63446	-1.07670	.57949	-1.01490
.77738	-.65770	.73127	-.60589
.89340	.22133	.87181	.24559
1.00000	1.00000	1.00000	1.00000

Table 3.5 Identified Springs; Mode Shapes Used After Orthogonalization
Average $\pm$ 90% Confidence Limits

No. of Modes Orthogonalized	k_1	k_2	k_3	k_4	k_5
2	$.9450 \pm .1830$	$.9275 \pm .4805$	$1.0213 \pm .2430$	$1.0196 \pm .1266$	$1.0261 \pm .1501$
3	$1.0067 \pm .1367$	$.9659 \pm .2045$	1.0132 ± 0.0770	$1.0097 \pm .1363$	$.9860 \pm .0590$
4	$.9980 \pm .0369$	$.9907 \pm .0467$	1.0188 ± 0.0684	1.0143 ± 0.0716	$.9957 \pm 0.0295$
5	$.9986 \pm 0.0063$	$1.0004 \pm .0038$	$1.0001 \pm .0018$	$1.0000 \pm .0016$	1.0000 ± 0.0016

a)   The exact mass matrix $[m_x]_{3x3}$.

b)   One measured natural frequency and the corresponding full length mode shape vector. In the present example we will use the exact values of these modal parameters which have been found by solving the eigenvalue problem of the system. They are;

natural frequency   =   0.107 Hz

mode shape   = $<1.0041, 1.0, 1.0484>^T$

It is required to identify the six springs using the above data.

For one mode the equation of motion provides only three linear equations in the unknown six springs. Therefore, initial estimates of these springs have to be used. Hence, Eqs. (3.14) using the pseudo-inverse as defined in Eq. (3.18) are to be applied.

The weighting matrix $[W]_{6x6}$ in Eqs. (3.14) was taken as,

$$[W]_{6x6} = \begin{bmatrix} 1 & & 0 \\ & \ddots & \\ 0 & & 1 \end{bmatrix}$$

The results of the identification process are listed in Table 3.6 for two sets of initial estimates of the six springs. As we can see the identified values are very close to the initial estimates in both cases.

3.2.2   Relevant Partial Mode Shapes

3.2.2.1   Procedure

There are some instances where the unknown parameters

Table 3.6   Identified Springs of the 3 Degrees
of Freedom System in Figure 3.4

Spring	Initial Estimate	Identified Value	Initial Estimate	Identified Value
k_1	1.25	1.0082	1.1	.9981
k_2	2.50	2.5866	2.2	2.2365
k_3	3.75	3.8288	3.2	3.2296
k_4	2.50	2.6011	2.3	2.3414
k_5	1.75	1.5518	1.6	1.5214
k_6	2.20	1.9733	2.1	2.0119

belong to a part of the structure, such that it is connected
to the rest of the structure on a small number of points.
In these cases it is still possible to apply the procedure
described in Section 3.2.1 even if only a part of the mode
shape was measured, the relevant section, i.e. that which
belongs to the strongly separated part of the structure. This
section contains the unknown parameters.

In other words, there are special cases where the
unknown elements to be identified are located in the mass,
damping, and stiffness matrices $[m_x]$, $[c_x]$ and $[k_x]$ in rows
which are partly filled with zeros. Therefore, the elements
of the mode shape vectors corresponding to these zero elements
will not be used in the identification process, and Eqs. (3.4)
are still applicable. Depending on the number of unknowns,
number of available equations and on the availability of
initial estimates we can, similarly, arrive at the expressions
in Eqs. (3.11) or (3.14).

However, we must realize, in the present case that,
correcting the available partial mode shapes is not possible,
and they have to be used directly as measured.

3.2.2.2 Example of Relevant Partial Mode Shapes

Consider the system shown in Fig. 3.5 which consists
of a rigid beam mounted on a flexible beam with two springs
k_1 and k_2. The flexible beam itself is mounted on an
immovable ground with the two springs k_3 and k_4. As can

be seen, the rigid beam is a strongly separated part from the rest of the structure. It is connected to it only on two points. It is required to identify the springs k_1 and k_2. Eqs. (3.4) for this system for mode i, in the coordinates x_1-x_9, is written as

$$
-\Omega_i^2
\begin{bmatrix}
\begin{bmatrix} m_{s1} & 0 \\ (2\times2) & \\ \hline & \\ 0 & \\ & m_{s2} \\ & 7\times7 \end{bmatrix}
\end{bmatrix}
+
\begin{bmatrix}
k_1 & 0 & 0 & 0 & -k_1 \dots 0 \\
0 & k_2 & 0 & 0 \dots -k_2 \dots 0 \\
\hline
0 & 0 & & & \\
\vdots & \vdots & & & \\
-k_1 & \vdots & & +k_1 & \\
\vdots & -k_2 & & +k_2 & \\
\vdots & \vdots & & k_{s2} & \\
0 & 0 & & & 7\times7
\end{bmatrix}
\begin{Bmatrix}
p_{1i} \\ p_{2i} \\ \vdots \\ \vdots \\ p_{5i} \\ p_{6i} \\ \vdots
\end{Bmatrix}
= 0
$$

(3.29)

where $[m_{s1}]$ is the mass matrix of the rigid beam and $[m_{s2}]$ is the mass matrix of the flexible beam.

$[k_{s2}]$ is the stiffness matrix of the flexible beam including the supports k_3 and k_4.

As can be seen, it is only the first two equations in Eq. (3.29) which contain the two unknown springs k_1 and k_2. Also, in this particular example, none of the elements of the mass and stiffness matrices $[m_{s2}]$ and $[k_{s2}]$ are involved in these two equations. The part of the mode shapes relevant to the identification process is that one measured only on coordinates x_1, x_2, x_5 and x_6.

Therefore, knowing the mass matrix of the rigid beam

$[m_{sl}]$, the measured eigenvalues Ω_i^2's and the measured relevant parts of the mode shapes $<p_{1i}, p_{2i}, p_{5i}, p_{6i}>$; $i = 1, p$, is sufficient to identify the unknown springs k_1 and k_2.

The eigenvalue problem of the system was first solved to yield the exact natural frequencies and mode shapes. The data of the first two modes are listed in Table 3.7. Only the relevant parts of the mode shapes are included.

Table 3.7 Exact First Two Modes of the Structure in Fig. 3.5

		Mode 1	Mode 2
Frequency Hz		38.13500	99.46900
Mode Shape	x_1	1.00000	1.00000
	x_2	.84579	-.64795
	x_5	.56461	-.38686
	x_6	.63961	-.50457

Then these relevant parts were corrupted with generated random numbers according to Eq. (3.28) to simulate experimental errors. These random numbers were generated and subsequently the identification process was carried out applying Eq. (3.11), one hundred times. The averages and 90% confidence limits of the two springs k_1 and k_2 were obtained as,

	k_1 N/m	k_2 N/m
First Mode	$(964.0 \overset{+}{-} 75.0123).10^3$	$(2087.7 \overset{+}{-} 414.6285).10^3$
First and Second Mode	$(984.1 \overset{+}{-} 70.7471).10^3$	$(1998.2 \overset{+}{-} 387.9480).10^3$

As can be seen these identified values are very close to the exact ones of $k_1 = 1E6$ N/m and $k_2 = 2E6$ N/m.

3.3   Incomplete Mode Shapes, Nonlinear Equations

3.3.1   Procedure.

In some instances significant coordinates of the model are not accessible for the measurement of the mode shapes, e.g. coordinates on the spindle inside a headstock. In these cases the formulation of linear equations as in Section 3.2 is not possible. Instead the following objective function is formulated in which the errors between the estimated and measured modal parameters are to be minimized,

$$U = \sum_{m=1}^{mm} [\sum_{j=1}^{P_m} \alpha_j \, (\frac{\Omega_j^2 - \Omega_{jex}^2}{\Omega_{jex}^2})^2 + \sum_{j=1}^{P_m} \beta_j \, (\frac{K_j^r - K_{jex}^r}{K_{jex}^r})^2$$

$$+ \sum_{i}^{\ell} \sum_{j=1}^{P_m} \gamma_{ij} \, (\frac{p_{ij} - p_{ijex}}{p_{ijex}})^2] \qquad (3.30)$$

where; the parameters with the subscript ex are those established experimentally.

α, β and γ are weighting factors introduced to represent

               our confidence in the measured parameters,

               α, β, γ = 0 - 1.

p_m is the number of measured modes, $p_m \leq n$

               where n is the number of degrees of freedom

ℓ is the number of accessible coordinates; $\ell \leq n$.

Ω_j^2 is the eigenvalue of mode j.

P_{ij} is the element measured on coordinate i in the

               mode shape j.

K_j^r is the modal stiffness of the mode j measured at

               coordinate r.

mm   is the number of available sets of modal parameters.

               For instance, if one set corresponding to the

               original structure and an additional set obtained

               when introducing some design changes are available,

               then mm = 2.

Therefore, the identification procedure starts with some initial estimates of the unknown elements in the mass and/or the stiffness matrices. Then the eigenvalue problem is solved to give the (estimated) eigenvalues Ω_j^2's, the mode shapes $\{\phi_j\}$'s and the modal stiffness K_j^r 's. These estimated modal parameters are plugged into the objective function in Eq. (3.30), and the optimization proceeds to obtain those values of the elements to be identified which give the minimum U.

Obviously, in the objective function in Eq. (3.30) the

range of the number of input data is quite large. It accepts
as small number as a single natural frequency and as large
number as several sets of n natural frequencies, n full
length mode shapes and n modal stiffnesses. In this sense
it represents a general expression for identifying the unknown
elements in the system mass and/or stiffness matrices. More-
over, any physical constraints on these unknown elements,
e.g., the masses and stiffnesses must be positive, can be
easily included. On the other hand, to ensure that U is
globally minimum, usually several trials with different
initial estimates are needed. In each trial the minimization
process takes many iterations, where in every iteration the
estimated modal parameters have to be updated.

3.3.2 Example of Using Incomplete Mode Shapes

The same structure in Fig. 3.2 of five degrees of
freedom will be used here. The exact mode shapes, obtained
by solving the eigenvalue problem, were corrupted according
to Eq. (3.28) to simulate experimental errors. Corrupted
modal stiffnesses were generated using these mode shapes,
which are in error, the exact mass matrix and the exact
eigenvalues. For example K_{ic}^{r} was obtained as follows;

$$K_{ic}^{r} = <\phi_i^{C}>^{T} [m_x]\{\phi_i^{C}\} \; \Omega_i^{2} \tag{3.31}$$

where; $\{\phi_i^{C}\}_{5x1}$ is the ith corrupted mode shape vector,

Ω_i^{2} is the corresponding exact eigenvalue.

$[m_x]$ is the exact mass matrix.

This process of generating what will be assumed as the experimental data was carried out for the original structure with the mass element $m_5 = 1$ kg., as well as for the structure with $m_5 = 2$, $m_5 = 3$ and $m_5 = 4$ kg. These last three cases represent artificial incorporated design changes.

Now, assume that the coordinates x_1 and x_2 are inaccessible. Therefore, the mode shapes are incomplete, they are measured only on the coordinates x_3, x_4 and x_5. Moreover, assume that only the first three modes are available. The simulated modal parameters are listed in Table 3.8 where O designates the original structure, M1 first modification, M2 second modification, etc. The exact mass matrix $[m_x]$ is available. It is required to identify the five springs k_1-k_5.

The optimization routine SEEK from the package OPTIVAR developed by Siddall [88] at McMaster University was used to identify these springs according to the objective function, Eq. (3.30). In this routine a direct search method is applied. All the weighting factors α, β and γ were taken as one. The identified values are listed in Tables 3.9 and 3.10 for two sets of initial estimates. As can be seen for both sets the corresponding identified values are practically identical which implies that a global minimum has been found.

Table 3.8 Simulated Modal Parameters
(Incomplete Mode Shapes)

			Mode		
			1	2	3
0: $m_5 = 1.$	Eigenvector	x_3	.74013	-.64290	-1.14456
		x_4	.96171	.31198	-.72552
		x_5	1.00000	1.00000	1.00000
	Modal Stiffness (N/m)		.23377	2.50705	7.75264
M1: $m_5 = 2.$	Eigenvector	x_3	.67431	-1.16285	-1.89462
		x_4	.88154	-.12170	-1.99813
		x_5	1.00000	1.00000	1.00000
	Modal Stiffness (N/m)		.20936	3.94885	25.36960
M2: $m_5 = 3.$	Eigenvector	x_3	.70880	-1.85048	-2.99007
		x_4	.88310	-.48621	-3.67492
		x_5	1.00000	1.00000	1.00000
	Modal Stiffness (N/m)		.211496	6.55573	69.51890
M3: $M_5 = 3.$	Eigenvector	x_3	.68525	-2.44074	-3.76099
		x_4	.86732	-.91621	-4.57628
		x_5	1.00000	1.00000	1.00000
	Modal Stiffness (N/m)		.20625	10.46770	105.22600

Table 3.9 Identified Springs

Initial estimates: $k_1 = .8$, $k_2 = 1.2$, $k_3 = 1.8$, $k_4 = .7$, $k_5 = 1.5$

	U	k_1	k_2	k_3	k_4	k_5
0	.01059	1.05711	1.16484	.93234	.96062	.99363
0 + M1	.02064	1.00600	1.13742	.95402	.96391	.99117
0 + M1 + M2	.06312	1.01539	1.03945	.98531	.99016	1.00172
0 + M1 + M2 + M3	.06954	1.02590	1.03334	.96937	.99179	1.00547

Table 3.10   Identified Springs

Initial estimates: $k_1 = .4$, $k_2 = 3.$, $k_3 = 4.$, $k_4 = .1$, $k_5 = 2.5$

	U	k_1	k_2	k_3	k_4	k_5
0	.01057	1.05703	1.16484	.93281	.96094	.99375
0 + M1	.02065	1.00781	1.13516	.95391	.96484	.99219
0 + M1 + M2	.06314	1.01406	1.04062	.98516	.98906	1.00078
0 + M1 + M2 + M3	.06965	1.02343	1.03672	.97031	.98984	1.00390

Tables 3.9 and 3.10 show that including the second set (M1) and then the third set (M2) of modal parameters into Eq. (3.30) has improved the estimates of the five springs. With the inclusion of the data associated with (M3) the improvements, or sometimes worsening of these estimates were not significant. This finding agrees with that observed in Section 3.2.1.2. This indicates that using too many additional sets of modal data into the identification process would not necessarily lead to better estimates of the unknown elements. As a matter of fact, from the practical point of view, performing an artificial design change and then obtaining an additional set of modal data is not an easy task. The lengthy operation of measuring the transfer functions can be prohibitive. For instance, sometimes the structure under investigation is only available for a specified length of time. Moreover, every additional modal set has its own errors.

With all this in mind, and from the presented examples, one can conclude that including a single additional set of measured modal parameters into the identification process is advantageous, especially when the modal data of the original structure are limited.

CHAPTER 4

APPLICATIONS OF IDENTIFICATION
SCHEMES ON MACHINE TOOL STRUCTURES

4.1   Introduction

In the previous chapter the schemes of identifying
the structure's mass and stiffness unknown elements using the
modal approach have been classified and applied on simulated
examples. The theoretical structures used were rather simple
and, of course, linear. The geometry, or in other words, the
model of the structure was known. In all these examples the
identified parameters obtained were very close in value either
to the exact ones when the data available were large enough or
to the initial estimates when the data available were less
than the number of unknowns.

In the present chapter these identification procedures
will be applied on actual machine tool structures. These
structures, which are actually distributed systems, will be
treated as linear lumped mass, spring, damper models. In doing
so, one must realize the following:

a)   The distributed system will theoretically have an
infinite number of modes compared to a finite number of the
lumped model. Thus it is reasonable to compare only the lower
frequency modes of the model and the actual structure. These
modes to be compared should lie within the frequency range of
interest.

b) In the actual structure there are always some non-linearities, e.g., the play in the gaps, the play between gears and spline shafts, etc. Therefore, the model to be established will be at best a linear approximation of a non-linear system.

c) A systematic way of establishing the proper lumped model of an actual complicated structure like machine tools from the test data has not yet been found. It is believed that the examples to be presented in this chapter will serve as a forward step towards achieving such a goal.

d) In general, the elements of the mass matrix of the lumped model of the structure are more accurately predictable than the stiffness elements. They can be calculated from the drawings or by weighing some of the components. Hence, in the examples presented in this chapter the mass matrix will be assumed to be accurately known and the unknown stiffness elements will be identified.

e) The assumption that the structure has proportional viscous damping will be used throughout this chapter, and consequently no attempt will be made to identify the dampers in the system. This assumption is justified on the basis that the imaginary parts of the measured mode shapes of all the structures considered here were at least one order of magnitude smaller than the real parts. This implies that these mode shapes were almost purely real which is a characteristic of a vibratory system with proportional viscous damping.

All of the above items, neglecting higher modes, neglecting nonlinearities, possibly the wrong choice of the proper model, assuming the mass matrix to be exact and assuming the damping to be proportionally viscous, in addition to the experimental errors, contribute to the overall inaccuracy of the established model. The validity of this model will be tested, as stated in the beginning of the previous chapter, by reproducing the test modal data as well as predicting design changes.

The first example presented here will be a case of a ram-type milling machine where full length mode shapes were measured. A complete model will be established.

The second example will be a case of establishing a complete model of a vertical milling machine where the measuring mode shapes were incomplete.

A third example to be presented in the next chapter will be a case of partial identification of the clamping characteristics of the chuck of a lathe.

4.2 Identifying Unknown Springs of a Milling Machine Using Full Length Mode Vectors

The structure under test is the ram-type milling machine shown in the photograph in Fig. 4.1. A long series of cutting tests have indicated that when chatter occurred the frequency associated with it was around 120 Hz. The exciter tests, which will be presented below in detail, have shown that there was a mode at 122 Hz associated mainly with the ram and the belt

housing. They also indicated that neither the spindle modes, around 750 Hz, nor the tool modes around 1400 Hz were detrimental to the chatter occurrence for this particular machine. Moreover, the exciter tests have shown that only the spindle and tool modes were evident in the measured relative transfer function between the tool and the workpiece in the Y direction.

From both the cutting and the exciter tests it was decided to concentrate on the lower structural modes in the X direction which are relevant to chatter. Therefore, the model to be established will represent only the behaviour of the structure in these modes.

4.2.1 Measured Mode Shapes

The hammer impact technique was used to measure the transfer functions at the different locations on the structure. The equipment used were:

a)   5451 A minicomputer based Fourier Analyzer.

b)   Pcb force impact transducer, model 203A with a
      Kistler charge amplifier model 5001.

c)   Pcb accelerometer model 308B.

d)   Proximity probe, capacitive type, Wyne Kerr Mcl used
      in the measurements of the relative transfer functions.

At each location the obtained transfer function was the average of ten measurements.

Figure 4.2 shows the relative transfer function between the tool and the workpiece in the X direction. In this figure, four modes can be seen in the range 0-625 Hz frequency. The frequencies of these modes are: 72.9, 122.3, 345.1 and 538 Hz. Apart from these four modes there is a fifth mode at 22 Hz in which the whole structure rocks on the floor. Obviously it can not be seen in the relative transfer function presented in Fig. 4.2. Fig. 4.3 shows the deformation of the structure in these five modes. These mode shapes are described as follows:

First mode at 22 Hz:

The whole machine vibrates in a rocking mode around the base as a pivot.

Second mode at 72.9 Hz:

. The whole head assembly swings around the end of the fork to which the headstock is attached. The motor goes farthest in one direction and the tool in the opposite direction, while the fork, the ram, the turret and the column counteract these motions.

Third mode at 122 Hz:

The headstock assembly moves almost in parallel in the longitudinal direction of the table, while the motor moves against this in the opposite direction, which causes a slight inclination of the head assembly.

Fourth mode at 345 Hz:

The main feature here is the headstock exhibiting a higher mode vibration, where the upper part moves in one direction while the lower part moves in the opposite direction.

Fifth mode at 538 Hz:

This mode is composed of the bending of the ram associated with the bending of the head assembly.

4.2.2 Establishing the Model

Studying the mode shape in Fig. 4.3 carefully, five main flexibilities in the system could be recognized. All of these flexibilities are torsional and are understood as being relative rotations between the two structural members associated in the given joint. These flexibilities, see Fig. 4.4, are explained as follows:

α_1 is the rotation of the whole ram around axis A_1. The flexibility γ_1 associated with α_1 includes flexibility of the "turret" (top of the column) and the guideways between the turret and the ram.

α_2 is the rotation around axis A_2. The flexibility γ_2 associated with α_2 consists of that of guideways of the ram, of the ram itself and of the U-shaped fork holding the headstock.

α_3 is the rotation around axis A_3. The flexibility γ_3 associated with α_3 consists of the twist of

the belt housing connecting the motor with the gear-
box on top of the headstock.

α_4 is the rotation around axis A_4. The corresponding
flexibility γ_4 is confined mainly to the fork.

α_5 is the rotation of the whole machine (rocking) around
axis A_5. The corresponding flexibility γ_5 is confined
to the mounting contact between the baseen, the base
and the floor. No appreciable flexibilities were
observed between the table and the knee and the column
in the covered frequency range. Moreover, the additional
flexibilities in the spindle and the tool do not
particularly affect the structural modes in the fre-
quency range of interest, 0-625 Hz.

Therefore, based on the mode shapes in Fig. 4.3 and
consequently on the interpretation of the different flexibilities
in the system it was reasonable to establish a model with five
degrees of freedom to describe the dynamics of the machine in
the frequency range of 0-625 Hz. The model will have five
design coordinates α_1-α_5. Associated with these coordinates
are the flexibilities γ_1-γ_5 or, alternatively, the stiffnesses
k_1-k_5 which are to be identified.

Having decided on a five degrees-of-freedom model it
was necessary to select five local coordinates on the structure
whose motions can best represent the deformations of the machine
in the five modes. These points must be chosen so that the

response at other locations could be obtained from the response of these selected points by interpolation.

The locations x_1-x_5 shown in Fig. 4.4 were found to satisfy the above requirements. The transformation matrix $[T_1]$ between the local coordinates x and the design coordinate α can be derived from the geometry of the model as,

$$
\begin{Bmatrix} \alpha_1 \\ \alpha_2 \\ \alpha_3 \\ \alpha_4 \\ \alpha_5 \end{Bmatrix} = \begin{bmatrix} 0 & 0 & 0 & .05556 & -.05556 \\ -0.1 & .1 & 0 & 0 & -.01818 \\ .24286 & -.1909 & .0909 & -.14286 & 0 \\ .14286 & 0 & 0 & .19841 & .05556 \\ 0 & 0 & 0 & 0 & .01818 \end{bmatrix} \begin{Bmatrix} x_1 \\ x_2 \\ x_3 \\ x_4 \\ x_5 \end{Bmatrix}
$$

i.e.

$$\{\alpha\} = [T_1] \{x\} \tag{4.1}$$

To establish the mass matrix of the model it was easier to find it directly in the local coordinates rather than the design ones. Nine masses were allocated at the positions shown in Fig. 4.4. These positions were chosen to be as close as possible to the actual mass distribution in the structure.

The mass m_a corresponds to the sum of the masses of the front half of the ram and the base of the fork, and m_b to the end of the fork and the central part of the headstock. The mass m_m represents the mass of the rear half of the ram. Since the turret, the column, the knee and the table did not show

any relative movement but acted as one body, these masses are represented by one concentrated mass m_g. The correspondence of the other masses to the actual parts of the machine is obvious, e.g. m_e corresponds to the motor, m_f to the pulley and part of the belt housing, m_{d2} to the top of the head assembly, m_{d1} to the gearbox and m_c to the quill end.

The masses were evaluated from the drawings of the machine. The mass m_e was obtained directly by weighing the motor. All the masses are listed in Table 4.1.

A matrix $[T_m]_{9*5}$ can be obtained from the geometry of the model to be used in transforming the coordinates of the individual masses into the main coordinates $x_1, x_2, \ldots, x_5$. $[T_m]$ is given in Appendix I .

Table 4.1 Estimated Masses (kg)

m_a	36.28
m_b	61.22
m_c	4.54
m_{d1}	11.34
m_{d2}	9.07
m_e	24.94
m_f	13.61
m_g	411.34
m_m	18.14

Summarizing

-) The model established shown in Fig. 4.4 has five

degrees of freedom α_1-α_5. Associated with these freedoms are the stiffnesses k_1-k_5.

- From the geometry of the machine a transformation matrix $[T_1]$ is obtained, such that

$$\{\alpha\} = [T_1] \{x\}$$

where the α's are the design coordinates, and the x's are the local coordinates where the transfer functions were obtained.

- Nine lumped masses are estimated from the drawings of the machine. They are interconnected by massless beams as shown in Fig. 4.4 The single line represents a flexible connection, while the double line represents a rigid one. These nine masses correspond to nine translative coordinates in the X direction. They can be transformed into the coordinates x_1-x_5 using the matrix $[Tm]$ formed from the geometry of the machine, i.e.

$$[m_x]_{5*5} = [Tm]^T \ \lceil m_{i\rfloor} \ [Tm] \tag{4.2}$$

are the individual estimated masses.

4.2.3 Identifying the springs k_1-k_5

The results obtained from curve fitting the measured transfer functions are given in Table 4.2. They include the natural frequencies, modal stiffnesses, modal damping ratios as well as the mode shapes at the coordinates x_1-x_5. Given these modal data and the mass matrix $[m_x]$, which is assumed to be

Table 4.2 Measured Modal Data of the Ram Type Milling
Machine (Motor on)

	Mode 1	Mode 2	Mode 3	Mode 4	Mode 5
Natural freq. (Hz)	22.103	72.910	122.110	345.012	538.327
Modal stiff (N/m)	.7162E7	.1727E9	.6798E8	.2533E9	.1737E11
Modal damp. %	1.3100	2.9480	3.2010	4.9470	3.4020
Mode shapes x_1	-.8110	-.1252	1.0500	-.2621	-1.9402
x_2	1.0	1.0	1.0	1.0	1.0
x_3	1.1921	4.7902	-.4072	-.4000	-.6615
x_4	.7702	-.3032	.3501	-.4921	4.1920
x_5	.7521	-.6001	-.1923	-.0110	-.0500

exact, as well as the transformation matrix $[T_1]$ between the design and local coordinates, it is requied to identify the five torsional springs in the system, k_1-k_5.

The procedure presented in section 3.2.1 has been followed to arrive at Eq. (3.26) where the unknowns are the stiffness elements. No initial estimates were used. The results of the identification process are given below.

4.2.3.1 Mode Shapes Used Directly

The modes as measured were used directly in Eq. (3.26). The identified springs using from one to five modes are listed in Table 4.3. Then these identified springs, except for those obtained using two modes where k_4 came out negative, to solve for the natural vibrations of the system. The computed modal data are given in Tables 4.4 - 4.7.

By comparing the computed data of the five modes with those measured given in Table 4.2, the following could be observed:

a) The use of the first mode in the identification process, although reproduced almost exactly the experimental input of mode 1, led to significant errors in reproducing the higher modes.

b) In practice the use of more input experimental data may not necessarily lead to better estimates of the unknown parameters. This is because in reality the errors associated with these data vary from one measured mode to another. They depend

primarily on the stiffness of the individual modes, as well as the closeness of the driving point (in the present case it is coordinate x_2) to a node. For instance, the inclusion of the data of the second mode to those of the first, has resulted in obtaining a negative value for k_4. Also, the inclusion of the data of the fifth mode to those of the first four, has resulted in worsening the estimate of k_5 which represents the main flexibility of the first mode.

c) The computed modal data using the first four modes, Table 4.6, are on the overall in a very good agreement with those measured, Table 4.2. The errors in reproducing the natural frequencies of the five modes are as follows:

Mode	1	2	3	4	15
Error %	-4.01	10.24	1.24	-8.14	-1.03

Figs. 4.5-4.9 show the measured and computed transfer functions at the coordinates x_1-x_5, respectively as synthesized from the data in Table 4.6 and Tables 4.2. The measured damping ratios were used in obtaining the computed transfer functions. As can be seen in these figures, using the identified springs from the first four modes have reproduced very closely the measured transfer functions which proves, considering the complexity of the structure, the validity of the established model.

4.2.3.2. Mode Shapes Used After Orthogonalization

The measured mode shapes were first orthogonalized with respect to the estimated mass matrix before using them in Eq. (3.11). The number of modes to be orthogonalized and

Table 4.3 Identified Springs $k_1 - k_5$ (N/m)

No. of Modes	k_1	k_2	k_3	k_4	k_5
1	.3184E8	.2525E7	.1238E7	.1151E7	.2428E8
2	.2349E8	.3747E7	.7866E6	-.3179E7	.2521E8
3	.3068E8	.3743E7	.7918E6	.3512E7	.2231E8
4	.3166E8	.4724E7	.9512E6	.4111E7	.2233E8
5	.3375E8	.5988E7	.9201E6	.4101E7	.6945E8

Table 4.4   Computed Modal Data Using the Identified
             Springs from One Measured Mode

	Mode 1	Mode 2	Mode 3	Mode 4	Mode 5
Natural freq. (Hz)	22.000	69.720	89.906	277.860	430.280
Modal stiff. (N/m)	.7241E7	.2712E9	.3097E8	.3036E9	.18722E10
Mode shapes x_1	.8100	-1.0307	.8842	-.3330	-.7997
x_2	1.0	-1.0	1.0	1.0	1.0
x_3	1.1900	-.2759	-.2759	-.5182	-.7203
x_4	.7700	.0461	.0461	.0461	1.7197
x_5	.7520	-.2023	-.2023	.0499	.0087

Table 4.5 Computed Modal Data Using the Identified Springs from Three Measured Modes

	Mode 1	Mode 2	Mode 3	Mode 4	Mode 5
Natural freq. (Hz)	21.170	72.741	118.680	289.220	497.340
Modal stiff. (N/m)	.7238E7	.3523E9	.6299E8	.2158E9	.2327E11
Mode shapes x_1	.8229	-.5839	.9507	-.3201	-2.5602
x_2	1.0	1.0	1.0	1.0	1.0
x_3	1.2331	6.8960	-.4217	-.730	-.8454
x_4	.8054	-.4932	.3022	-.4501	6.0817
x_5	.7859	-.7308	-.2014	-.0174	.0542

Table 4.6   Computed Modal Data Using the Identified
            Springs from Four Modes

	Mode 1	Mode 2	Mode 3	Mode 4	Mode 5
Natural freq. (Hz)	21.216	80.375	123.610	316.930	532.790
Modal stiff. (N/m)	.7361E7	.3980E9	.7256E8	.2529E9	.1991E11
Mode shapes x_1	.8287	-.4729	.98522	-.2877	-2.3045
x_2	1.0	1.0	1.0	1.0	1.0
x_3	1.2177	6.6378	-.4589	-.4010	-.7934
x_4	.8127	-.4152	.3415	-.4743	5.1549
x_5	.7936	-.7065	-.2038	.0126	.0583

Table 4.7   Computed Modal Data Using the Identified
            Springs from Five Modes

		Mode 1	Mode 2	Mode 3	Mode 4	Mode 5
Natural freq.	(Hz)	36.640	85.222	126.970	336.580	537.250
Modal stiff.	(N/m)	.1906E8	.1697E10	.7653E8	.2862E9	.1592E11
Mode shapes	x_1	.8042	-1.3678	.9651	-.2869	-2.05
	x_2	1.0	1.0	1.0	1.0	1.0
	x_3	1.3251	12.8810	-.3846	-.3532	-.6956
	x_4	.7591	-1.0508	.3104	-.4965	4.5351
	x_5	.7056	-1.4940	-.2264	.0092	.0440

subsequently used in identifying the five springs was from
2 to 5 modes.

The results obtained were not satisfactory in compari-
son with those obtained using the mode shapes directly. This
may be attributed to the following:

a)   As was established in Chapter 3, orthogonalizing a
number of mode shapes smaller than the order of the system with
respect to the exact mass matrix does not make these modes
exact. Simply stated, the orthogonalization process does not
correct for the missing modes. In the present case, the actual
order of the system is   greater than 5 (the number assumed
here). This eventually makes the orthogonalization process
ineffective.

b)   In addition to the reason in a), the estimated mass
matrix, although very close to the actual mass distribution in
the system, is not necessarily the true one. Consequently, the
orthogonalization of the measured mode shapes with respect to
this estimated mass matrix may lead to worsening rather than
improving these modes. For instance, the orthogonalization of
four modes, in the present case, with respect to $[m_x]$ has returned
the mode shapes as given below.

Orthogonalized Mode Shapes

Mode	1	2	3	4
Coordinate x_1	.842	.058	1.100	-1.73
x_2	1.0	1.0	1.0	1.0
x_3	1.16	2.580	.032	-.063
x_4	.832	-.061	.618	-2.300
x_5	.807	-.771	-.197	.115

These mode shapes, although perfectly orthogonal to $[m_x]$, have diverted away from the measured ones. When these modes were used in identifying the springs k_1-k_5 and subsequently solving for the natural vibrations of the system, the computed natural frequences were as follows:

Mode	1	2	3	4	5
Nat. freq. (Hz)	21.636	60.171	85.834	260.220	358.140

As can be seen, these natural frequencies, with the exception of that of the first mode, are not as accurate (with respect to reproducing the measured ones in Table 4.2), as those obtained using the mode shapes directly, (Table 4.6).

This finding is significant as to whether or not to make the measured mode shapes orthogonal to an estimated mass matrix before using them in identifying the unknown springs in the system. From the theoretical example in section 3.2.1.2 and the actual complicated structure presented here, the following observation can be made: unless the number of available modes is equal to the order of the system and mainly, the mass matrix is the correct one, the mode shapes should not be orthogonalized before using them in the identification process.

4.2.4 Performing Design Changes

So far, the established model of the machine using the estimated mass matrix, together with the identified springs from the first four modes (without being orthogonalized) has proven valid in terms of reproducing the input modal data. However, for this model to be accepted as a good one it should also have

the potential of predicting accurately the effects of design changes on the dynamics of the system in the frequency range of interest, 0-625 Hz. To fulfill this condition the motor was removed, which simulates a design change, and subsequently the transfer functions were measured at the coordinates x_1, x_2, x_4 and x_5. The measured modal data obtained from curve fitting these transfer functions are listed in Table 4.8.

On the model side, the mass element m_e which corresponds to the motor was set to zero, and then the natural vibrations of the system was solved. The computed modal data are listed in Table 4.9.

Comparing the measured modal data, Table 4.8, with those computed, Table 4.9, the errors in predicting the new natural frequencies are as follows:

Mode	1	2	3	4	5
Error %	-3.83	7.56	10.57	-8.11	-.76

Figs. 4.10-13 show the measured and computed transfer functions (motor off) at the coordinates x_1, x_2, x_4 and x_5. As can be seen in these figures, the established model could predict the effect of removing the motor on the dynamics of the system very closely.

Consequently, the model is to be accepted as a good one;

- it reproduced the experimental model data used in identifying its unknown springs,

- it, also, could predict, with sufficient accuracy, the

Table 4.8   Measured Modal Data of the Ram Type Milling
            Machine (Motor Off)

	Mode 1	Mode 2	Mode 3	Mode 4	Mode 5
Natural freq. (Hz)	23.055	109.881	168.310	456.950	583.972
Modal stiff. (N/m)	.7312E7	.4721E8	.8986E9	.8203E9	.2361E10
Damping ratio %	1.4100	3.1270	3.6210	5.0220	3.8740
Mode shapes x_1	.8266	.7234	-1.3567	-.0148	-.7402
x_2	1.0	1.0	1.0	1.0	1.0
x_4	.7867	.2058	-.6121	-1.096	1.1026
x_5	.7701	-.2091	-.0891	.0651	.0484

Table 4.9   Computed Modal Data (Motor Off)

		Mode 1	Mode 2	Mode 3	Mode 4	Mode 5
Natural freq.	(Hz)	22.170	117.458	186.101	419.908	579.547
Modal stiff.	(N/m)	.7484E7	.5183E8	.7607E9	6450E9	.2650E10
Mode shapes	x_1	.8413	.6993	-1.6426	.1152	-.6639
	x_2	1.0	1.0	1.0	1.0	1.0
	x_3	1.1554	.8431	8.4313	-3.7492	-4.6779
	x_4	.8223	.2295	-.7011	-.9202	1.3284
	x_5	.8043	-.2199	.0223	.0066	.0227

effect of a significant design change on the dynamics
of the machine.

This model can then be used in predicting the effects
of other design changes with sufficient reliability.

4.3 Identifying Unknown Springs of a Milling Machine Using Incomplete Mode Shapes

The structure under test is the vertical milling machine
shown in the schematic in Fig. 4.14. Cutting tests of steel
1020 with end mills have indicated that when chatter occurred
the frequency associated with it was around 550 Hz. The modal
analysis testing, given below in some details, has shown that
such a frequency belongs basically to the spindle itself
including the flexibility of the bearings.

Moreover, it was demonstrated in the cutting tests that
the modes in the X direction, see Fig. 4.14, were more sensi-
tive to chatter. This together with the spindle being X-Y
symmetrical, which implies that its properties can be recognized
from a measurement in either one of these directions, has led
to concentrating on the modes in the X direction only.

The situation here is different from the Ram-type
milling machine presented in the previous section in the
following:

a) It is the flexibility of the spindle itself with its
bearings rather than the structure (belt housing, ram, turret)
which are causing the tendency to machining instability.
Consequently, the model to be established here has to encompass

the modes associated with the spindle.

- b)   Some of the relevant coordinates on the spindle
and the bearings inside the headstock are inaccessible for
measurement. Therefore; the mode shapes obtained here are
incomplete as compared to full length mode shapes in the
previous example.

Recapitulating; the model to be established for the
present machine will represent its dynamics only in the X
direction in the frequency range 0-2000 Hz which covers the
significant modes of the spindle. A complete model will be
established based on the measured modal data with the mode
shapes being incomplete.

4.3.1 Measured Mode Shapes

The same equipment used in the previous example were
used here. Greater emphasis was put on the tool, tool holder
and the end of the spindle. At each location the obtained
transfer function was the average of ten measurements.

A mandrel 15.875 mm in diameter and 76.2 mm in over-
hang was clamped in a collet holder (Weldon type) which fits
the taper #50 of the spindle. The mandrel was used instead of
a real end mill as to facilitate the measurements. A flat
was ground at the end of the mandrel to provide a surface
parallel to the surface of the proximity probe. Moreover,
the mandrel was preloaded with a 200 N weight using a piano
wire 0.8 mm in diameter to eliminate any possible plays. The

piano wire was long enough (0.8 m) not to alter significantly the stiffness at the end of the mandrel. Fig. 4.15 shows the arrangement for measuring the relative vibration between the tool (mandrel) and the table.

Fig. 4.16 shows the measured relative TF at the end of the mandrel (only the real part). Five modes can be recognized in this figure. They are at 150, 350, 525, 975 and 1330 Hz.

Another mandrel 19.05 mm and 76.2 mm in overhang was clamped in the holder and the relative TF at the end was measured. The five recognized modes are now at 150, 350, 520, 970 and 1680 Hz. The first two modes did not change, the third and fourth changed very little while the fifth mode has moved from 1330 to 1680 Hz. This has clearly indicated that the fifth mode is basically associated with the tool itself with its bending as a cantilever as well as the clamping in the collet as the main flexibility.

Three other tools in heavier holders differing in stiffness and mainly in mass were also used. The frequencies measured including the two tools above are listed below.

Tool	f_1(Hz)	f_2(Hz)	f_3(Hz)	f_4(Hz)	f_5(Hz)
a	150	350	525	975	1330
b	150	350	520	970	1680
c	150	349	505	910	1220
d	149.5	349	450	900	1400
e	149.5	349	500	970	1400

It is obvious that the weight and stiffness of the tool and tool holder affected mainly the higher three modes:

- The fifth mode changed alot; it is the tool mode.
- The third and fourth modes also changed. They are spindle modes.

The first and second modes practically did not change. Further measurements on the headstock and the column have confirmed that they belong to the machine tool structure.

The measured mode shapes are shown in Fig. 4.17 for the headstock and in Fig. 4.18 for the spindle end and tool (mandrel 15.875 mm). Here is a short description of these modes.

150 Hz: - This is based on the torsion of the column with the headstock front moving in the opposite direction than the back of the column. The whole headstock and spindle and tool move so that there is no twist of the headstock around a horizontal axis parallel with the Y axis. The spindle axis remains vertical all the time.

350 Hz: This a a higher mode to the previous one. Both the back of the column and the front of the headstock move in the same direction while the front of the column moves in the opposite direction. Flexibility is in the guideways and slide of the Z motion. Again, there is very little twist of the headstock around the Y axis.

525 Hz: The end of the tool moves the most, the spindle end moves in the same direction and the headstock

participates by some twist around the Y·axis while its lower end goes in the same direction as the spindle end.

975 Hz: The tool and spindle end move very much, the headstock moves a little in the opposite direction.

In both the 525 and 975 Hz modes deflections are due to spindle bending, some flexibility in the tool holder as it is connected to the spindle, in the collet and tool bending.

1330 Hz: The tool moves a lot to one side while the spindle end and the tool holder move a little to the other side.   Flexibility is in the collet and mainly in the tool itself.

4.3.2   Establishing the Model

By carefully examining the mode shapes, and interpreting the different flexibilities in the system as mentioned above, and in order to encompass the modes from 150 to about 2000 Hz the model shown in Fig. 4.19 has been established.

There are two base rigid bodies, one representing the upper part of the column and the other one the headstock. Springs k_1 and k_2 represent the flexibility of the column and k_3 and k_4 the flexibility between the column and the headstock. The column is constrained so that it can only translate in the X direction.   The headstock translates in X but also rotates so that springs k_3 and k_4 do not compress equally. The amount of the corresponding twisting flexibility is varied

by varying the distance L between springs k_3 and k_4.

Modelling the spindle, tool holder and tool is rather straightforward. They are computed as finite beam elements; the spindle is divided into 12 elements to accommodate the variations in cross section, the tool holder is divided into two elements and the tool is divided into two elements.

The spindle is connected to the headstock by the bearings whose stiffnesses are k_5 and k_6. There is an angular flexibility between the spindle end and the tool holder as well as an angular flexibility between the collet and the tool. These two flexibilities are represented by the two torsional stiffnesses k_7 and k_8, respectively.

The local coordinates shown on Fig. 4.19, x_1-x_8, x_{13}-x_{26} are translative while x_9-x_{12} are rotational. The torsional spring k_8 is working between x_9 and x_{10}, while k_7 is working between x_{11} and x_{12}.

Therefore, the model can be looked at as being composed of two substructures:

Substructure 1:

This includes the headstock and the upper part of the column. It has three degrees of freedom; x_1, x_2, x_3. There are four springs in this substructure. However due to constraining the motion of the upper part of the column to be purely translative, the two springs k_1 and k_2 represent actually one single spring. To be compatible with the connection points on the headstock this spring is split into two and it would be

natural to put $k_1 = k_2$. The springs k_3 and k_4 will allow
to vary as well as the distance L to match the behaviour
of the headstock in the measured modes of vibration.

The mass matrix of this substructure is estimated
from the drawings of the machine. Twelve mass elements are
allocated along the headstock and the upper part of the column
to account for the mass distribution in the substructure.
They are interconnected by massless rigid beams. In Appendix II
it is shown how they are transformed into the coordinates
x_1, x_2 and x_3 in order to obtain the mass matrix of size
3x3. Also given in the Appendix II is a matrix which trans-
forms the springs k_1, k_2, k_3 and k_4 into the same coordinates.

The unknowns in this substructure are k_1, k_3, k_4 and L.

Substructure 2:

This includes the spindle, tool holder and the tool.
The mass and stiffness matrices of these members are readily
available from the finite elements computations. All angular
coordinates, except those between the end of the spindle
and the tool holder and between the tool holder and the tool,
were reduced statically using the Guyan method [89]. Accord-
ingly, the order of this substructure is 23. The unknowns
in this substructure are the torsional springs k_7 and k_8.

Substructure 1 is connected to substructure 2 via the
two translative springs k_5 and k_6 which represent the bearings.
They are unknown.

Summarizing:

The model established here is of total order of 26.

The mass matrix is obtained partially by computations (spindle, tool holder and tool) ánd partially by estimation (headstock, upper part of the column). It will be assumed to be exact. The unknowns in the model are: the translative springs k_1, k_3, k_4, k_5, k_6, the torsional springs k_7, k_8, in addition to the distance L, which add up to a total of 8 unknowns.

4.3.3 Identifying the Unknown Parameters in the Model

The available measured modal parameters are: 5 eigen-values Ω_1^2 - Ω_5^5, and the corresponding five incomplete eigenvectors $\{\phi_1\}$ - $\{\phi_5\}$ measured only on the accessible coordinates x_1 - x_8, and five modal stiffnesses K_1^4 - K_5^4 at the end of the tool, x_4. Also available is the mass matrix which will be assumed to be exact. It is required to identify the unknown stiffness elements k_1, k_3-k_8 and the distance L.

. The situation here fits into the class of identification schemes presented in section 3.3. Accordingly, the objective function as per Eq. (3.30) is written for the present system, and taking the weighing factors as 1's, as:

$$U = \sum_{j=1}^{5} \left(\frac{\Omega_j^2 - \Omega_{jex}^2}{\Omega_{jex}^2}\right)^2 + \sum_{j=1}^{5} \left(\frac{K_j^4 - K_{jex}^4}{K_{jex}^4}\right)^2$$

$$+ \sum_{i=1}^{8} \left(\frac{p_{ij} - p_{ijex}}{p_{ijex}}\right)^2 \qquad (4.3)$$

where; the parameters with the subscript ex are those established experimentally.

Ω_i^2 is the eigenvalue of mode j.

p_{ij} is the element measured on coordinate i in the mode j.

K_j^4 is the modal stiffness of the mode j measured at coordinate x_4 (4 here refers to the reference point at which the mode shapes have been normalized).

The parameters in Eq. (4.3) without the subscript ex are those obtained from solving the eigenvalue problem of the system using initial estimates of the unknown parameters.

In trying to minimize U, two problems arise, namely:

a)   how to obtain reasonable initial estimates of the unknown parameters.

b)   and how to match the computed and the experimentally measured modal parameters. Or in other words, which computed mode to be compared with which measured mode.

In the theoretical example in section 3.2.3. these two problems did not represent any difficulty:

-    the initial estimates of the unknown springs were deliberately chosen close to the exact values (which were known).

-    the modal parameters of the first three modes were used in the identification process. Consequently it was obvious as to compare the first computed mode with the first measured, the second computed with the second measured, etc.

For the present complicated structure of the milling machine whose established model has a large order (26) solving those problems becomes more involved as illustrated below.

4.3.3.1 Obtaining Initial Estimates

a) Initial estimate of distance L:

It is reasonable to consider the two springs k_3 and k_4 as being located at the end points of the headstock. Hence, a logical initial estimate of the distance L would be; $L = \ell$, where ℓ is the length of the headstock.

b) Initial estimates of k_1, k_2 and k_3:

Based on the measured mode shapes, the model established for the machine included the springs k_1, k_2 and k_3 to represent the main flexibilities in the first two modes at 150 and 350 Hz. In these two modes it is expected that the flexibilities included in substructure 2 (spindle-tool holder-tool) would have little effect. Consequently, in order to obtain initial estimates of k_1, k_3 and k_4 it is justified to assume the elements of substructure 2 as well as the connections between them to be rigid. Moreover, due to the small total mass of substructure 2 compared to that of substructure 1, (headstock-column), the connections between them will also be assumed to be rigid.

Having introduced these assumptions, the model reduces to a three degrees of freedom system. Its local coordinates are x_1, x_2 and x_3. These coordinates were accessible for

measurement.

Therefore, we have now a case of a vibratory system of order 3, its mass matrix $[m_x]_{3 \times 3}$ is known, and available are the modal data: two natural frequencies 150 and 350 Hz and the corresponding full length mode shapes at the coordinates x_1, x_2 and x_3. Identifying the unknown springs in such a case has been discussed in section 3.2.1. An equation similar to Eq. (3.26) could be arrived at, such that:

$$\begin{Bmatrix} k_1 \\ k_3 \\ k_4 \end{Bmatrix} = [[D^T][D]]^{-1} [D]^T \begin{Bmatrix} g_1 \\ \vdots \\ \vdots \\ g_6 \end{Bmatrix} \qquad (4.4)$$

where $[D]_{6 \times 6}$ and $\{g\}_{6 \times 1}$ contain the data of the two modes as well as the mass matrix (see section 3.2.1.2). From Eq. (4.4) the values of k_1, k_3 and k_4 could be estimated in the least square sense.

c) Initial estimates of k_5 and k_6:

Normally the manufacturer of the rolling bearings provides estimates of their stiffnesses. However, these estimates may vary over a relatively wide range depending on the base structure and mainly on the preloading. Nevertheless, it would be feasible to take the values furnished by the manufacturer as initial estimates of the bearing stiffnesses k_5 and k_6.

d) Initial estimates of k_7 and k_8:

k_7 and k_8 are located in the stiffness matrix of sub-

structure 2 as illustrated in diagram 4.5 below.

$$\begin{bmatrix} & & & & 0 & \\ & \boxed{\text{Spindle}} & & & & \\ & k_7 \;-\!-\!\mid\!-\; -k_7 \;-\!-\!-\!-\!-\!-\!-\!-\!-\!-\!-\!- & x_{12} \\ & & -\!-\!-\!-\!-\!-\!-\!-\!-\!- & x_8 \\ & -k_7 \quad\; k_7 \;-\!-\!-\!-\!-\!-\!-\!-\!- & x_{11} \\ & \quad k_8 \;\mid\!-k_8 \;-\!-\!-\!-\!-\!- & x_{10} \\ & & -\!-\!-\!-\!- & x_6 \\ & \text{Tool Holder} \quad -k_8 \quad k_8 \;-\!-\!-\!-\!- & x_9 \\ & & \boxed{\text{Tool}} & \\ & 0 & & \end{bmatrix}$$
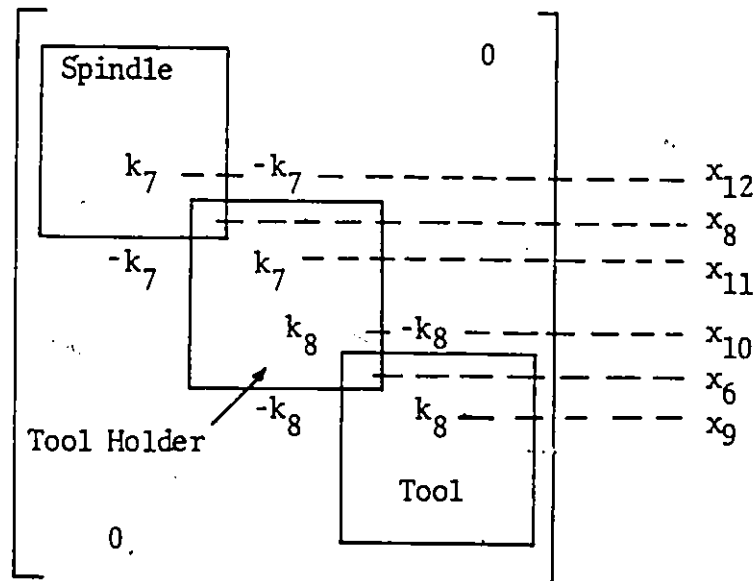
Examining this diagram it is immediately realized
that the situation here fits into that class of indentifica-
tion schemes presented in section 3.3.2. Only a relevant
part of the mode shape vector is needed to identify the
unknown springs, using linear equations assembled from the
equations of motion of the system. In the present case the
relevant parts are:

    i)   the elements at x_{12}, x_8 and x_{11}. They are needed
to identify the spring k_7.

    ii) the elements at x_{10}, x_6 and x_9. They are needed
to identify the spring k_8.

    The elements of the mode shapes corresponding to the
displacement coordinates x_6 and x_8 were readily available from
modal analysis testing. On the other hand, those elements

corresponding to the angular coordinates $x_9 - x_{12}$ were not

measured. They could be estimated from the displacements

measured on the tool, tool holder and at the end of the

spindle. These estimates are, however, unreliable due to the

short lengths of the tool holder and especially of the spindle

end.

The data of the fifth mode at 1330 Hz, where the

relative rotation between the tool and the tool holder was

largest, were used to identify the spring k_8, while the data

of the fourth mode at 975 Hz, were used to identify the spring

k_7. These identified values will be used as initial estimates.

4.3.3.2 Mode Matching

Apart from the crucial step of finding initial esti-

mates of the unknown parameters, the problem of mode matching

is of great significance.

In a measured transfer function over a certain fre-

quency range we might encounter a situation where very stiff

modes in this range do not show. Accordingly, the immediate

impression would be that these modes do not exist. Consequently,

the minimization of U in Eq. (4.3) by comparing the computed

and measured modal data in an ascending order of modes will

lead to erroneous results.

The problem of modal matching becomes more severe as

the order of the mode increases.

Fortunately, in the present case, the mode matching

problem was not critical for the following reasons:

a)   Only a few low ranked modes were considered.

b)   Very good initial estimates of the unknown parameters could be obtained.

c)   Additional information about the system were available (data obtained when changed tools and tool holders).

Therefore, the problem of mode matching could be addressed here intuitively.   The eigenvalue problem of the system was solved using the initial estimates and the different tool-tool holder arrangements (the estimate of k_8 was changed in every case).   It became obvious that the measured and computed modes could be matched as follows:

Computed	Measured
1	1
2	2
3	3
5	4
6	5

The computations have shown that there was a very stiff mode in the range 600-800 Hz.

4.3.3.3   Identified Values

The modal data corresponding to the tool 15.875 mm diameter and 76.2 mm long were used in Eq. (4.3).   The initial estimates were: $L/\ell = 1$, $k_1 = .1875E6$ (N/m), $k_3 = 0.1660E6$ (N/m), $k_4 = .1690E6$ (N/m), $k_5 = .1500E6$ (N/m), $k_6 = .2150E6$ (N/m),

k_7 = .3000E6 (N.m/rad), k_8 ≜ .7850E5 (N.m/rad).

The optimization routine SEEK from the package OPTIVAR [88] was used to minimize U. The eigenvalue problem was solved in every iteration with the updated estimates. After 41 iterations a global minimum was found. The final values of the parameters to be identified were: L/ℓ = 1.500, k_1 = .1745E9 (N/m), k_3 = .1496E9 (N/m), k_4 = .15109 (N/m), k_5 = .2510E9 (N/m), k_6 = .3936E6 (N/m), k_7 = .2280E6 (N.m/rad), k_8 = 0.1000E6 (N.m/rad)

With these identified values the first six computed natural frequencies were obtained as; 153.44, 349.53, 533.92, 717.21, 934.36 and 1334.70 Hz. Comparing these values with the corresponding measured natural frequencies, the errors are:

Mode	1,1	2,2	3,3	5,4	6,5
Error %	2.23	-.13	1.70	-4.17	.35

Fig. 4.20 shows the computed TF at the end of the tool which is in a very good agreement with that measured in Fig. 4.16.

The computed mode shapes are shown in Fig. 4.21. The lowest modes at 153 and 350 Hz which match almost exactly the measured data are not shown here. The graphs of all modes are drawn in the same scale of flexibility. Here we can see the "inside" of the headstock, the deformation in the bearings and that of the spindle itself. The triangles a, b

indicate the locations of the bearings and the points c, d
indicate the location of the spindle end and of the tool
holder end, respectively. Point e is the tool end. The
dashed line represents the headstock. At each mode its
corresponding modal stiffness K in N/m is given.

It is obvious, that the three important modes are
characterized each mainly by:

534   - deflections in bearings

934   - bending of the spindle

1334   - bending of the tool

The modes at 534, 934 and 1334 are in a very good agreement
with those measured at 525, 975 and 1330 Hz, respectively.

Therefore, the model established could reproduce the
input experimental modal data from which its parameters have
been identified. This proves its validity.

4.3.4   Performing Design Changes

In the model the computed data of the 15.875 x 76.2 mm
tool were replaced by that of the 19.05 x 76.2 mm tool. Also
the identified torsional spring k_8 = 0.1E6 (N.m/rad) was
replaced by an estimate k_8 = 0.15E6 (N.m/rad) to account for
the difference in diameter. All other parameters remained the
same. Subsequently, the eigenvalue problem of the system was
solved to yield the natural frequencies: 153.44, 349.52,
528.21, 707.07, 927.63 and 1713.41 Hz. These values again

are in a very good agreement with those measured with this
a tool.

In conclusion, the model established is a good one:
it reproduced the input experimental modal data as well as
predicted the effects of design changes accurately. The
model has shown clearly that it is the bearings which are
responsible for the high flexibility of the mode at 525 Hz
where chatter occurs. Accordingly, replacing the current
bearings with bigger size ones with higher stiffness should
alleviate the problem of machining instability. Although the
tool mode is much more flexible than the spindle mode at 525 Hz,
yet it does not represent any problem in milling steel for
reasons to be explained in Chapter 6.

CHAPTER 5

DYNAMICS OF A WORKPIECE
CLAMPED ON A LATHE

5.1   Introduction

In this chapter a procedure is presented whereby the experimental modal data are used to predict the dynamics of a lathe with various workpieces. The procedure includes both the identification and the modification approaches as outlined in Chapter 2.

In the case of a lathe the dynamics of the machine is practically constant and the largest variable in every application is the workpiece which, mainly through its inertial properties, affects the resulting stability against chatter. Therefore, it would be a great advantage to establish once, experimentally, the dynamics of the machine and subsequently, through computation, to predict the limit of stability for any workpiece.

The treatment here is limited to one plane only. In reality it has to be applied to two mutually perpendicular planes. Also, only cylindrical workpieces are considered. However, they represent the majority of workpieces.

The examples given here were measured on a typical conventional lathe with .4 m swing over bed and 1 m between centers.

5.2 Typical Mode Shapes

On a lathe two distinct cases must be considered:

a)   a long workpiece clamped in the chuck and tailstock.

c)   a short workpiece clamped in the overhang in the chuck only.

First, the case a): In Fig. 5.1 three mode shapes are illustrated as measured on a rather rigid workpiece with 127 mm diameter and 616 mm length. The highest mode with frequency 107 Hz is drawn in an axonometric view for a better impression of the machine. The lower two modes are drawn in the top view only. This will also be the case for all the following mode shape illustrations. It can be seen that with this bulky and rigid workpiece the 29 Hz mode is a rocking mode of the whole machine as a rigid body on the "springs" of the connections to the floor. The 49 Hz mode is similarly one of the machine essentially as a rigid body with a little twist of the bed and the ends of the machine moving against each other. In both these low modes there is very little relative motion between the tool and the workpiece.

Such a relative motion occurs in the 107 Hz mode where the mass of the workpiece moves to one side on the springs of the spindle and the chuck at one end and of the tailstock and quill and center (much more compliant) at the other end. The bed and saddle, carriage and toolpost move to the other side.

In Fig. 5.2 seven mode shapes are shown for a more

flexible workpiece with 61 mm diameter and 603 mm length. The first three modes at 31, 56 and 150 Hz are analogous to those in Fig. 5.1. In the 205 Hz mode the ends of the headstock and of the tailstock move against the workpiece. In the following higher modes at 270, 650 and 740 Hz the headstock and spindle and chuck - the workpiece - the center and quill and tailstock undergo higher and higher shapes with more and more deformation of the workpiece and with an increasing number of nodal points.

In Fig. 5.3 the Transfer Function at a point on the workpiece at its tailstock end is given which shows the relative importance of the modes shown in Fig. 5.2. The plots give the real (top) and imaginary (bottom) parts of the Transfer Functions in acceleration scale which is used to make also the higher modes visible. In reality, for flexibility (displacement scale), both curves should be divided by ω^2. Thus, e.g., the 740 peak would be 24 times smaller than shown if the 150 peak was left at the here given size. The Transfer Function indicates that modes of 150 Hz and 270 Hz are most significant while those of 560 and 740 Hz could almost be neglected.

For the second case, of the workpiece clamped in overhang in the chuck only, typical mode shapes are shown in Fig. 5.4. These measurements correspond to a workpiece 43 mm diameter, 260 mm long. An unusually long workpiece was used deliberately in order to exaggerate the case. In the 212 Hz mode the chuck and workpiece move in the same directions and

in the 350 Hz mode they move in opposite directions.

5.3 Establishing the Model of the Lathe

For the task of representing the system with various different workpieces we look at it as consisting of three parts, see Fig. 5.5. Part 1 is the lathe, part 2 is the workpiece and part 3 are the connections between the two: the chuck and the center. The whole system is the sum of these three parts and we will call it the assembly. The connections are considered separately from the lathe because their characteristics may vary with the workpiece. Especially, both the flexibility and damping of the chuck may vary with the diameter of the workpiece clamped and, also it may exhibit non-linear characteristics.

Reviewing all the mode shapes as shown in Fig. 5.1, 2, and 4 it may be seen that the chuck acts essentially as a rotational spring and the center as a translative spring between the body of the center and the end of the workpiece. This is illustrated in Fig. 5.6 where the outline of the model of the system is shown. The local coordinates of the lathe are denoted x, those of the workpiece are y. At the chuck there are the translative coordinates $x_1 = y_1$ and the rotary coordinates x_2, y_2 the latter two differing by the rotational displacement in the chuck. The translative motion at the other end of the workpiece is denoted y_3 and that of the center body is x_3. The stiffness of the rotational spring between x_2 and

y_2 will be called k_1 and the stiffness of the center will be called k_2. We will assume damping factors c_1 and c_2 associated with these springs. We may be interested in the Transfer Function at coordinate y_4 on the workpiece.

The workpiece is a well geometrically defined body of a uniform material with well defined elastic properties. Its dynamic behaviour can rather easily and accurately be determined by computation. Because its own damping is usually very small as compared to the damping of the lathe structure and of the connecting elements it will be completely neglected. Thus, only its elastic and inertial properties need to be computed.

Considering workpieces whose form is cylindrical or close to cylindrical and analyzing visually the mode shapes and frequency ranges as given in Figs. 5.1, 2 and 4 it becomes obvious that it is satisfactory to simplify the workpiece as a free-free body by considering its three lowest mode shapes only out of the first four shown in Fig. 5.7. The frequencies given in this figure correspond to the workpiece which was used in the measurements reproduced in Fig. 5.2 It is obvious that the fourth mode did not show in them. The three lowest modes are the first two rigid body modes and the first bending mode. These modes may locally be represented at coordinates y_1, y_2, y_3. The dynamics of the workpiece may be obtained by computations using finite beam elements. The nodes must include the connection coordinates as well as any other additional coordinates y_4, y_5... These will have to include

those points on which we will want to compute the resulting

Transfer Function of the whole system. Let us consider one

such point y_4 located arbitrarily on the workpiece as shown

in Fig. 5.6.

In the case of the workpiece clamped in the chuck

only it can be simply considered as rigid mass.

The lathe structure and the flexibilities and damping

of the chuck and of the center cannot be computed with sufficient

accuracy. They have to be determined experimentally.

5.4 Determining the Properties of the lathe by Subtracting the Workpiece from the Assembly

The procedure of predicting the dynamics of the lathe

with any workpiece consists of:

a)   first, measuring the modal parameters of the whole

system with a workpiece.

b)   second, computing the elastic and inertia properties

of this workpiece and subsequently subtracting it, together

with the connection elements of the chuck and tailstock,

from the assembly. In this way the properties of the lathe

alone at the connecting coordinates x_1, x_2 and x_3 can be

determined.

c)   finally, computing the new workpiece and adding it,

together with the corresponding connecting elements of the

chuck and tailstock which might be different from the ones

above, at the connection coordinates.

Therefore, the starting point is the modal analysis

testing. It is carried out by exciting at a selected point, say y_4 and measuring vibrations at this point as well as at all other points of interest. These will have to include the "end" points of the lathe x_1, x_2, x_3 and the end points of the workpiece $y_1 \equiv x_1$, y_2, y_3. The immediate result of the measurement is the "direct" transfer function (TF) on y_4 and the "cross" TF's between y_4 and all other points. When these TF's are curve fitted on a number of modes p within the measured frequency range, the modal parameters for the assembly can be extracted. On the example in Fig. 5.2 we identify 7 modes, i.e. p=7. Assuming non-proportional viscous damping to exist, and assuming that all lower modes are taken into account while the residual flexibilities of the higher missing modes are negligible, then the modal parameters will be as follows:

eigenvalues:
$$\lambda_i = \mu_i + j \, \nu_i$$
$$\lambda_i^* = \mu_i - j \, \nu_i \qquad \dots; \; i = 1,p \qquad (5.1)$$

modal matrix $[P]_{12 \times 2p}$. where,

$$
\begin{Bmatrix} x_1 \equiv y_1 \\ x_2 \\ x_3 \\ y_2 \\ y_3 \\ y_4 \\ \dot{x}_1 \\ \vdots \\ \dot{y}_4 \end{Bmatrix}_{12 \times 1}
=
\underbrace{\begin{bmatrix} \begin{Bmatrix} \psi_1 \end{Bmatrix} & \begin{Bmatrix} \psi_1^* \end{Bmatrix} & \cdots & \begin{Bmatrix} \psi_p^* \end{Bmatrix} \\ \begin{Bmatrix} \lambda_1 \psi_1 \end{Bmatrix} & \begin{Bmatrix} \lambda_1^* \psi_1^* \end{Bmatrix} & \cdots & \begin{Bmatrix} \lambda_p^* \psi_p^* \end{Bmatrix} \end{bmatrix}}_{[P]_{12 \times 2p}}
\begin{Bmatrix} q_1 \\ q_2 \\ \cdot \\ \cdot \\ \cdot \\ \cdot \\ \cdot \\ \cdot \\ q_{2p} \end{Bmatrix}
\qquad (5.2)
$$

where q_i's are the modal coordinates of the assembly.

and,
$$\lceil a \rfloor_{2p \times 2p} \tag{5.3}$$

The diagonal matrix $\lceil b \rfloor$ of the assembly can be obtained from a_i,s and λ_i's according to Eq. (2.27). (See section 2.3.2.2 for more details).

For the workpiece, the mass and stiffness matrices, $[m_w]$ and $[k_w]_{4 \times 4}$, respectively, are computed in the local coordinates y_1, y_2, y_3 and y_4.

Furthermore, we need the stiffness and damping of the connections k_1, c_1, k_2, c_2, as simple discrete springs and dampers between coordinates x_2, y_2 and x_3, y_3, respectively. Assume here that they are already known. By correspondingly overlapping them with $[m_w]$ and $[k_w]$ the $[A_{w,c}]$ and $[B_{w,c}]$ matrices as per Eq. (2.2) are assembled: i.e.

$[A_{w,c}]_{12 \times 12}$ and $[B_{w,c}]_{12 \times 12}$, in coordinates $<y_1, x_2, x_3, .. y_4, y_1 ... y_4>^T$

$$\tag{5.4}$$

Let $[P_{w,c}]_{12 \times 2p}$ be that part of the measured modal matrix $[P]$ which corresponds to the coordinates of $[A_{w,c}]$ and $[B_{w,c}]$. Then the workpiece and connections can be transformed into the modal coordinates of the assembly as follows:

$$[a_{w,c}]_{2p \times 2p} = [P_{w,c}]^T [A_{w,c}][P_{w,c}] \tag{5.5}$$

and similarly

$$[b_{w,c}] = [P_{w,c}]^T [B_{w,c}][P_{w,c}] \tag{5.6}$$

where $[a_{w,c}]$ and $[b_{w,c}]$ are not diagonal, however they

correspond to the coordinates q.

Now by subtracting the workpiece and connections from the assembly, the matrices $[a_L]$ and $[b_L]$ of the lathe alone in the modal coordinates of the assembly q are obtained:

$$[a_L]_{2px2p} = \begin{matrix} \ulcorner \\ a \\ \lrcorner \end{matrix} - [a_{w,c}] \qquad (5.7)$$

$$[b_L]_{2px2p} = \begin{matrix} \ulcorner \\ b \\ \lrcorner \end{matrix} - [b_{w,c}] \qquad (5.8)$$

The lathe structure may, in the p measured modes of the assembly contribute by a number of modes d. This number is most likely smaller than p; i.e. $d < p$. In other words, the lathe structure alone acts in the measured frequency range as having $d < p$ freedoms. Therefore, the matrices $[a_L]$ and $[b_L]$ will be singular. However, as it is shown in Appendix III, any submatrices of order 2d located diagonally in $[a_L]$ and $[b_L]$ will contain all the information about the system. These submatrices eventually will not be singular. Consequently, the main question would be how to determine the order d of the structure. To answer this question a method (which proved successful on theoretical examples) is suggested below:

Arrange for solving the natural vibrations as follows;

$$\lambda [a_L]_{2px2p} \{q\} + [b_L]_{2px2p} \{q\} = 0 . \qquad (5.9)$$

This leads to p pairs of conjugate eigenvalues. If the order of $[a_L]$ and $[b_L]$ is smaller than 2p, say by 4, then 2 conjugate pairs of these eigenvalues will be much smaller

than the first eigenvalue measured on the assembly (If there were no errors involved in the whole process, then these 2 pairs would have a typical value of zero). Hence, the actual order of the lathe structure alone is obtained as

$$d = \frac{2p-4}{2} \qquad\qquad (5.10)$$

Having determined d, then two matrices $[a'_L]$ and $[b'_L]$ of order $2d$ can be taken out of $[a_L]$ and $[b_L]$, respectively, say at the upper left corner, as;

$$\begin{bmatrix} \boxed{a'_L} & \\ & a_L \end{bmatrix} \quad , \quad \begin{bmatrix} \boxed{b'_L} & \\ & b_L \end{bmatrix} \qquad\qquad (5.11)$$

In this way the matrices $[a'_L]$ and $[b'_L]$ correspond to the lathe structure alone, expressed in the coordinates q' which are the first $2d$ modal coordinates of the assembly.

Furthermore, out of the modal matrix $[P]_{2p \times 2p}$ measured on the assembly, we take a matrix $[P_L]_{6 \times 2d}$ which relates the local coordinates of the lathe at the connections to q', i.e.

$$\begin{Bmatrix} x_1 \\ x_2 \\ x_3 \\ \dot{x}_1 \\ \dot{x}_2 \\ x_3 \end{Bmatrix} = [P_L] \; \{q'\} \qquad\qquad (5.12)$$

The matrices $[a'_L]$, $[b'_L]$ and $[P_L]$ represent the dynamics of the lathe structure alone and they can be used to assemble other workpieces as explained in the next section.

5.5 Assembling a New Workpiece

The new workpiece is computed and by overlapping the corresponding connecting elements (assuming they are already known), then the following matrices as per Eq. (2.22) are assembled;

$[A'_{w,c}]$ and $[B'_{w,c}]$ in coordinates $\langle y_1, x_2, x_3, y_2, y_4, \dot{y}_1, \ldots \dot{y}_4 \rangle^T$

$$(5.13)$$

To assemble these matrices with $[\dot{a}'_L]$ and $[b'_L]$ of the lathe structure a procedure described by Klosterman [69] can be followed:

Establish the matrix $[P']$ to be used in transforming $[a'_{w,c}]$ and $[B'_{w,c}]$ into a system of coordinates which includes q' as well as the local coordinates on the workpiece that are not involved in the connections. $[\dot{P}]$ thus is formed such that;

$$
\underbrace{\begin{Bmatrix} y_1 \\ x_2 \\ x_3 \\ \dot{y}_1 \\ \dot{x}_2 \\ \dot{x}_3 \\ \hline y_2 \\ \vdots \\ y'_4 \\ \dot{y}_2 \\ \dot{y}'_4 \end{Bmatrix}}_{\substack{\text{connecting coordinates} \\ \text{rest of coordinates}}}
=
\underbrace{\begin{bmatrix} [P_L] & 0 \\ 0 & I \end{bmatrix}}_{[P']}
\begin{Bmatrix} q' \\ \hline y_2 \\ \vdots \\ y'_4 \\ \dot{y}_2 \\ \dot{y}'_4 \end{Bmatrix}
\qquad (5.13)
$$

The transformation is then carried out, to obtain the
matrices $[A''_{w,c}]$, $[B''_{w,c}]$ in the new system of coordinates;

$$[A''_{w,c}] = [P']^T [A'_{w,c}][P'] \qquad (5.14)$$

$$[B''_{w,c}] = [P']^T (B'_{w,c}][P'] \qquad (5.15)$$

Subsequently, the matrices $[A''_{w,c}]$ and $[B''_{w,c}]$ are
overlapped on the matrices $[a'_L]$ and $[b'_L]$, respectively,
over the coordinates q' to form the matrices [A'] and [B']
of the new assembly;

$$(5.16)$$
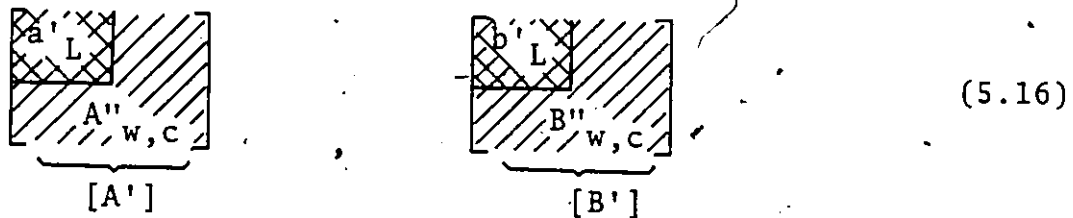
The matrices [A'] and [B'] can then be used to compute the dynamics of the new system;

$$[\lambda[A'] + [B']] \begin{Bmatrix} q' \\ Y \end{Bmatrix} = \begin{Bmatrix} 0 \\ F \end{Bmatrix} \qquad (5.17)$$

where; the vector {Y} contains those local coordinates on the workpiece not rigidly connected to the lathe, while the force vector {F} contains the forces acting on {Y}.

5.6 A Theoretical Example

The procedure presented above for disassembling a substructure (workpiece) from the assembly and subsequently determining the characteristics of the remaining substructure (lathe), is demonstrated here on a theoretical example.

Fig. 5.8, shows the substructures S_L and S_W and the assembly S_Z. Substructure S_W represents a workpiece, while S_L is a theoretical model which has been so chosen as to loosely approximate the behaviour of a lathe. In the assembly S_W is rigidly connected to S_L at the coordinates $x_1 \equiv y_1$ and $x_2 \equiv y_5$.

5.6.1 Generating Modal Data of Assembly

S_W alone is a six degrees of freedom system, its masses and stiffnesses are:

masses m_1-m_5; 1.25, 10, 20, 150, 300 (kg)

stiffnesses: k_1-k_5; 20,000, 10,000, 35,000, 30,000,
80,000 (N/mm).

These data were used to form the mass and stiffness matrices $[m_L]$ and $[k_L]$ of order 6 in the coordinates; x_3, x_4, x_5, x_6, x_1, x_2. The damping matrix $[c_L]$ was generated assuming proportional viscous damping in the way shown in Appendix IV. The results of solving the eigenvalue problem of S_L alone are given in Table 5.1. These results are shown, however, as if S_L had non-proportional damping to be compatible with the further presentation.

S_W is a cylindrical workpiece of constant cross section, its dimensions are 30 mm diameter and 350 mm long. Its mass and stiffness matrices $[m_W]$ and $[k_W]$ of order 5 were computed in the coordinates y_1, y_5, y_2, y_3 and y_4 in the way shown in Appendix V. S_W is assumed to have no damping, i.e. $[C_W]$ is a null matrix.

Subsequently, the matrices in local coordinates of S_L and S_W were overlapped on the connecting coordinates $x_1 \equiv y_1$ and $x_2 \equiv y_5$ to form $[A_z]$ and $[B_z]$ of order 18 of S_Z as follows.

$$[A_z] = \begin{bmatrix} \begin{matrix} c_L & \\ & c_W \end{matrix} & \begin{matrix} m_L & \\ & m_W \end{matrix} \\ \text{Symm} & 0 \end{bmatrix} \begin{matrix} \cdots\cdots x_1 = y_1 \\ \cdots\cdots x_2 = y_5 \\ \cdots\cdots \dot{x}_1 = \dot{y}_1 \\ \cdots\cdots \dot{x}_2 = \dot{y}_2 \end{matrix}$$

$$[B_z] = \begin{bmatrix} \begin{matrix} k_L & \\ & k_W \end{matrix} & 0 \\ \text{Symm} & \begin{matrix} -m_L & \\ & m_W \end{matrix} \end{bmatrix}$$

(5.17)

Table 5.1   Computed Modal Data of S_L

Mode	λ_L (1/sec)	a_L (N.sec/mm)
1	$-.150E2 \pm j \ .500E3$	$0 \pm j \ .582E6$
2	$-.205E2 \pm j \ .682E3$	$0 \pm j \ .298E6$
3	$-.379E2 \pm j \ .126E4$	$0 \pm j \ .405E7$
4	$-.539E2 \pm j \ .180E4$	$0 \pm j \ .295E5$
5	$-.129E2 \pm j \ .430E4$	$0 \pm j \ .128E5$
6	$-.587E2 \pm j \ .293E5$	$0 \pm j \ .296E11$

Mode Shapes:

	Mode					
	1	2	3	4	5	6
x_1	1.0	1.0	1.0	1.0	1.0	1.0
x_2	$1.244 \pm j0$	$-1.156 \pm j0$	$9.728 \pm j0$	$-.027 \pm j0$	$-.000 \pm j0$	$1920. \pm j0$

The matrices $[A_z]$ and $[B_z]$ were used to solve the eigenvalue problem of S_Z. The results obtained were:

- eigenvalues; $\lambda_i = \mu_i \overset{+}{-} j\,\mu_i$, $i = 1,9$

- complex conjugate pairs of the paramters a_i's , $i = 1,9$.

- modal matrix $[P_z]$ of size 18 x 18 which contains 9 complex conjugate pairs of eigenvectors.

These computed λ_i's and a_i's are listed in Table 5.2. Also given is that part of $[P_z]$ normalized at x_1 which corresponds only to the displacements x_1 and x_2. The undamped natural frequencies f_n (Hz) of the modes are also included. Fig. 5.9 shows the nine mode shapes (real parts).

The so computed modal paramters of the assembly will now be assumed to be the data obtained from the modal analysis testing. Furthermore, it will be assumed that only the first 7 modes measured only on the coordinates of the workpiece y_1 - y_5 are available. No simulated errors will be introduced on these data.

5.6.2 Subtracting Substructure S_w From Assembly To Obtain Substructure S_L

Starting with the modal parameters of the assembly;
λ_i, λ_i^* ; $i = 1,7$
a_i, a_i^* ; $i = 1,7$

and the modal matrix $[P_w]$ of size 10 x 14, which relates the displacements and velocities of the local coordinates $\dot{y}_1$, y_5, y_2, y_3, y_4 to the modal coordinates of the assembly q_i, $i = 1,14$.

Table 5.2   Computed Modal Data of Assembly

Mode	f_n (Hz)	λ_i (1/sec)	a_i (N.sec/mm)
1	79.454	$-.149E2 \pm j\ .499E3$	$.123E \pm j\ .559E6$
2	108.274	$-.204E2 \pm j\ .680E3$	$.269E3 \pm j\ .293E6$
3	195.841	$-.353E2 \pm j\ .123E4$	$.618E5 \pm j\ .113E7$
4	270.662	$-.458E2 \pm j\ .170E4$	$-.412E2 \pm j\ .277E5$
5	358.136	$-.327E2 \pm j\ .224E4$	$.293E7 \pm j\ .413E7$
6	531.663	$-.602E2 \pm j\ .334E4$	$-.430E4 \pm j\ .493E5$
7	749.743	$-.853E2 \pm j\ .471E4$	$.921E3 \pm j\ .241E5$
8	2164.526	$-.577E2 \pm j\ .136E5$	$.160E5 \pm j\ .549E6$
9	4711.030	$-.128E3 \pm j\ .296E5$	$.314E5 \pm j\ .283E7$

Mode shapes:

	x_1	x_2
1	1.0	$.126E1 \pm j\ .727E-3$
2	1.0	$-.117E1 \pm j\ .872E-3$
3	1.0	$.568E1 \pm j\ .118E0$
4	1.0	$.996E-1 \pm j\ .124E-1$
5	1.0	$-.157E2 \pm j\ .527E-1$
6	1.0	$-.130E1 \pm j\ .886E-1$
7	1.0	$.521E0 \pm j\ .231E-1$
8	1.0	$-.960E0 \pm j\ .828E-2$
9	1.0	$.991E0 \pm j\ .376E-2$

In addition to the known local matrices of S_W; $[m_w]$, $[k_w]$ and $[c_w]$, it is required to determine the characteristics of S_L at the connecting points x_1 and x_2.

The modal parameters a_i's fill on the diagonal the matrix $\ulcorner a \lrcorner$ of size 14 x 14. Moreover, the parameters a_i's and the eigenvalues λ_i.s are used to form the diagonal matrix $\ulcorner b \lrcorner$ of size 14 x 14 such that $b_i = -\lambda_i a_i$.

Without repeating, the matrice $[A_w]$ and $[B_w]$ of S_W were formed, and the steps 5-5 to 5-8 followed as to arrive at $[a_L]$ and $[b_L]$ of size 14 x 14 which belongs to S_L alone.

The eigenvalue problem (Eq. (5.9)) was subsequently solved to yield the eigenvalues listed in Table 5.3. Obviously, the eigenvalues of the first mode are wrong and they are much smaller than the eigenvalues associated with the first mode measured on the assembly. The rest of the computed eigenvalues of S_L fall within the measured frequency range. The immediate conclusion would be that the actual order of S_L alone is only 6, i.e. $d = 6$.

By comparing the computed eigenvalues of S_L after sub-traction (modes 2 - 7) in Table 5.3 with those obtained directly in Table 5.1, it becomes clear that they are practically the same. The very small differences occur basically due to the fact that only 7 modes were assumed to be known out of 9 of the assembly.

With the order of S_L known ($d = 6$), two matrices $[a'_L]$ and $[b'_L]$ of size 12 x 12 may now be taken out, say at the upper left corner, of the matrices $[a_L]$ and $[b_L]$, respectively.

Table 5.3   Computed Eigenvalues of S_L
After Subtracting S_W from S_Z.

Mode	λ_L
1	$.261E\text{-}1 \pm j\ .312E\text{-}1$
2	$-.152E2 \pm j\ .501E3$
3	$-.209E2 \pm j\ .680E3$
4	$-.383E2 \pm j\ .127E4$
5	$-.543E2 \pm j\ .178E4$
6	$-.127E2 \pm j\ .428E4$
7	$-.577E2 \pm j\ .287E5$

Those matrices are in the coordinates q_1-q_{12} of the original assembly. In addition we take the matrix $[P_L]$ of size 4 x 12 out of $[P_Z]$ which relates the connecting coordinates $x_1 \equiv y_1$, $x_2 \equiv y_5$, $\dot{x}_1 \equiv \dot{y}_1$, $\dot{x}_2 \equiv \dot{y}_5$, to the coordinates q_1-q_{12}.

The matrices $[a'_L]$, $[b'_L]$ and $[P_L]$ represent the dynamics of S_L alone at the connecting coordinates and consequently can be used directly in assembling other substructures at these points as shown in section 5.5.

If it is required to transform $[a']$ and $[b']$ into a set of coordinates which contains explicitly the local coordinates x_1 and x_2, a matrix $[P_{Lx}]$ of size 12x12 can be formed such that:

$$
\begin{Bmatrix} x_1 \\ x_2 \\ \dot{x}_1 \\ \dot{x}_2 \\ \hline q_3 \\ q_4 \\ q_{11} \\ q_{12} \end{Bmatrix} = \begin{bmatrix} & P_L & \\ & 4{\times}12 & \\ \hline 0 & 0 & \\ 0 & 0 & \\ \vdots & \vdots & I_{8{\times}8} \\ 0 & 0 & \end{bmatrix} \begin{Bmatrix} q_1 \\ q_2 \\ \vdots \\ \vdots \\ \vdots \\ \vdots \\ q_{11} \\ q_{12} \end{Bmatrix} \tag{5.18}
$$

$$[P_{Lx}]$$

Subsequently, the transformation into the new set of coordinates is carried out;

$$[A_{Lq}] = [P_{Lx}]^{-T} [a'_L][P_{Lx}]^{-1}$$

$$[B_{Lq}] = [P_{Lx}]^{-T} [b'_L][P_{Lx}]^{-1} \tag{5.19}$$

The matrices $[A_{Lq}]$ and $[B_{Lq}]$ can be used in solving the eigenvalue problem of S_L;

$$[\lambda [A_{Lq}] + [B^{\cdot}_{Lq}]] \{^x_q\} = 0 \qquad (5.20)$$

For the present theoretical model, the modal parameters obtained from solving Eq. (5.20) were practically the same as those listed in Table 5.1.

$[A_{Lq}]$ and $[B_{Lq}]$ can be overlapped directly on the connecting points with the matrices $[A'_w]$ and $[B'_w]$ of a new substructure S'_W (without performing the transformations (5.14) and (5.15)).

5.7   Identifying the Connecting Elements

Going back to the actual case of a lathe-connections-workpiece assembly, it is presented in this section how the connecting elements k_1, c_1, k_2 and c_2, can be identified.

In section 5.3 the assembly has been modelled as three separate substructures. The connections, substructure S_c, includes discrete springs and dampers but have no masses. The matrices $[A_c]$ and $[B_c]$ of S_c assembled according to Eq. (2.22) will have the form in Eq. (5.21).

$$[A_C]=\begin{bmatrix} c_2 & 0 & 0 & 0 & -c_2 & \vline & \\ 0 & c_1 & 0 & -c_1 & 0 & \vline & \\ 0 & 0 & 0 & 0 & 0 & \vline & 0 \\ 0 & -c_1 & 0 & c_1 & 0 & \vline & \\ -c_2 & 0 & 0 & 0 & c_2 & \vline & \\ \hline & & 0 & & & \vline & 0 \end{bmatrix}_{10\times10} , [B_C]=\begin{bmatrix} k_2 & 0 & 0 & 0 & -k_2 & \vline & \\ 0 & k_1 & 0 & -k_1 & 0 & \vline & \\ 0 & 0 & 0 & 0 & 0 & \vline & 0 \\ 0 & -k_1 & 0 & k_1 & 0 & \vline & \\ -k_2 & 0 & 0 & 0 & k_2 & \vline & \\ \hline & & 0 & & & \vline & 0 \end{bmatrix}_{10\times10} \begin{matrix} x_3 \\ x_2 \\ x_1 \\ y_2 \\ y_3 \\ \dot{x} \\ \dot{y} \end{matrix}$$

(5.21)

In the $[A_z]$ and $[B_z]$ matrices of the assembly the matrices $[A_L]$, $[B_L]$, $[A_C]$, $[B_C]$, $[A_w]$, and $[B_w]$, (L: lathe, w: workpiece), overlap on corresponding rows as shown in Eq. (5.22).
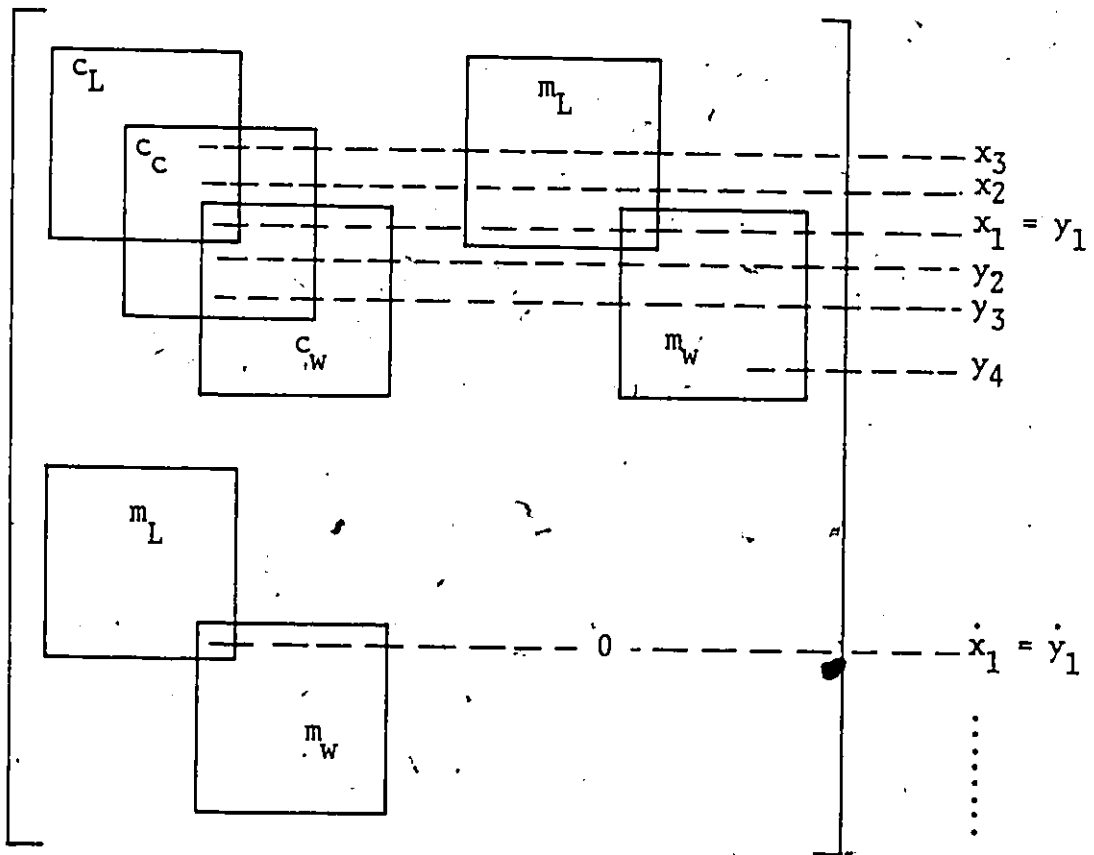
Let us look at the row of the assembly which corresponds to the coordinate y_2. The lathe matrices do not contribute there. The row stretches over columns corresponding to x_3, $x_2 \ldots, \dot{y}_4$. These columns are specified in Table 5.4, where the row is obtained for $[A_z]$ and $[B_z]$ as the sum of contributions from $[A_c]$ and $[A_w]$ and from $[B_c]$ and $[B_w]$ respectively:

Table 5.4 Contributions of S_c and S_w into the Row of S_z Corresponding to Coordinate y_2

Columns	x_3	x_2	y_1	y_2	y_3	y_4	$\dot{x}_3$	$\dot{x}_2$	$\dot{y}_1$	$\dot{y}_2$	$\dot{y}_3$	$\dot{y}_4$
from $[A_c]$	0	$-c_1$	0	c_1	0	0	0	0	0	0	0	0
from $[A_w]$	0	0	0	0	0	0	0	0	m_{21}	m_{22}	m_{23}	m_{24}
$[A_z]=[A_c]+[A_w]$	0	$-c_1$	0	c_1	0	0	0	0	m_{21}	m_{22}	m_{23}	m_{24}
from $[B_c]$	0	$-k_1$	0	k_1	0	0	0	0	0	0	0	0
from $[B_w]$	0	0	k_{21}	k_{22}	k_{23}	k_{24}	0	0	0	0	0	0
$[B_z]=[B_c]+[B_w]$	0	$-k_1$	k_{21}	k_1+k_{22}	k_{23}	k_{24}	0	0	0	0	0	0

m_{21}, $m_{22} \ldots$ are elements of $[m_w]$.

The natural vibration equation for one mode of the assembly is written as;

$$\lambda_i [A_z] \left\{ \begin{matrix} \psi_i \\ \lambda_i \psi_i \end{matrix} \right\} + [B_z] \left\{ \begin{matrix} \psi_i \\ \lambda_i \psi_i \end{matrix} \right\} = 0 \qquad (5.23)$$

Let us use the following notation:

$$\{\psi_i\} = \left\{ \begin{matrix} \vdots \\ \vdots \\ p_{imn} \\ \vdots \end{matrix} \right\} \qquad \text{where} \quad m = x \text{ or } y$$
$$n = 1,2,3\ldots\text{etc.}$$

e.g., the element of the ith eigenvector corresponding to coordinate y_2 will be denoted p_{iy2}.

Then the row associated with the y_2 coordinate of Eq. (5.23) will read:

$$\lambda_i[c_1(p_{iy2}-p_{ix2})+\lambda_i(m_{21}p_{iy1}+m_{22}p_{iy2}+m_{23}p_{iy3}+m_{24}p_{iy4})]+$$

$$+k_1(p_{iy2}-p_{ix2})+k_{21}p_{iy1}+k_{22}p_{iy2}+k_{23}p_{iy3}+k_{24}p_{iy4}=0$$

$$(5.24)$$

Equation (5.24) is written in unknowns c_1, k_1. It contains terms obtained from the measurement of the ith mode shape on the two end coordinates of this connection: x_2 and y_2, and elements of the workpiece mass and stiffness matrices which have been computed from the workpiece dimensions. Here the workpiece is meant which was used in the measured assembly.

Eq. (5.24) can be split into its real and imaginary parts. In this way the necessary two equations are obtained to determine k_1 and c_1.

In an analogous way, by selecting another row of Eq. (5.23), the one corresponding to coordinate y_3 the parameters k_2 and c_2 of the connection at the center can be obtained.

By using information about more than one mode a redundant system of equations is obtained for $\hat{k}_1$, c_1 and, similarly for k_2, c_2. Such a system will lead to:

$$\left\{ \begin{matrix} k_i \\ c_i \end{matrix} \right\} = [[D^T][D]]^{-1} [D]^T \{g\} \tag{5.25}$$

which is similar to Eq. (3.11) with replacing m_i by c_i.

5.8 An Example of Experimental Identification of the Connecting Elements

Of the whole procedure described in the preceding sections the most critical part is the question of how well can the connections and, especially the chuck, be expressed by a simple spring, k and a simple damper c. This aspect will be most discernible in the case of a workpiece clamped in overhang where the deformations of the chuck are rather large. An experiment was conducted to check on this question. In order to emphasize the possible problem rather long workpieces were used having large inertia for the rotational displacement in the chuck.

First a workpiece diameter 43 mm, 260 mm long was used. The two mode shapes measured are shown in Fig. 5.4.

The corresponding eigenvalues were

$$\lambda_1 = -86.76 + j\,1285$$
$$\lambda_2 = -191 + j\,2188.$$

The workpiece was considered as a rigid body. Its mass matrix is obtained as

$$[m_w] = \begin{bmatrix} m & m\ell \\ & \cdot \\ m\ell & m\ell^2 + J \end{bmatrix} \dots \begin{Bmatrix} y_1 \\ y_2 \end{Bmatrix}$$

where m is the total mass of the workpiece, ℓ is half its overhang length and J is the mass moment of inertia around the middle point.

Next a workpiece 43 mm diameter, 196 mm long was used. The eigenvalues of the two corresponding modes were

$$\lambda_1 = -80 + j\,1642$$
$$\lambda_2 = -138 + j\,2665.$$

The coordinate y_2 is understood here as being the relative rotation between the workpiece and the chuck. It was estimated from the displacements measured on both.

The values of the rotational stiffness of the chuck k_1 and of the corresponding damping coefficient c_1 as obtained from the measurement on the two workpieces using Eq. (5.25) are listed in Table 5.5.

If we take the values of k_1 and c_1 obtained from all the measured data of the two workpieces as references, and

Table 5.5   Identified Spring and Damper of a Chuck

Workpiece	Data Used	k_1 (N.m/rad)	c_1 (N.m.sec/rad)
260x43 mm	Mode shape at λ_1	.1051E6	.9706E1
	λ_2	.6943E5	.3429E1
	Mode shapes at λ_1, λ_2	.1043E6	.7931E1
196x43 mm	Mode shape at λ_1	.1271E6	.5568E2
	λ_2	.1195E6	.1208E2
	Mode shapes at λ_1, λ_2	.1256E6	.4632E2
Two work-pieces	All mode shapes	.1224E6	.4366E2

compare them to those obtained using two modes of either

workpiece, the percentage differences would be as follows:

	k_1	c_1
Workpiece 1	-14.78	-98.93%
Workpiece 2	2.61	6.09%

Obviously, the damping coefficient as estimated
here is not reliable. This could be attributed to its very
small value compared to the stiffness coefficient which makes
it more sensitive to experimental errors. Also it could be
due to its improper modelling as a linear damper. On the
other hand, it is seen that the stiffness coefficient k_1
behaves within reasonable limits. This makes the suggested
modelling of the clamping stiffness of the chuck as a discrete
linear spring acceptable.

CHAPTER 6

USING MODAL DATA IN STUDYING
CHATTER IN MACHINING

6.1   Introduction

Many aspects of chatter in machining have been investigated, among them the basic theory of the limit of stability, the role of the structural dynamics of the machine tool and the dynamic cutting force coefficient for the part of the mechanics of the cutting process. However, most of the theoretical and experimental knowledge was oriented to continuous cutting as it is represented by turning and boring operations and not enough was done yet to properly understand chatter in milling with its periodically interrupted cutting process. Moreover, all these studies were done in the frequency domain.

In this chapter, the use of the modal parameters of the structure in studying the chatter phenomenon in machining is demonstrated. Both the continuous (turning) and the interrupted (milling) cutting operations will be considered. This study will help formulate an acceptance test of machine tools based on dynamic stability.

The modal parameters as obtained by the exciter test will be used in the simulation of the cutting process to determine the limits of stability under different cutting

conditions. The simulation here will be carried out in the time domain, which represents, to the knowledge of the author, an original work in the field of chatter in machining.

The simulation will be applied first, on theoretical vibratory systems, then on an actual machine with experimental verification.

6.2 Basic Principles of Chatter in Machining

The three basic principles of chatter in machining [8] are: regeneration, mode coupling and the velocity component. A brief description of these principles is given below.

6.2.1 Regeneration

The mechanism of the regenerative principle is shown in Fig. 6.1. In this case, a vibratory tool cuts the workpiece and a chip is produced whose both sides are undulated. The undulation $z(n+1)$ is produced due to the vibrating tool during the $(n+1)^{th}$ pass and undulation $z(n)$ has been left on the workpiece surface during the nth pass. The instantaneous chip thickness is determined by the amplitude and phase relation between $z(n+1)$ and $z(n)$. The phase shift ε between $z(n+1)$ and $z(n)$ is determined by the frequency of tool oscillation f and the rotational speed and the diameter of the workpiece in the case turning or the rotational speed and the number of teeth of the tool in the case of milling. At the onset of chatter, frequency f and angle ε adjust themselves

so that a maximum energy is delivered to the system which may be sufficient to overcome the available damping energy in the system, causing self-excitation and dynamic instability in the cutting process.

The mechanism of regenerative chatter was applied to predict the limit width of the cut b_{lim} in conjunction with the vibratory system of the machine tool. This limit width of the cut was derived in [8] as,

$$b_{lim} = - \frac{1}{2\ r\ G_{min}} \qquad (6.1)$$

where;

   r = the dynamic cutting force coefficient

   G_{min} = the minimum real part of the relative transfer

              function between the tool and the workpiece after

              multiplying by the proper directional orientation

              factor.

6.2.2 Mode Coupling

The principle of mode coupling is illustrated in Fig. 6.2. For this principle to apply, it is necessary that the vibratory system of the machine tool should have at least two degrees of freedom in different directions, which is in fact always the case in machine tool structures. During cutting under vibratory conditions, the tool describes an ellipse. Assuming that $k_1 < k_2$ the cutting force acts along the direction as shown in Fig. 6.2, during the tool motion from A

to B the cutting force F acts against the tool motion, thus vibration energy is dissipated. During the second half of the cycle, motion B to A, vibration energy is imparted to the system which is greater than the dissipation energy, since during the second half of the cycle the tool faces a larger average depth of cut. Thus for each cycle an excess energy is available which may supercede the damping energy and maintain vibrations in the system.

6.2.3 Velocity Component

This principle is based on the existence of a phase shift between the change of the chip thickness and the change of the cutting force as depicted in Fig. 6.3.a where;

$z(n)$ is the undulation amplitude left behind in the nth pass

$z(n+1)$ is the vibration amplitude in the $(n+1)^{th}$ pass

$z(n+1)-z(n)$ is the chip thickness variation in the $n+1)^{th}$ pass

ε is the phase shift between $z(n+1)$ and $z(n)$

$F(n+1)$ is the cutting force in the $(n+1)^{th}$ pass

α is the phase shift between the cutting force $F(n+1)$ and the chip thickness $z(n+1)-\dot{z}(n)$.

The principle is called the "velocity component principle" by which is meant that the cutting force contains a variable component in phase with the velocity of vibration

$z(n+1)$. This component is denoted $F_d(n+1)$ where d designates damping. Therefore, if the phase shift angle α is positive, i.e. $F(n+1)$ is leading $z(n+1)-z(n)$, the velocity force component $F_d(n+1)$ will be added to the damping force exerted by the vibratory system $c\,\dot{z}(n+1)$ resulting in an increase in the overall damping in the system. However, if α is negative, i.e. $F(n+1)$ is lagging the chip thickness $z(n+1)-z(n)$, the velocity force component $F_d(n+1)$ will be subtracted from $c\,\dot{z}(n+1)$ the damping force to reduce the overall damping in the system. If $|-\alpha|$ exceeds the angle ψ as shown in the figure, the vibratory system will behave as if it has negative damping and the cutting process will be unstable.

The positive damping generated in the cutting process [90], which is represented by the force component $F_d(n+1)$ is due to the interference of the flank of the tool with the slope of its motion with the cut as depicted in Fig. 6.3b. In position 1 the tool is moving upwards and there is enough clearance between it and the surface it has just cut. In position 2 it moves into the material and the clearance is diminished. The increased thrust force acts against the velocity of the motion and generates damping. Up to a certain slope the cutting force is not much affected but as soon as the slope reaches or exceeds the relief angle γ of the tool the thrust force increases. The slope of the wave is proportional to the amplitude of vibration and to the ratio of frequency f and cutting speed v, its maximum value is

$$\sigma_{max} = 2\pi\ A\ f/v \qquad\qquad\qquad (6.2)$$

Thus, e.g. for f = 500 Hz, cutting steel with a high speed tool with v = 30 m/min the wave length is w = v/f = 500 (mm/sec)/500 (1/sec) = 1 mm and the slope will reach 6° at A = 0.017 mm. For cutting aluminum with v = 1200 m/min, the wavelength is 40 mm and the same slope would be reached at A = 0.66 mm. Cutting steel and considering f = 1600 Hz, the wavelength is 0.3 mm and the critical amplitude is A = 0.005 mm.

Thus, for low cutting speeds and high frequencies · damping is high. If, for simplicity, we consider the wavelength a good indicator of wave reproducibility, Table 6.1, lists the combination of standard cutting speeds and typical frequencies measured on a milling machine, 200, 600 and 1600 Hz. where the 200 Hz is the headstock mode, 600 Hz is the spindle mode and 1600 Hz is the end mill mode.

Table 6.1

Tool/workpiece Combination	Cutting Speed	Surface Wave Length, mm		
		200 Hz	600 Hz	1600 Hz
a) HSS/steel	30 m/min	2.5	0.83	0.31
b) Carbide/steel	150 m/min	12.5	4.2	1.56
c) HSS/aluminum	600 m/min	50	.17	6.25

If, as a rule of thumb, we consider a wavelength w = 0.5 mm the shortest to reproduce then for the case a) the

end mill mode becomes inactive and the spindle mode is also strongly damped. On the other hand, in milling aluminum the end milling mode can easily participate.

6.3 Simulation of Chatter in Machining

6.3.1 Machine Tool Vibratory Model

The machine tool structure can be modelled as a vibratory system with many masses, located quite generally in the three-dimensional space, interconnected with springs or massless beams. A two-dimensional diagrammatical representation of one such system is depicted in Fig. 6.4. The mass a_1 represents the tool and the mass a_2 represents the workpiece. This vibratory system is assumed to have several modes in several directions x_i, x_j...etc. (Several modes can eventually have one common direction). In the present work it is assumed that either all these directions are different or for th modes which have a common direction the system exhibits proportional viscous damping.

Since we are interested in the relative vibrations between the tool and the workpiece, which are relevant, in the exciter test we must measure the direct relative transfer functions between these two. This means to get the parameters of the mode i in the direction x_i we apply a force between a_1 and a_2 and measure the relative vibrations between them in the same direction X_i. Therefore, for mode i we obtain;

K_i: The relative modal stiffness between a_1 and a_2.

M_i: The relative modal mass between a_1 and a_2.

C_i: The relative modal damping between a_1 and a_2.

These parameters are to be obtained for all the modes $i, j, \ldots p$.

6.3.2 Cutting Forces

In general, several cutting forces $F_j(n) - F_m(n)$ in different directions will be acting simultaneously between a_1 and a_2. This could be due to several cutting edges that are engaged in cut at the same time and/or the cutting edge is divided into segments where the cutting force on each of these segments is treated separately (in the case of complicated geometry of the cutter). Each of these forces, e.g. $F_j(n)$, can be looked at as two forces $F_{jr}(n)$ and $F_{jd}(n)$, where $F_{jr}(n)$ is in phase with the chip thickness and $F_{jd}(n)$ is in phase with the velocity. n is a subscript used for the time step.

6.3.3 Geometry of the Cut

Corresponding to each cutting force $F_j(n)$ there is a direction $Z_j(n)$ normal to the machined surface. This direction in general changes from one time step to the next. The angle between $F_j(n)$ and $Z_j(n)$ is β_j. The angle between the direction X_i of the mode of vibration i and $Z_j(n)$ is $\alpha_{ij}(n)$. These angles will always be measured in the direction from positive $Z_j(n)$ to positive $F_j(n)$ as shown in Fig. 6.4. The differential

equation of the mode i in the direction X_i at the time step n is written as

$$M_i \ddot{x}_i(n) + C_i \dot{x}_i(n) + K_i x_i(n) = \sum_{\alpha=1}^{m} F_j(n) \cos (\beta_j - \alpha_{ij}(n)) \qquad \alpha = 1 - p \qquad (6.3)$$

If we decompose the forces $F_j(n)$'s into their components $F_{jr}(n)$'s and $F_{jd}(n)$'s, Eq. (6.3) can be written as

$$M_i \ddot{x}_i(n) + C_i \dot{x}_i(n) + \sum_{j=1}^{n} F_{jd}(n) \cos (\beta_j - \alpha_{ij}(n)) + K_i x_i(n)$$

$$= \sum_{j=1}^{m} F_{jr}(n) \cos (\beta_j - \alpha_{ij}(n)) \qquad (6.4)$$

6.3.4 Basic Non-Linearity

All existing theories and analysis of chatter in machining are based on assumptions of a linear vibratory system and, mostly, also of a linear effect of vibration on the cutting force. However, it is well known that when chatter starts it does not grow indefinitely but stabilizes at a finite amplitude of vibration. There is an obvious basic non-linearity in the process which is due to the fact that once the vibration is large enough the tool jumps out of the cut for a part of its vibratory period. During this time the force is not any more proportional to chip thickness but it is simply zero.

This basic non-linearity will be investigated here. Its inclusion is important especially in milling operations where the cut may start or end with zero chip thickness which

implies that any small vibrations would lead to the tool jumping out of the cut.

6.3.5 Simulation Procedure

The simulation is carried out in small time steps Δt. Subsequent cuts follow one another after L steps (after the time L $\times$ Δt). The average chip thickness which corresponds to the force $F_j(n)$ is $h_j(n)$ (average chip thickness is the instantaneous chip thickness to be removed if there are no undulations on both sides of the chip, i.e. no vibrations occurred either in the preceding cuts nor in the current cut). The instantaneous chip thickness which corresponds to $F_j(n)$ in the direction $Z_j(n)$ is usually taken as a result of waviness $z_j(n)$ and $z_j(n+1)$ but as the vibrations grow more preceding cuts than one may be involved (See later Fig. 6.9). Let us take three preceding cuts into account. At any instant n we may ask which of the preceding cuts reached the lowest in the material and denote such a position z_{jmin}:

z_{jmin} is the lowest of $z_j(n-L)+h_j(n)$, $z_j(n-2L)+2h_j(n)$

$$, z_j(n-3L)+3h_j(n) \qquad (6.5)$$

and the instantaneous chip thickness $y_j(n)$ is:

$$y_j(n) = z_{jmin} - z_j(n) \qquad (6.6)$$

and the cutting force is

$$F_j(n) = r \times b \times y_j(n) \qquad (6.7)$$

where;

r: the dynamic cutting coefficient

b: the width of the cut

$F_j(n)$ can further be written as:

$$F_{jr}(n) = r_r \times b \times y_j(n)$$

$$F_{jd}(n) = r_d \times b \times y_j(n)$$

$$\left.\right\} \qquad (6.8)$$

where;

r_r: represents the stiffness of the cut which produces the cutting force $F_{jr}(n)$ in phase with the chip thickness $y_j(n)$.

r_d: represents the damping of the cut which produces the damping force $F_{jd}(n)$ in phase with the velocity $\dot{z}_j(n)$.

but, if $F_{jr}(n) < 0$, then $F_{jr}(n) = F_{jd}(n) = 0$ (6.9)

where Eq. (6.9) expresses the basic non-linearity in the system; if the force should be negative it would mean that the tool jumps out of the cut and then the force is actually zero.

The differential equations of the different modes of vibrations are written according to Eq. (6.4). The motion $z_j(n)$ in the direction $z_j(n)$ which modulates the chip thickness is obtained from the contributions of all modes $x_i(n)$ to $x_p(n)$ as;

$$z_j(n) = \sum_{i=1}^{p} x_i(n) \cos \alpha_{ij}(n), \quad j=1,m \tag{6.10}$$

In the simulation, for each mode the acceleration in the time step n is determined and then the displacement in the next time step $(n+1)$ is obtained by double integration. Thus, e.g., for mode i:

$$\ddot{x}_i(n) = [\sum_{j=1}^{m} F_{jr}(n) \cos (\beta_j - \alpha_{ij}(n)) - (C_i \dot{x}_i(n) + \sum_{j=1} F_{jd}(n)\cos$$

$$(\beta_j - \alpha_{ij}(n))) - K_i x_i(n)]/M_i \tag{6.11}$$

$$\dot{x}_i(n+1) = \dot{x}_i(n) + \ddot{x}_i(n) \quad \Delta t \tag{6.12}$$

$$x_i(n+1) = x_i(n) + \dot{x}_i(n+1) \quad \Delta t \tag{6.13}$$

Similarly, for the other modes and, then $z_j(n+2)$; $j=1, m$ are obtained. The procedure is to be continued until the amplitudes of vibration stabilizes. In the following two sections the simulation procedure will be applied to theoretical vibratory systems for two machining operations, continuous and interrupted.

6.4 Continuous Cutting (Turning)

The model used for simulation is shown in Fig. 6.5. A system with two mutually perpendicular degrees of freedom X_1 and X_2 is used. A tool is attached to the mass of the system and it cuts an undulated surface and leaves another

undulated surface behind. There is only one force F acting
on the system which does not change direction from one time
step to the next. Consequently the direction normal to the
machined surface z, and the angles between the directions
of X_1 and X_2 and Z are constant. And assuming that the force
does not have a component in phase with the velocity, Eq. (6.4)
for, say X_1, becomes;

$$M_1 \ddot{x}_1(n) + C_1 \dot{x}_1(n) + K_1 x_1(n) = F(n) \cos (\beta - \alpha_1) \quad (6.14)$$

and, similarly, for X_2. The subscript j has been dropped here,
since there is only one force acting.

The parameters of the simulated system were chosen
so that the stiffnesses of both modes are equal, $K_1 = K_2 = K =$
18,000,000 N/m, but the frequencies differ, $f_1 < f_2$. Various
values of the ratio $R = f_1/f_2$ were used. Damping ratios of both
modes were taken $\xi_1 = \xi_2 = 0.05$. Cutting stiffness (DCFC)
was chosen as, $r = 2 \times 10^9$ N/m^2.

With a system of two degrees of freedom oriented like
the one in Fig. 6.5 the values of b_{lim} depends on the ratio
R of the two frequencies. The values of b_{lim} versus this ratio
as established from Eq. (6.1) and using the above mentioned
parameters of the system are plotted in Fig. 6.6. It is
seen that b_{lim} is minimum for $R = f_1/f_2 = 0.94$ and that for
R = 1.0 the value of b_{lim} is 2.5 times larger than that. The
case of R = 0.94 is selected here for simulation.

In Fig. 6.7.a) vibration in Z during the first three
cuts (passes) is plotted versus time $T = n \times \Delta t$, where

$\Delta t = 0.0002$ sec. The chip width is chosen $b = 1.212$ mm which is slightly above b_{lim}. The length of one cut corresponds to one revolution of the workpiece per 0.1 sec. This means that the number of simulation steps between subsequent cuts is taken here $L = 500$. The individual workpiece revolutions are correspondingly indicated as L, 2L, 3L, etc. It is seen that at the entry of the tool into the first cut natural decaying vibration of the system is produced which leaves undulations on the surface and these begin to reproduce during the second and third cuts, etc. Between the second and third cuts a growth is seen indicating instability. However, already the first cut is not purely natural vibration because of "mode coupling". This is explained later. In Fig. 6.7b) simulation of a case is presented with larger chip width $b = 2.2 \times b_{lim} = 2.222$ mm. The vertical scale of the graph is 70 times larger than that in Fig. 6.7b) to accommodate the much faster rate of increase of vibration amplitude. Here it is seen that there is practically no decay at the beginning. This is due to a larger self excitation energy arising from the larger chip width. In the fourth revolution the vibration z reaches an amplitude of 0.22 mm which is 1.5 times the average chip thickness h.

The details of the process are shown in Figs. 6.8 and 6.9 which expand on sections of Fig. 6.7b).

In Fig. 6.8a) vibrations z are plotted for sections S1, S2, S3, S4 of Fig. 6.7b). These sections follow each other exactly always after one revolution and they represent

subsequent undulations on one and the same section of the
circumference of the workpiece. It is seen that in the 4th
cut the tool already jumps out of the cut for a part of the
vibration cycle. The shaded area represents the material
removed in this cut. The horizontal coordinate in this case
is the angle of workpiece rotation in degrees. There are
about 17 waves per circumference of the workpiece. In
Fig. 6.8b) the cutting force F is shown for the last cut,
$z(n)$, of Fig. 6.8b). It is seen that repeatedly, the force
becomes zero for a part of the cycle. In Fig. 6.8c) vibration
$z(n)$ of Fig. 6.8a) is plotted versus $u(n)$, see Fig. 6.5.
The graph shows the actual motion of the tip of the tool in
the Z-U coordinates. The tool moves on this elliptical path
in the direction of the arrow and during the motion from point
A to point B it moves outside of the cut. The cutting force F
has the direction as indicated at two arbitrary points along
the path. During the motion from point 1 to point 2 the force
has a positive component into the direction of the velocity
of motion - it drives the tool. During the motion from
point 2 to point 1 the force component acts against the motion -
the force brakes the motion. Even without the tool jumping
out of the cut, with the direction of motion as shown here the
1-2 motion is carried out deeper in the cut than 2-1 and there-
fore during the 1-2 part the force is greater and the work
supplied is greater than during 2-1 and a surplus of self
excitation energy results. This is the mechanism of "mode
coupling" which acts here in addition to the "regeneration of

waviness'' mechanism and increases the intensity of self excitation. For a single degree of freedom system the tool moves on a straight line and mode coupling is not active. Similarly for $f_1=f_2$ the tool moves on a straight line (both vibrations have the same phase) and therefore the case of R=1 has higher stability in the graph, Fig. 6.6.

Now, with the tool jumping out of the cut the braking action works only from B to 1 and there is still more energy left for self excitation.

In Fig. 6.9a) vibration z is shown in sections over the same part of workpiece revolutions 99 to 103 after the start of the cut. So, this graph actually follows the one in Fig. 6.8a) after another 98 revolutions of the workpiece. By this time vibration z has stabilized at an amplitude of 0.35 mm (2.3 times the average chip thickness). The tool leaves the cut for a little more than half the vibratory cycle. The shaded area shows the material cut during each cycle. In Fig. 6.9b) the tool motion is shown in coordinates Z, U. Again, during motion 1-2 the force drives the tool. Between A and B the tool does not cut. Thus, there is no force to brake the tool along the path 2-1.

The diagrams in Figs. 6.7, 6.8 and 6.9 illustrate very clearly the process of self excitation in turning. Due to the non-linearity of the tool leaving the cut the amplitude of the chatter does not grow indefinitely but it stabilizes after a sufficiently large number of workpiece revolutions at a finite value. This value is easily obtained by simulation

computations as described here. This value depends on the chip width b, on how much it is larger than the value b_{lim}.

In Fig. 6.10 results of a number of computations are summarized. The amplitudes z of fully established self excited vibrations are plotted versus the chip width b for a system shown in Fig. 6.5 for various values of the ratio R of the two natural frequencies. There is no vibration below the values b_{lim} as determined by Eq. (6.1). The various values b_{lim} are those found on the z = 0 axis. The lowest b_{lim} corresponds to R = 0.94 and the highest to R = 1.0. The value of b_{lim} would further grow for R > 1 (i.e. $f_1 > f_2$). For any value of $b > b_{lim}$ the amplitude of vibrations grows until it exceeds the average chip thickness h (the feed per revolution). In our case h = 0.15 mm. Then the tool starts jumping out of the cut and the amplitude of vibration stabilizes at a value which increases with any further increase in b.

The vibration with an amplitude larger than h is usually considered unacceptable. Correspondingly, one may conclude that the boundary between stable and unstable machining with continuous cuts (turning, boring) is very sharp.

6.5 Interrupted Cutting (Milling)

The model used for simulation is shown in Fig. 6.11. A system with two mutually perpendicular degrees of freedom X_1 and X_2 is used. X_1 and X_2 will be denoted here X and Y, respectively. The arc of the cut goes from ϕ_s to ϕ_e. Several

teeth are engaged in the cut over this arc. At any time step n there are as many forces acting on the system as the number of teeth cutting, assuming for simplicity the teeth are straight. In the figure there are three forces $F_1(n) - F_3(n)$. Along with each force $F_j(n)$ there is a direction $Z_j(n)$ normal to the machined surface. Both $F_j(n)$ and $Z_j(n)$ rotate with the cutter. The angle between $F_j(n)$ and $Z_j(n)$ is β which is constant and has the same value for all the forces. The angles between the modes and the normals to the surface, e.g., between X and $Z_1(n)$ and $Z_3(n)$ are $\alpha_{11}(n)$ and $\alpha_{13}(n)$ respectively as shown in the figure. The average chip thickness, e.g., $h_1(n) = f_t \sin \phi(n)$; where f_t is the feed/tooth and $\phi(n)$ is the angle position of the first tooth. Similarly, $h_2(n) = f_t \sin(\phi(n) + \phi_t)$; where ϕ_t is the angle between tooth 1 and tooth 2. f_t used here = 0.15 mm.

The particular geometries of the milling operations considered here are those depicted in Fig. 6.12 which will be further analyzed. These are: half-immersion (radial depth of cut equals half cutter diameter) up-milling, b) half-immersion down-milling, c) full-immersion milling, i.e., slotting. The cases a) and b) represent the first and second half of the case c) respectively. We will consider an end milling cutter with four teeth having straight edges (non helical).

The two modes of vibrations have the same stiffness $K_x = K_y = 2 \times 10^7$ N/m and damping ratio $\xi_x = \xi_y = 0.05$ but different natural frequencies, f_x, f_y.

In the following we will be discussing five different

arrangements of the vibratory system:

a) $f_x = f_y = 660$ Hz

b) $f_x = 633$ Hz $< f_y = 660$ Hz, b') $f_x = 660$ Hz $> f_y = 633$ Hz

c) $f_x = 660$ Hz $< f_y = 960$ Hz, c') $f_x = 960$ Hz $> f_y = 660$ Hz

The cases a), b), and c) differ by the ratio of
the natural frequencies of the two modes of vibration. In
all these three cases the direction of the feed is X as
shown in Fig. 6.12. The cases b') and c') are reverse to
b) and c) respectively. They will be indicated as milling
with the feed in the Y direction because they act as b) and
c) if f_x and f_y are interchanged.

In analyzing chatter in milling it has, so far, always
been done so that instead of the variable directional factors
such ones were used which correspond to the mean directional
orientation [8]. This is illustrated for the up-milling case
in Fig. 6.12a).   They would correspond to a) $\phi = 45°$,
b) $\phi = 135°$, c) $\phi = 90°$ and for $\beta = 70°$ their values would be:
a) $u_x = 0.64$, $u_y = -0.3$, b) $u_x = -0.3$, $y_u = 0.64$, c) $u_x = 0.34$,
$u_y = 0$. This is, of course, an oversimplification of reality.
If the variation of the directional factors is appreciated it
is realized that during the cut either the X or Y mode takes
over and the frequency of vibration may change.

If excitation were an instantaneous phenomenon then
the limit of stability against chatter would vary during the
rotation of the cutter as the directional factors and consequently

the contribution of the modes to the undulation of the machined surface vary. This variation is illustrated in graphs in Fig. 6.13 where "instantaneous" values of b_{lim} as obtained from Eq. (6.1) are plotted versus the angle of rotation for up- and down-milling of the above cases a) and b). The broken line parts of the graph correspond to chatter with the higher of the two frequencies and the full line to the lower one. However, excitation cannot vary instantaneously, vibrations decay or increase rather slowly, time is needed for transitions. Especially chatter cannot start with one frequency and change instantaneously into another frequency. Obviously in each of the presented cases there is some "average" value of b_{lim}. It is not certain whether it corresponds to the values at 45° and 135°, respectively which are usually used.

Furthermore, the variation of chip thickness has also strong implications for the "saturation" of the force as expressed by the non-linearity condition Eq. (6.9). At the beginning of the cut in a), at the end of the cut in b) and both at the beginning and the end of the cut in c) the average thickness is zero and, therefore the tool will jump out of the cut at even the smallest vibration.

The cutting forces F_j's are periodically variable also in the case of stable cutting, without chatter. This variation has a basic period equal to the interval between the teeth which in our case is 1/80 sec. We will not discuss the form of the variation of the forces; it will be visible in the

following plots. It is, however, necessary to point out that in the cases a) and b) the sudden changes at the exit and entry, respectively, of the cut periodically·excite decaying natural vibrations in both X and Y. In the case c) where two teeth cut simultaneously the sum of their forces is constant and it has a constant direction (if the cutter has no run-out). Therefore, in this case, the cutting force itself does not excite any vibration unless self excitation occurs. All these aspects, the varying directional orientation, the varying chip thickness and the forced and transient natural vibrations due to the variation of the cutting forces make the analysis of milling much more complicated than that of turning. Probably the only way that it can be properly done is simulation which also permits, with no difficulty, to include the basic non-linearity of the tool jumping out of the cut.

The transition between stable and unstable cutting is "blurred" by the transient natural vibrations excited per every tooth period which occur already below the limit of stability. This is illustrated in Figs. 6.14 and 6.15. In Fig. 6.14 the x and y vibrations are plotted (as simulated) for the first eight tooth periods for the above a) case, $f_x = f_y$, up-milling, for chip width b = 0.6 mm which is slightly below the limit of stability (as is shown later b_{lim} = 0.7 mm for this case). The basic periodicity per cutter tooth is clearly visible as well as the transient vibrations with the natural frequencies of the system. In Fig. 6.15 the

x and y vibrations of the same case are shown but a larger chip width b = 1.2 mm is used. This is already beyond the limit of stability and vibrations are increasing in amplitude per every tooth period. The vertical scale of this graph is 5 times larger than that of Fig. 6.14.

Some insight into the self-excitation process in milling is provided in Figs. 6.16 to 6.20. In Fig. 6-16a) vibration in the Z direction (normal to the cut - radial to the cutter) in four subsequent cuts (subsequent teeth) number 51 to 54 (after 50 cuts from the beginning) is shown for the $0^o < \phi < 90^o$ up-milling cut of case a) and chip width b = 1.2 mm. This is obviously well established chatter. The shaded area shows the actual removed material in cut number 54. Fig. 6.16b) shows the corresponding tangential component of the cutting force. Fig. 6.16c) shows the tool tip trajectory in the Z, U coordinates. It is interesting to see that, now, unlike in turning, even for $f_x = f_y$, the trajectory is not a straight line but evolving ellipses and "mode coupling" is active. The arrow shows the direction of motion. For two of the cycles the points A, B, C and D are indicated. From the start S to A the tool moves outside of the cut, from A to B it cuts, etc., from D to E it does not cut, etc. In a way similar to Fig. 6.16a) the case of down-milling is shown in Fig. 6.17 for cuts 100 to 103 and in Fig. 6.18 the case of slotting (b=0.4 mm) for cuts 100 to 103. Again, in both these cases chatter is fully established, vibration does not vary from cut to cut (tooth after tooth).

In Fig.s 6.19 and 6.20 the case b) of f_x = 633 Hz and f_y = 660 Hz and b') of f_x = 660 Hz and f_y = 633 Hz are shown respectively, for up-milling and b = 1.2 mm. In Fig. 6.19a) the vibration z is shown for cuts 50' to 53 and in Fig. 6.19b) the trajectory of the tool tip is shown in the Z, U coordinates. It is seen that chatter is fully developed and the "mode coupling" mechanism is strongly active; the ellipses are wide and the tool moves in the right direction for mode-coupling self excitation; notice the direction of the cutting force F.

In Fig. 6.20 the case of the reversed-frequencies is shown (f_x > f_y, milling in Y). In Fig. 6.15a) vibration z is shown for cuts 50 to 53 and in Fig. 6.15b) the corresponding tool tip trajectory is shown. The direction of the motion is correct for mode-coupling self excitation but the ellipses become very flat in the latter part of the cut and this mode of self excitation is, therefore, weak. Although there is sustained chatter which is fully developed its amplitude is much smaller than in the case of Fig. 6.19.

Computations of the various cases were carried out for a number of values of chip width b and sufficient cycles carried out to each established vibrations. The summary of the results is presented in Fig. 6.21. The three diagrams correspond to slotting (S), down-milling (D) and up-milling (U) respectively.

In each graph the a), b), c) and b'), c') cases

of the various frequency combinations: 660/660, 633/660, 660/960 are included with always $f_x < f_y$ while X means milling in direction X (cases a), b), and c) of the previous classification) and Y means milling in the Y direction (cases b') and c') of X with reversed frequencies).

The following observations can be made:

1.   In slotting, the transition between stable and unstable machining is rather sharp and for any $b > b_{lim}$ the amplitudes of chatter increase fast. In up-milling and down-milling (half-immersion milling) the boundary between stable and unstable cutting is wide; with chip width b increasing the amplitude of established vibration increases first rather gradually. It is not easy to clearly define the limit of stability b_{lim}. It is suggested to extrapolate the part of the individual lines to PTP = 0 and take the intersect as b_{lim}.

2.   In slotting b_{lim} is in the average about half that in the half-immersion cuts. This is due to the fact that twice as many teeth cut simultaneously. However, for $f_x = f_y$ it is less than half and it is the lowest stability of all cases. (This is contrary to turning where the case of R = 0.94 which corresponds here to 633/660 Hz system which was much less stable than R = 1.0). This is due to the rotation of the cutting force.

3.   In slotting the direction of the cut does not matter as long as the parameters of the two modes are the same. Stability of the case c) with frequencies f_1 and f_2 far

apart is much higher than for R = 1 and R = 0.95. The same applies to up- and down-milling for the cases b) and b') with frequencies f_x and f_y not equal but close; R = 0.95 and 1.05. In these cases (b) and b')) the direction of the feed has a strong effect.

The final recapitulation of the simulation results for the theoretical vibratory systems is presented in Fig. 6.22 where just the b_{lim} values are assembled (black bars) and they are compared with the values b_{lim} (blank bars) as they were always calculated in the past under the assumption of the mean directional orientation.

First, the same main conclusions can be repeated as for Fig. 6.21:

Up- and down-milling is about the same and feed direction does not matter if f_x and f_y are either equal or far apart; but they differ and feed direction has an effect if f_x and f_y are different but close. Slotting is about half as stable as half-immersion except for $f_x = f_y$ where it is still less stable.

Secondly, computing the limit width of cut using the mean directional factors are satisfactory for f_x and f_y strongly different. As f_x and f_y get closer they lead to larger and larger errors; the actual stability is smaller; for $f_x = f_y$ it is less stable than half of that calculated in this approximate way.

6.6   Experimental Verification

In this section the simulation procedure, applied above on theoretical vibratory systems, will be applied on an actual milling machine. The modal parameters, as obtained from the measurements of the relative transfer functions between the tool and the workpiece will be used to predict the limit of stability through the computer simulation. Then cutting tests will be carried out to verify the simulation results.

6.6.1   Milling Machine Vibratory Model

The machine used here is a TOS FA4 milling machine (5.5 KW). Figs. 6.23 and 6.24 show the direct relative transfer functions between the end of a 101.6 mm diameter face milling cutter and the workpiece in the X and Y directions, respectively.   They were measured using:

- a piezoelectric impact transducer (pcb 218A) mounted on a hammer.
- a proximity probe, capacitive type (MC1, range 0.254 mm, resolution 0.0127 mm for 1-10 KHz range) mounted on the workpiece.

From these transfer functions, we can identify two main modes in the X direction at 250 and 518 Hz and two modes in the Y direction at 165 and 603 Hz. The parameters of these modes are listed below;

	Mode	Frequency Hz	Damping Ratio %	Modal Stiffness N/mm
X	1	250	2.7	510648.6
	2	518	7.6	142492.0
Y	1	165	6.5	483698.6
	2	603	8.08	131016.2

Complete measurement of the mode shapes of the machine showed that the first modes (the first in X and the first in Y) are associated with the headstock and the column. Fig. 6.25 shows the 250 Hz mode in the X direction where the column bending contributes most., Also, the measurements showed that the higher modes (518 Hz in X and 603 in Y) are associated with the spindle.

As can be seen from Fig. 6.23, the two modes are far apart with the first mode being much stiffer than the second one. The same applies on Fig. 6.24. Since the objective here is the analysis of chatter rather than redesigning the machine, only the parameters of the spindle modes (518 Hz in X and 603 Hz in Y) will be introduced into the simulation program. Consequently, the vibratory model of the machine here is reduced to that one in Fig. 6.11 with two mutually perpendicular degrees of freedom.

6.6.2 Simulation Results

The cutter used here has six straight edges. The cutting speed is 111.5 m/min which corresponds to a tooth

frequency of 35.5 Hz. The feed per tooth is $f_t = 0.1$ mm.
Four different modes of milling are considered; a) up-milling
in X, b) down-milling in X, c) up-milling in Y, d) down-
milling in Y. In all these cases the cutter is half immersed
(half of the diameter of the cutter is engaged radially in the
cut). The cutting force is taken as being proportional and
in phase with the instantaneous chip thickness. The DCFC
r is 2×10^9 N/m^2. Using these data and the modal parameters
of the spindle modes mentioned above, the results of the
simulation were obtained as follows;

a) Up-milling in X:

By increasing the axial depth of the cut b, the limit
of stability was found at 8 mm. Fig. 6.26 shows the force
components F_x and F_y and their autopower spectra respectively
for b = 5 mm. As we can see in Figs. 6.26a) and b) the force
components, although the cut is still stable, contain the
spindle mode frequencies which are repeatedly excited by the
tooth impacts. The autopower spectra c) and d) show the
tooth frequency and its harmonics. Fig. 6.27 is similar to
Fig. 6.26 but for b = 9 mm where the process is already
unstable. The spindle modes are dominating the individual
signals.

b) Down-milling in X:

The limit of stability here was found at an axial
depth of cut b = 22 mm. Figs. 6.28,9 show the force components
F_x and F_y and their autopower spectra respectively for

b = 15, 19 mm where the cut is still stable.

c) Up-milling in Y:

The limit of stability here was found at an axial depth of cut, b = 18 mm. Fig. 6.30 shows a stable case at b = 15 mm while Fig. 6.31 shows an unstable case at b = 17 mm.

d) Down-milling in Y:

The limit of stability here was found at b = 10 mm. Fig. 6.32 shows a stable case at b = 5 mm while Fig. 6.33 shows the unstable case at b = 10 mm.

6.6.3 Cutting Tests

6.6.3.1 Experimental Set-Up

Fig. 6.34 is a schematic of the experimental set-up. It consists of; a) two-components table dynamometer, b) multichannel visicorder (Honeywell), c) two channel structural dynamic analyzer (Hewlett Packard 5423 A). . The description and calibration of the dynamometer is given in Appendix VI. The visicorder was used to get the time records of the force components F_x and F_y, while the analyzer was used to get their autopower spectra. The tool used was a face milling cutter, 101.6 mm diameter, double positive (positive radial rake angle of 5° and positive axial rake angle of 7°), with 6 carbide inserts; SPU 634-KC850. Cutting conditions were mentioned in Section 6.6.2. The workpiece material was

1020 hot rolled steel, BHN = 125, in the form of a flat 406.4 mm long, 203.2 mm wide and 50.8 mm thick. It was clamped to the table dynamometer.

6.6.3.2 Cutting Test Procedure

The cutting tests were carried out for the four cases mentioned in Section 6.6.2; half immersion a) up-milling in X, b) down-milling in X, c) up-milling in Y and d) down-milling in Y. The experiment for each case was to keep all conditions constant but the axial depth of cut b which was to be increased until chatter developed. One important aspect in these tests was to watch for tool wear, should the inserts chip or the wear land on the flank exceed 0.1 mm, the cutting edges would be replaced by fresh ones.

6.6.3.3 Identifying Stability Limit

Reaching the stability limit, and eventually exceeding it, is readily discernible by a characteristic noise, characteristic chatter marks on the machined surface, see photograph in Fig. 6.35, and by a characteristic dissected chip form, see photograph in Fig. 6.36. This chip form shows clearly that the tool does jump out of the cut for some time of its vibratory period.

In order to improve the safe recognition of chatter and to correlate the cutting tests to the simulation results, the recording of the cutting force components and their

autopower spectra was necessary. These cutting force
components are direct indicators of the relative vibration
between the tool and workpiece relevant to chatter. As soon
as they show the natural frequencies of that part of the
structure responsible for chatter dominating (here it is
the spindle), it is recognized as chatter. This could be
recognized from both, their time records and their auto-
power spectra.

6.6.3.4 Cutting Test Results

a) Up-milling in X:

The limit axial depth of the cut was found at b = 7 mm.
Fig. 6.37 shows the time records of F_x and F_y and their auto-
power spectra for a stable cutting at b = 5 mm. Fig. 6.38
is similar to Fig. 6.37 but for b = 7 mm where the cut is
already unstable. These figures are to be compared with Figs.
6.26 and 6.27. They show a very good agreement between the
simulation results and the cutting test results.

b) Down-milling in X:

The axial depth of the cut was increased here up to
15 mm without chatter developing fully. Figs. 6.39 and 6.30
show the force components and their autopower spectra for
b = 6 mm and 15 mm respectively. In both cases the cut was
considered as being still stable. The depth of the cut could
not be increased any further due to the finite length of the

insert's edge. The cutting test is again in good agreement
with the simulation results which showed that the limit
of stability occurs at b = 22 mm.

c) Up-milling in Y:

Similar to the previous case, an axial depth of the
cut of 15 mm could be reached without encountering chatter.
Fig. 6.41 shows the time records of F_x and F_y at b = 15 mm.
Again, the agreement between the simulation results and the
cutting test results is good.

d) Down-milling in Y:

The limit axial depth of the cut was found at b = 10
mm. Figs. 6.42 and 6.43 show the time records of F_x and
F_y and their autopower spectra for a stable cutting at b = 5 mm
and unstable cutting at b = 10 mm respectively. Comparing
these figures with figures 6.32 and 6.33 respectively,
reveals that the agreement between the simulation results and
the cutting results is good.

Summarizing, in all the cases handled here both results
of the simulation and cutting tests are in good agreement.

6.6.3.5 Stability Limits Using Mean Directional
         Orientation Factors

In this section the limit axial depth of the cut b_{lim}
for the cases a), b), c) and d) will be calculated using the

mean directional orientation factors which are:

for a) and d) $u_x = 0.64$, $u_y = -0.3$,

for b) and c) $u_x = -0.3$, $u_y = 0.64$

The transfer functions, only the real part, in
Figs. 6.23 and 6.24 are, first, multiplied by the correspond-
ing directional factor, and then added together, to get the
oriented transfer functions, Fig.s 6.44 and 6.45. From these,
oriented, we get the minimum real parts G_{min}'s. Applying
Eq. (6.1) and using $r = 2 \times 10^9$ N/m^2 we get:

i) for cases a) up-milling in X and d) down-milling in Y

$b_{lim} = 7.94$mm

ii) for case b) down-milling in X and c) up-milling in Y

$b_{lim} = 9.26$ mm.

Before making a final comparison between the results
obtained here, let us consider first the following set of
cutting tests.

6.6.3.6 Cutting Tests of Aluminum

These tests were designed such that the flexible tool
mode would participate in the chatter process. The tool used
was a HSS (high speed steel) end mill, 25.4 mm diameter, 76.2
mm overhang, 4 teeth. The workpiece material was 7075 Al,
BHN=112. The cutting speed was 112 m/min, feedrate $f_t = 0.1$
mm/tooth.

Figs. 6.46 and 6.47 show the direct relative transfer functions between the end of the tool and the workpiece in the X and Y directions, respectively. The parameters associated with the tool modes are,

	Frequency Hz	Damping Ratio %	Modal Stiffness N/mm
X	1587	1.93	11623
Y	1600	2.58	10770

The vibratory model of this system can, again, be considered as having two mutually perpendicular degrees of freedom in the X and Y directions respectively. The wavelength at the 1600 Hz and cutting speed 112 mm/min, is 1.17mm which could be reproduced.

As we can see from Figs. 6.46 and 6.47 the two modes associated with the tool have almost the same parameters except for the damping ratios. And since the tool has four teeth the cutting tests here can be compared in the general trend with the simulation results of the theoretical vibratory system with $f_x = f_y$ in Section 6.5.

The cutting tests conducted gave the results in Table 6.2.

Table 6.2 Al Cutting Tests Results

	Direction					
	X			Y		
	1/2 imm U	1/2 imm. D	S	1/2 imm. U	1/2 imm. D	S
b_{lim}(mm)	10	12	4	14	15	6

6.7 Discussion

a) The theoretical vibratory systems handled in Section 6.5 had, always, the same stiffness and damping ratio in both directions. The tool had four straight teeth (non-helical) and the tooth frequency was kept at 80 Hz. Consequently, the observations and conclusions derived in Section 6.5 are concerned only with such systems. No attempt was made here either to study the effect of the number of teeth of the tool nor the tooth frequency. Gygax has found in his theoretical study [92] that these parameters have an effect on the dynamics of the milling operations. However, their effect on the stability limit has yet to be explored through the simulation procedure described here. This could be subject to future work.

b)   Fig. 6.48 shows a comparison between limits of stability obtained through: simulation, cutting tests and using the mean directional orientation factors when using the face milling cutter on steel. All results are close for up-milling in X and

down-milling in Y. They differ very much between; simulation and cutting tests on one hand, and using the mean directional orientation factors (as used to be taken in the past) on the other hand, for down-milling in X and up-milling in Y. This proves the validity of the mathematical simulation procedure presented here over the previous treatment of chatter based on Eq. (6.1).

c) The cutting tests of 7075 aluminum showed that the limit of stability in slotting, in both the X and Y directions, is about 0.4 of b_{lim} obtained in half-immersion millings in the corresponding direction. It was mentioned in Section 6.6.3.6 that the vibratory model of the machine, in that particular case, could be compared with the theoretical one in Section 6.5 with $f_x = f_y$. For that system, the latter, slotting gave $b_{lim} \cong 0.4 \ b_{lim}$ in half-immersions. The ratio between the limit of stability in slotting and in half-immersions was also calculated using the mean directional orientation factors and it was found as, $b(slotting) \cong 0.6 \ b_{lim}$ (half immersions). As we can see both the simulation and cutting tests resulted in the same ratio which is different by more than 30% than that obtained using the mean directional factors. This, again, verifies the simulation procedure.

CHAPTER 7

CONCLUSIONS

In this chapter the summary, contributions and main
conclusions of this work are presented. Also some ideas
about possible future work are suggested.

Summary

1. Identification

In identifying the unknown structural parameters
of the system from the experimental data obtained from the
Modal Analysis Testing, two situations arise:

a)   If all relevant coordinates are available then a
system of linear equations can be assembled from: either
the equations of motion alone in the case that only parts of
the mode shape vectors are measured, or from the equations of
motions as well as the orthogonality relationships in the case
that full length mode shape vectors are measured.

The unknown parameters are then obtained in the least
square sense using the pseudoinverse method.

b)   If some relevant coordinates in the mode shape vectors
are missing, like coordinates on the bearings and spindle
inside a headstock, then establishing linear equations in the
unknown parameters is not possible. Consequently, a non-
linear optimization routine could be used to minimize

the errors between the experimental modal data and those
computed using initial estimates.

2. Modelling

The identification techniques were illustrated on
two examples. Mathematical models of two actual milling
machines have been established from the experimental modal
data. As a special case a model for a lathe is suggested.

3. Disassembling a Substructure

A procedure was developed to obtain the dynamic
characteristics of a substructure using the experimental
modal data measured on the whole assembly. This is demon-
strated on the example of the lathe mentioned in 2.

4. Chatter in Machining

The problem of chatter in machining in this thesis
is treated in an original way, through digital simulation
in the time domain.

The main contributions to general knowledge may be
summarized as follows:

1. Identification procedures were formulated in a
   systematic coherent way and examples were
   provided of their applications to theoretical
   structures   as   well   as   Machine   Tool

structures which present special difficulties
because of the rather nonuniform distribution
of masses and flexibilities and because of
the strong influence of nonlinear joints on
higher modes.

2.   The pseudoinverse method, which was first used
in this area by Berman and Flannelly [50] for
identifying unknown masses from the orthogon-
ality relationships, was extended to include
also the equations of motion.

3.   It was shown that in orthogonalizing mode
shapes with respect to the known mass matrix
using Targoff [59] algorithm before applying
them to the identification of unknown springs
of the structure can be of advantage only if:
the number of available modes is equal to the
order of the system and, mainly, if the mass
matrix is exact. This procedure is ineffective
if the number of available modes is small and
it can lead to erroneous results if the mass
matrix is inaccurate.

4. It is proposed: If the available experimental
    modal data are limited, e.g. only very few
    modes could be measured in the frequency range
    concerned, or the number of accessible co-
    ordinates is very small, then a suitable change
    of the structure should be introduced in the
    experiment so as to obtain additional modal
    information. E.g. a small mass can be added
    to selected coordinate.

5. In modelling machine tool structures, it is
    important to concentrate on those flexible modes
    responsible for chatter. This may be a difficult
    problem.

         The work presented here contributes to
    its solution by providing two examples of modell-
    ing typical machine tools. The rational approach
    of interpreting the flexibilities in the structure
    based on the measured mode shapes and consequently
    establishing the geometry of the model as well as
    obtaining initial estimates of the unknown para-
    meters, could be followed in modelling similar
    machines.

6. In this work a typical model of a lathe structure is suggested based on the measured mode shapes. A procedure is developed for obtaining the dynamic characteristics of the lathe structure alone by subtracting a known workpiece using the measured modal parameters of the assembly. The lathe structure characteristics are obtained in this way rather than measuring them directly. The weak coupling between the headstock and tailstock might make the data obtained in the latter way unreliable. The procedure is general and can be applied to other structures.

7. In this work an original approach to machining chatter is presented. The digital simulation of the cutting process including chatter in the time domain is carried out. The vibratory models of the machines used in the simulations are established from the experimental data obtained through the Modal Analysis Testing.

    For the first time in the field of investigations of chatter the variation in the cutting force direction as well as the variation in the chip thickness during milling are considered in

estimating the limit of stability.

Cutting test results carried out in this project have confirmed the results obtained through simulation.

Significance of the Work

1. Identification and Modelling

Establishing mathematical models of mechanical structures from the experimental data and, identifying the unknown parameters in these models is an important tool for assessing a wide range of design changes. This is especially valuable when the coordinates at which the design changes are intended are inaccessible.

The identification also can enhance the Finite Element applications by providing the data on joints and possibly on damping.

2. Dynamics of a Lathe

The procedure developed in this work to predict the limit of stability against chatter for any workpiece before-hand could be implemented in the Postprocessors of Numerically Controlled Turning Centers, in order to be included in the process of determining cutting conditions.

3. <u>Chatter in Machining</u>

The cutting tests carried out in this work have shown that the digital simulation approach to the problem of chatter in machining represents the reality very closely. Based on that, new acceptance tests procedures of Machining and Turning Centers were formulated [93]. Also, milling cutters can be designed [94], and the effects of cutting speed on chatter can be investigated [95] under more realistic conditions.

<u>Ideas for Future Work</u>

Future work should concentrate on developing the identification and modelling procedures presented in this thesis into well packaged and easy to use computer software.

REFERENCES

1. Peters, J., "Modal Analysis of Mechanical Structures",
   Modal Analysis Seminar, Mech. Eng. Dept., Univ.
   of Leuven, Dec. 1977.

2. Van Loon, P., "Modal Parameters of Mechanical Structures",
   Ph.D. dissertation, Catholic University of Leuven,
   Sept. 1974.

3. Richardson, M., "Measurements and Analysis of the
   Dynamics of Mechanical Structures", Hewlett
   Packard Publication, Hewlett Packard, Santa Clara,
   Cal., DSA/Laser Division, 1981.

4. Bach, N., Burdekin, M., Cowley, A., "A Review of the
   Research on Fixed and Sliding Joints", Proc. 13th
   MTDR Conf., Pergamon Press, 1973, pp. 87-97.

5. Hijink, J., Van Der Wolf, A., "Survey on Stiffness and
   Damping of Machine Tool Elements", Paper presented
   at the 23rd General Assembly of CIRP, August, 1973.

6. Tlusty, J., Moriwaki, T., "Experimental and Computational
   Identification of Dynamic Structural Models",
   Annals of the CIRP, V. 25/2/1976, pp. 497-503.

7. Peters, J., "Damping in Machine Tool Construction",
   Report MC8 - CIRP, 1965.

8. Koenigsberger, F., Tlusty, J., "Machine Tool Structures",
   Vol. 1, Pergamon Press, Oxford, 1970.

9. Klosterman, A., "On the Experimental Determination and
   Use of Modal Representations of Dynamic Character-
   istics", Ph.D dissertation, University of Cincinnati,
   1971.

10. Taylor, S., "The Design of a Machine Tool Structure Using
    A Digital Computer", Proceedings of 7th Int. MTDR
    Conf., Bermingham, 1966, pp. 369-383.

11. Richardson, M., Potter, N., "Viscous Versus Structural
    Damping in Modal Analysis", 46th Shock and Vibra-
    tion Symposium, San Diego, Cal., Oct. 1975.

12. Hurty, W. C., Rubinstein, M. F., "Dynamics of Structures",
    Prentice Hall, 1964.

13. Caughey, T. K., O'Kelly, M. E. J., "Classical Normal Modes in Damped Linear Dynamic Systems", Journal of Applied Mechanics, Vol. 32, 1965, pp. 583-588.

14. Richardson, M., "Modal Analysis Using Digital Test Systems", Seminar on Understanding Digital Control and Analysis in Vibration Test Systems, Shock and Vibration Information Center Publication, Naval Research Lab., Wash., D.C., May 1975.

15. Potter, R, "A General Theory of Modal Analysis for Linear Systems", Shock and Vibration Digest, Nov. 1975.

16. Klosterman, A., Zimmerman, R., "Modal Survey Activity via Frequency Response Functions", SAE, National Aerospace Engineering and Manufacturing Meeting, Culver City, Los Angeles, Nov. 17-20, 1975.

17. Richardson, M. and Potter, R., "Identification of the Modal Properties of an Elastic Structure from Measured Transfer Function Data", 20th International Instrumentation Symposium, Albuquerque, N.M., May 1974.

18. Frazer, R. A., Duncan, W. J., Collar A. R., "Elementary Matrices", Cambridge University Press, London, 1946.

19. Bleiweis, P. B., Hart, G., Smith, C., "Enirco Fermi Plant Dynamic Response During Blasting", Transactions of the ANS, Vol. 13, No. 7, July 1970, pp. 231-238.

20. Moriwaki, T., Mutch, G. and Tlusty, J., "Identification of Mode Shapes of #3 Turbine Generator at Lakeview Generation Station", MWRG Report No. 68, Dec. 1975.

21. Veck, M., Prossler, K., "Untersuchung Des Dynamischen Verhasltens Spanender Werkzengmaschinene Und Deren Einzelner Bauelemente Und Kopplungsstellen Mit Hilfe Aperiodischer Testsignale", WZL, TH, Aachen, West Germany, March 1977.

22. Moriwaki, T., Iwata, K., Veno, S., "A New Technique in Shock Excitation Testing for Improvement of Measuring Accuracy", Procceddings of 9th NAMRC Conf., 1979, pp. 214-221.

23. Moriwaki, T., Iwata, K., Veno, S., "Optimizing Dynamic Force in Shock Excitation Testing", Proceedings of 8th NAMRC Conf., 1979, pp. 427-434.

24. Brown, D., "Grinding Dynamics", Ph.D Dissertation, University of Cincinnati, 1976.

25. Ramsey, K. A., "Effective Measurements for Structural Dynamic Testing", Sound and Vibration Magazine, April, 1976, pp. 18-31.

26. Trail-Nash, R. W., "On the Excitation of Pure Natural Modes in Aircraft Resonance Testing", Journal of Aerospace Sciences, Vol. 25, 1958.

27. Tlusty, J., Lau, K. C. and Parthiban, K., "Use of Shock Compared with Harmonic Excitation in Machine Tool Structure Analysis", Trans. ASME, J. Eng. for Ind., Feb. 1974, pp. 187-195.

28. Van Brussel, H., Peters, J., "Comparative Assessment of Harmonic, Random, Swept Sine and Schock Excitation Methods for the Identification of Machine Tool Structures with Rotating Spindles", Annals of the CIRP, Vol. 24, No. 1, 1975, pp. 291-296.

29. Halvorsen, W. G., Brown, D. L., "Impulse Technique for Structural Frequency Response Testing", Sound and Vibration Magazine, Nov. 1977, pp. 8-21.

30. Moriwaki, T., Tlusty, J., "Eliminating Noise in Shock Excitation Testing", Annals of CIRP, Vol. 25, No. 1, 1976, pp. 267-271.

31. Ewins, D. J., "Measurement and Application of Mechanical Impedance Data", Part 2: Measurement Techniques", Journal of the Society of Environmental Engineers, Dec. 1975, pp. 23-30.

32. McKinny, W., "Band Selectable Fourier Analysis", Hewlett-Packard Journal, April 1975, pp. 20-24.

33. Ewins, D. J., "Measurement and Application of Mechanical Impedance Data, Part 1: Introduction and Ground Rules", Journal of the Society of Environmental Engineers, Dec. 1975, pp. 3-12.

34. Mergeay, M., "Curve Fitting: Theoretical and Practical Problems", Modal Analysis Seminar, Mech. Eng. Dept., Univ. of Leuven, Dec. 1977.

35. Weck, M. et al., "Visual Representation of the Dynamic Behaviour of Machine-Tool Structures", Annals of the CIRP, Vol. 25, No. 1, 1976, pp. 263-266.

36.   D'Ans, G., "Critical Speeds and Modal Analysis of
           Anisotropic Shafts", Modal Analysis Seminar,
           Mech. Eng. Dept., Univ. of Leuven, Dec. 1977.

37.   Tlusty, J., Ismail, F., Prossler, K., "Identifica-
           tion, Modelling and Modification of Struct-
           ures Defined from Experimental Data",
           WZL, TH Aachen, June 1978.

38.   Bekey, G. A., "System Identification - An Introduc-
           tion and Survey", Simulation V. 15, No. 4,
           1970, pp. 151-166.

39.   Kozin, F., Kozin, C. H., "Identification of Linear
           Systems, Final Report on Simulation Studies",
           NASA CR-98738, April 1968.

40.   Kozin, F., Kozin, C. H., "A Moment Technique for
           System Parameter Identification", Shock and
           Vibration Bulletin, No. 38, pt. 2, August,
           1968, pp. 119-131.

41.   Young, J. P., On, F. J., "Mathematical Modelling
           Via Direct Use of Vibration Data", SAE National
           Aeronautic and Space Engineering and Manufact-
           uring Meeting, Los Angeles, Calif., October
           1969, SAE paper 690615.

42.   Distefano, N., Rath, A., "Modelling and Identifica-
           tion in Nonlinear Structural Dynamics - One
           Degree of Freedom Models", Report No. 74-15,
           Earthquake Eng. Research Center, Univ. of
           Calif., Berkeley, California, Dec. 1974.

43.   Dale, O. B., Cohen, R., "Multiparameter Identifica-
           tion in Linear Continuous Vibratory Systems",
           Trans. ASME, Journal of Dynamic Systems,
           Measurement and Control, March 1971.

44.   Mains, R. M., Noonan, W. E., "Stiffness, Mass and
           Damping Matrices from Measured Mobilities",
           AIAA/ASME/SAE 15th Structures, Structural
           Dynamics and Materials Conference, Las Vegas,
           Nevada, April 1974.

45.   Caravani, P., Watson, M. L., Thomson, W. T.,
           "Recursive Least-Square Time Domain Identifica-
           tion of Structural Parameters", ASME J. of
           Applied Mechanics, March 1977, pp. 133-140.

46. Flanneylly, W. G., McGarvey, J. H., Berman, A. "A Theory of Identification of the Parameters in the Equations of Motion of a Structure Through Dynamic Testing", Symposium on Structural Dynamics, Univ. of Technology, Loughborough, England, March 1970.

47. Ibanez, P., "Identification of Dynamic Structural Models from Experimental Data" UCLA-ENG. 7225, March 1972.

48. Raney, J. P. and Howlett, J. T., "Identification of Structural Systems by Use of Near-Resonance Testing", NASA TN D-5069, February 1969.

49. Thoren, A. R., "Derivation of Mass and Stiffness Matrices from Dynamic Test Data", AIAA/ASME/ SAE 13th Structures, Structural Dynamics and Materials Conf. San Antonio, Texas, April 1972, AIAA paper 72-346.

50. Berman, A., Flannelly, W. G., "Theory of Incomplete Models of Dynamic Structures", AIAA Journal, V. 9, No. 8, August 1971, pp. 1481-1487.

51. Hall, B. M. Calicin, E. D., Sholar, M. S., "Linear Estimation of Structureal Parameters from Dynamic Test Data", AIAA/ASME 11th Structure, Structural Dynamics and Materials Conference, April 1970, pp. 193-197.

52. Ross, R. G., "Synthesis of Stiffness and Mass Matrices from Experimental Vibration Modes", SAE National Aeronautic and Space Engineering and Manufacturing Meeting, Los Angeles, Calif., September 1971, SAE paper 710787.

53. Collins, J. D., Young, J., Kiefling, L., "Methods and Application of System Identification in Shock and Vibrations", ASME Winter Meeting, November 1972.

54. Collins, J. D., Hart, G. C., Gabler, R. T., Kennedy, B., "Structural Model Optimization Using Statistical Evaluation", Interim. Report, J. H. Wiggins Co., NASA Contract NAS8-27331.

55. Inamura, T., Sata, T., "Stiffness and Damping Identification of the Elements of a Machine Tool Structure", Annals of the CIRP, V. 28, No. 1, 1979, pp. 235-239.

56. Greville, T. N. E., "The Pseudoinverse of a
     Rectangular or Singular Matrix and Its
     Application to the Solution of System of
     Linear Equations", SIAM Review, V. 1, No. 1,
     January 1959, pp. 38-43.

57. Gravitz, S. I., "An Analytical Procedure for
     Orthogonalization of Experimentally Measured
     Modes", Journal of Aerospace Sciences, V. 25,
     No. 25, 1958, pp. 721-722.

58. McGrew, J., "Orthogonalization of Measured Modes
     and Calculation of Influence Coefficients",
     AIAA Journal, V. 7, No. 4, April 1969, pp. 774-
     776.

59. Targoff, W. P., "Orthogonality Check and Correction
     of Measured Modes", AIAA Journal, V. 14, No. 2,
     Feb. 1976, pp. 164-187.

60. Hurty, W. C., "Dynamic Analysis of Structural Systems
     by Component Mode Synthesis", AMCE, J. Eng.
     Mech., V. 86, August 1960, pp. 51-69.

61. Hurty, W. C., "Dynamic Analysis of Structural Systems
     by Using Component Modes", AIAA Journal, V. 3,
     No. 4, April 1965, pp. 678-685.

62. Gladwell, G. M. L., "Branch Mode Analysis of Vibration
     Systems", Journal of Sound and Vibration, V. 1,
     January 1964, pp. 41-59.

63. Craig, R. and Bamptor, M. C., "Coupling of Sub-
     structures for Dynamic Analysis", AIAA Journal,
     V. 6, No. 7, July 1968, pp.

64. Banfield, W. A. and Hruda, R. F., "Vibration Analysis
     of Structures by Component Mode Substitution",
     AIAA/ASME 11th Strctures, Structural Dynamics
     and Material Conference, Denver, Colorado,
     April 1970.

65. Tolani, S. K. Rocke, R. D., "Modal Truncation of Sub-
     structures Used in Free Vibration Analysis",
     ASME/Design Eng. Tech. Conference, Washington,
     D.C., Sept. 17-19, 1975, paper No. 75-DET-82.

66. Klosterman, A. L., Lemon, J. R., "Building Block
     Approach to Structural Dynamics", ASME Publication,
     VIBR-30, 1969.

67. Klosterman, A. L., "A Combined Experimental and Analyti-
     cal Procedure for Improving Automotive System
     Dynamics", SAE 720093, January 1972.

68.   Klosterman, A. L., McClelland, W. A., "Combining
      Experimental and Analytical Techniques for
      Dynamic System Analysis", Tech. Paper
      presented at the 1973 Tokyo Seminar on Finite
      Element Analysis, Nov. 5-10, 1973.

69.   Klosterman, A. L. McClelland, W. A., Sherlock, I. E.,
      "Dynamic Simulation of Complex Systems Utiliz-
      ing Experimental and Analytical Techniques",
      ASME, 75-WA/Aero-9, Dec. 1975.

70.   Formenti, D., Richardson, M., "Modal Synthesis",
      Modal Analysis Seminar, Mech. Eng. Dept., Univ.
      of Leuven, Dec. 1977.

71.   Vanhonacker, P., "Modelling", Modal Analysis Seminar,
      Mech. Eng. Dept., Univ. of Leuven, Dec. 1977.

72.   Arnold, R. N., "The Mechanism of Tool Vibration in
      the Cutting of Steel", Proc. Inst. of Mech. Eng.,
      London, No. 154, 1946, pp. 261-276.

73.   Doi, S., Kato, S., "Chatter Vibration of Lathe Tools",
      Trans. ASME, V. 78, July 1956, pp. 1127-1132.

74.   Cook, N. H., "Self Excited Vibrations in Metal Cutting",
      Trans. ASME, J. Eng. Industry, V. 81, 1959,
      pp. 183-185.

75.   Boothroyd, G., "Fundamentals of Metal Machining and
      Machine Tools", McGraw Hill, 1975.

76.   Tlusty, J., Spacek, L, "Self Excited Vibrations in
      Machine Tools", Nakl, CSAV, Prague, 1954.

77.   Tlusty, J. Polacek, M., "The Stability of the Machine
      Tool Against Self-Excited Vibration in Machining",
      ASME Prod. Eng. Res. Conf., Pittsburgh, 1963.

78.   Tlusty, J., Polacek, M., "Experience with Analyzing
      Stability of Machine Tools Against Chatter,
      MTDR Conf., Birmingham, 1968, Program Press.

79.   Merritt, H. E., "Self Excited Machine Tool Chatter",
      Trans. ASME, J. Eng. Industry, V. 87, No. 4,
      Nov. 1965, pp. 447-454.

80.   Tobias, S. A., "Machine Tool Vibration", Blackie and
      Son, Glasgow, 1965.

81.   Weck, M., Teipel, K., "Assessing the Chatter
         Behaviour of Machine Tools", Annals of the
         CIRP, V. 27/1, 1978, pp. 333-343.

82.   Van Brussel, H., Vanherck, P., "A New Method for
         the Determination of the Dynamic Cutting Coeff-
         icient", 12th MTDR Conf., Manchester, 1971,
         Pergamon Press.

83.   Peters, J., Vanherck, P. Van Brussel, H., "The Measure-
         ment of the Dynamic Cutting Coefficient", Annals
         of the CIRP, v. 21/2/1972.

84.   Tlusty, J., Goel, B. S., "Measurements of the Dynamic
         Cutting Force Coefficient", Proc. of 2nd NAMRC
         Conf., Univ. of Wisconsin, Madison, 1974,
         pp. 649-659.

85.   Tlusty, J., Rao, S., "Verification and Analysis of
         Some Dynamic Cutting For,e Coefficient Data",
         Proc. 6th NAMRC Conf., Univ. of Florida, SME,
         1978, pp. 420-426.

86.   Tlusty, J., "Analysis of the State of Research in
         Cutting Dynamics", Annals of the CIRP, V. 27/2/
         1978, pp. 583-589.

87.   Tlusty, J., Heczko, O., "Improving Tests of Damping
         in the Cutting Process", Proc. of 8th NAMRC.
         Conf., University of Missouri-Rolla-Missouri,
         1980, pp. 372-376.

88.   Siddall, J. N., "Optimal Engineering Design: Princi-
         ples and Applications", Marcel Dekker Inc.,
         New York and Basel, 1982.

89.   Guyan, R. J., "Reduction of Stiffness and Mass Matrices",
         AIAA Journal, V. 3, No. 2, Feb. 1968, pp. 380-384.

90.   Tlusty, J., Ismail, F., "Special Aspects of Chatter
         in Milling", ASME/DET Conference, Hartford, Conn.,
         Sept. 20-23, 1981, Paper No. 81-DET-18.

91.   Tlusty, J., Ismail, F., "Dynamic Structural Identifica-
         tion Tasks and Methods", Annals of the CIRP, V. 29/1/
         1980, pp. 251-255.

92.   Gygax, P. E., "Dynamics of Single-Tooth Milling", Annals
         of the CIRP, V. 28/1/1979, pp. 65-69.

93.   Tlusty, J., Ismail, F., Hoffmanner, A., Rao, S.,
         "Theoretical Background for Machining Tests of
         Machining Centers and of Turning Centers", 10th
         NAMRC Conf., McMaster Univ., Hamilton, Ontario,
         May 23-24, 1982.

94. Tlusty, J., Zaton, W., Ismail, F., "Digital Simulation of Chatter of Milling Cutters with Irregular Tooth Pitch", Contract A-14818, Project LAO19 of Kennametal Inc., MWRDG, Report No. 180, McMaster University, July 19, 1982.

95. Tlusty, J., Ismail, F., Zaton, W., "Use of Special Milling Cutters Against Chatter", To be published in the NAMRC-11, University of Wisconsin-Madison, Madison, Wisconsin, May 24-26, 1983.

APPENDIX I

TRANSFORMATION MATRIX FOR RAM-TYPE MILLING MACHINE

.The coordinates of the lumped masses in the model of the Ram-Type machine in Figure 4.4 are related to the main coordinates x_1, x_2...x_5 according to:

$$
\begin{Bmatrix} x_a \\ x_b \\ x_c \\ x_{d_1} \\ x_{d_2} \\ x_e \\ x_f \\ x_g \\ x_m \end{Bmatrix} = \underbrace{\begin{bmatrix} 0 & 0 & 0 & 1 & 0 \\ 1 & 0 & 0 & 0 & 0 \\ 1.5 & -.5 & 0 & 0 & 0 \\ -.45 & 1.45 & 0 & 0 & 0 \\ 0 & 1 & 0 & 0 & 0 \\ 0 & 0 & 1 & 0 & 0 \\ 0 & .55 & .45 & 0 & 0 \\ 0 & 0 & 0 & 0 & 1 \\ 0 & 0 & 0 & -.83 & 1.83 \end{bmatrix}}_{[T_m]_{9\times5}} \begin{Bmatrix} x_1 \\ x_2 \\ x_3 \\ x_4 \\ x_5 \end{Bmatrix}
$$

The matrix $[T_m]$ is used to transform the estimated lumped masses to the main coordinates according to Equation 4.2.

APPENDIX II

MASS MATRIX OF MILLING MACHINE (SUBSTRUCTURE 1)

Figure II.1 shows only substructure 1 of the milling machine model in section 4.3. The mass distribution of the headstock is represented by seven lumped masses m_1-m_7 while that of the column by the masses m_8-m_{12}. e, f, g, h, p and q are the ratios between the distances between the individual masses to the length of the headstock. The transformation matrix between the local coordinates y_1-y_{12} to the main coordinates of the substructure x_2, x_3 and x_1 can be derived as given in II.1.

$$
\begin{Bmatrix} y_1 \\ y_2 \\ y_3 \\ y_4 \\ y_5 \\ y_6 \\ y_7 \\ y_8 \\ y_9 \\ y_{10} \\ y_{11} \\ y_{12} \end{Bmatrix} = 1/(g+f) \begin{bmatrix} (p+q+e+f+g) & -(p+q+e) & 0 \\ (q+e+f+g) & -(q+e) & 0 \\ (e+f+g) & -e & 0 \\ 1 & 0 & 0 \\ 2 & f & 0 \\ 0 & 1 & 0 \\ -h & (f+g+h) & 0 \\ 0 & 0 & 1 \\ 0 & 0 & 1 \\ 0 & 0 & 1 \\ 0 & 0 & 1 \\ 0 & 0 & 1 \end{bmatrix} \begin{Bmatrix} x_2 \\ x_3 \\ x_1 \end{Bmatrix} \quad \text{II.1}
$$

$$[T]$$

196

The matrix [T] can then be used to transform the individual masses into the main coordinates,

$$[m_x]_{3\times3} = [T]^T \ulcorner m_{i\lrcorner} [T] \qquad \text{II.2}$$

With respect to stiffnesses the transformation matrix is obtained as:

$$\begin{Bmatrix} y_{13} \\ y_{14} \\ y_8 \\ y_{12} \end{Bmatrix} = 1/(g+f) \underbrace{\begin{bmatrix} [(L-1)/2+e+f+g+p+q] & -[(L-1)/2+e+p+q] & 0 \\ -[h+(L-1)/2] & [h+f+g+(L-1)/2] & 0 \\ 0 & 0 & 1 \\ 0 & 0 & 1 \end{bmatrix}}_{[T]} \begin{Bmatrix} x_2 \\ x_3 \\ x_1 \end{Bmatrix} \text{II.3}$$

Then,

$$[k_x]_{3\times3} = [T']^T \ulcorner k_{i\lrcorner} [T'] \qquad \text{II.4}$$

where k_i contains k_3, k_4, k_1 and k_2.

The individual masses were astimated as:

mass	m_1	m_2	m_3	m_4	m_5	m_6	m_7	m_8-m_{12}
value(kg)	10.8	20.7	18	18	13.5	5.4	3.6	45

The ratios e, f,...etc. were:

e	f	g	h	p	q
.2	.14	.16	.09	.21	.2

APPENDIX III

SUBDIAGONAL MATRIX CONTAINING DYNAMIC
CHARACTERISTICS OF A SYSTEM

Let $[A]$ be a square nonsingular matrix of order n, say $n = 6$, defined in a set of coordinates x_1 to x_6. Let $[D]_{9x6}$ be a transformation matrix which relates coordinates x to the independent coordinates q_i; $i = 1, 9$.

$$\{x\} = [D]\{q\} \qquad\qquad III.1$$

The matrix $[D]$ transforms $[A]$ into the q coordinates,

$$[A_q]_{9x9} = [D]^T[A][D] \qquad\qquad III.2$$

The matrix $[A_q]$ is thus singular being of order 9 and rank 6. Let us rewrite III.2 with partitioning the matrix $[D]$ into $[D_1]$, $[D_2]$ and $[D_3]$ of which $[D_2]$ is square 6x6, then

$$[A_q] = \begin{bmatrix} D_1^T(1x6) \\ D_2^T(6x6) \\ D_3^T(2x6) \end{bmatrix} [A] \begin{bmatrix} D_1 & D_2 & D_3 \end{bmatrix} \qquad III.3$$

The multiplication leads to

$$[A_q] = \begin{bmatrix} D_1^T A D_1 & D_1^T A D_2 & D_1^T A D_3 \\ \hline \text{Symm.} & D_2^T A D_2 & D_2^T A D_3 \\ & (6x6) & \\ \hline & & D_3^T A D_3 \end{bmatrix} \qquad III.4$$

The submatrix $[D_2^T A D]$ is nonsingular and it

198

represents a simple transformation of [A] into the coordinates q_2-q_7. Therefore, the eigenparameters of [A] are preserved.

As the partitioning of [D] was arbitrary it is obvious that any diagonal 6x6 submatrix of $[A_q]$ would satisfy the same condition .

APPENDIX IV

GENERATING THE DAMPING MATRIX FOR A SYSTEM
WITH PROPORTIONAL VISCOUS DAMPING

For substructure S_L in 5.6.1 whose mass and stiffness matrices $[m_L]$ and $[k_L]$ of size 6x6 could be assembled according to the geometry in Figure 5.8, the damping matrix $[c_L]$ was generated as follows:

a) The eigenvalue problem of the system was first solved, assuming there was no damping. The modal parameters obtained were; Ω_i^2, $\{\phi_i\}$, K_i^1, $i = 1, 6$.

where Ω_i^2's are the eigenvalues, $\{\phi_i\}$'s are the eigenvectors and K_i^1's are the modal stiffnesses at coordinates x_1.

b) Modal damping ratios $\S_1 - \S_6 = 0.03$ were assumed and subsequently used in computing the modal damping coefficients C_i^1 as:

$$C_i^1 = 2 \, \S_i \, K_i^1 / \Omega_i \; ; \qquad i = 1, 6 \qquad \text{IV.1}$$

C) Since it was assumed that S_L had proportional damping, then the modal matrix $[P]$ assembled from $\{\phi_i\}$'s obtained in a) could be used to get $[c_L]$ by back transformation, i.e.

$$[c_L] = [P]^{-T} \lceil C_i^1 \rfloor [P]^{-1} \qquad \text{IV.2}$$

DYNAMIC CONDENSATION OF WORKPIECE MASS
AND STIFFNESS MATRICES

In 5.6.1 the workpiece mass and stiffness matrices $[m_w]$ and $[k_w]$ of size 5x5 were obtained from the first five modes of a free-free continuous beam in transverse vibrations.

The displacements at the coordinates y_1, $y_2 \cdots y_5$ in the first five modes, and taking the displacement y_1 as 1, were computed as:

$$\begin{Bmatrix} y_1 \\ y_5 \\ y_2 \\ y_3 \\ y_4 \end{Bmatrix} = \begin{bmatrix} 1. & 1. & 1. & 1. & 1. \\ 1. & -1. & 1. & -1. & 1. \\ 1. & .5 & -.099 & -.585 & -.621 \\ 1. & .0 & -.607 & .0 & .712 \\ 1. & -.5 & -.099 & .525 & -.621 \end{bmatrix} \qquad \text{V.1}$$

$$\underbrace{\qquad\qquad\qquad\qquad\qquad\qquad\qquad\qquad}_{[P_w]_{5x5}}$$

The modal masses M_1^1-M_5^1 were computed as; $m\ell$, $m\ell/3$, $.2499977\ m\ell$, $.2500323\ m\ell$, $.2546481\ m\ell$, where $m\ell$ is the total mass of the beam. The modal stiffnesses K_1^1-K_5^1 were obtained from M_i^1's and the computed eigenvalues Ω_i^2, such that, $K_i^1 = \Omega_i^2 M_i^1$.

Then $[m_w]$ and $[k_w]$ were obtained from

$$[m_W] = [P_W]^{-T} \ulcorner M^r_{\searrow} [P_W]^{-1} \text{ and } [k_W] = [P_W]^{-T} \ulcorner K^1_{\searrow} [P_W]^{-1} \quad V.3$$

In this way $[m_W]$ and $[k_W]$ are dynamically condensed over the first five modes.

APPENDIX VI

TABLE DYNAMOMETER

The table dynamometer used in the cutting tests in Chapter 6 measures the force components in two mutually perpendicular directions. It was used throughout the tests to measure the forces F_x and F_y in the X and Y directions respectively. The dynamometer was fixed to the table of the milling machine while the workpiece was clamped on top if it.

A schematic of the table dynamometer is shown in Figure VI.1. The load-sensitive elements are piezo-electric force transducers with built-in charge amplifiers, in the form of thick washers (Pcb 201A). There are two load cells on each side. The voltages coming out of the two load cells on one side are summed together.

Figure VI.2 shows the static calibration of the dynamometer. It is linear in both X and Y directions. The static calibration gave the same results in both tension and compression. The cross sensitivity in both directions was less than 5% and consequently there was no need for compensation.

Figures VI.3, 4 show the frequency characteristics of the dynamometer. They are reasonably flat up to 600 Hz.

FIGURES

a)

b)   c)
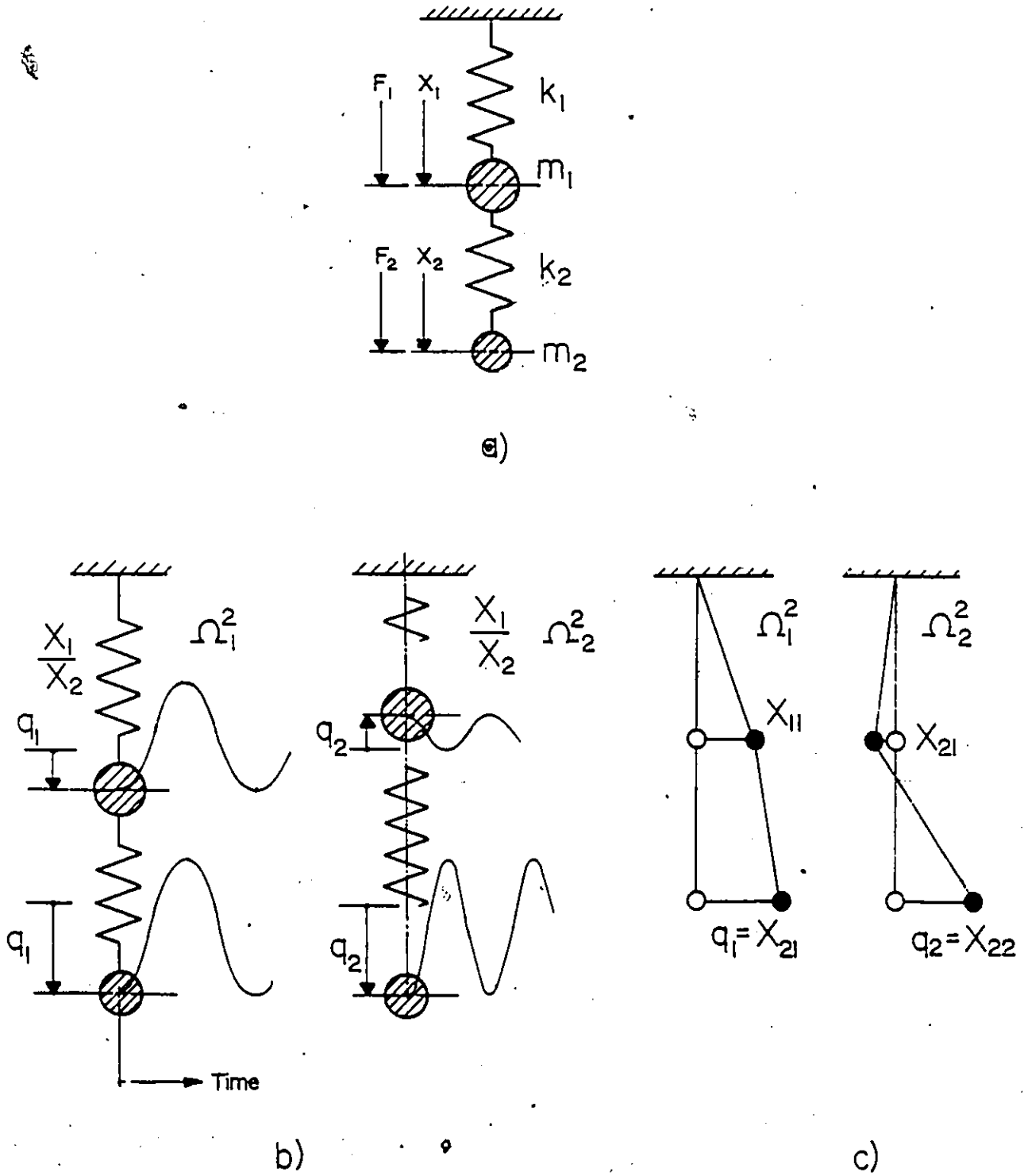
Figure 2.1   Local and Modal Coordinates
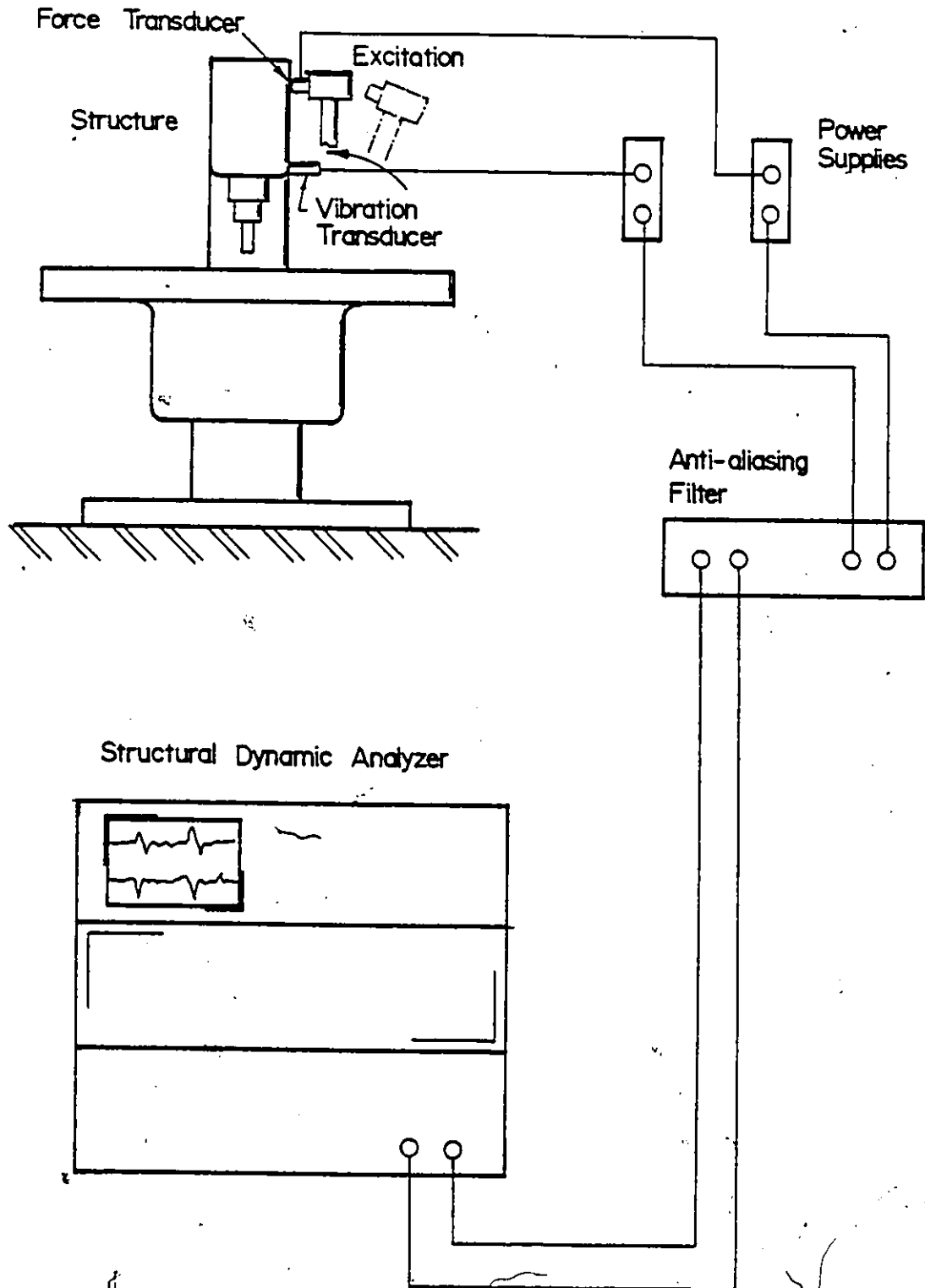
Figure 2.2   Modal Parameters from Modal Analysis
Testing
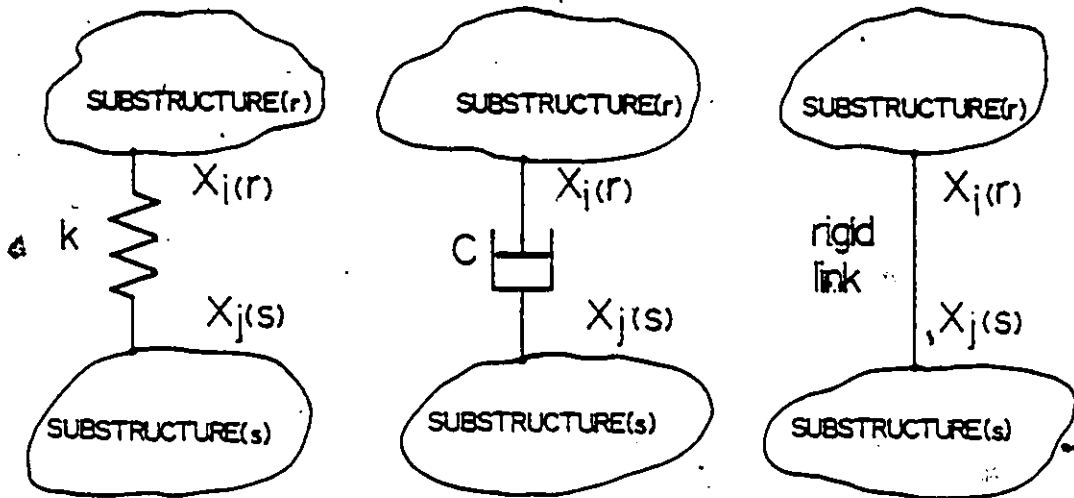
Figure 2.3   Different Connecting Elements Between
            Substructures
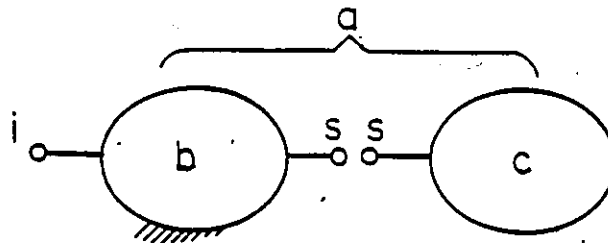
Figure 2.4   Synthesizing Substructures b and c
            to Form Assembly a
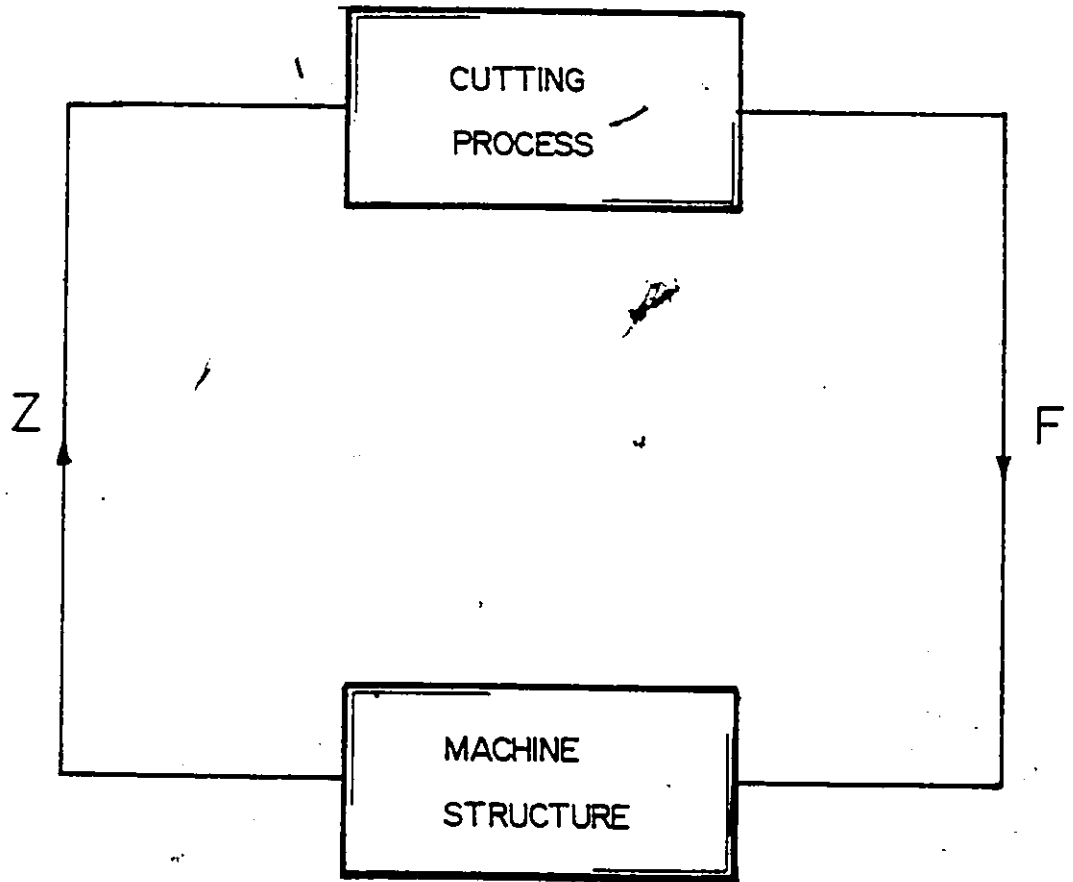
Figure 2.5   Chatter Closed Loop
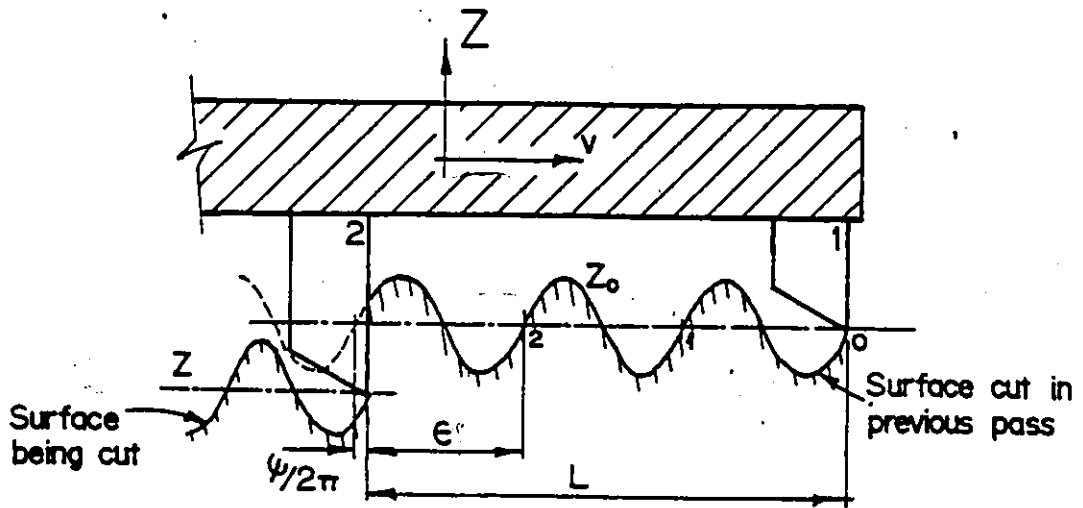
Figure 2.6   Phase Shift Between Outer and
Inner Undulations
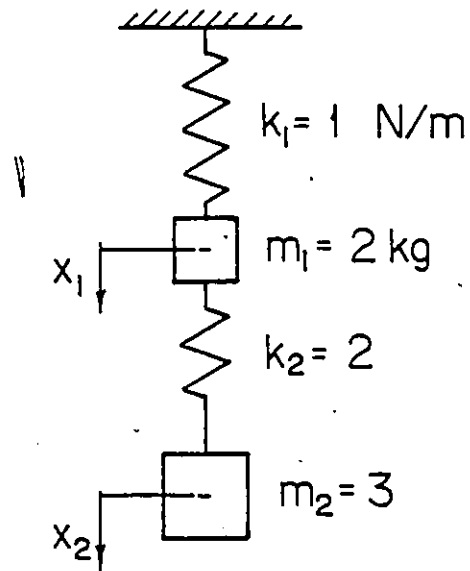
Figure 3.1   Two Degrees of Freedom System
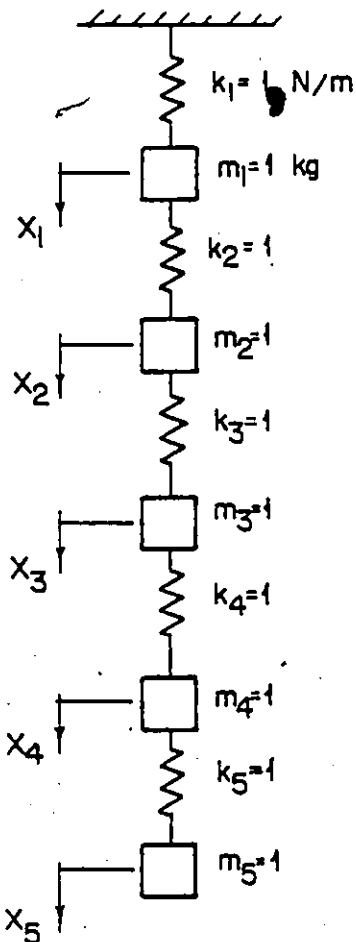
Figure 3.2   Five Degrees of Freedom System
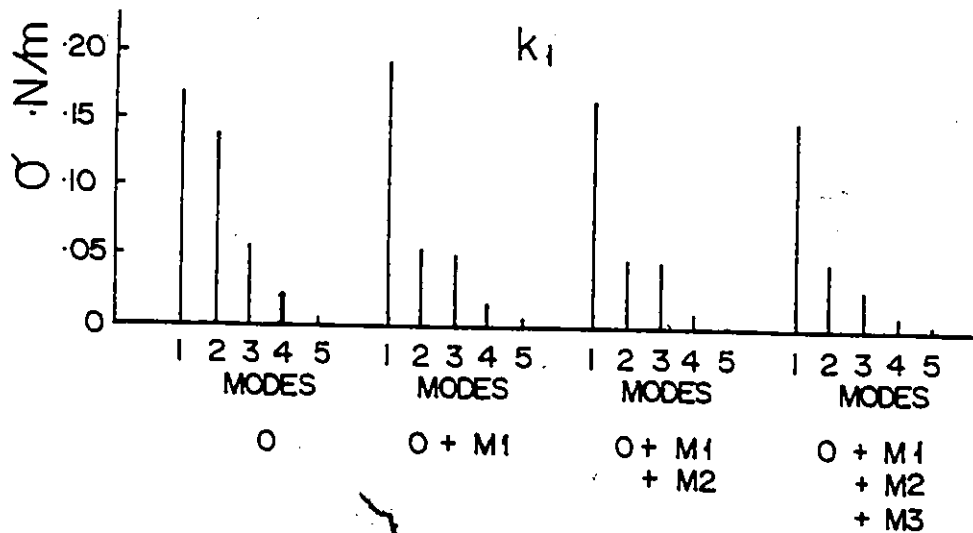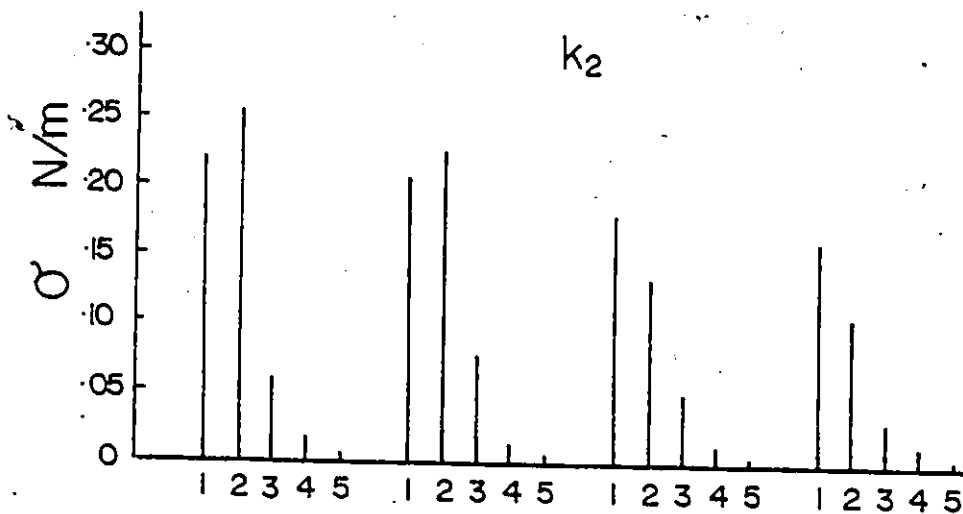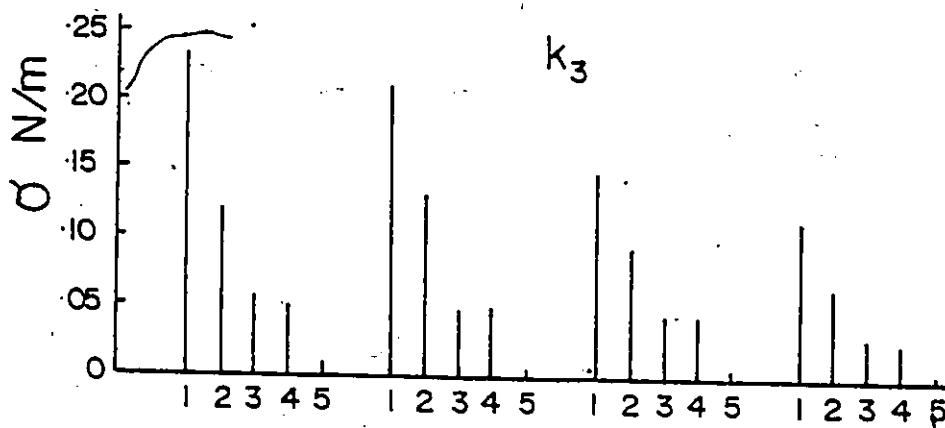
Figure 3.3   Standard Deviations of Springs k_1-k_5
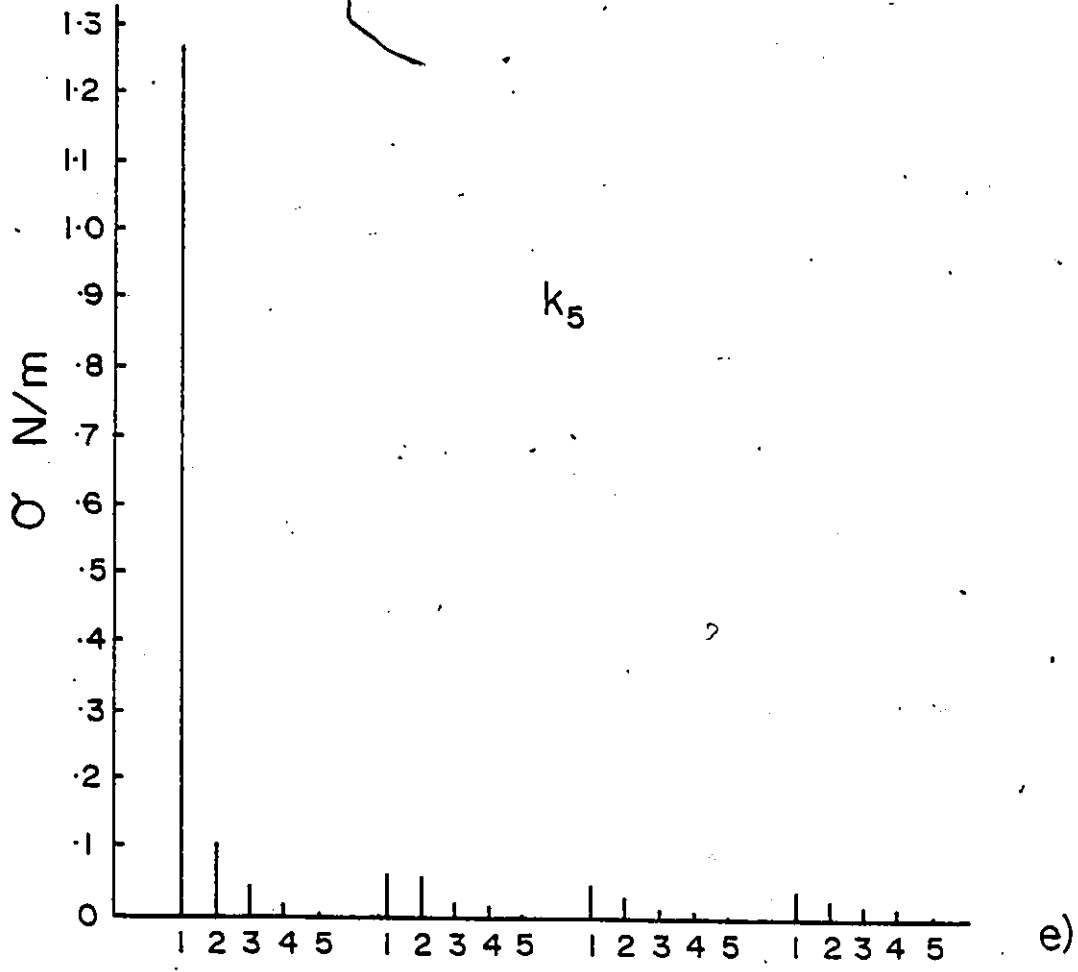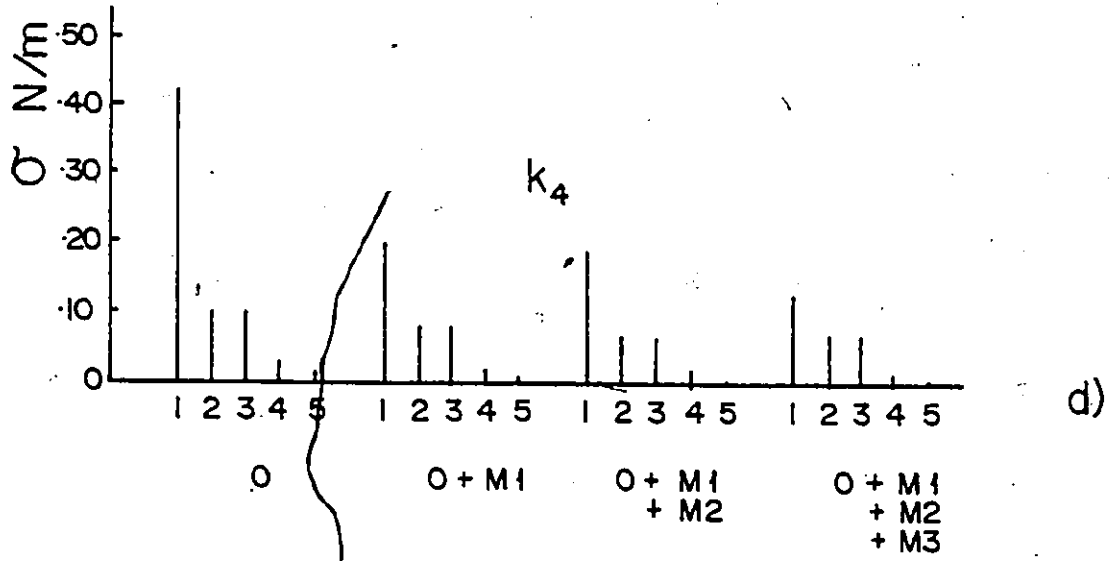
Figure 3.3 Standard Deviations of Springs k_1-k_5
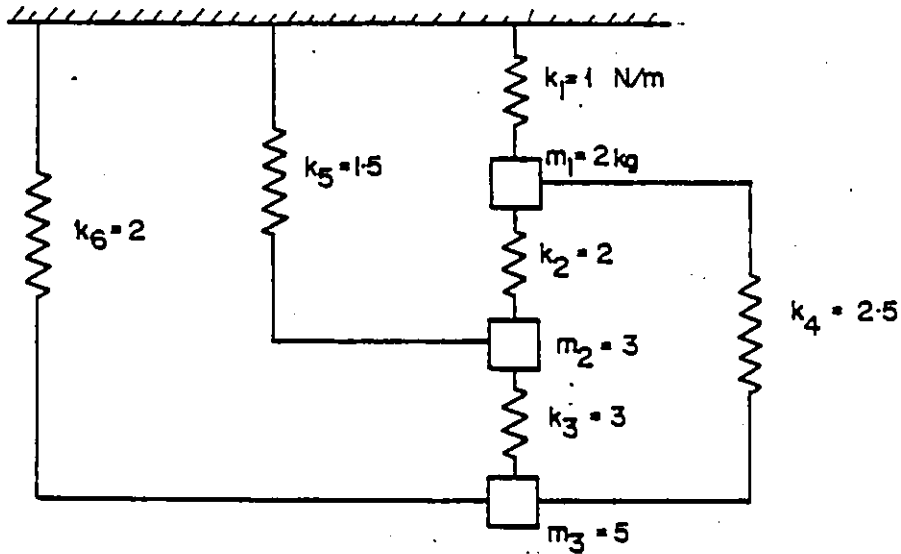
Figure 3.4 Three Degrees of Freedom System with
Six Springs
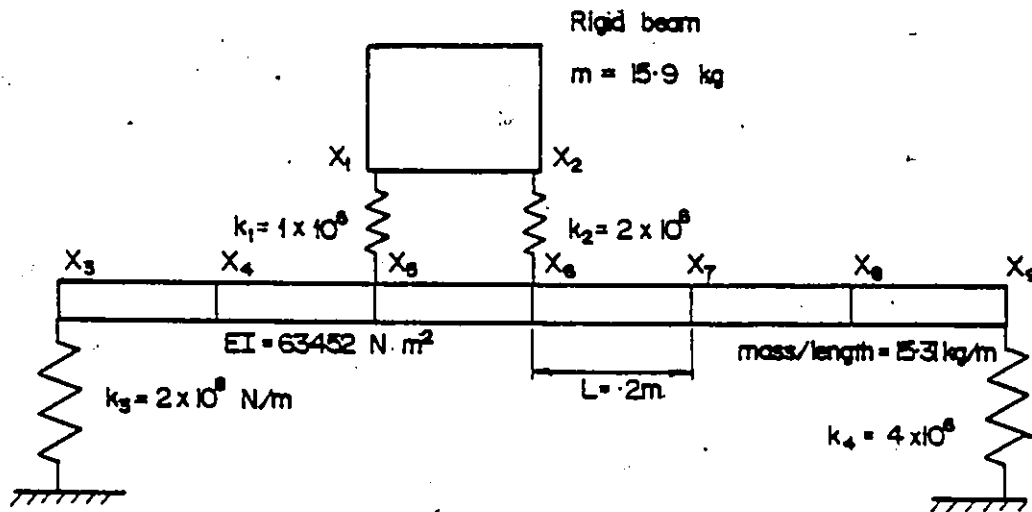
Figure 3.5 Theoretical Structure Used for Partial
Identification
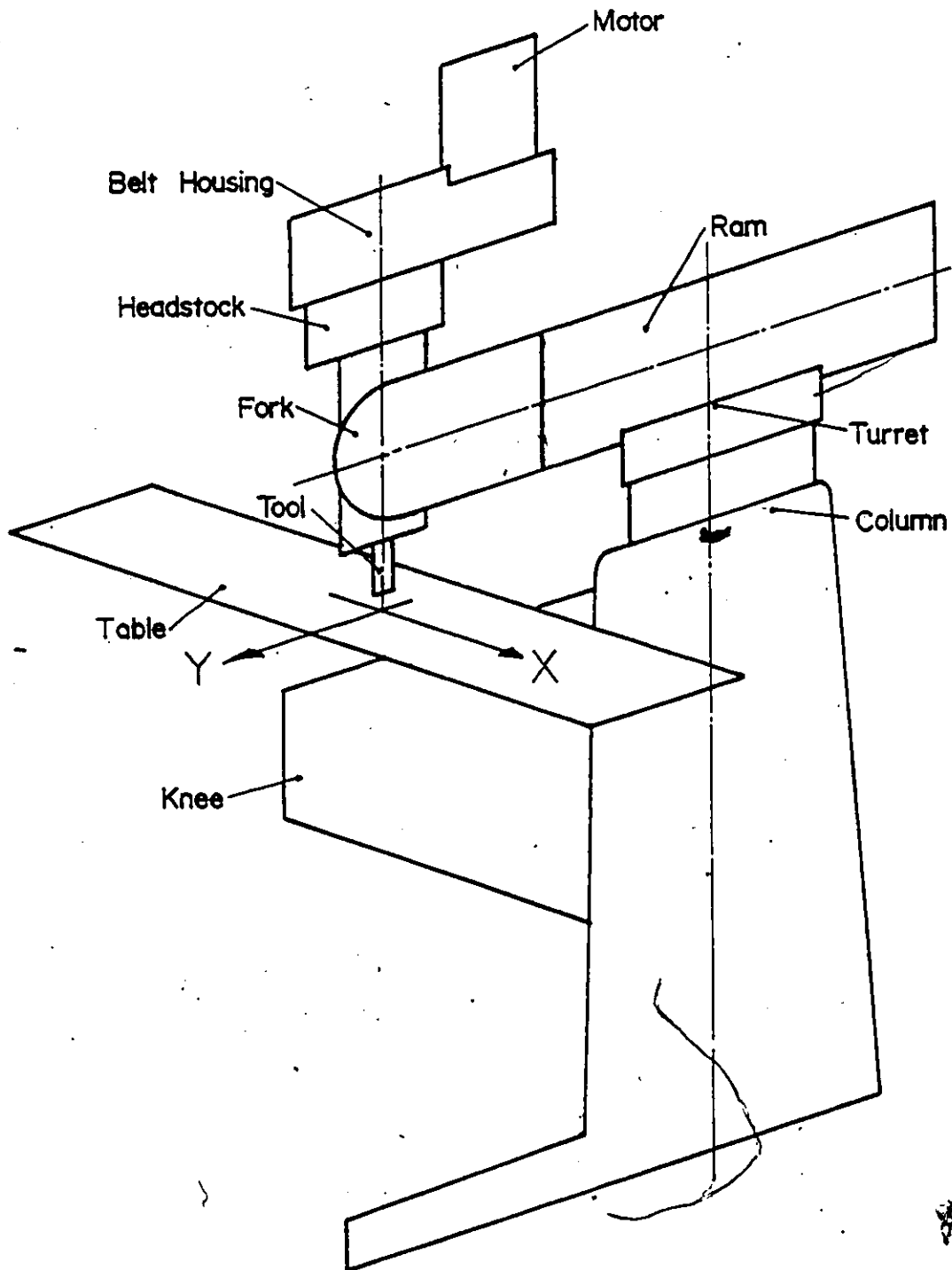
Figure 4.1 Ram Type Milling Machine
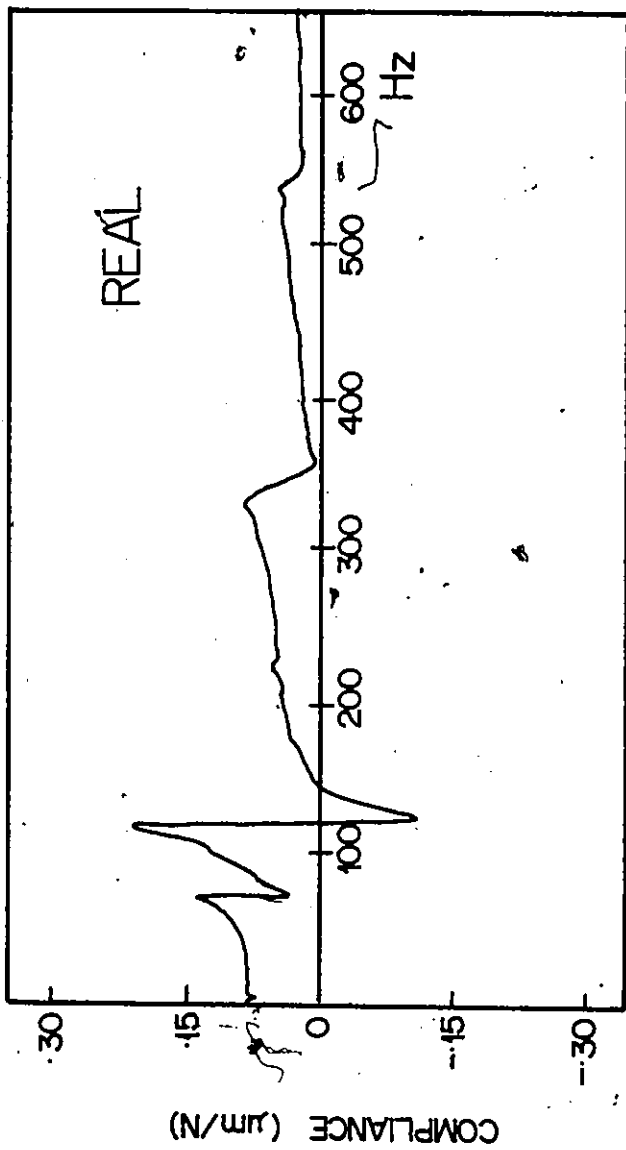
Figure 4.2   Real Part of Measured Relative TF Between Tool
and Workpiece, Motor On

214

f₁= 22 Hz

f_2= 72·9 Hz

$X_2=1$
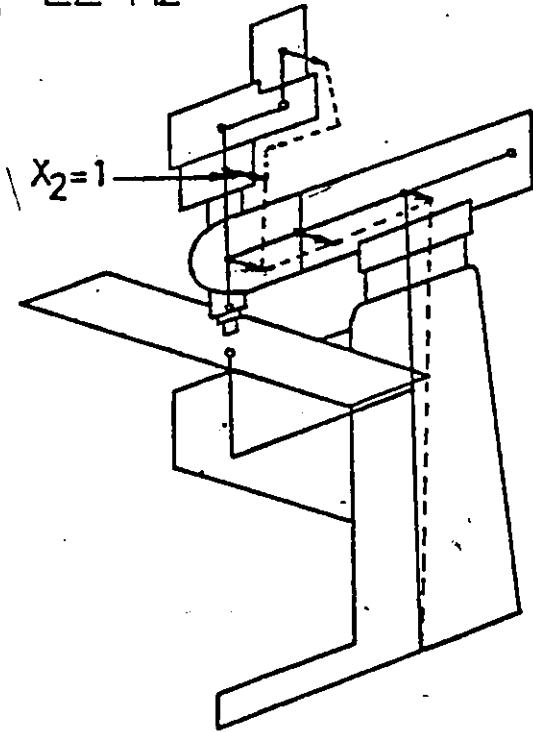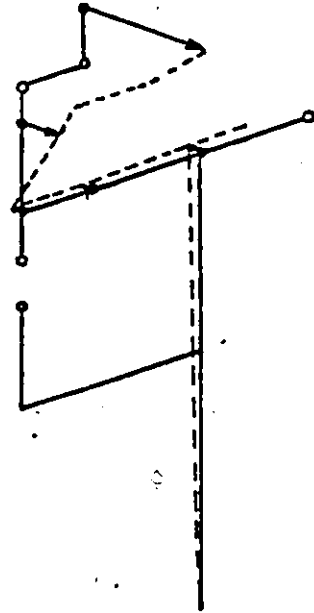
f_3 =122·1 Hz

f_4= 345 Hz

f_5= 538·3 Hz
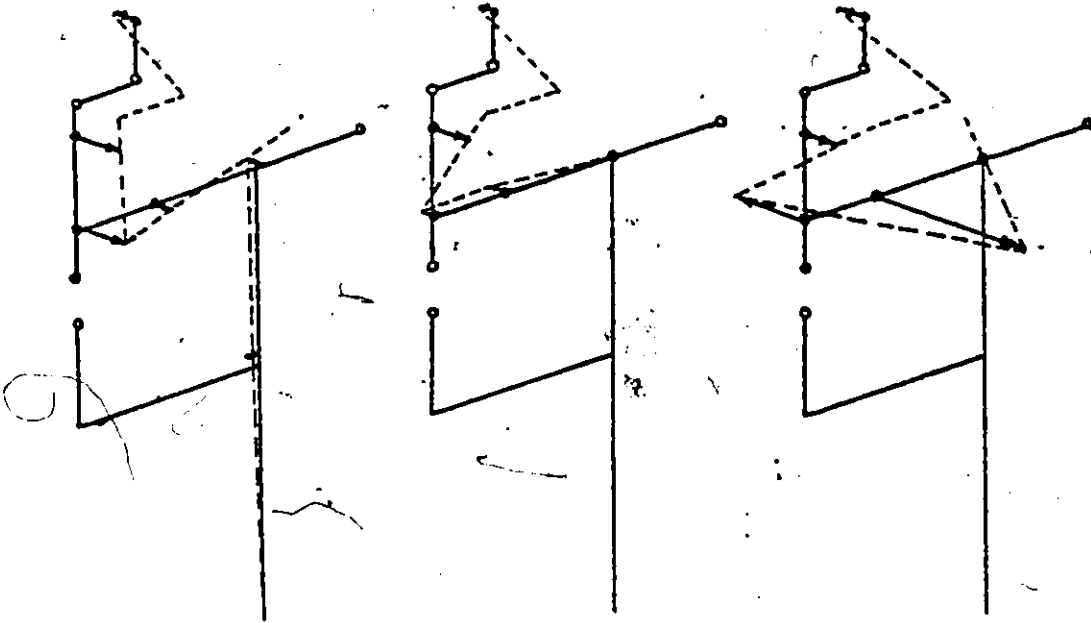
Figure 4.3   Measured Mode Shapes, Motor On
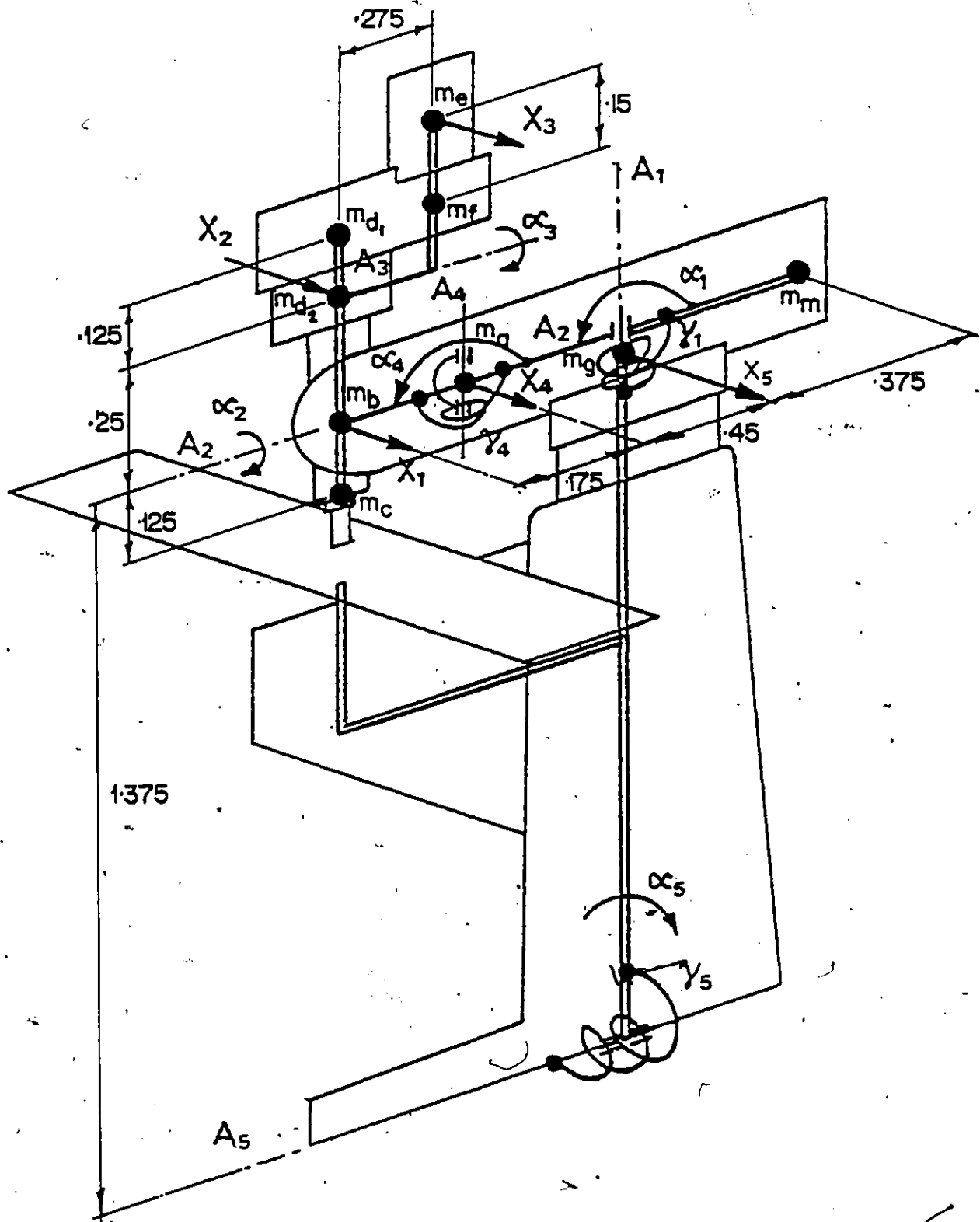
Figure 4.4 Vibratory Model of the Ram-Type Milling Machine
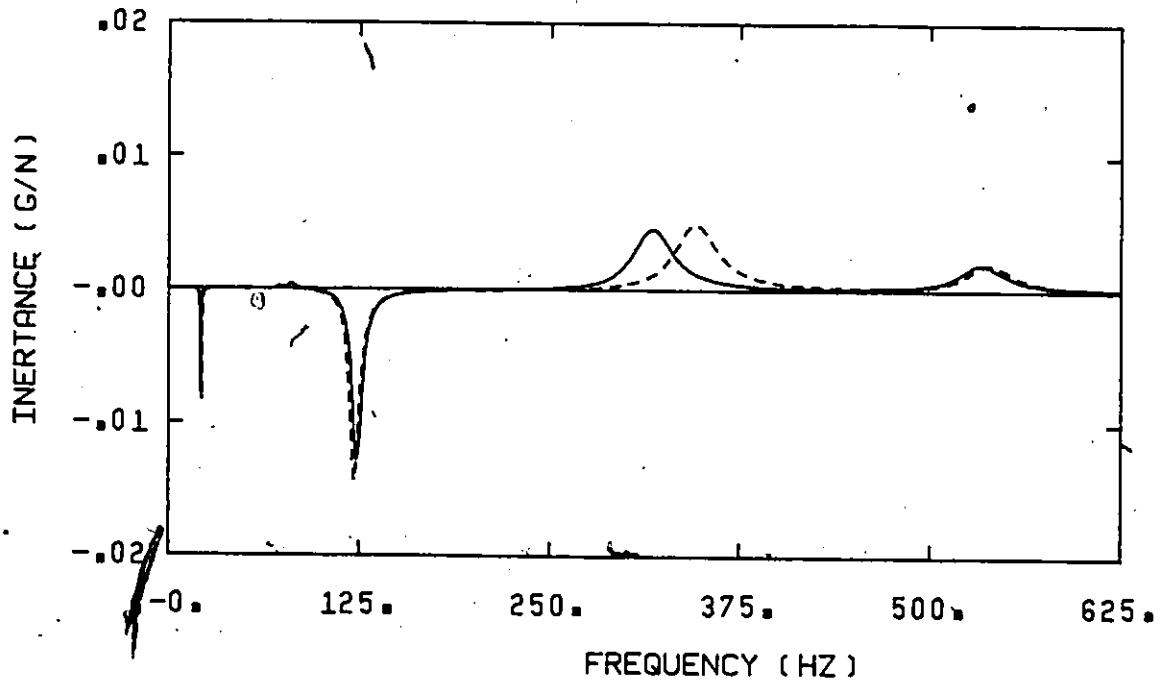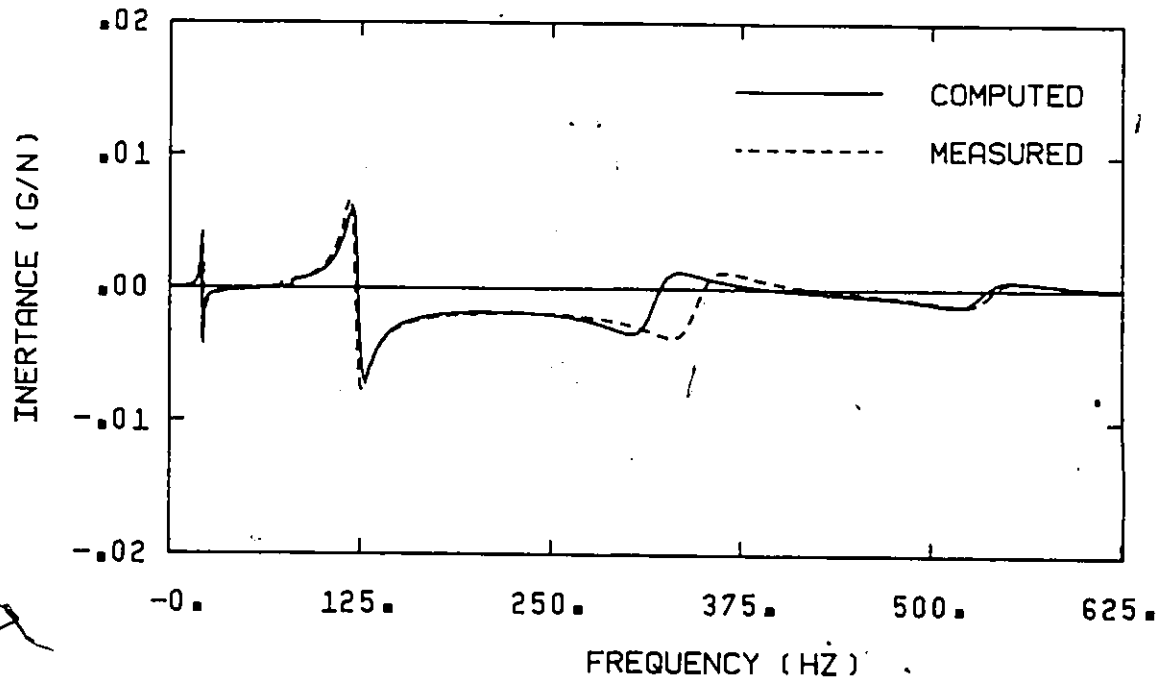
Figure 4.5   Measured and Computed Transfer Functions at
Coordinate x_1, Motor On
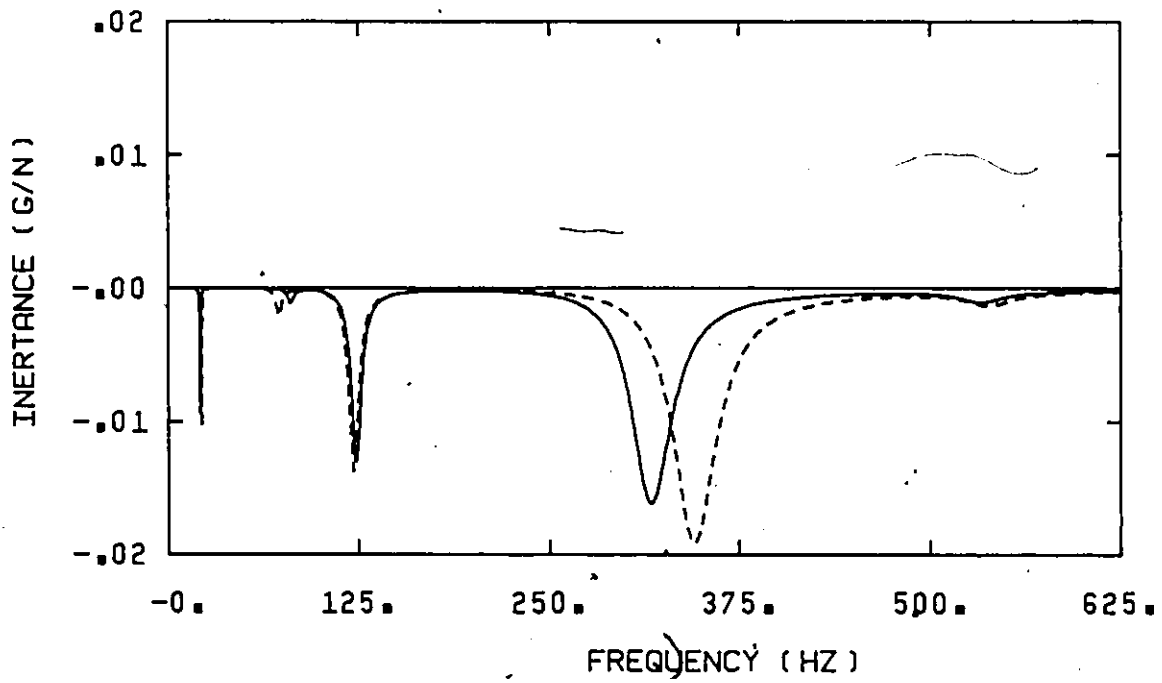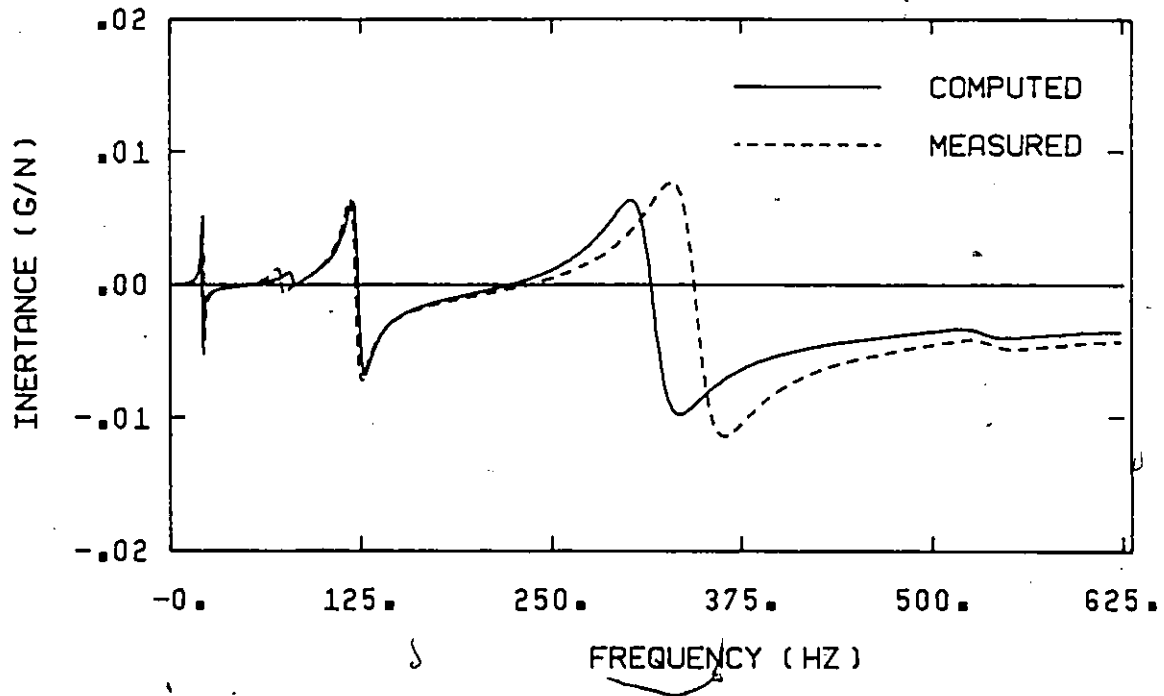
Figure 4.6   Measured and Computed Transfer Functions at
Coordinate x_2, Motor On
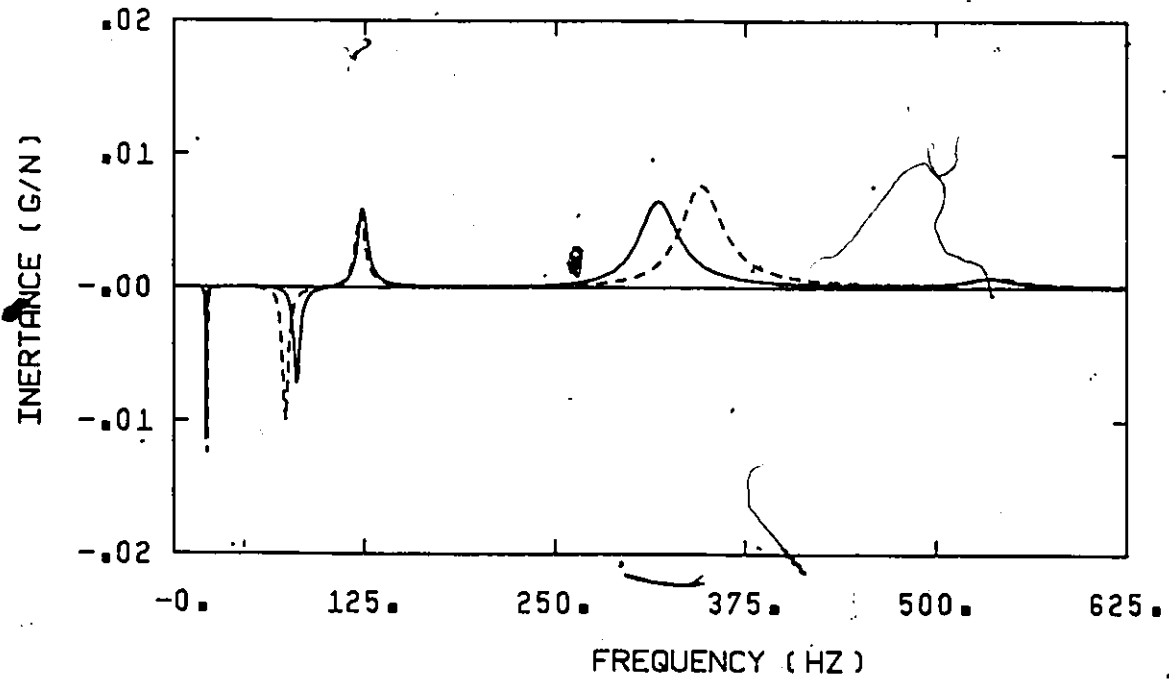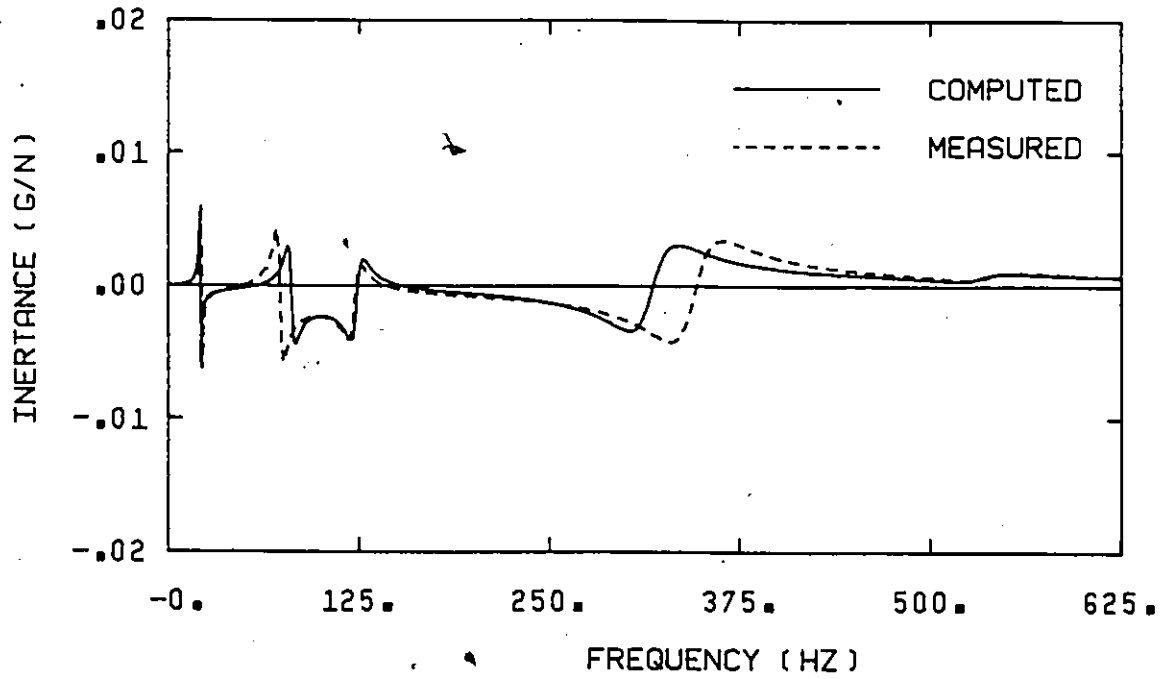
Figure 4.7   Measured and Computed Transfer Functions
             at Coordinate x_3, Motor On
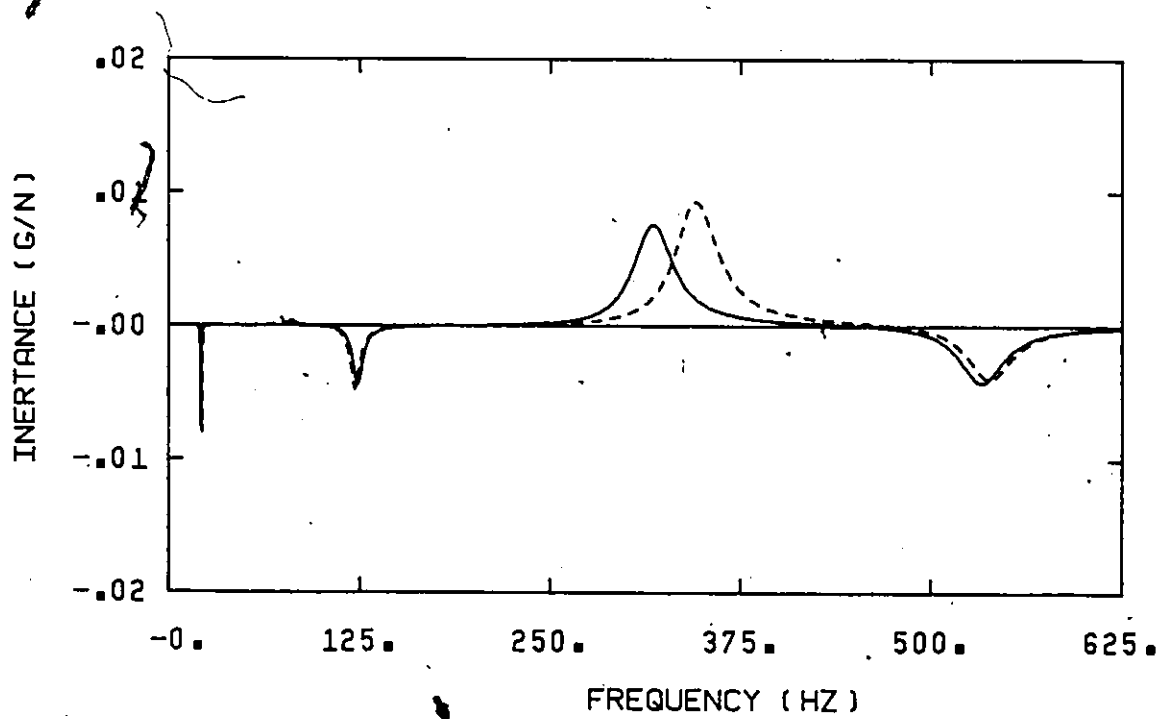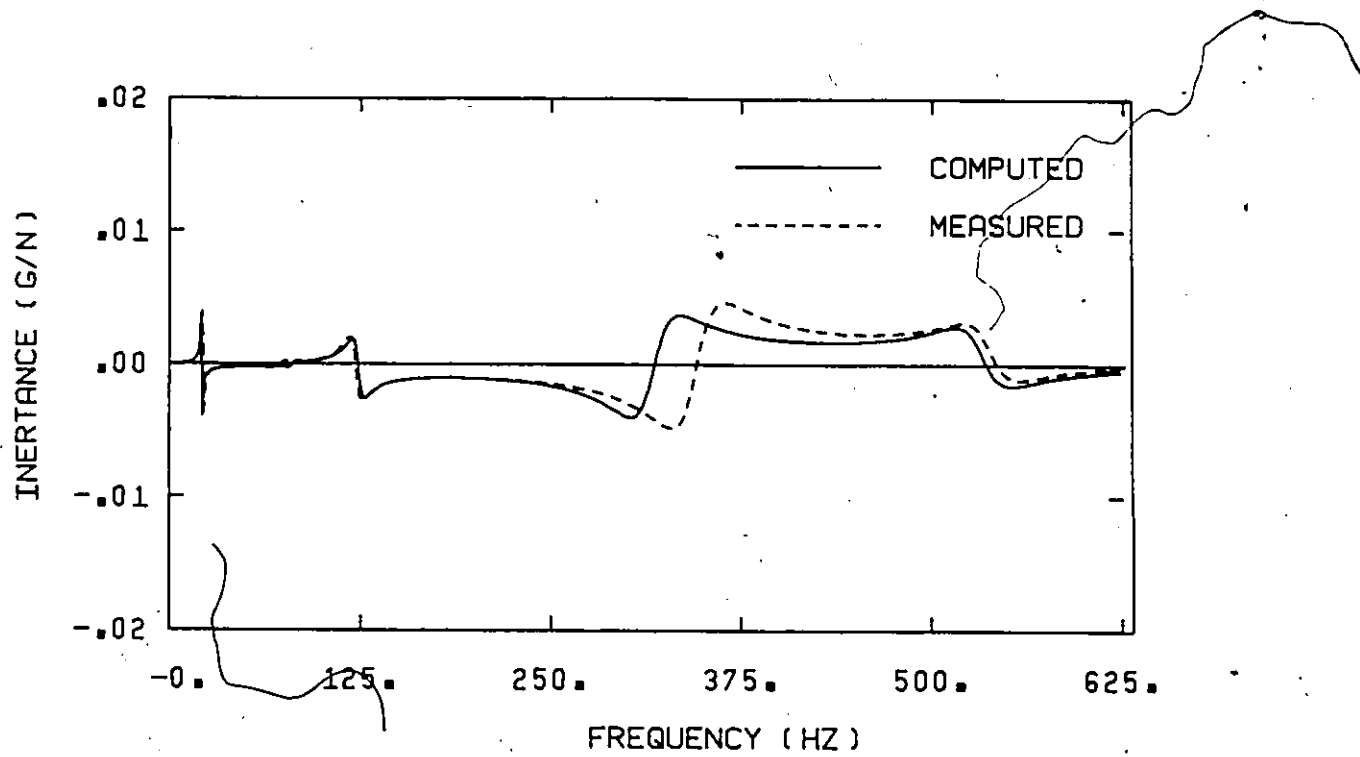
Figure 4.8   Measured and Computed Transfer Function at
Coordinate x_4, Motor On
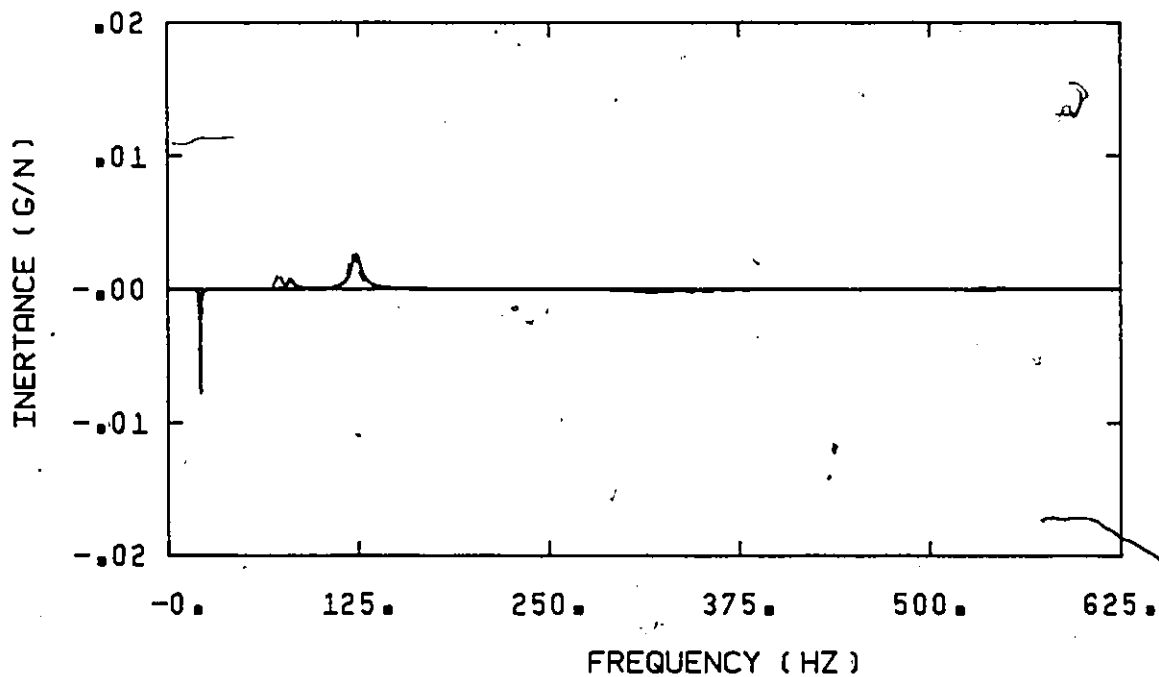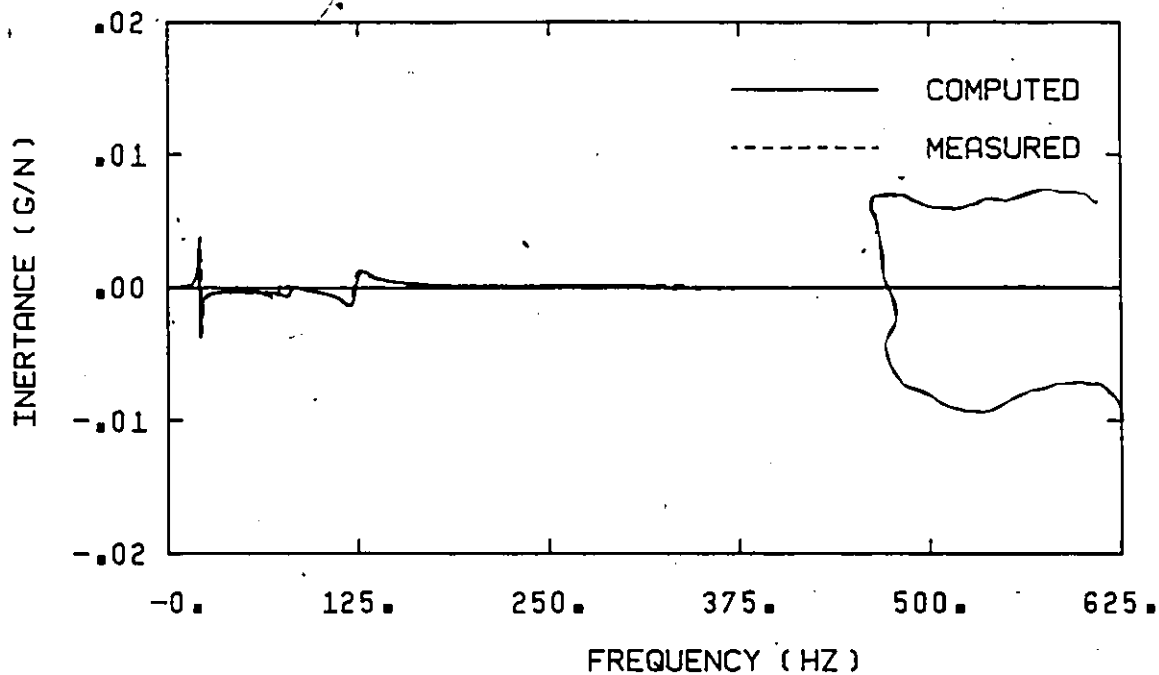
Figure 4.9   Measured and Computed Transfer Functions at
Coordinate x_5, Motor On
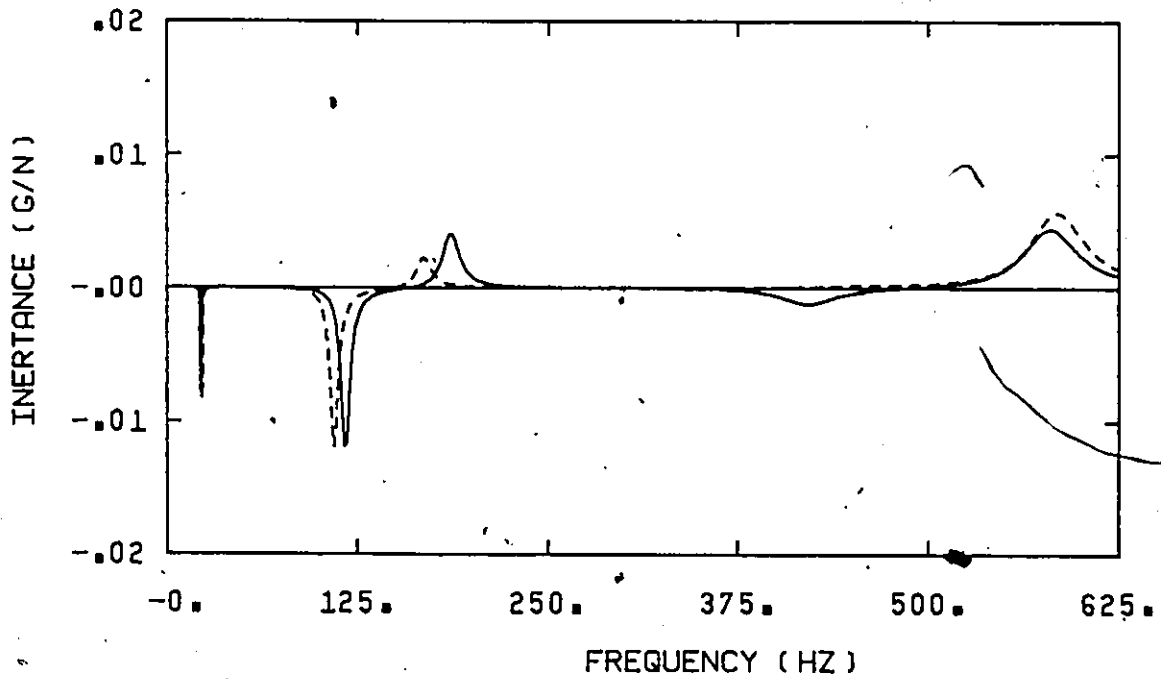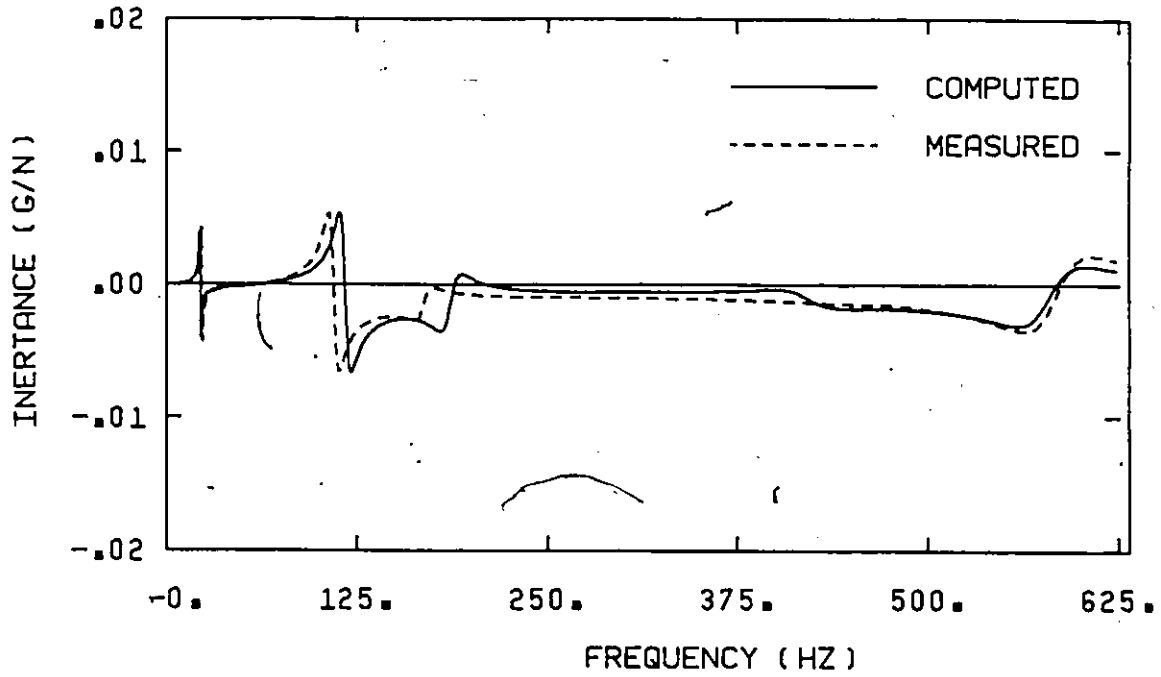
Figure 4.10   Measured and Computed Transfer Functions at
Coordinate x_1, Motor Off
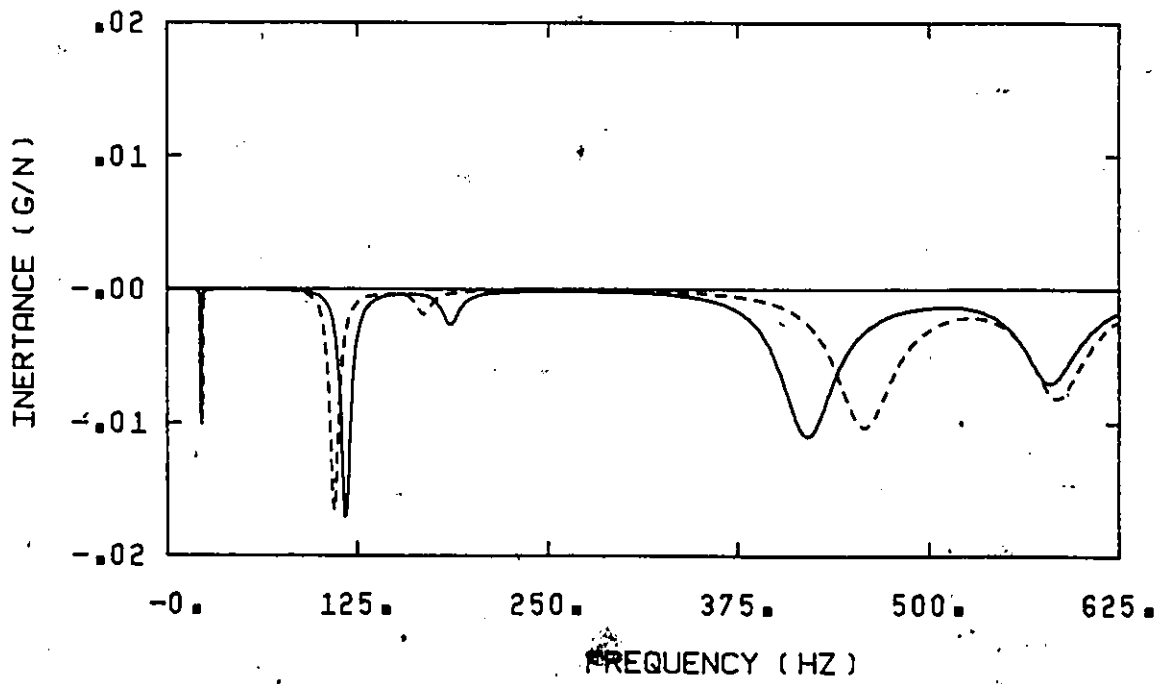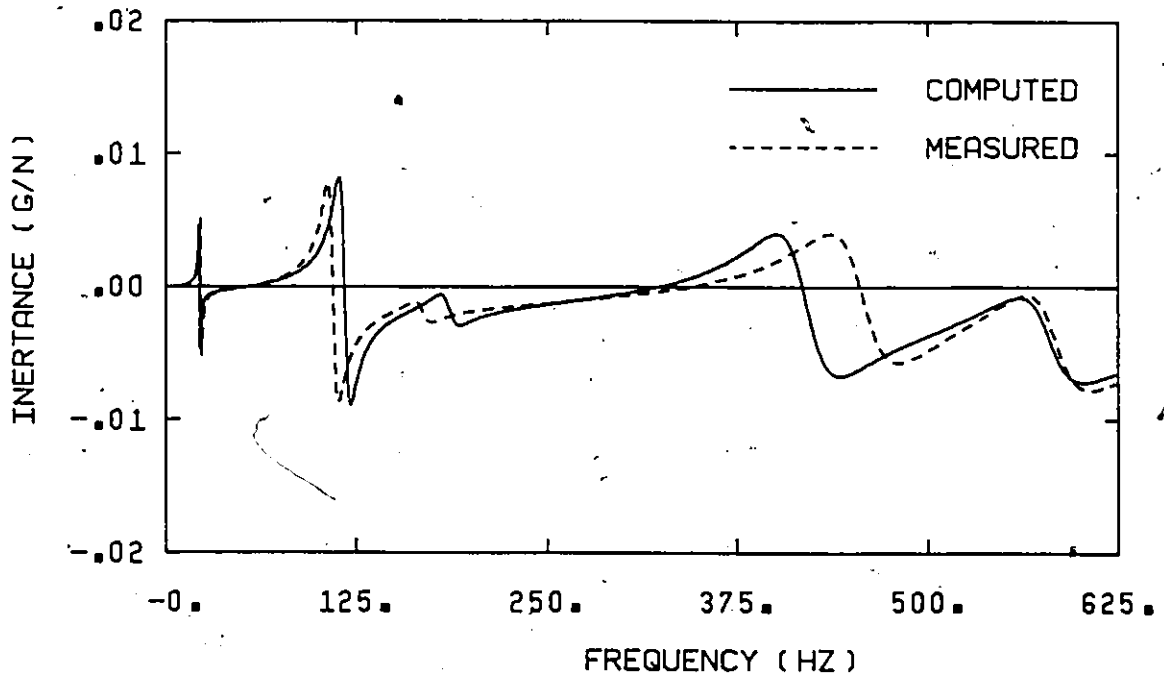
Figure 4.11   Measured and Computed Transfer Functions at
Coordinate x_2, Motor Off
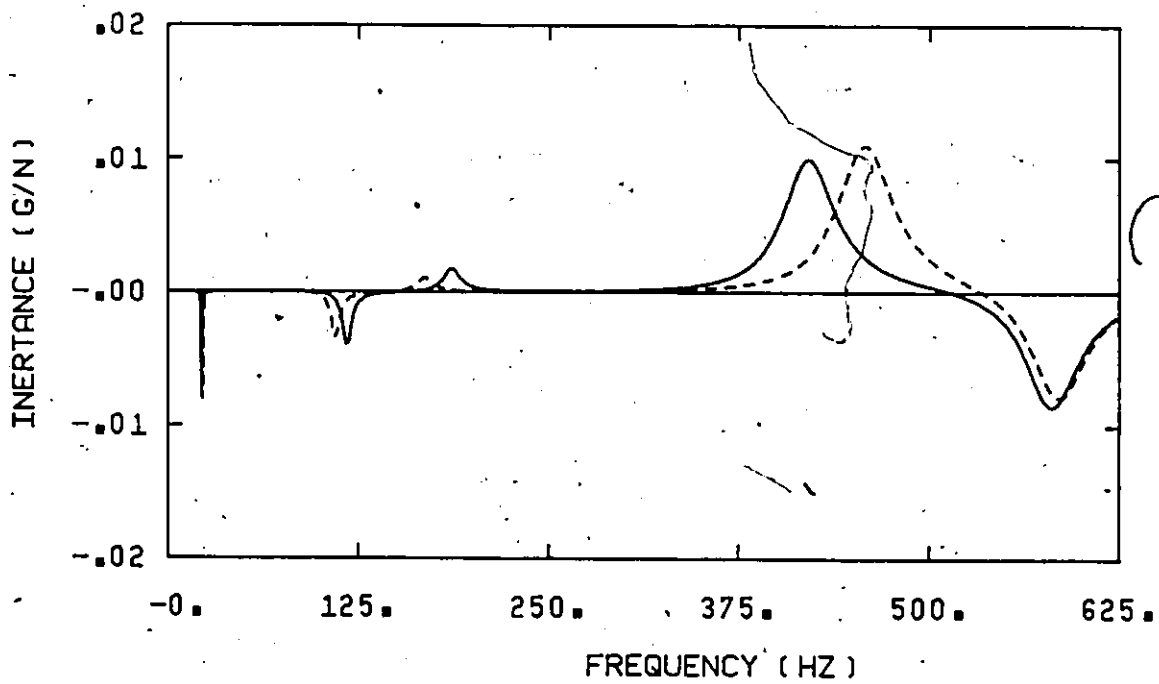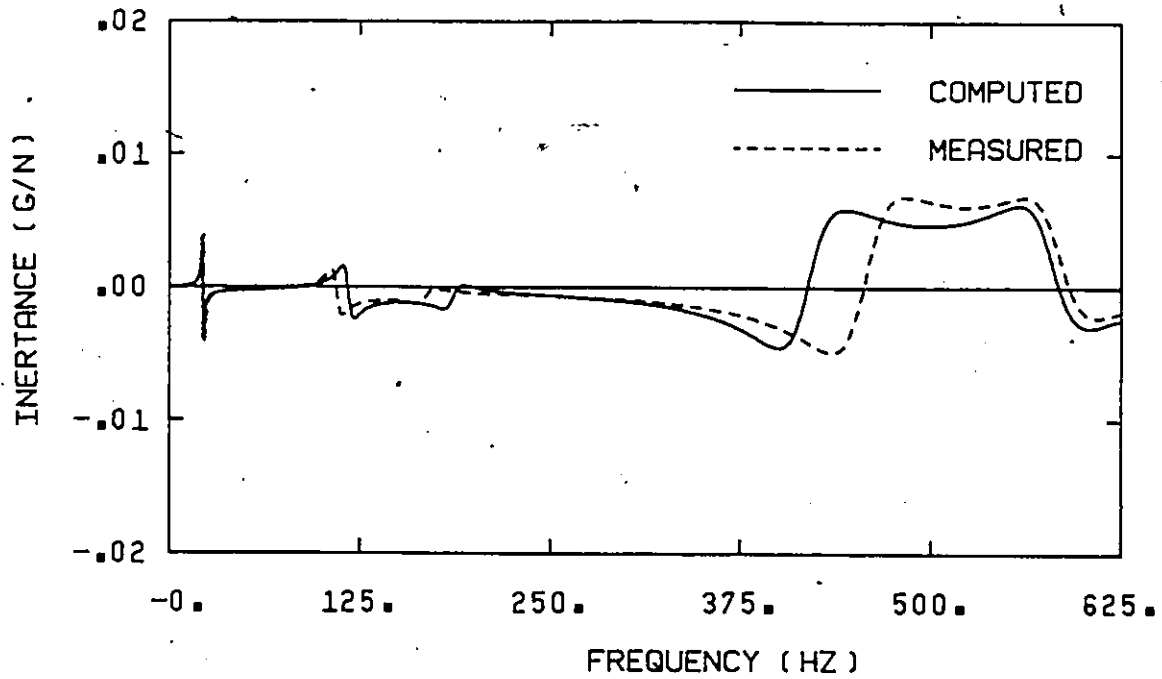
Figure 4.12   Measured and Computed Transfer Functions at
Coordinate x_4, Motor Off
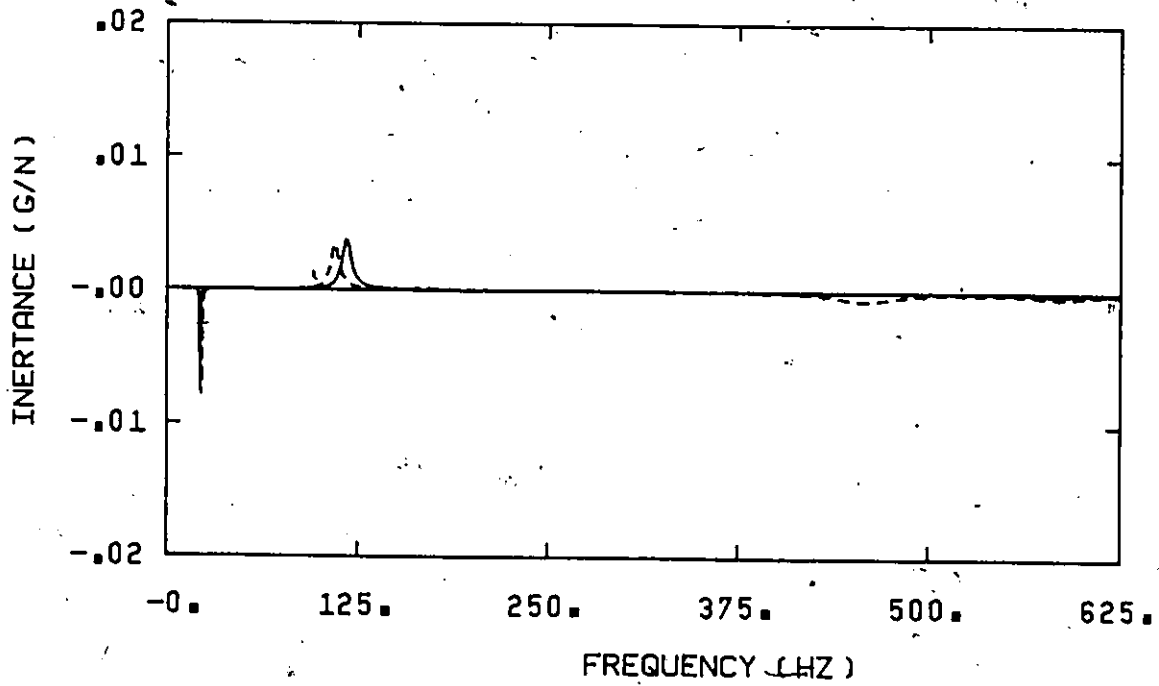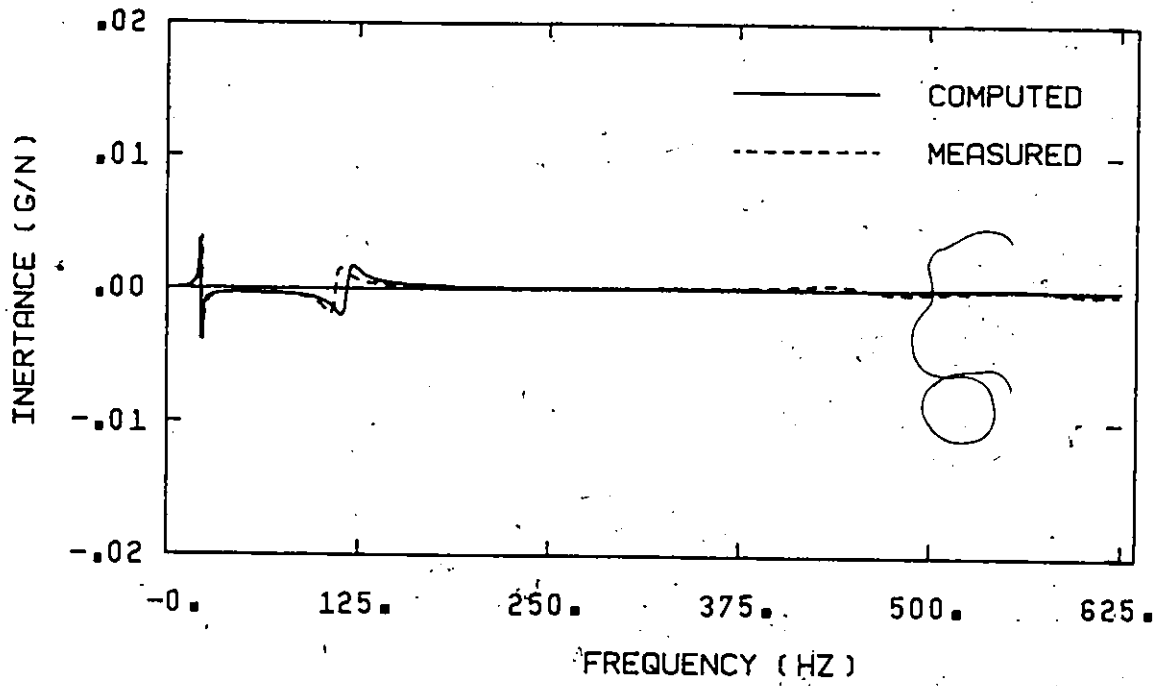
Figure 4.13 Measured and Computed Transfer Functions
at Coordinate x_5, Motor Off
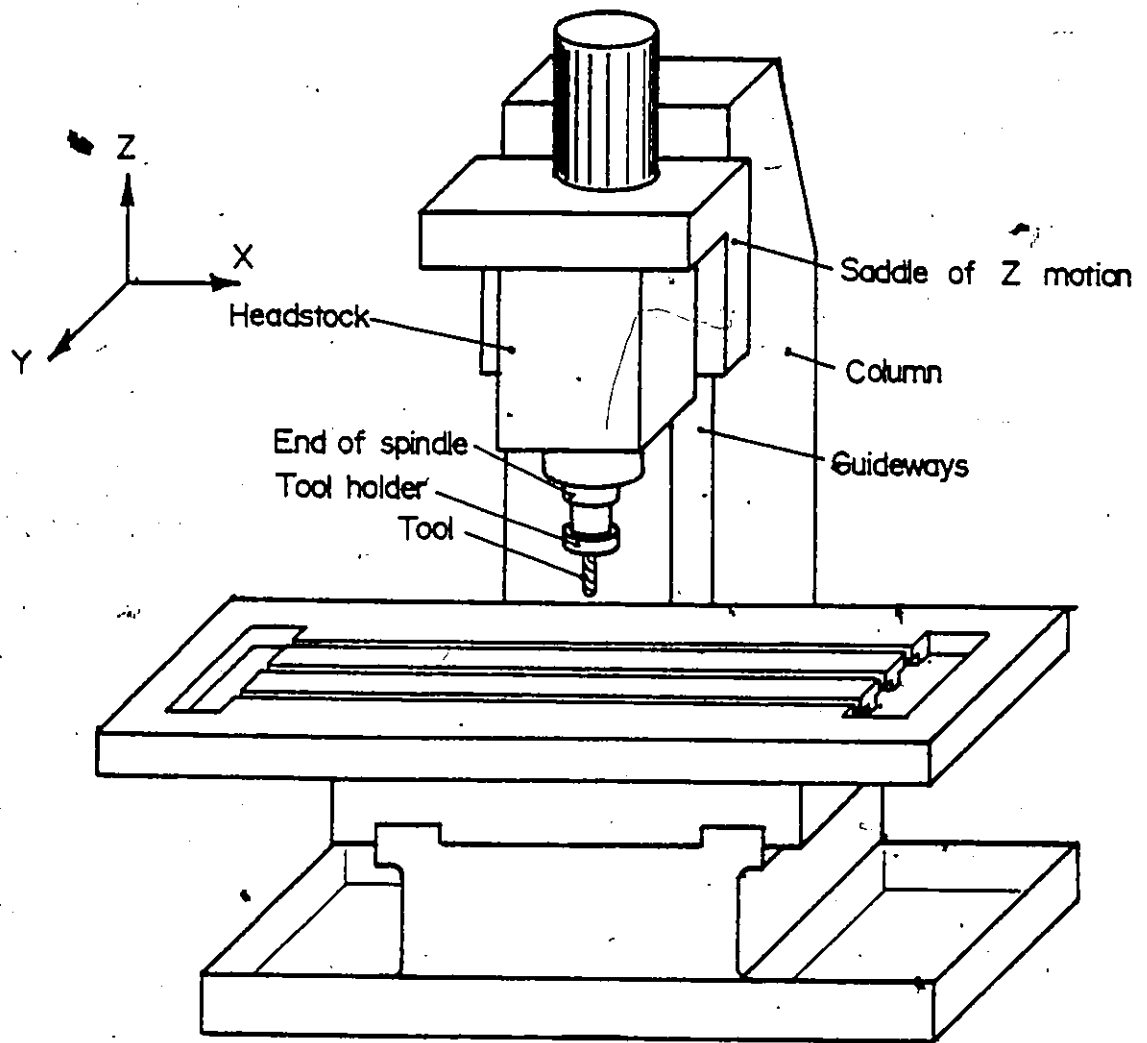
Figure 4.14 Schematic of Milling Machine
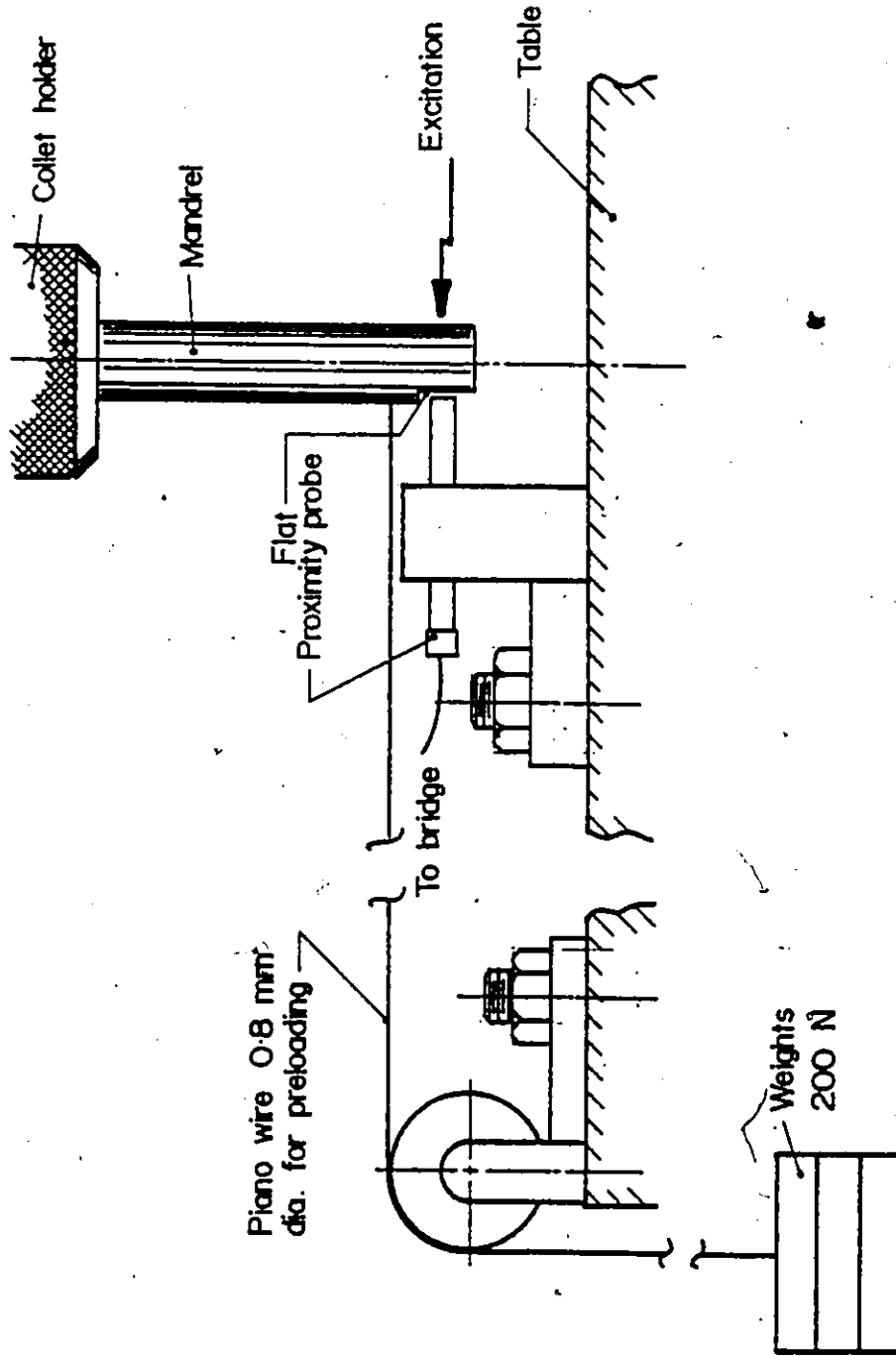
Figure 4.15 Measuring Relative TF
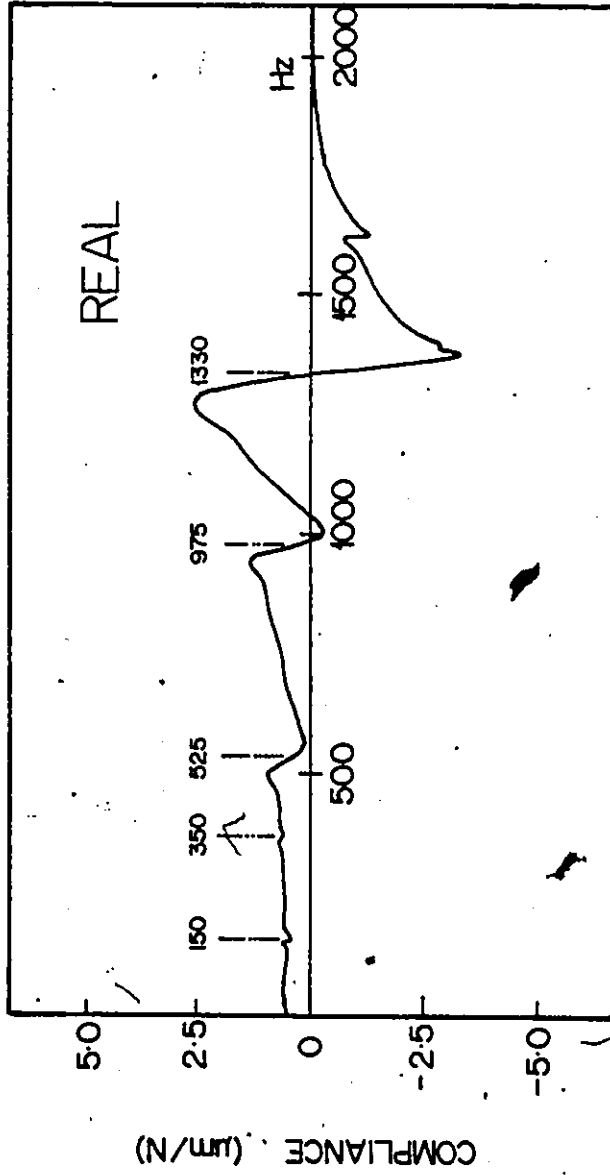
Figure 4.16 Measured Relative Transfer Function

TOP VIEW
Modes are shown
at levels ② and ③

Column

525 Hz

150 Hz

Headstock

350 Hz

X_1
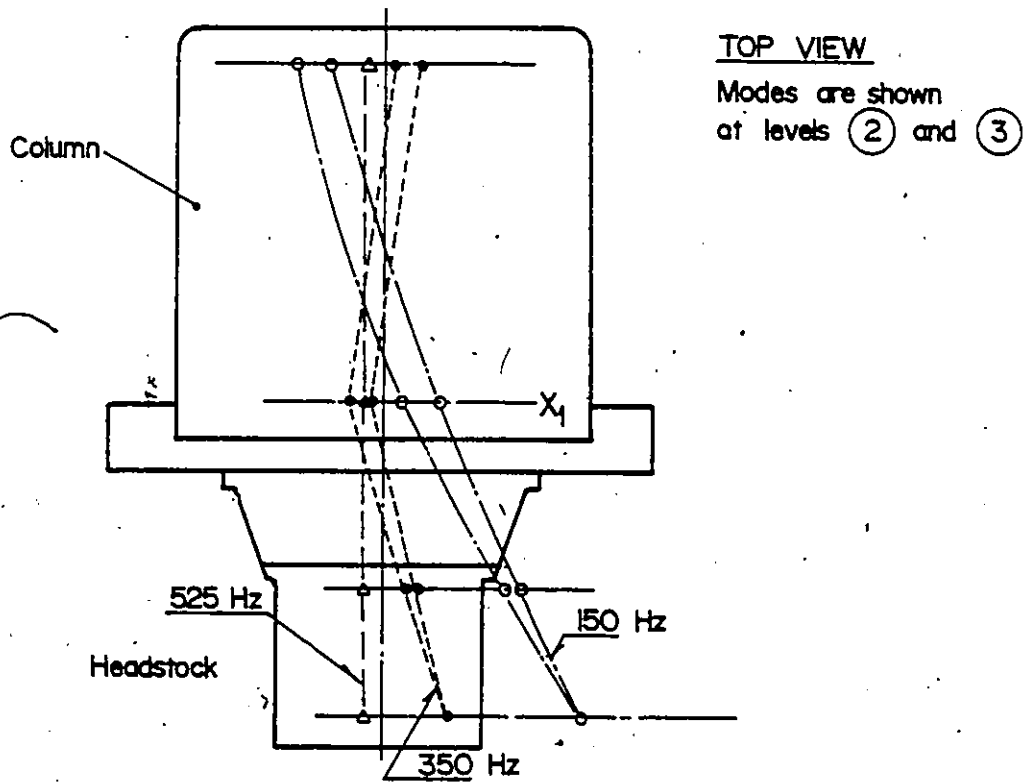
FRONT VIEW
Modes shown in
plane of spindle

③

350 Hz

X_2

150 Hz

②

X_3

①

525 Hz

Spindle end
Tool holder
Tool
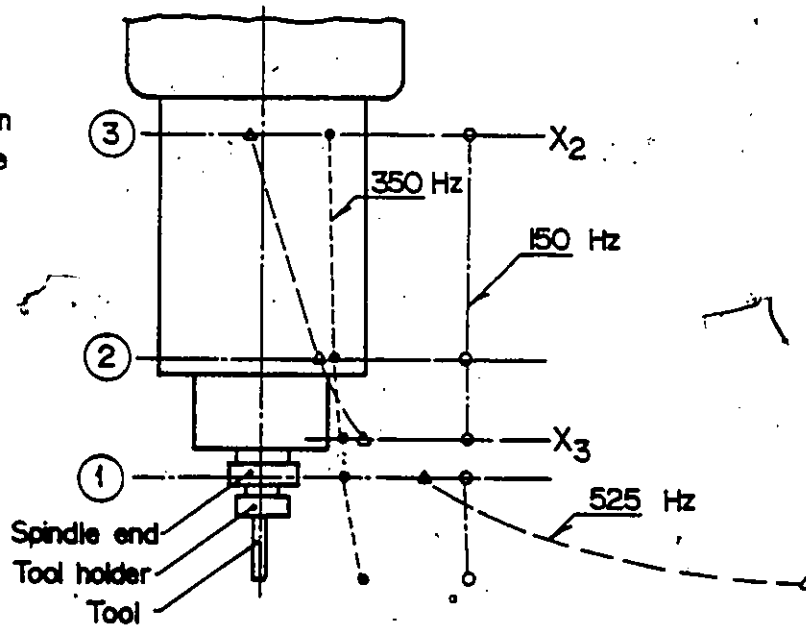
Figure 4.17   Measured Mode Shapes (Headstock and
Column)
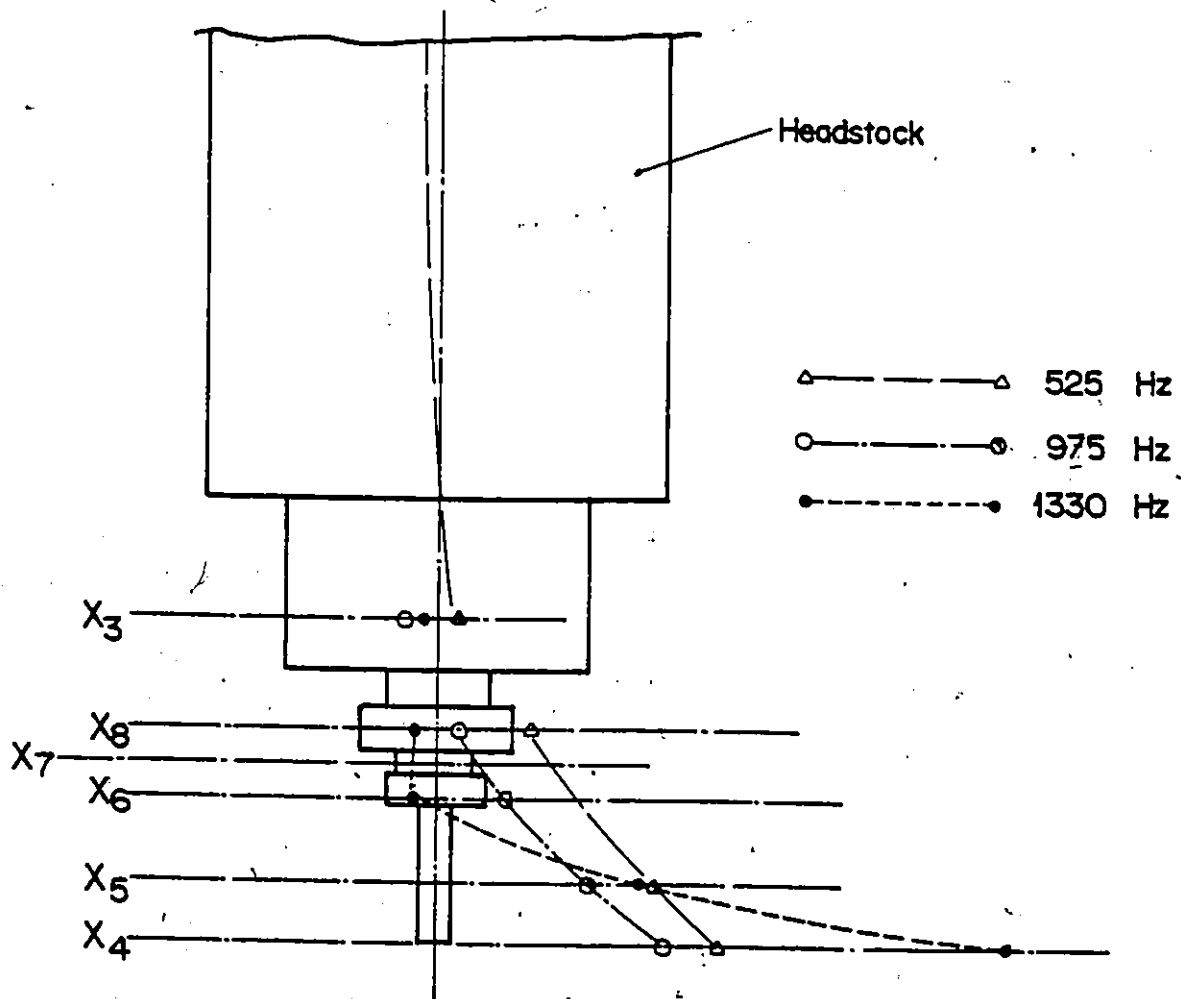
Figure 4.18 Measured Mode Shapes (Spindle-Tool
Holder-Tool)
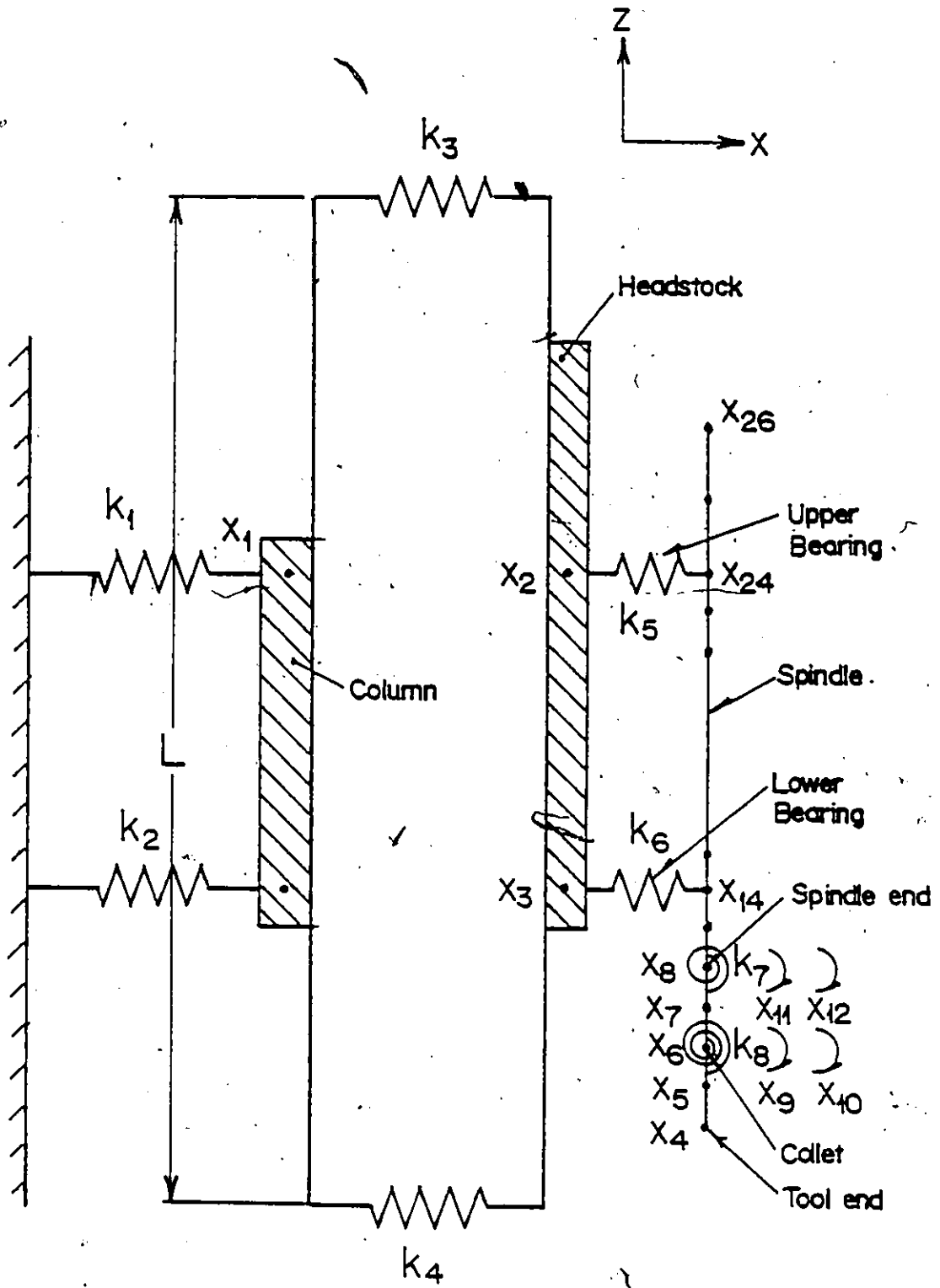
Figure 4.19 Model of Milling Machine
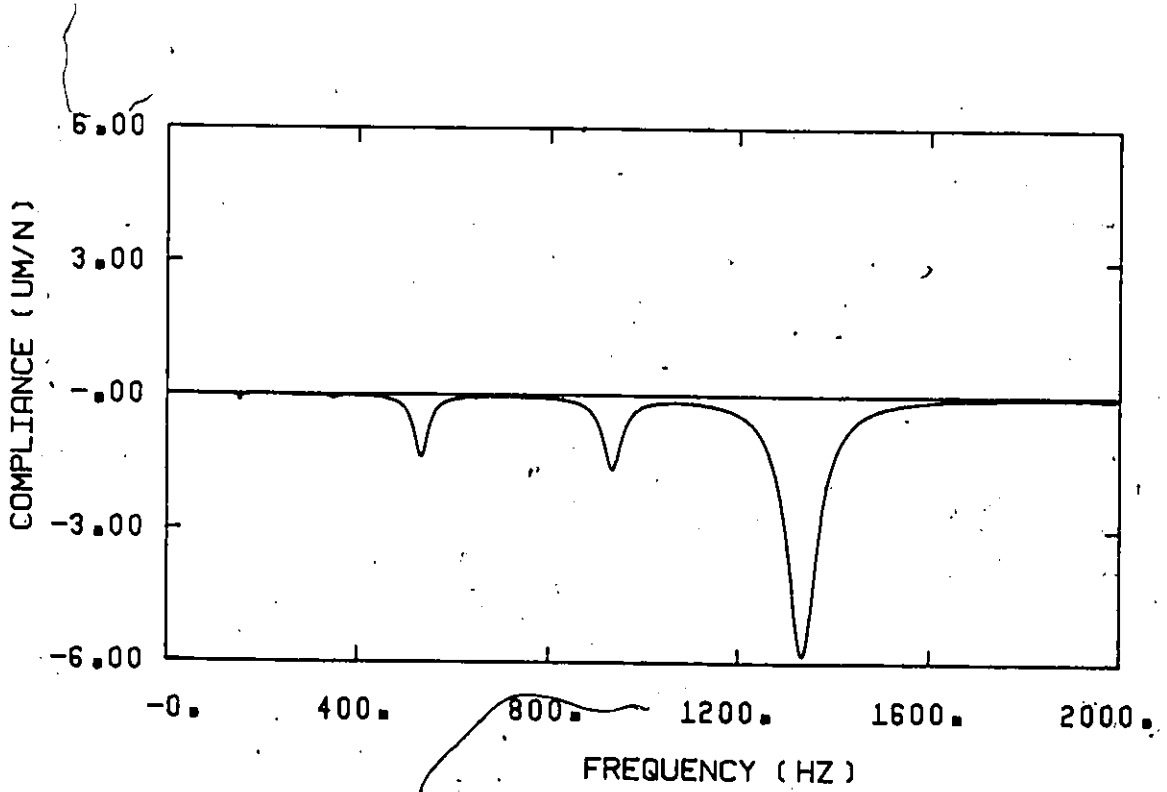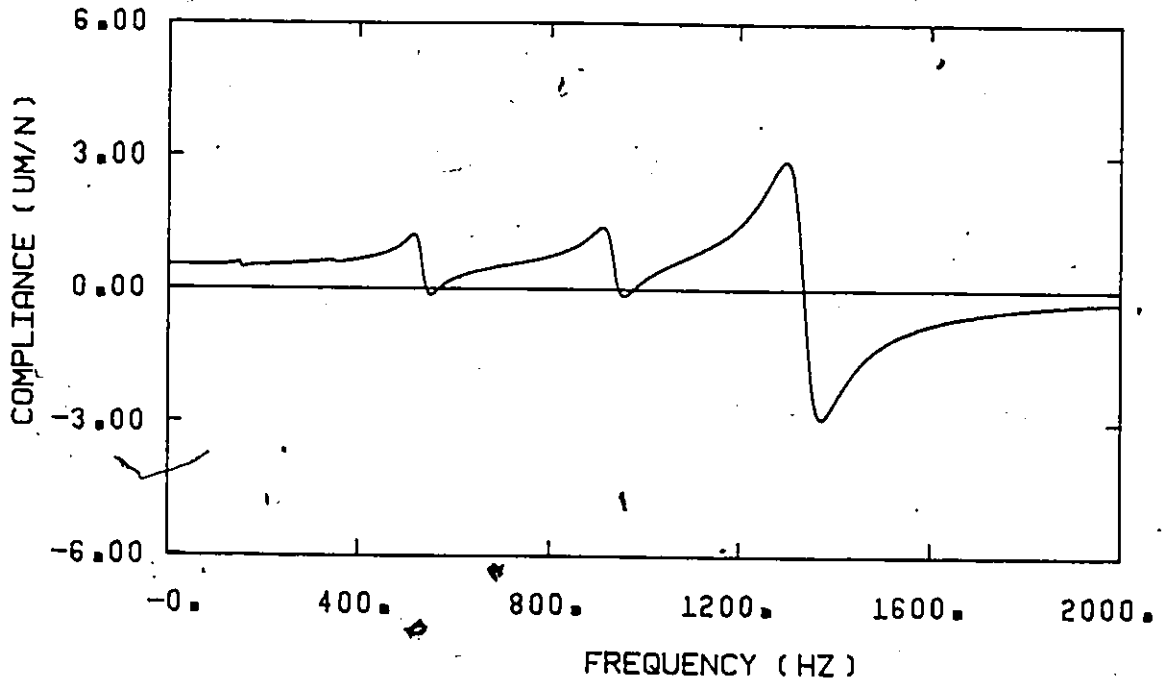
Figure 4.20 Computed Relative Transfer Function
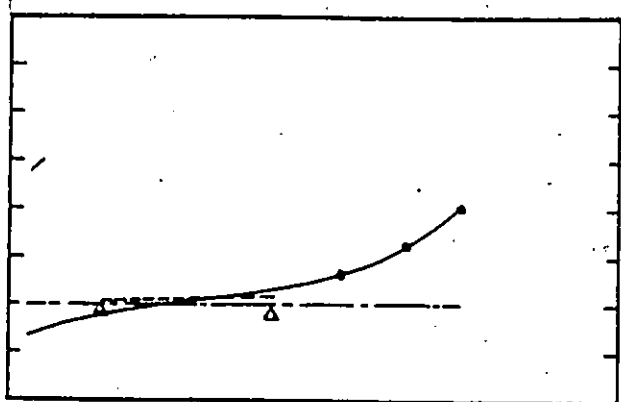
F = 534 Hz   K = 1·091 E7
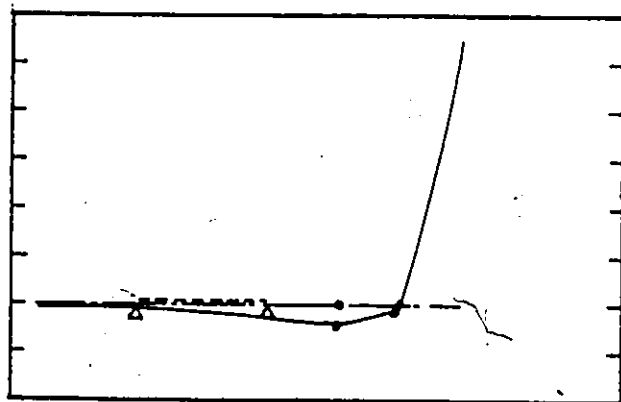
F = 1335 Hz   K = 3·060 E6
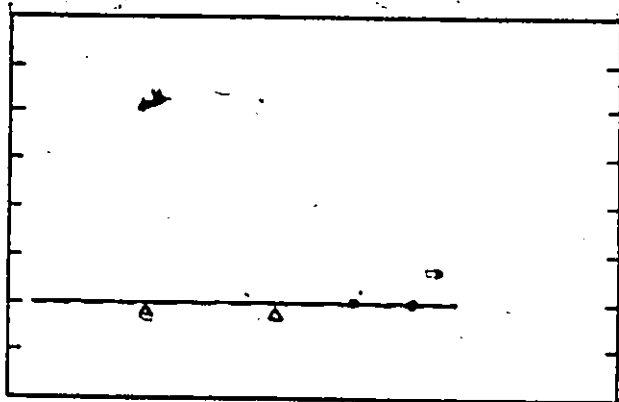
F = 717 Hz   K = 5·608 E9
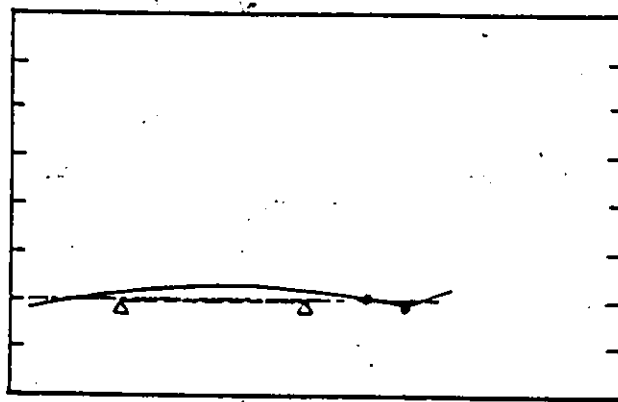
F = 2017 Hz   K = 2·170 E8
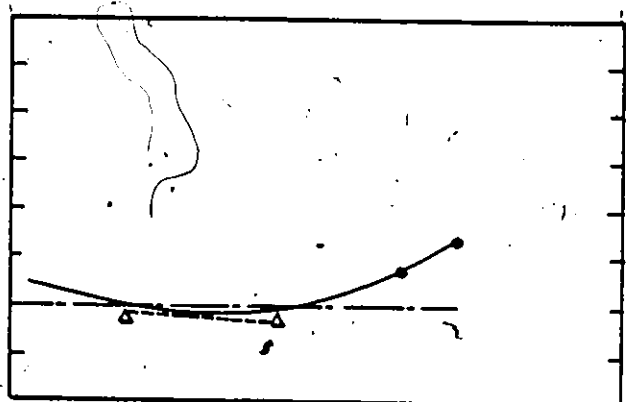
F = 934 Hz   K = 1·226 E7
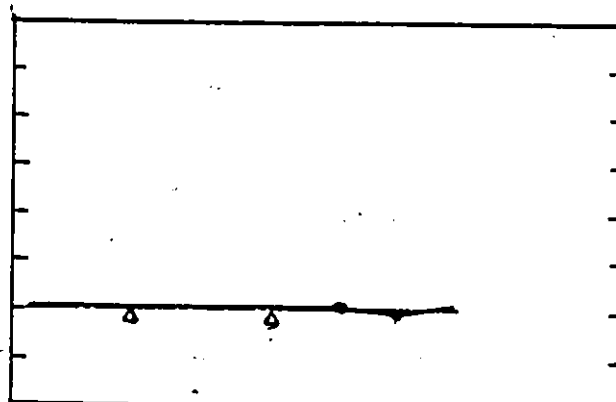
F = 3770 Hz   K = 9·951 E8

Figure 4.21   Computed Mode Shapes of Milling Machine

233
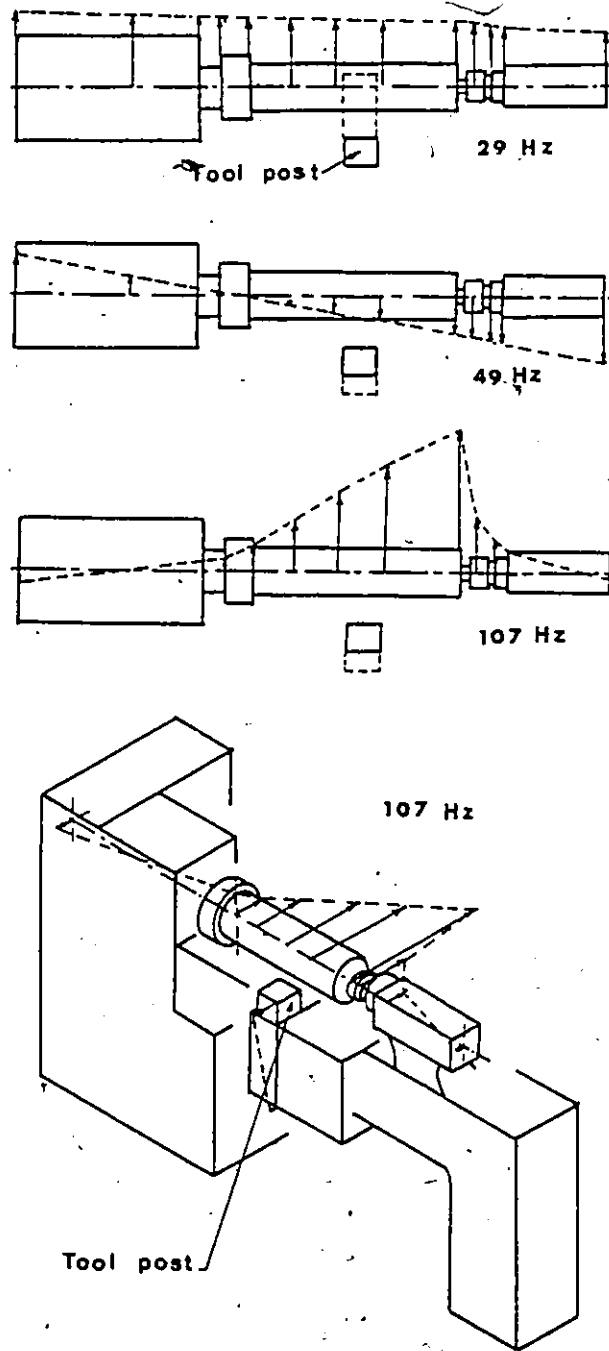
Figure 5.1 Mode Shapes of Heavy Workpiece

31 Hz

56 Hz

150 Hz

205 Hz

270 Hz

650 Hz

740 Hz
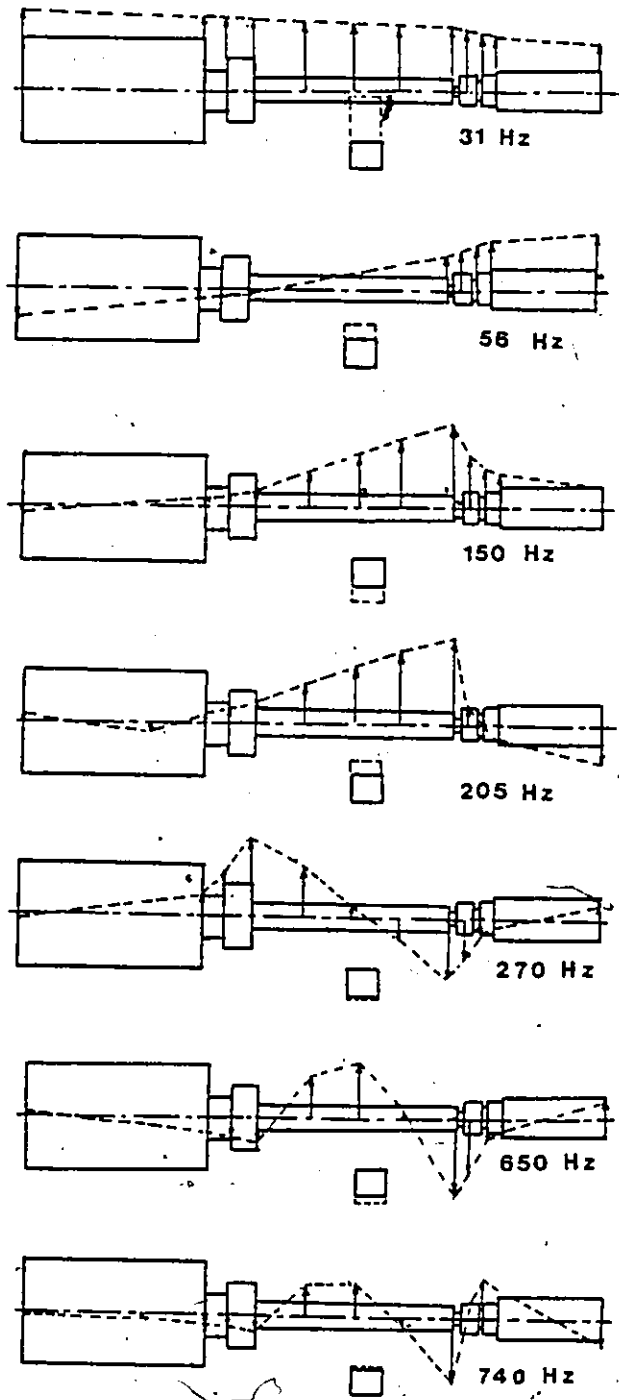
Figure 5.2   Mode Shapes of Slender Workpiece
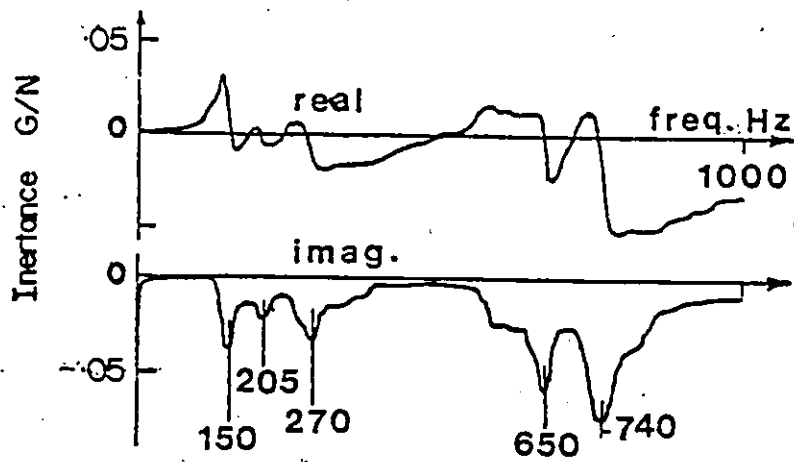
Figure 5.3 Measured TF at Tailstock End of Workpiece
in Figure 5.2
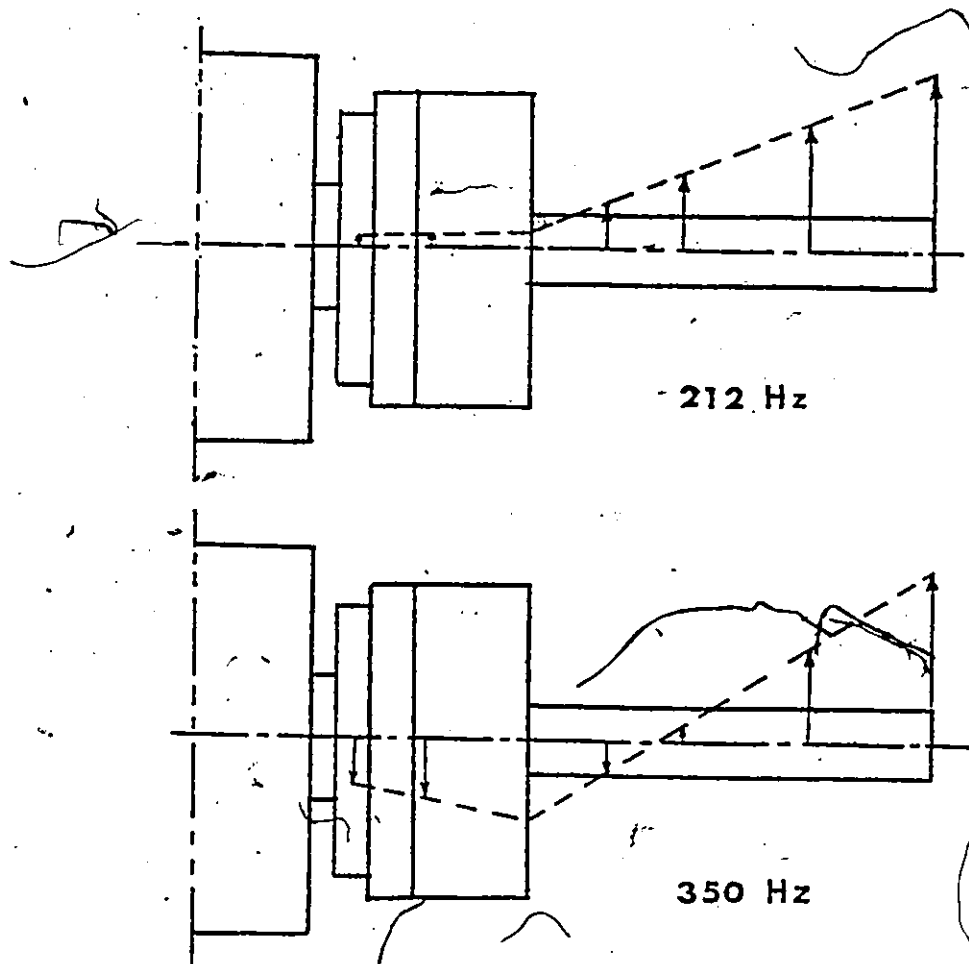
Figure 5.4 Mode Shapes of a Workpiece in Overhang
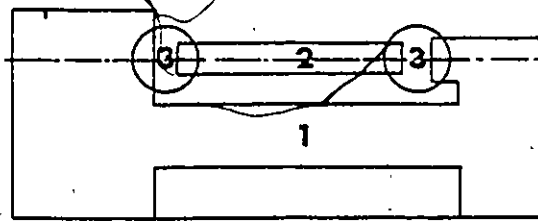
Figure 5.5 Three Components of a Lathe
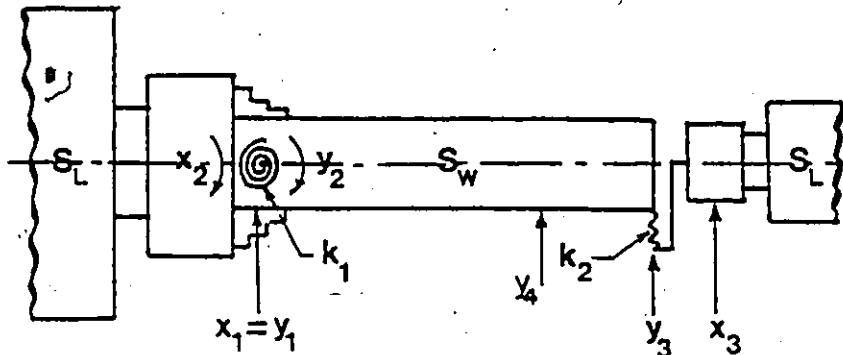
Figure 5.6 Model of a Lathe

0 Hz

0 Hz

775 Hz

2135 Hz
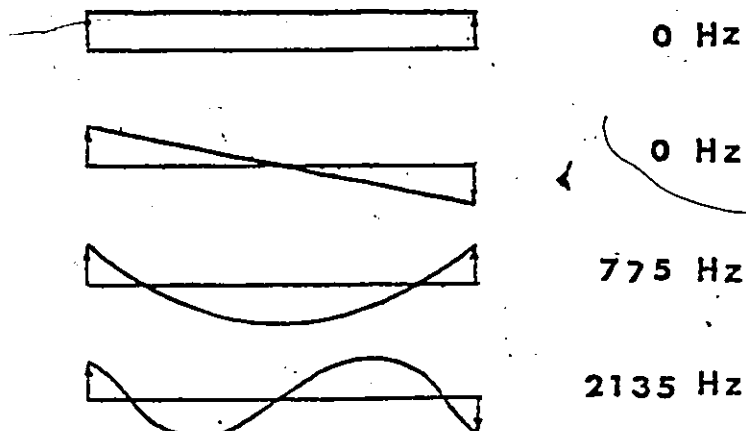
Figure 5.7 Free-Free Modes of Workpiece in Figure 5.2
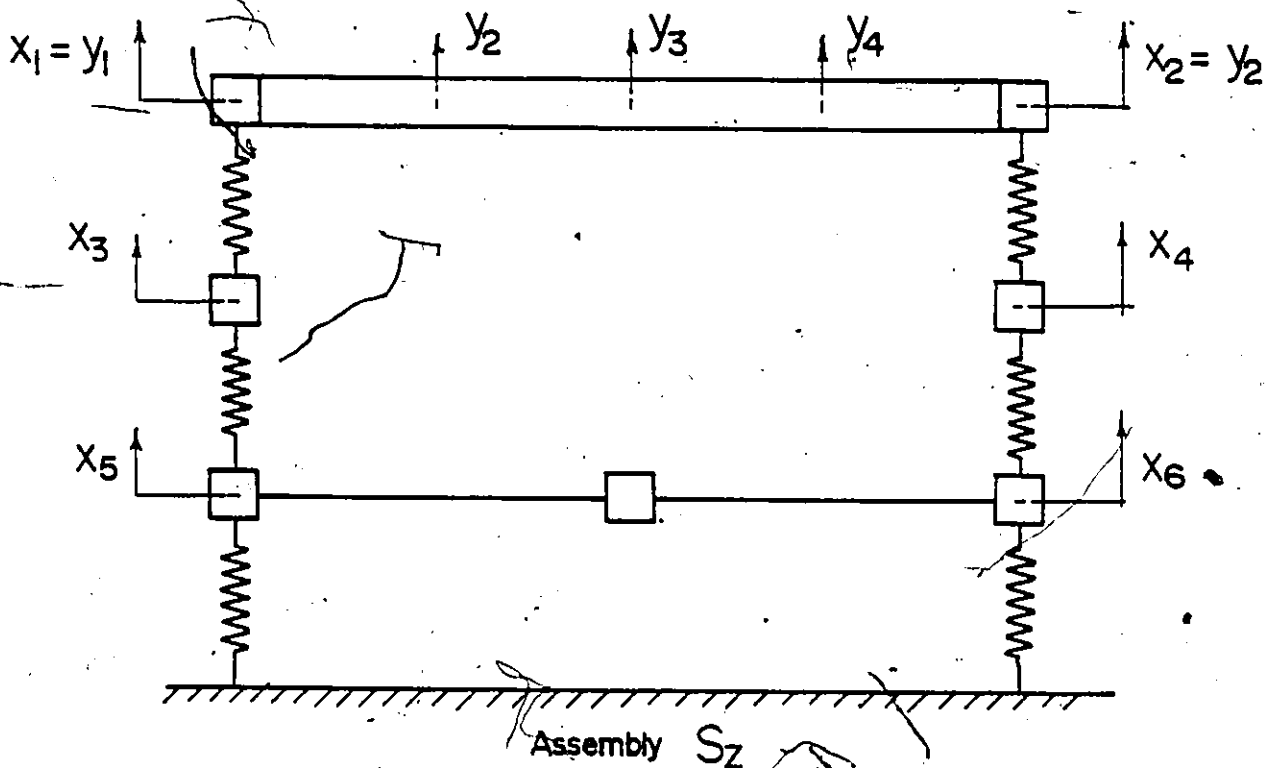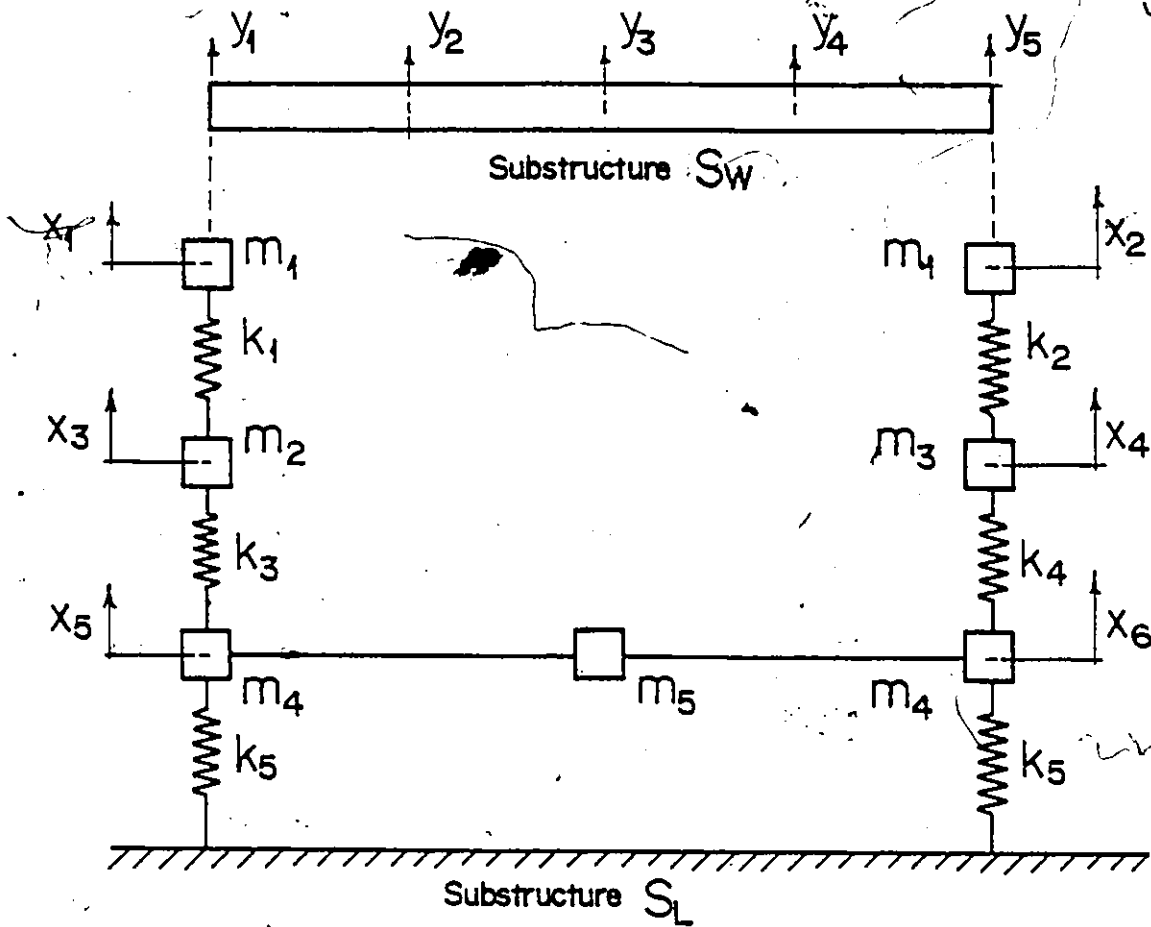
Figure 5.8 Theoretical Structure: Substructures S_W
and S_Z and Assembly S_Z
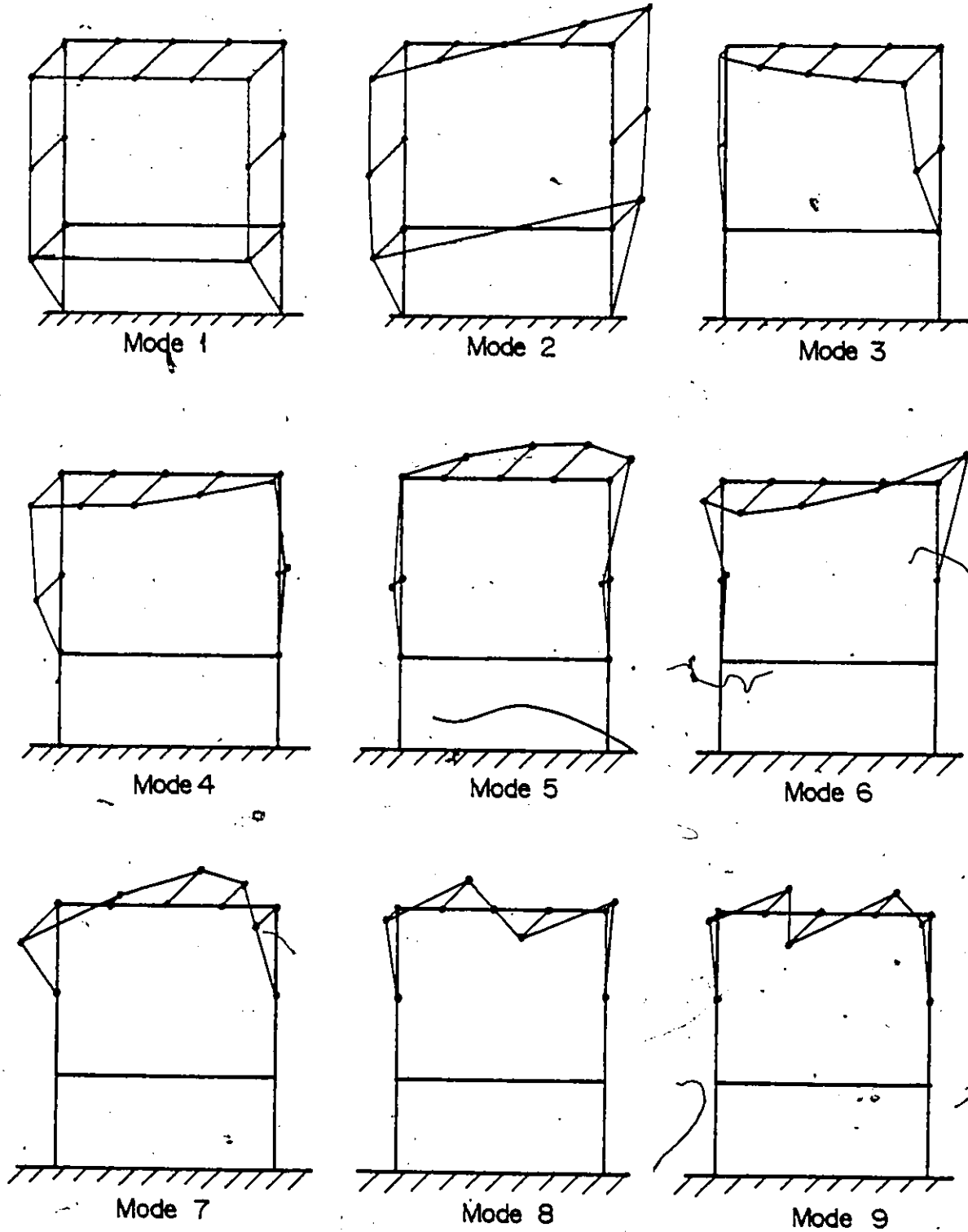
Figure 5.9   Mode Shapes of Assembly in Figure 5.8
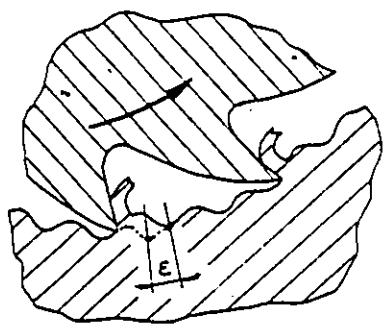
Figure 6.1 Regenerative
Principle
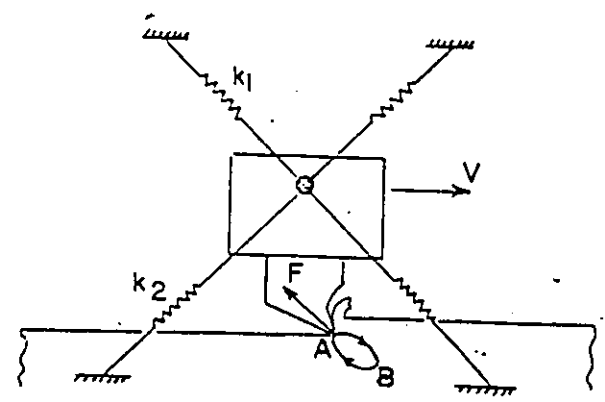
Figure 6.2 Mode Coupling
Principle

Figure 6.3.a Velocity
Component
Principle
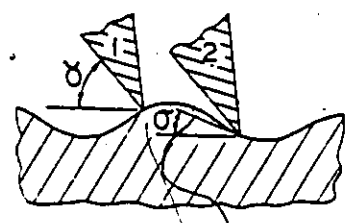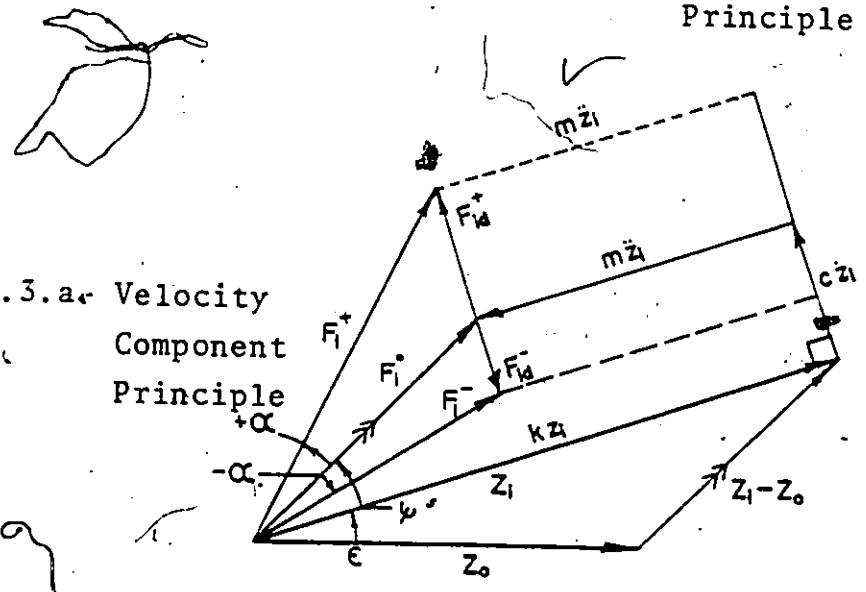
Figure 6.3.b Source of Process Damping
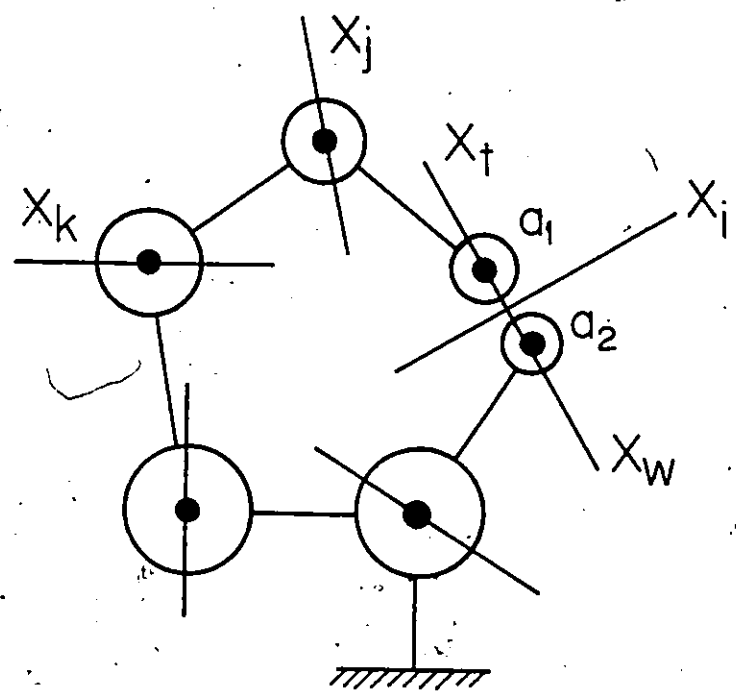
Figure 6.4   Machine Tool Vibratory System
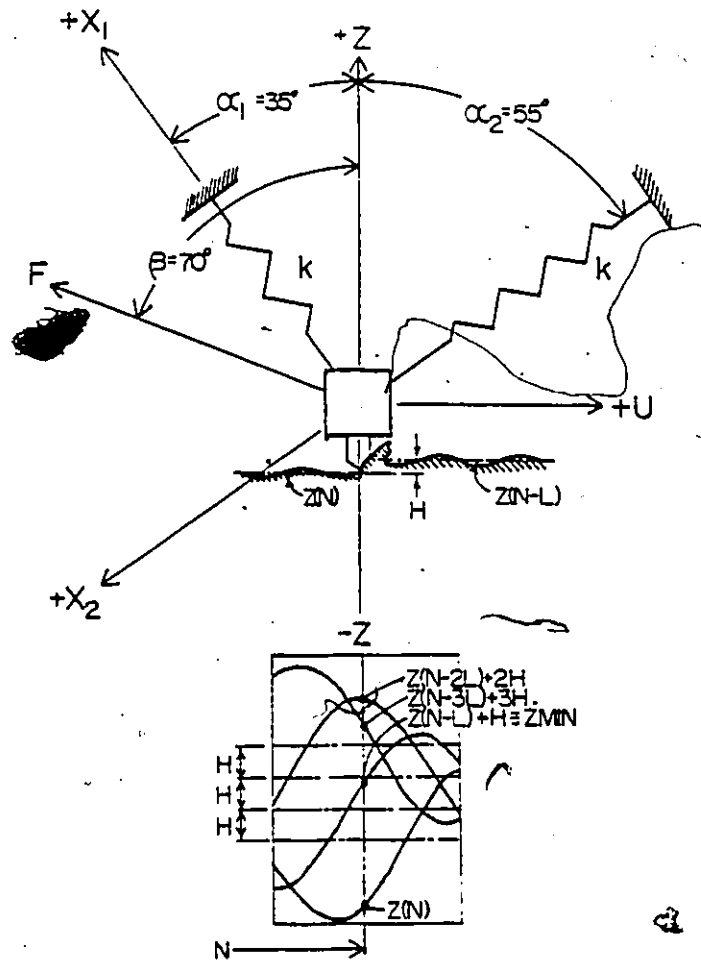
Figure 6.5   Model for   Simulation of Turning
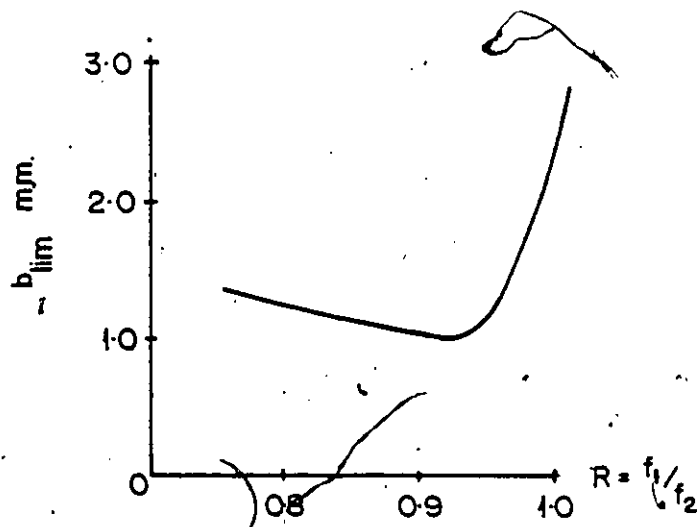
Figure 6.6   Limit of Stability Versus the Ratio
of Two Frequencies
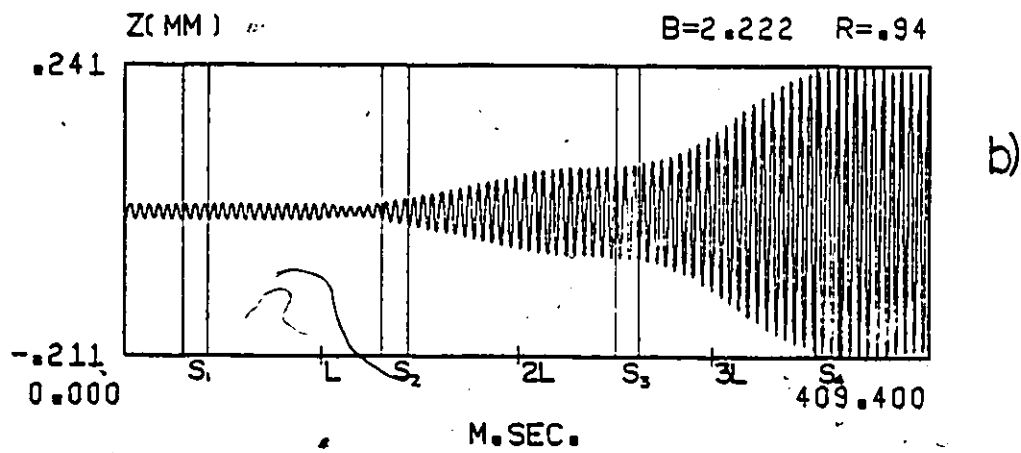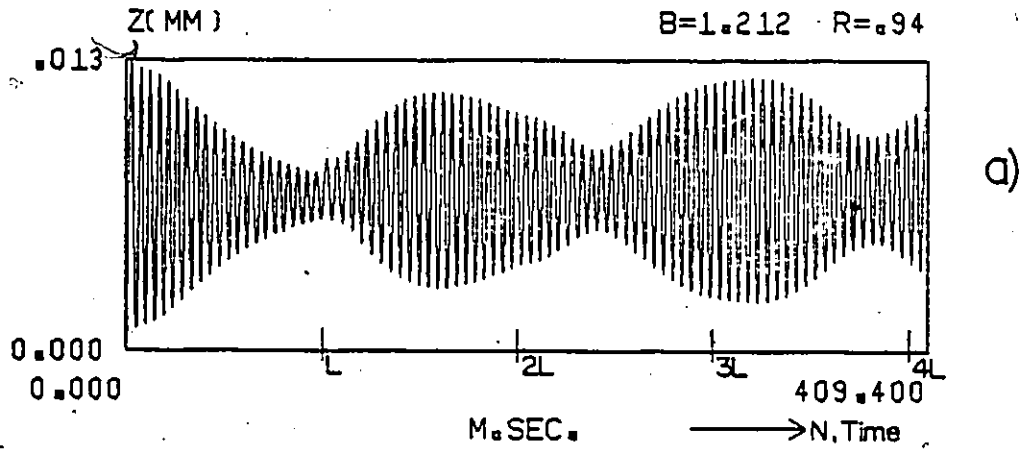
Figure 6.7   Development of Chatter in Turning at
Two Different Chip Widths:
a)   b = 1.212 mm
b)   b = 2.222 mm
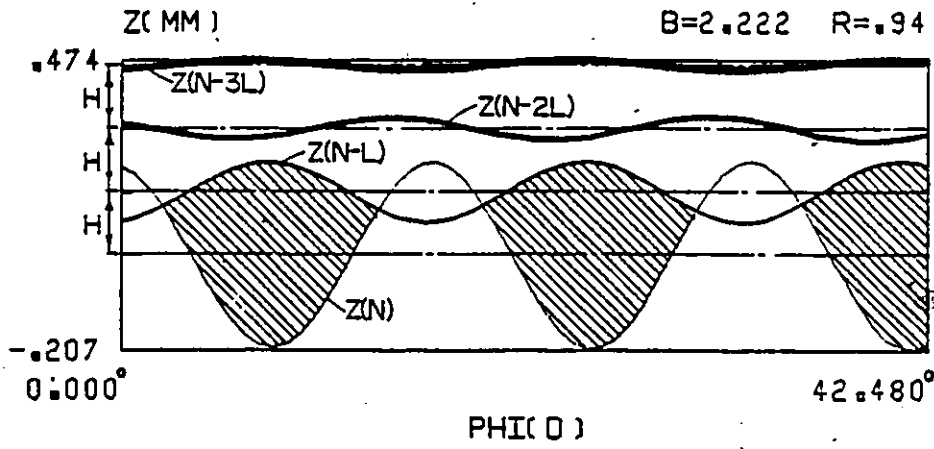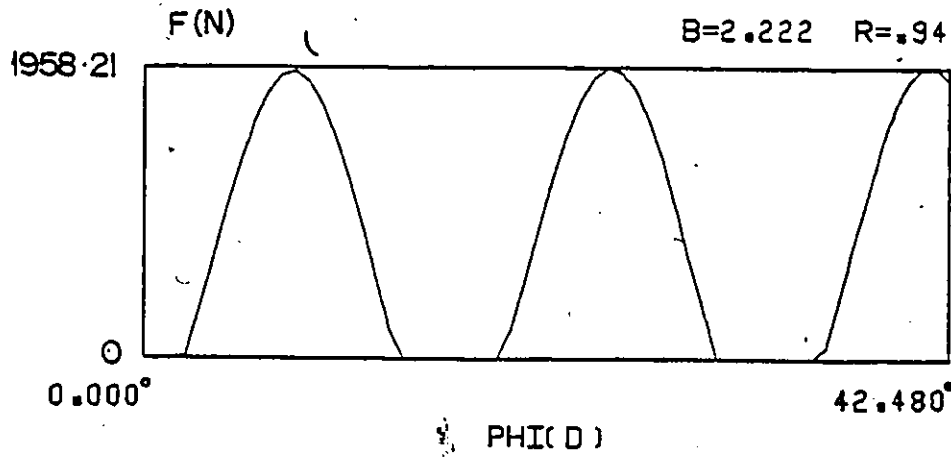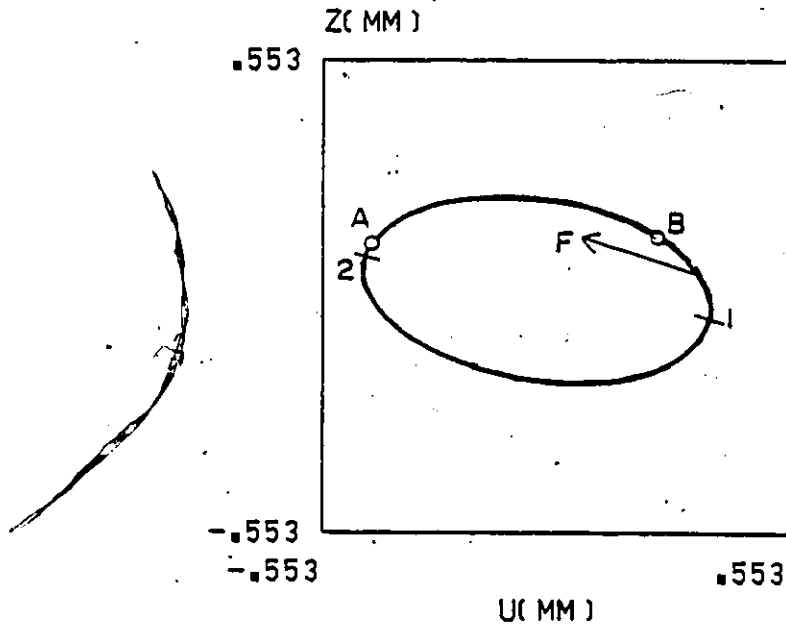
Figure 6.8 Details of Developing Chatter
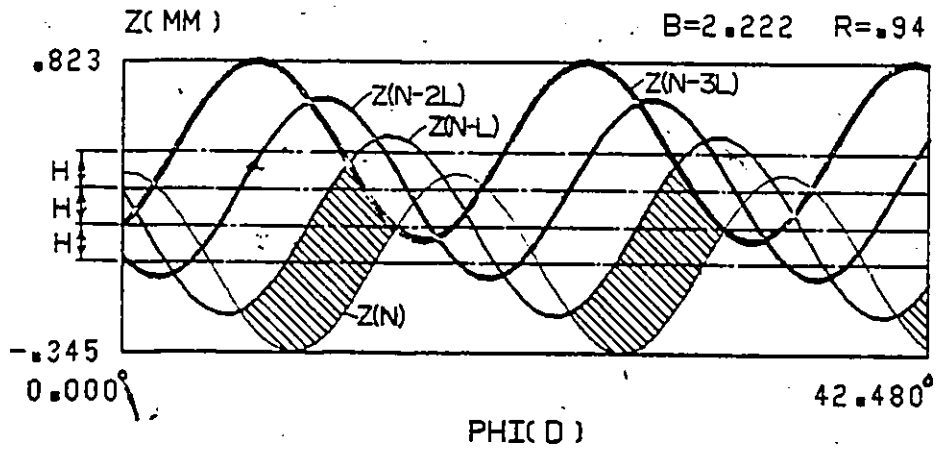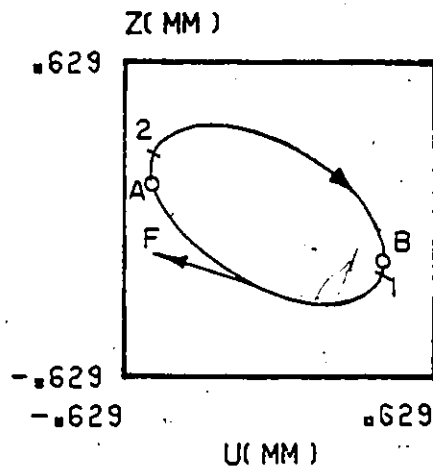
Figure 6.9 Details of Fully Developed Chatter
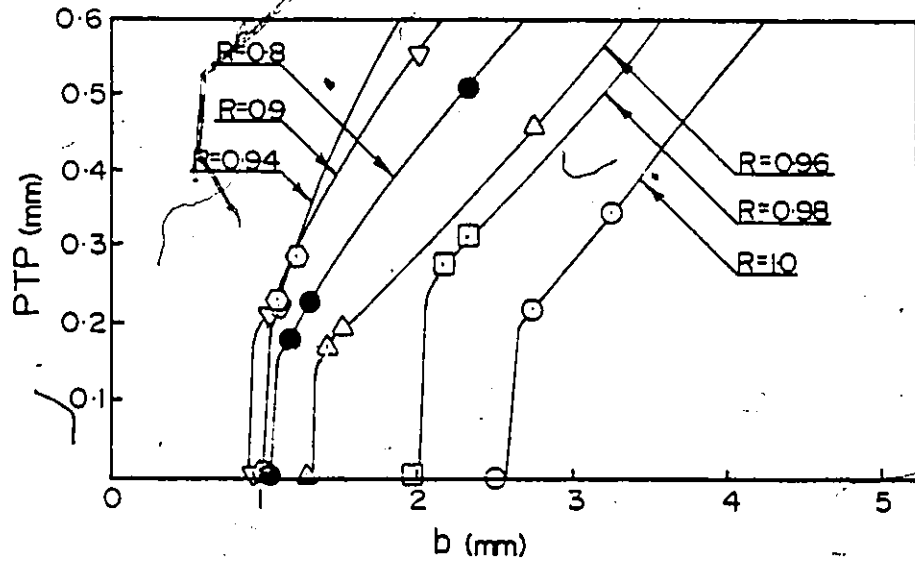
Figure 6.10   Amplitudes of Chatter in Turning
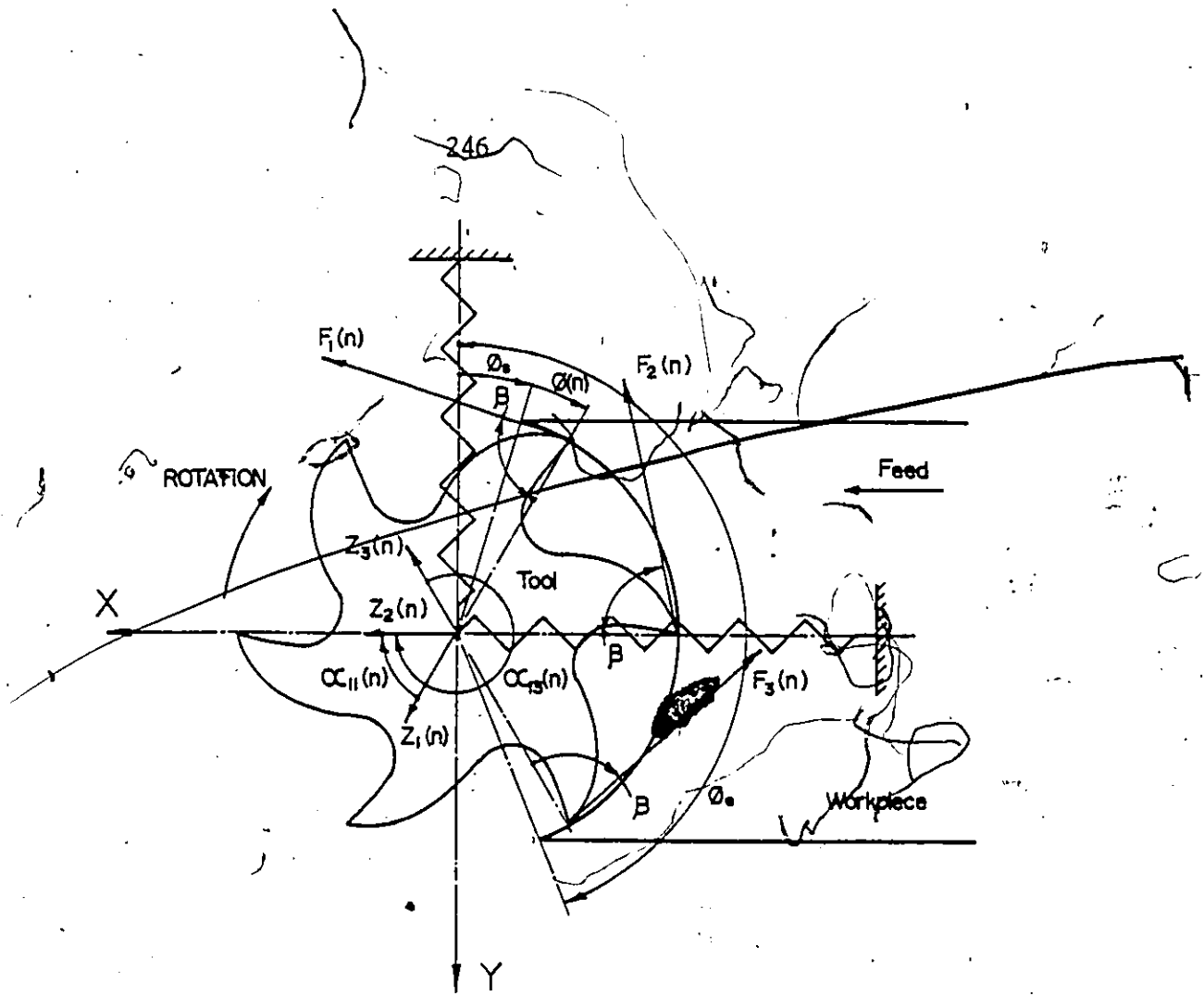
Figure 6.11 Model for Simulation of Milling
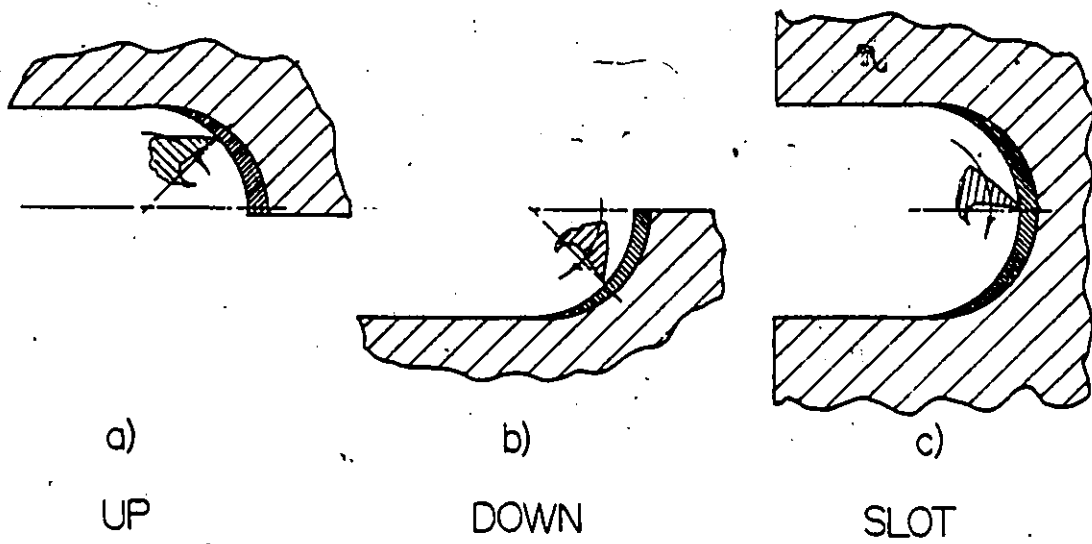
Figure 6.12 Modes of Milling Operations

UP   DOWN

(633-660)

(660-960)
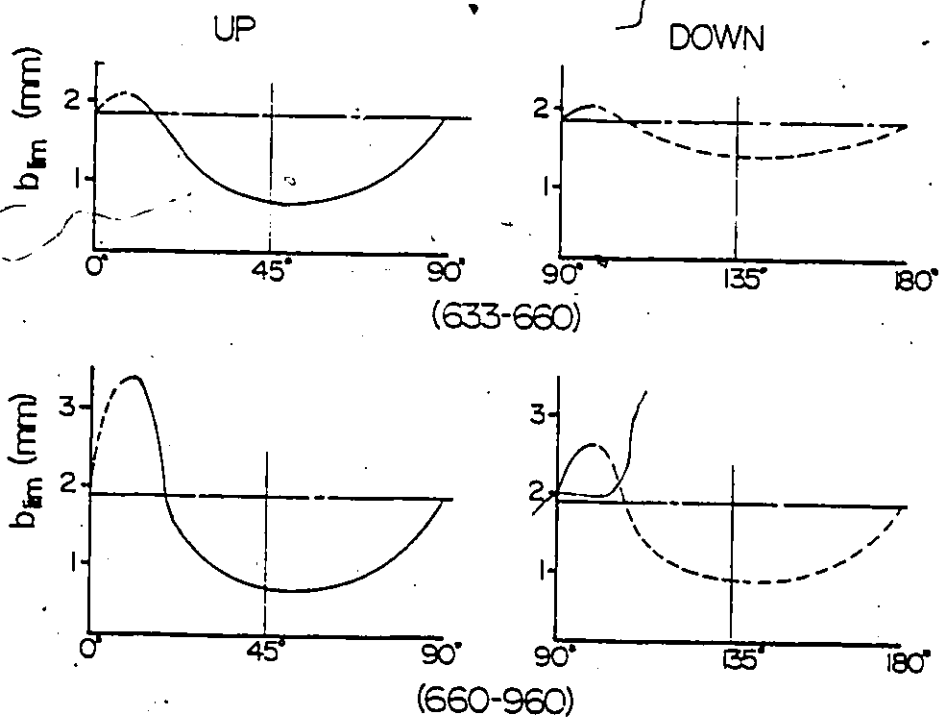
Figure 6.13   Effect of Varying Directional Orientation on "Instantaneous Stability"
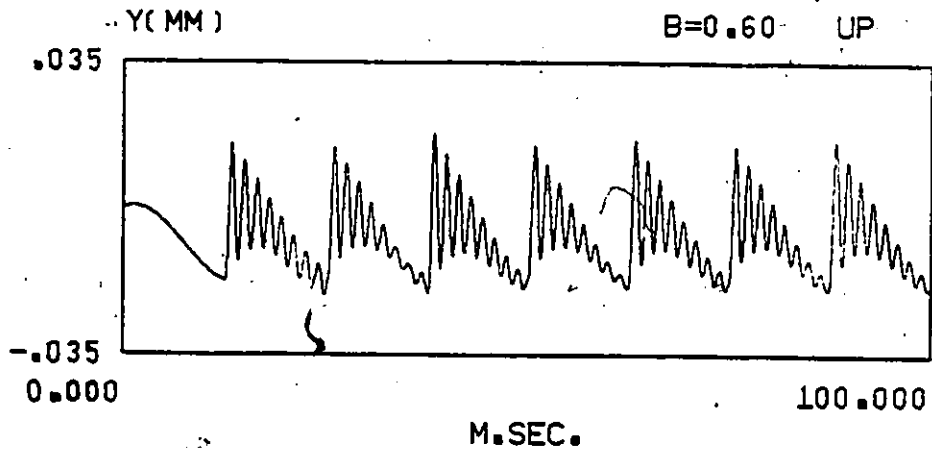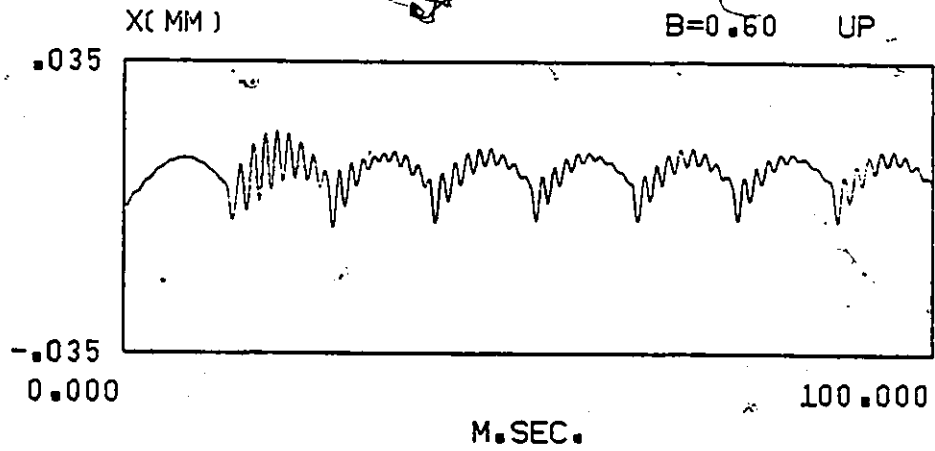
Figure 6.14   Vibrations in Stable Up-Milling
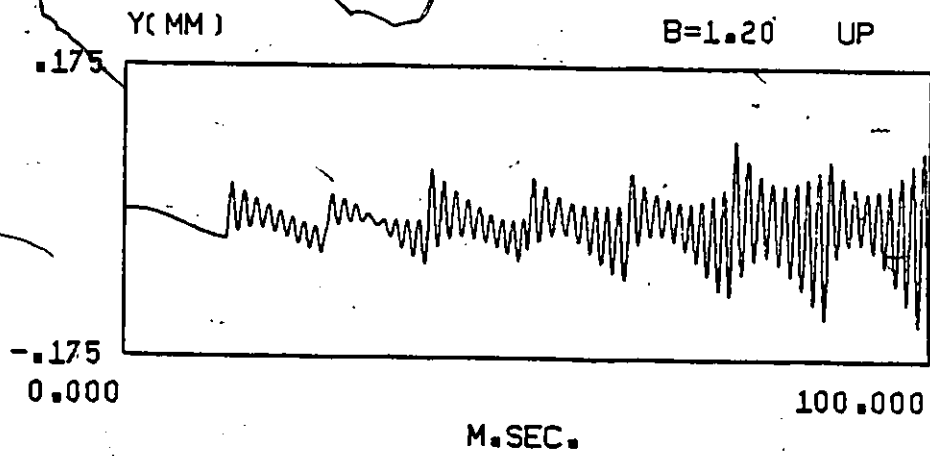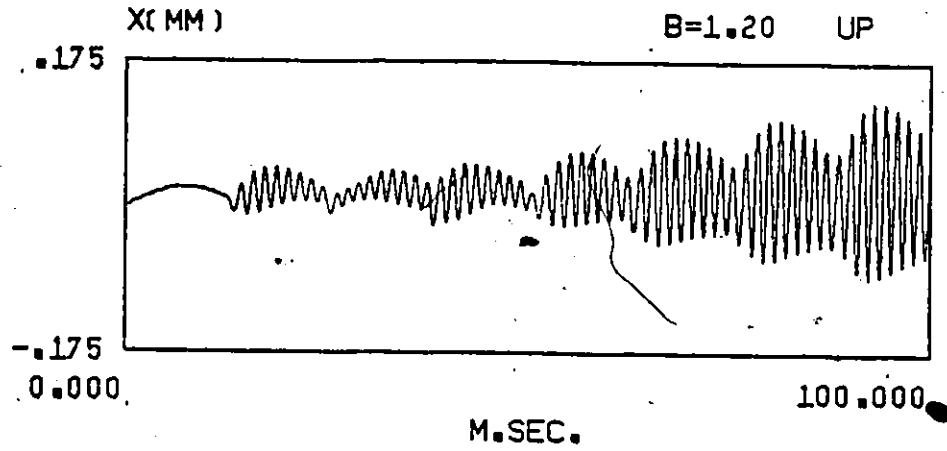
Figure 6.15   Vibrations in Up-Milling with
Incipient Chatter
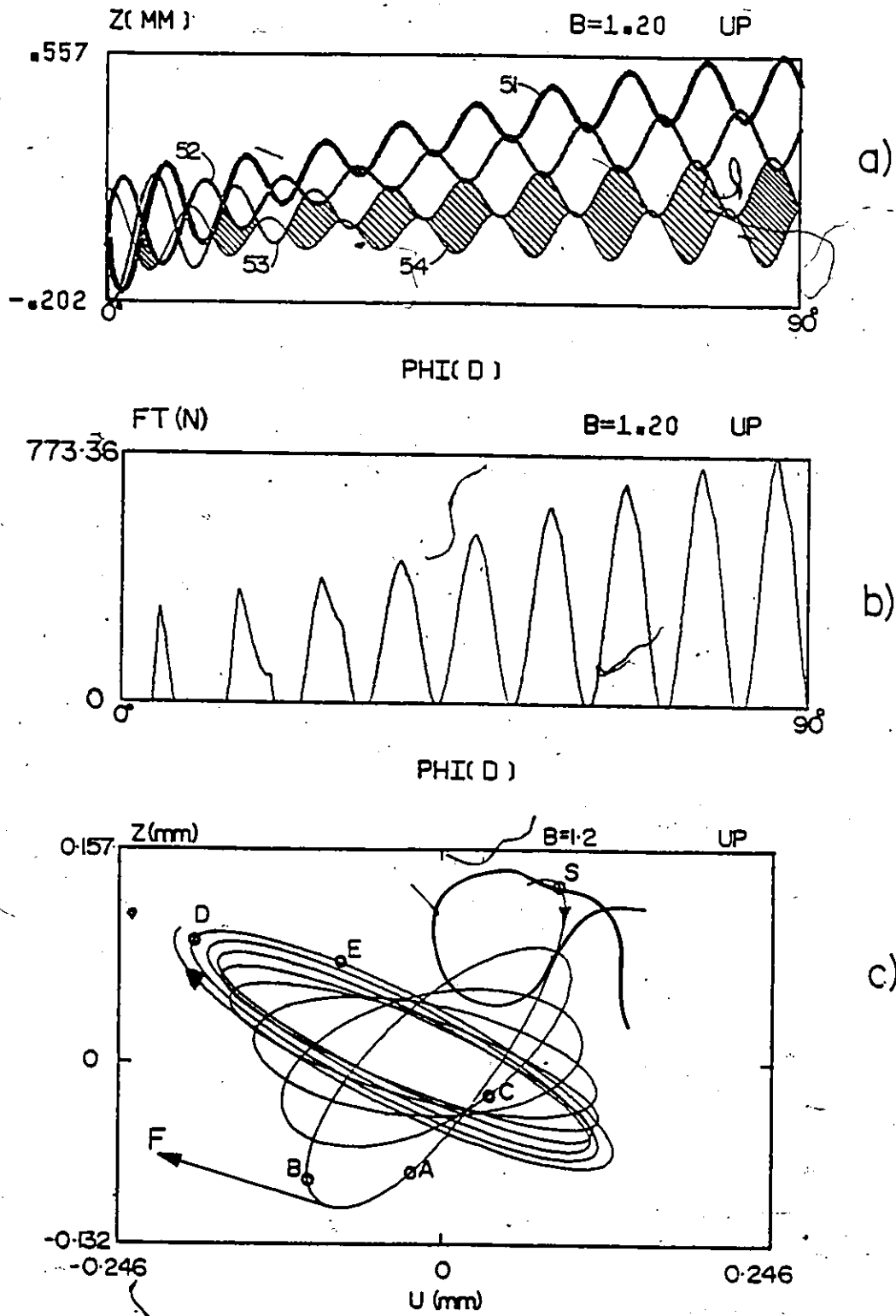
Figure 6.16   Details of Chatter in Up-Milling

Z(MM) B=1.2 DOWN

.497

101 100

103 102

-.171 90° 180°

PHI(D)
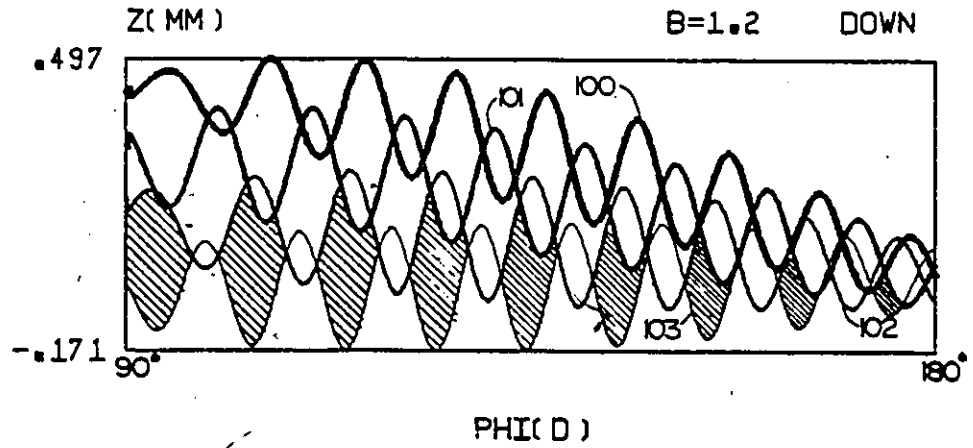
Figure 6.17 Details of Chatter in Down-Milling

Z(MM) B=0.4 SLOT

.547

100
101
102
103

-.101 0° 180°

PHI(D)
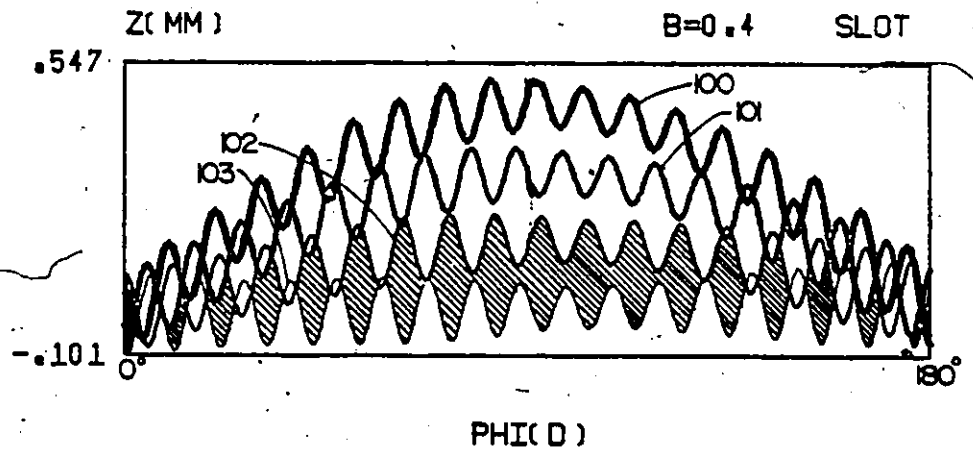
Figure 6.18 Details of Chatter in Slotting
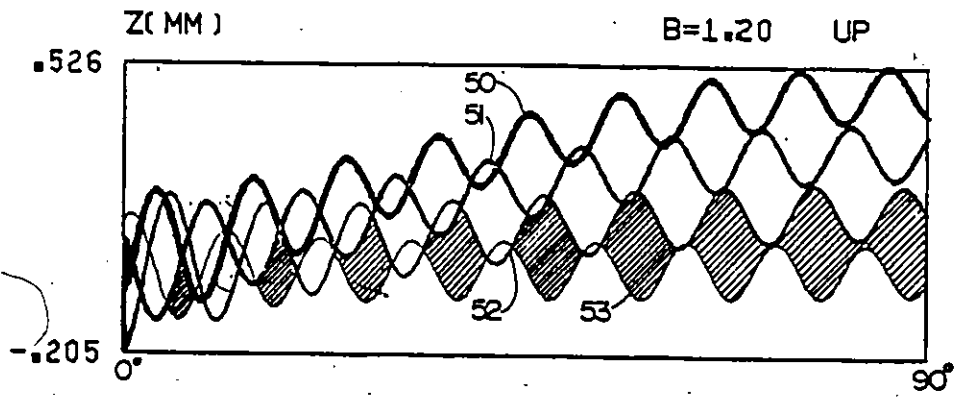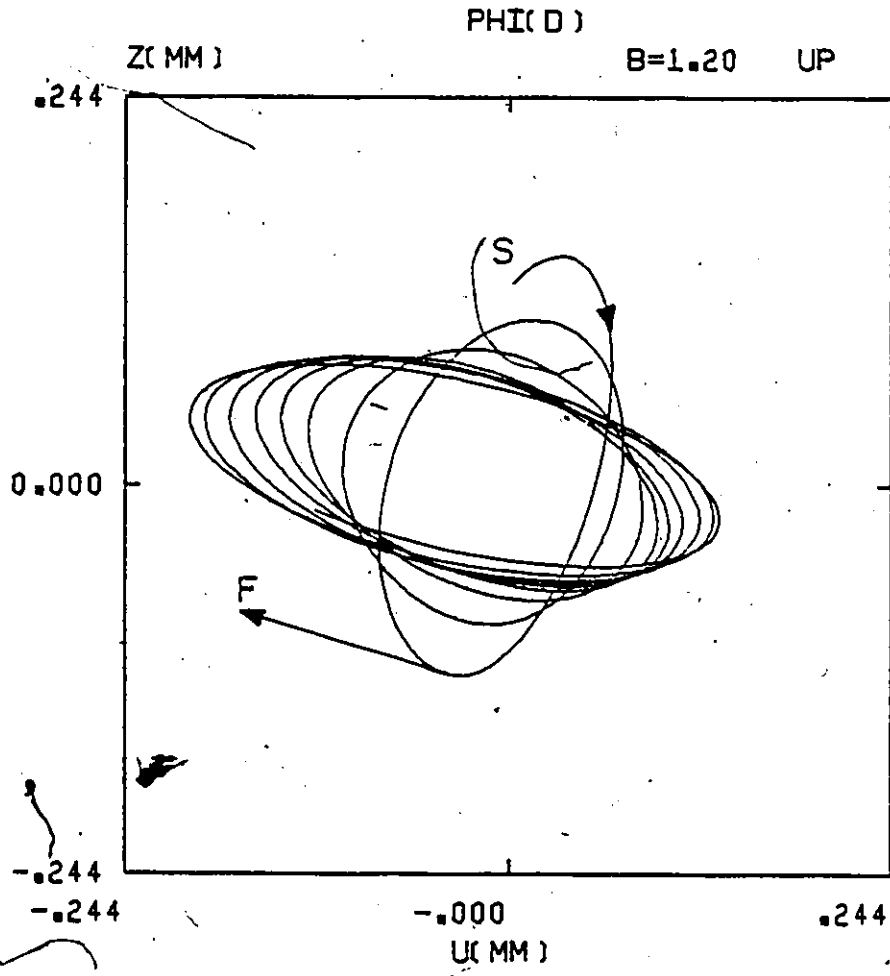
Figure 6.19   Details of Chatter with Unequal
but Close Frequencies
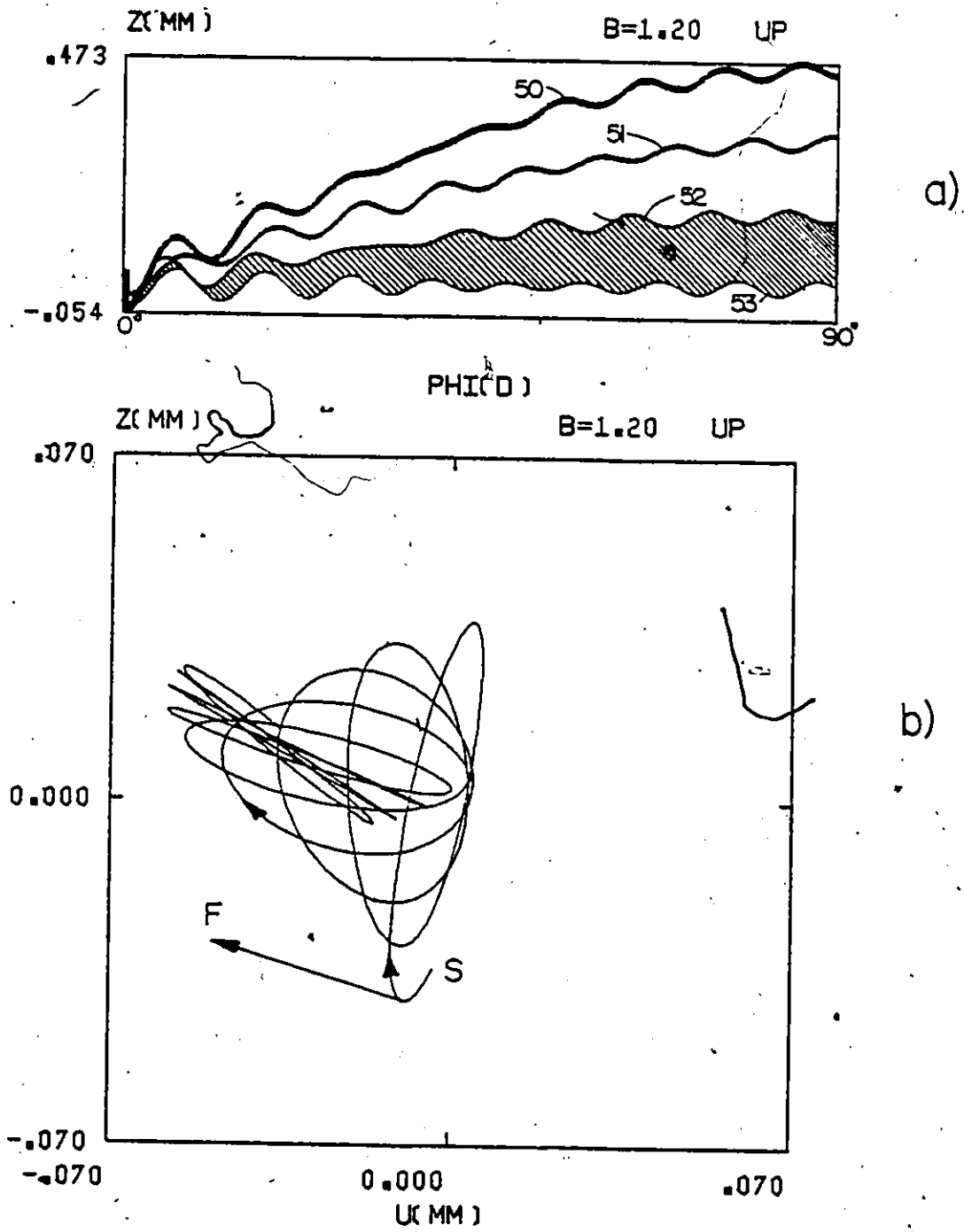
Figure 6.20   Details of Chatter with Frequencies
Reversed
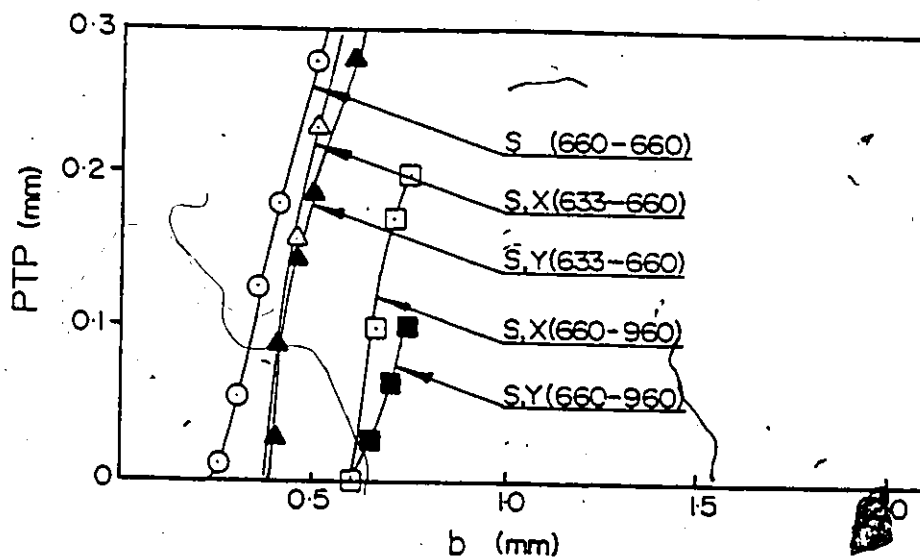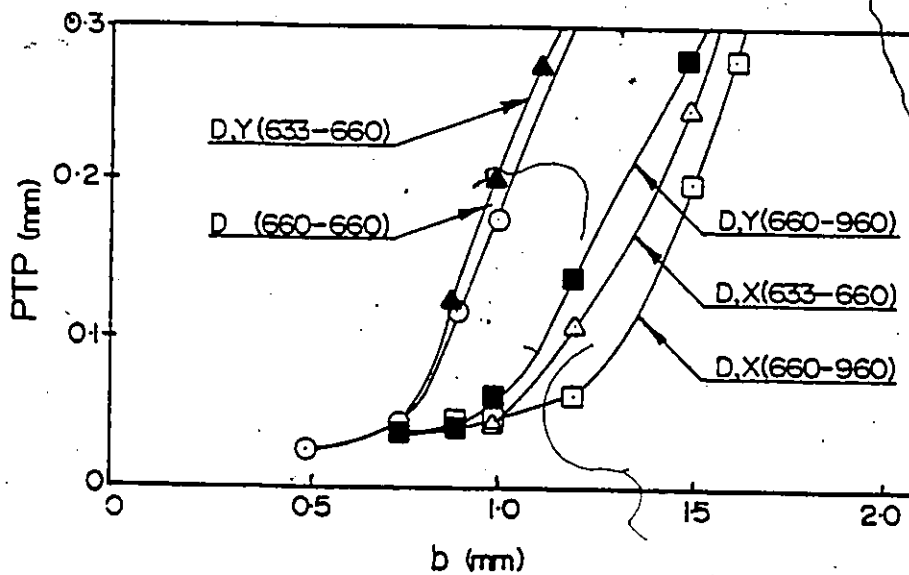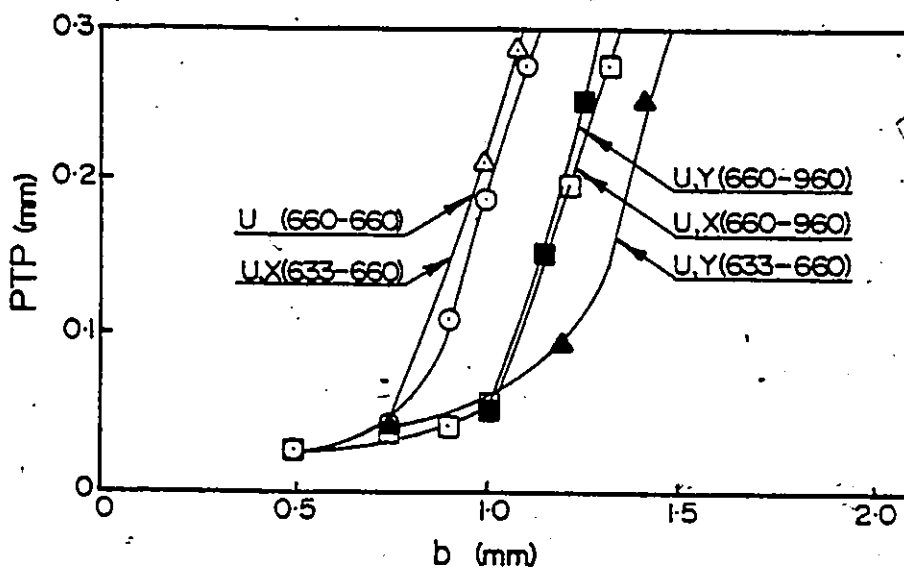
Figure 6.21 Amplitudes of Chatter in Milling
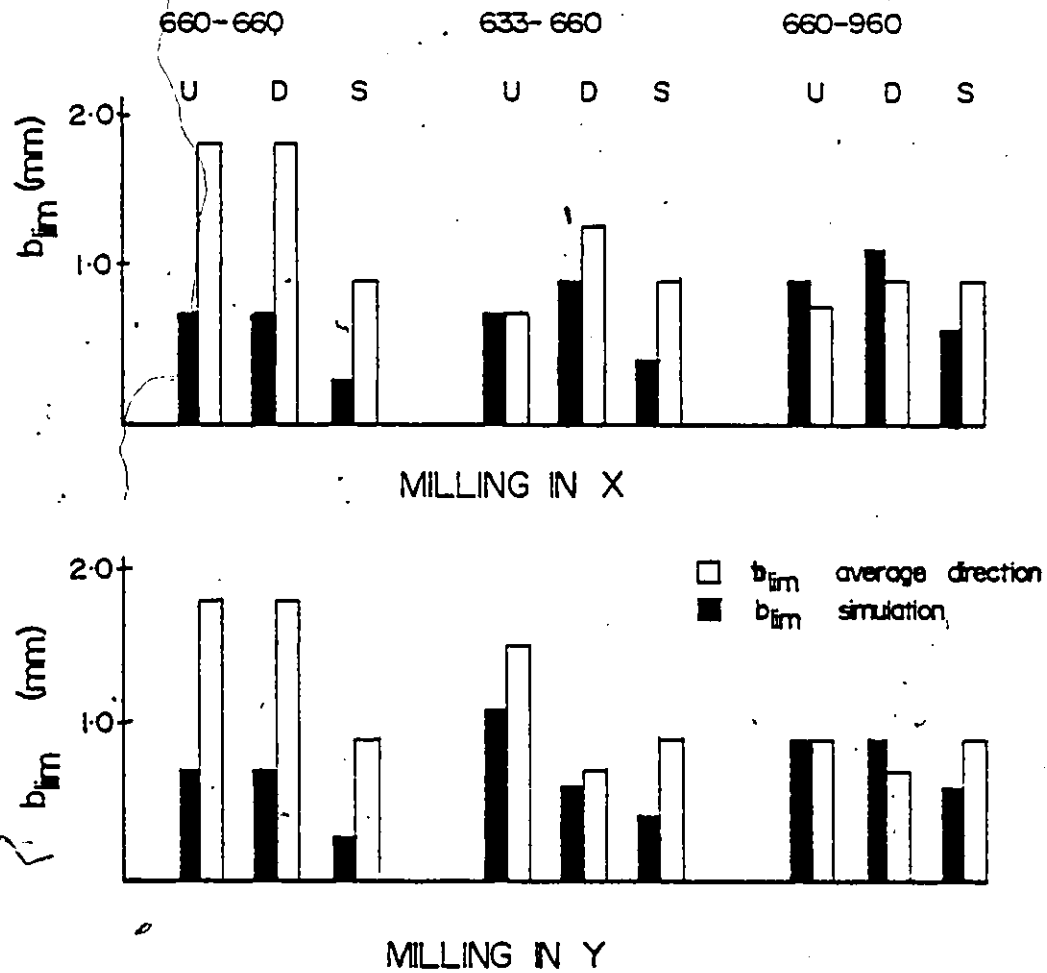
Figure 6.22   Comparison of Limits of Stability
               Calculated with Constant and with
               Varying Directional Orientation
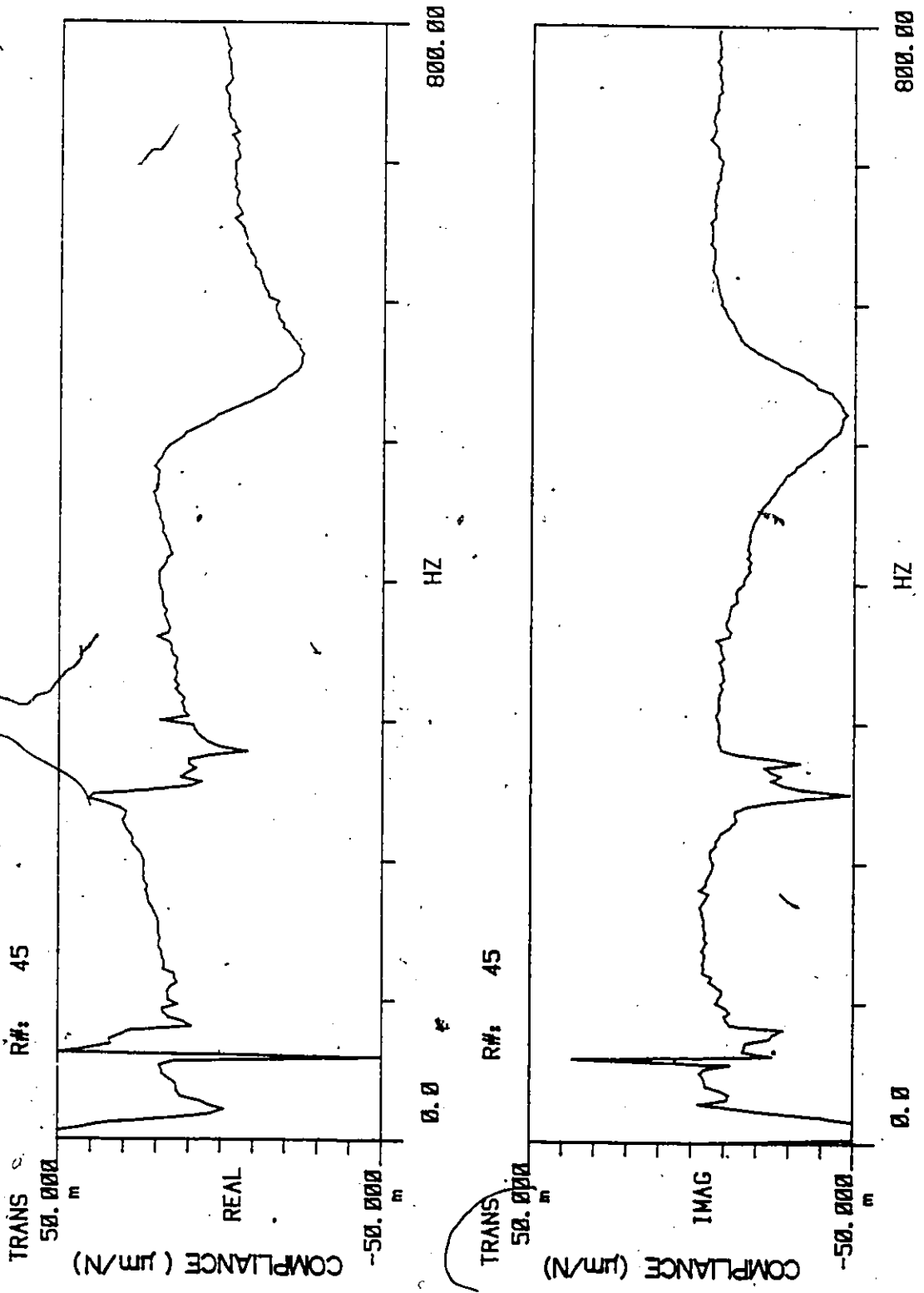
Figure 6.23 Direct Relative Transfer Function for the Face Milling Cutter in Direction X
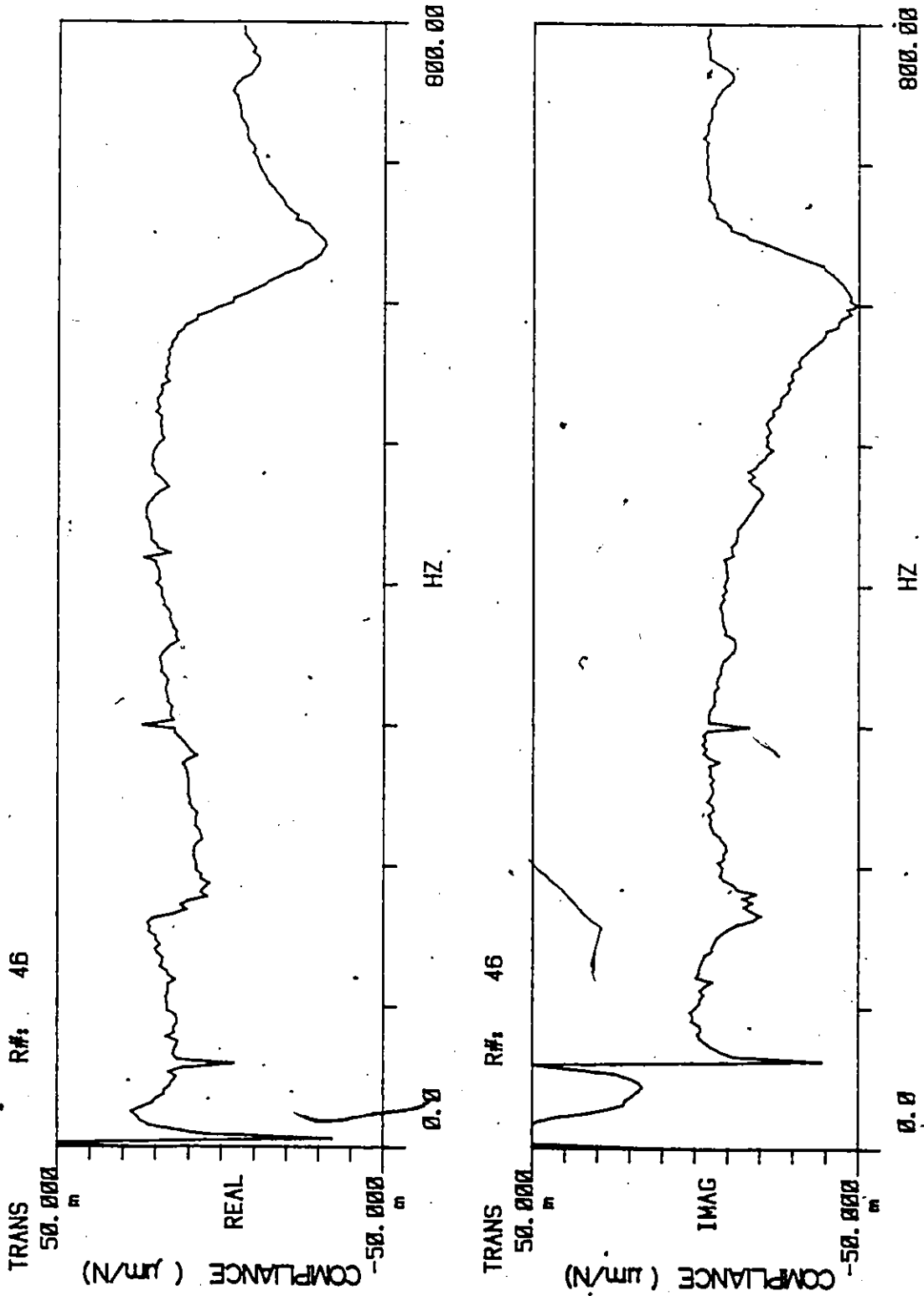
Figure 6.24   Direct Relative Transfer Function for the Face Milling
Cutter in Direction Y
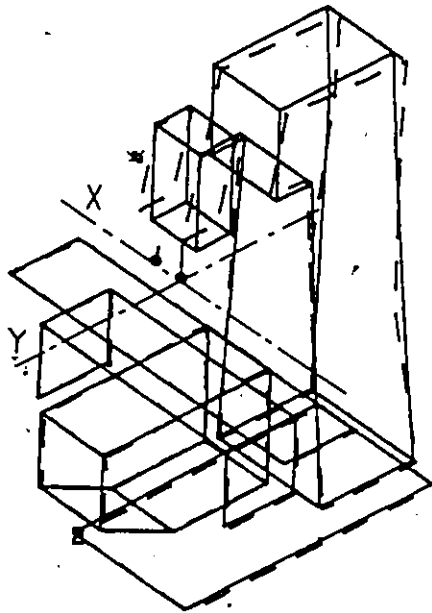
Fig. 6.25   Mode of milling machine at 250 Hz
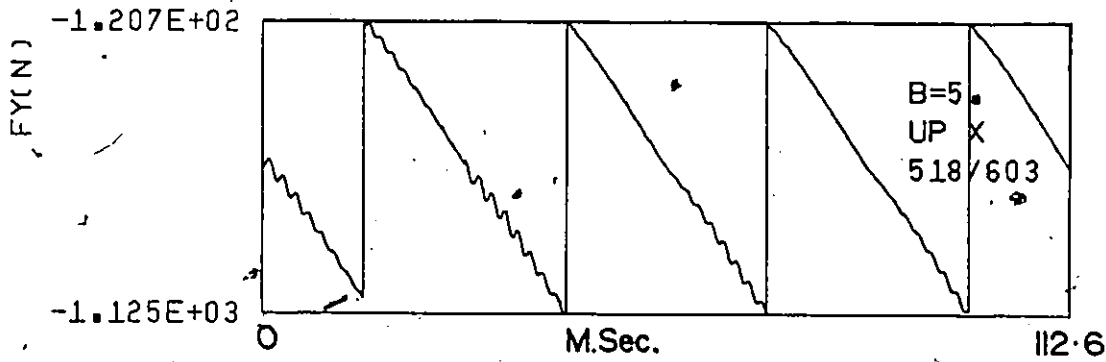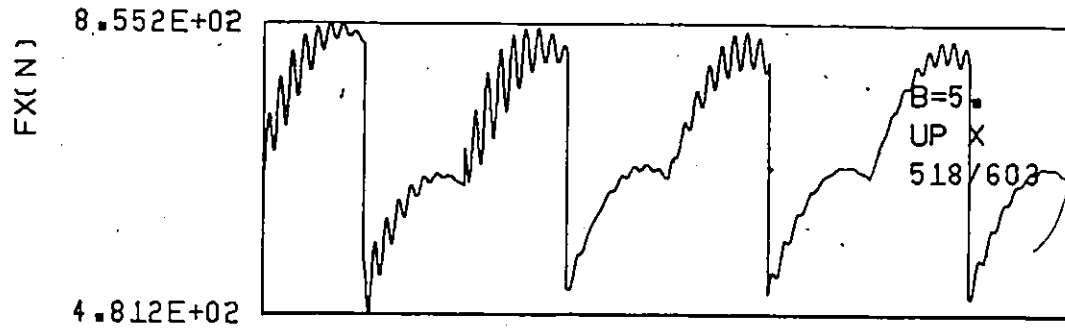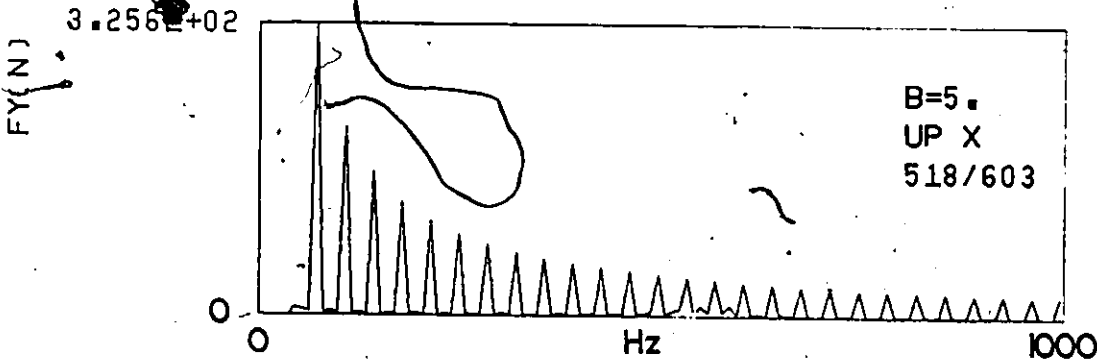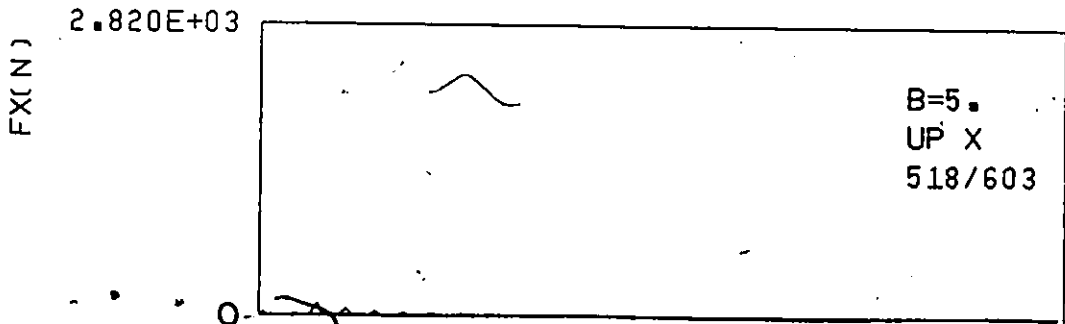
Figure 6.26   Simulation of Up-Milling in X, b = 5 mm
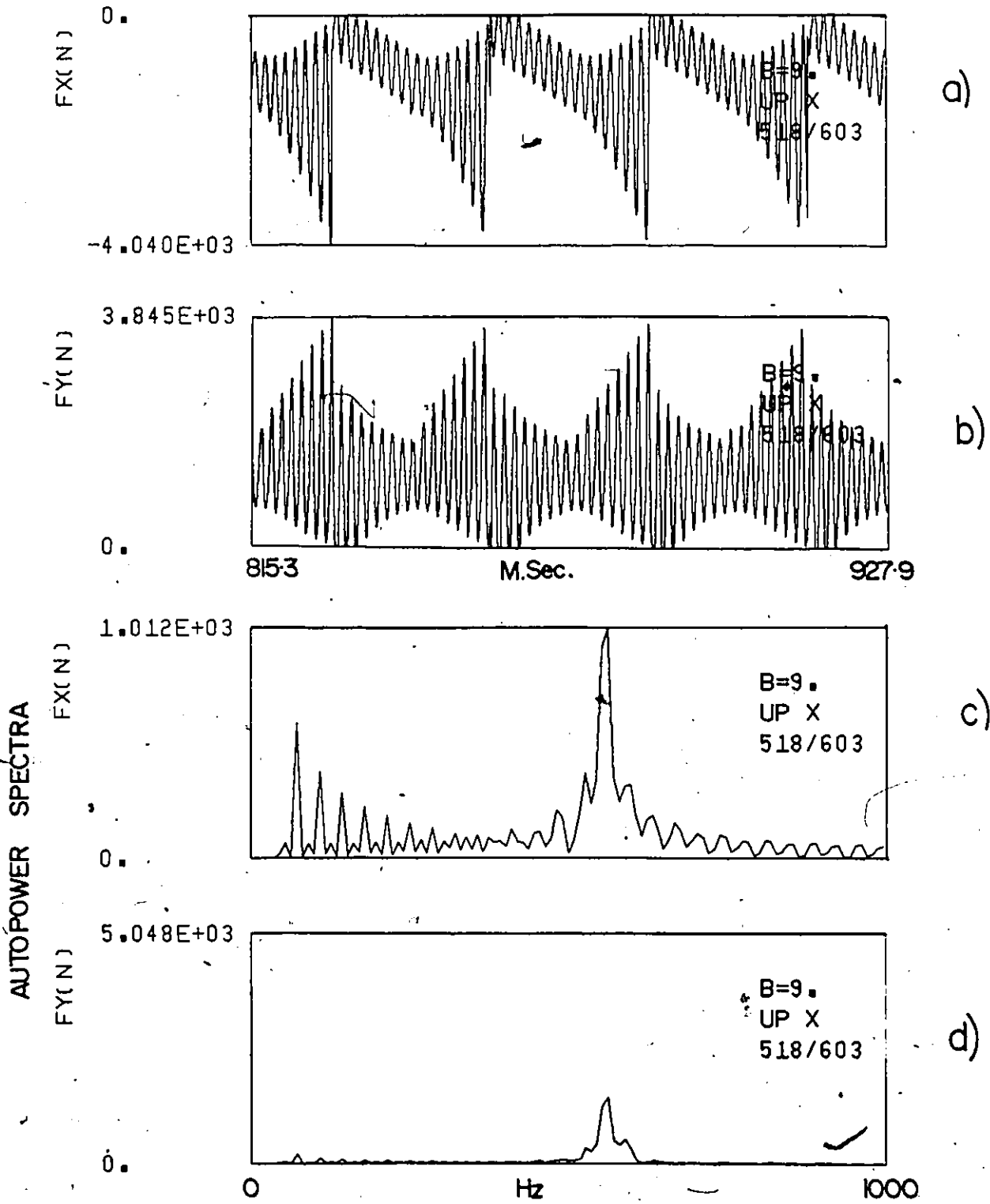
Figure 6.27   Simulation of Up-Milling in X, b = 9 mm
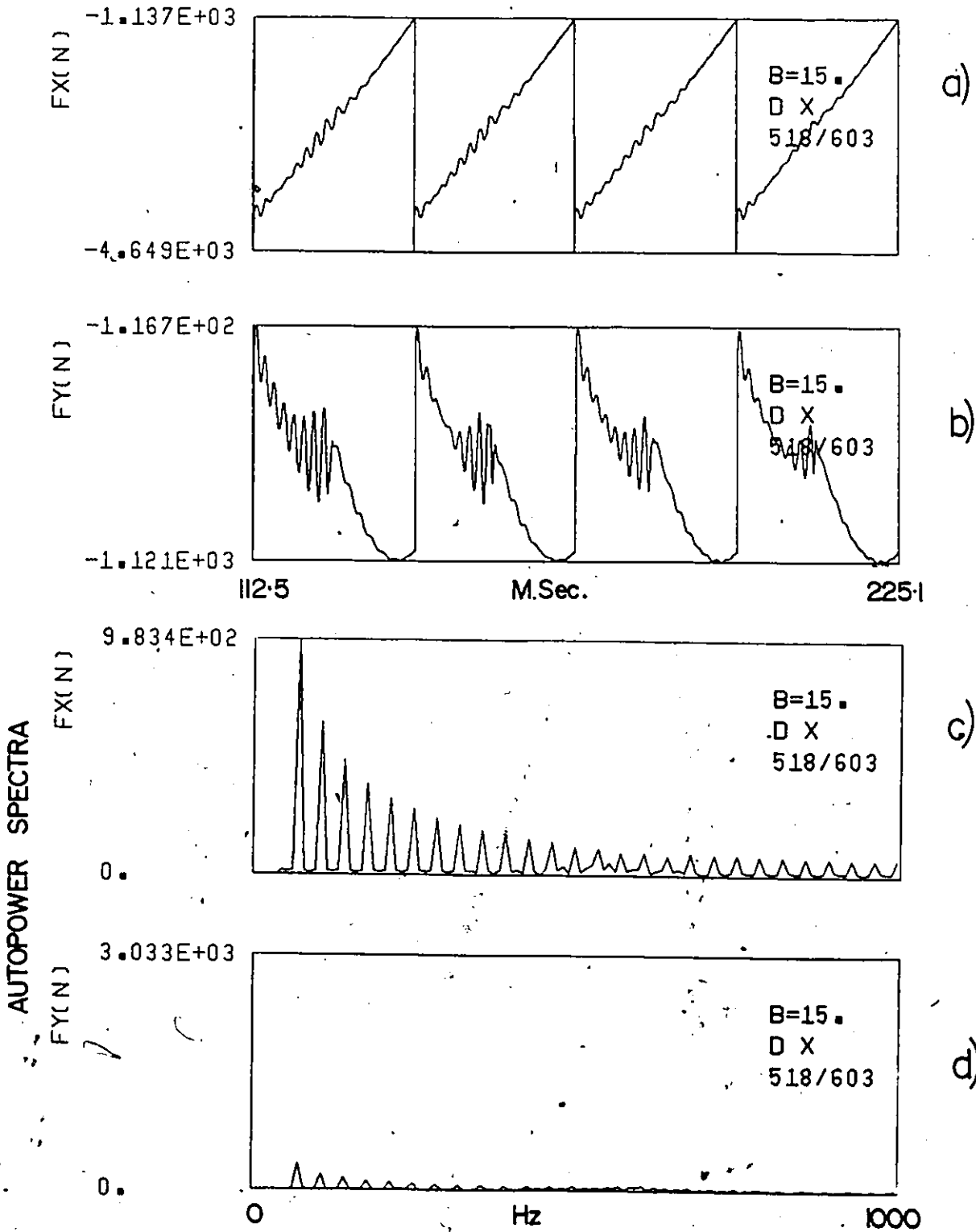
Figure 6.28   Simulation of Down-Milling in X, b = 15 mm
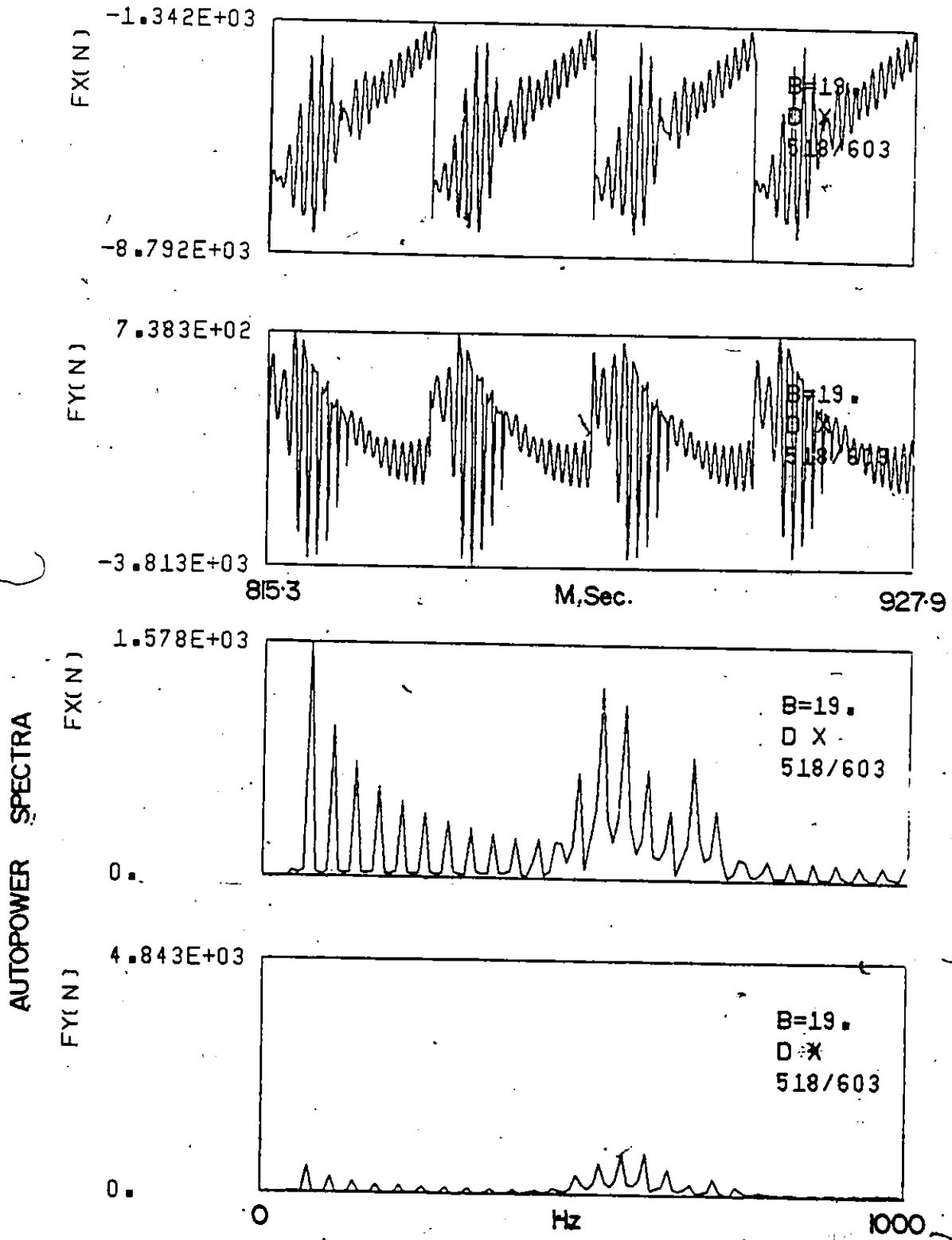
Figure 6.29   Simulation of Down-Milling in X, b = 19 mm
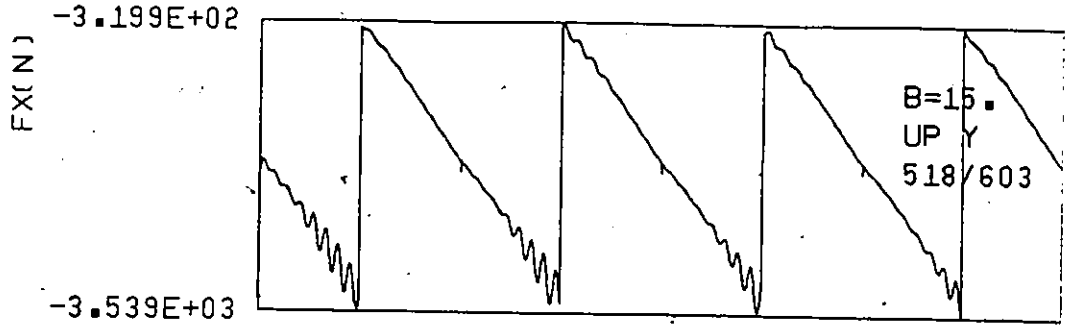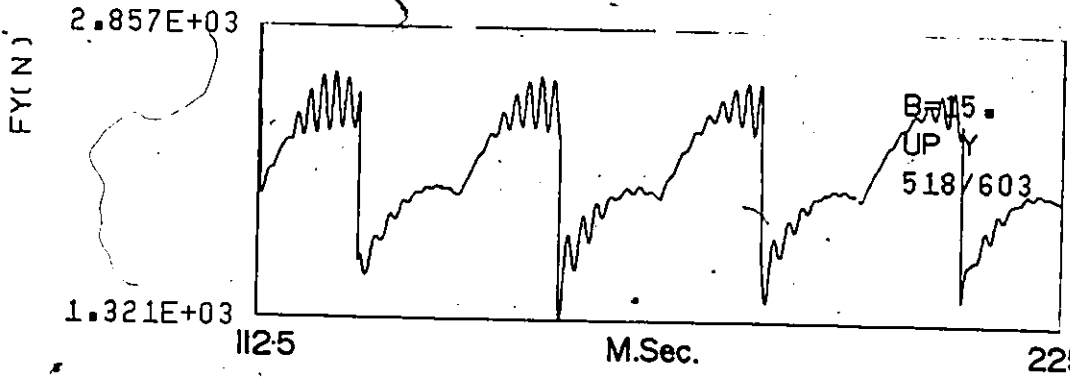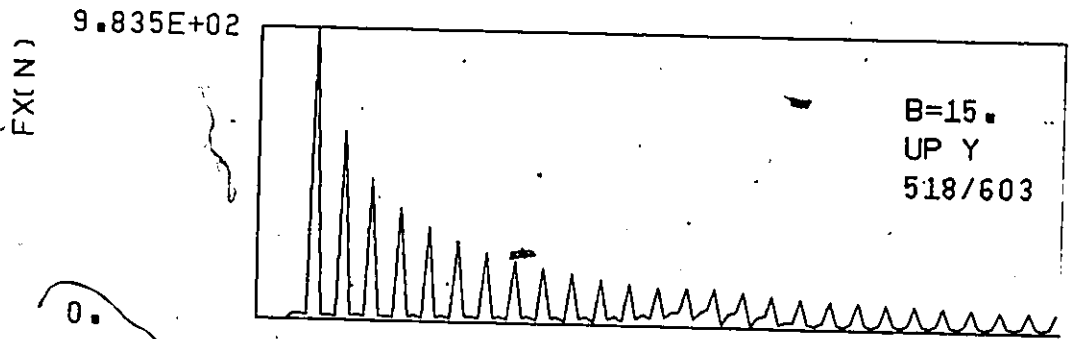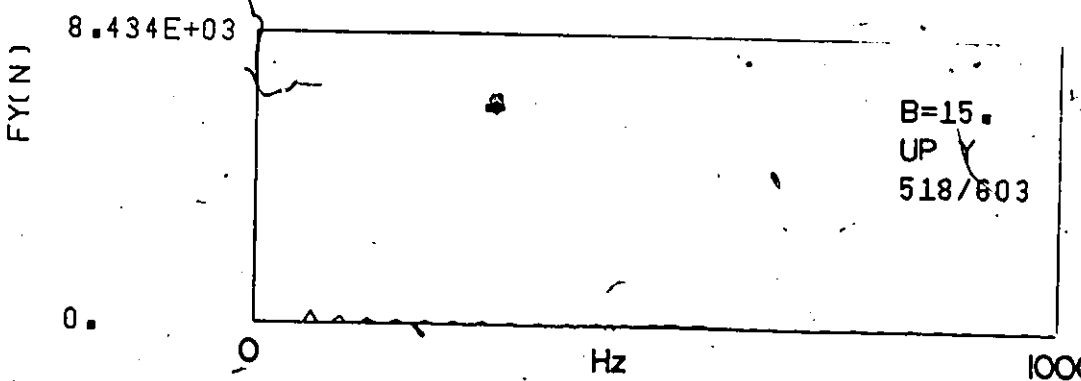
Figure 6.30   Simulation of Up-Milling in Y, b = 15 mm

AUTOPOWER SPECTRA

a)

FX(N) 0.

−1.129E+04

B=17.
UP Y
518/603

b)

FY(N) 7.219E+03

0.

815·3   M.Sec.   927·9

B=17.
UP Y
518/603

c)

FX(N) 2.482E+03

0.

B=17.
UP Y
518/603

d)

FY(N) 1.351E+04

0.

0   Hz   1000

B=17.
UP Y
518/603
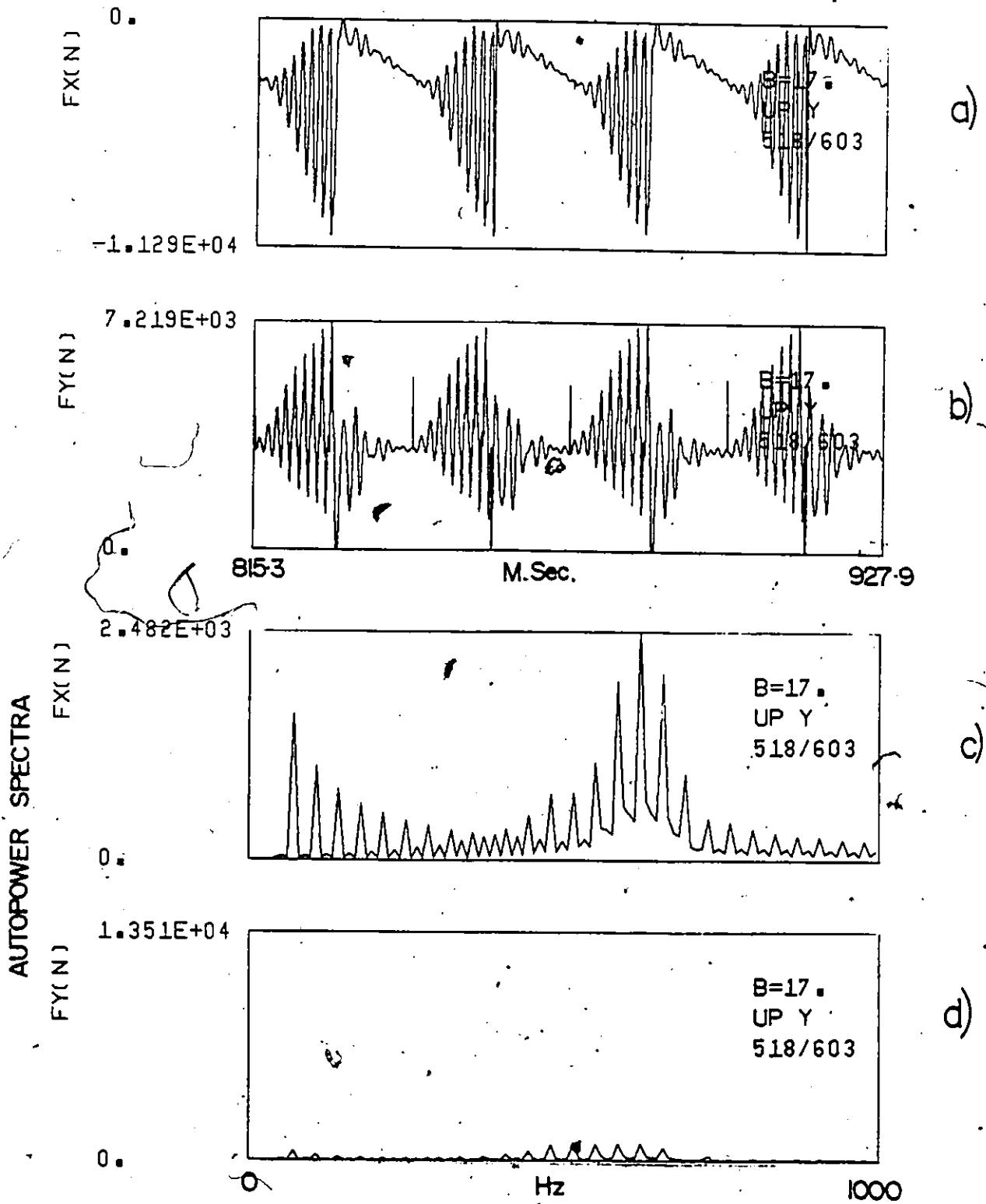
Figure 6.31   Simulation of Up-Milling in Y, b = 17 mm
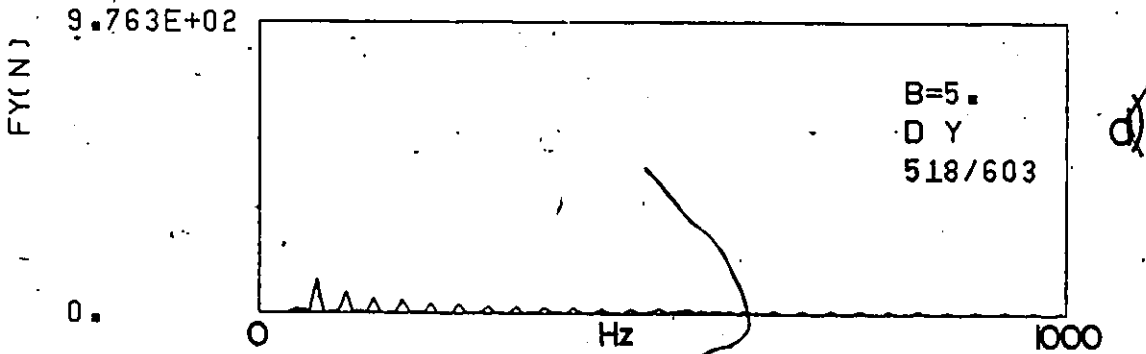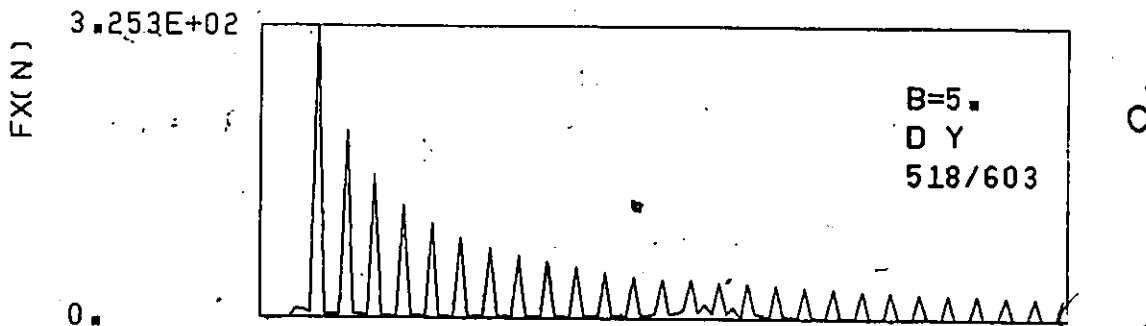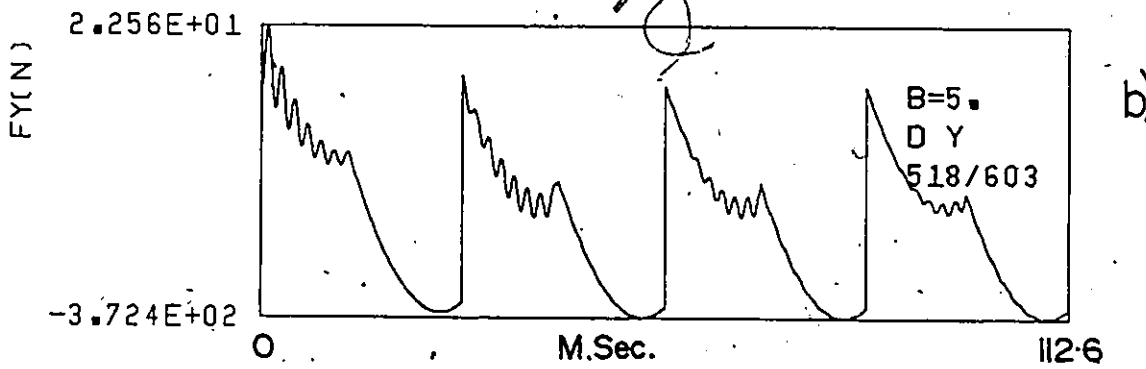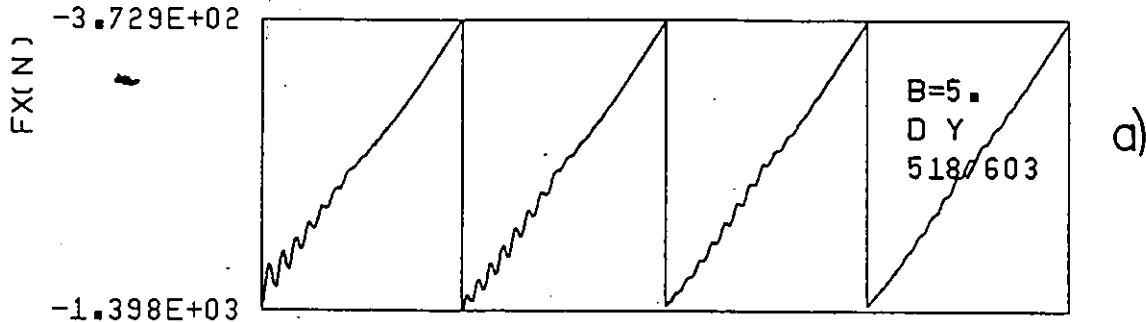
Figure 6.32   Simulation of Down-Milling in Y, b = 5 mm
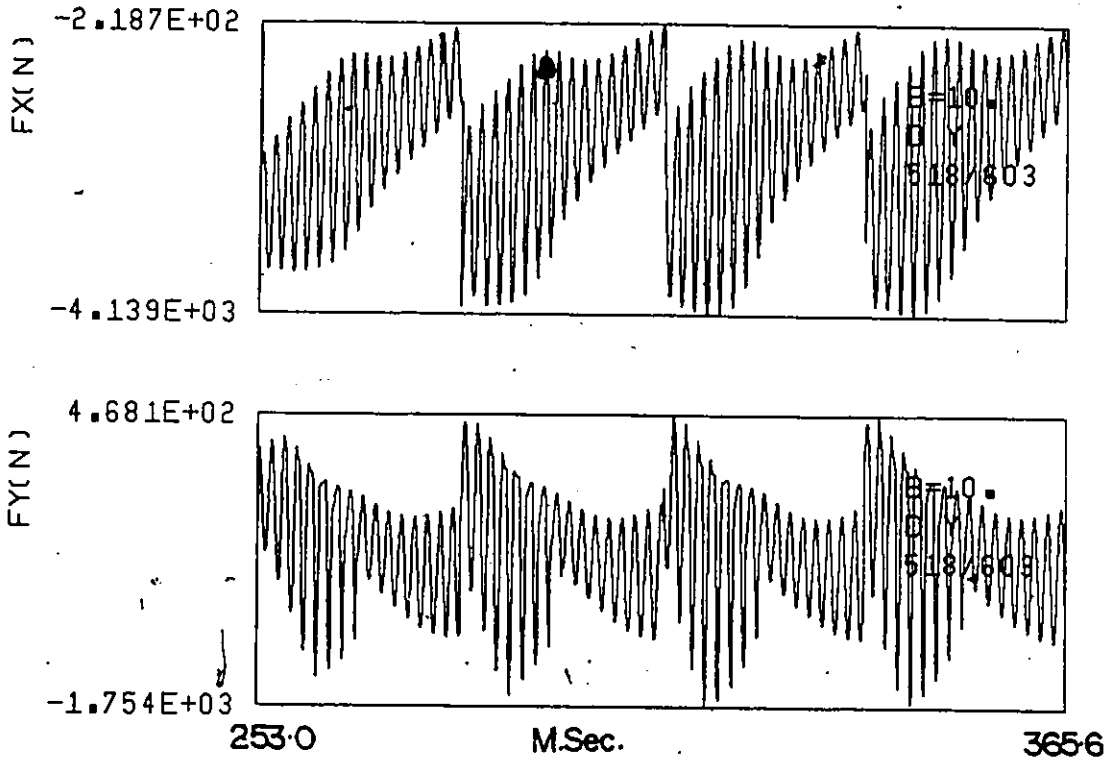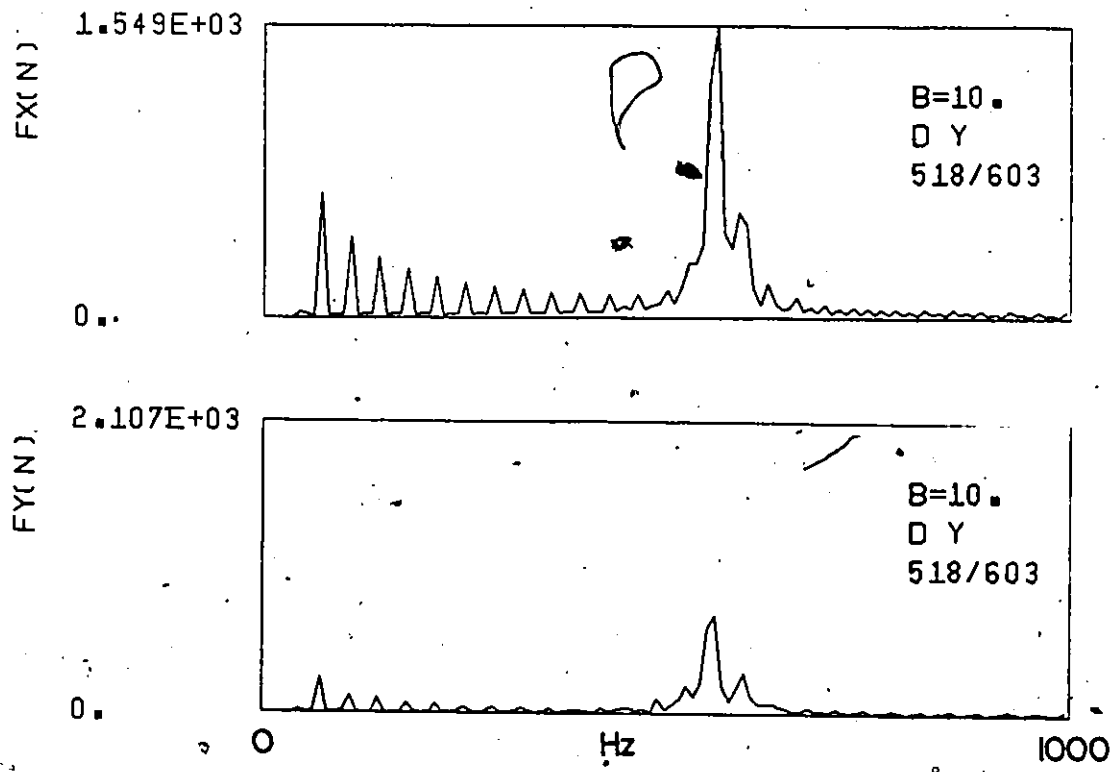
Figure 6.33   Simulation of Down-Milling in Y, b = 10 mm
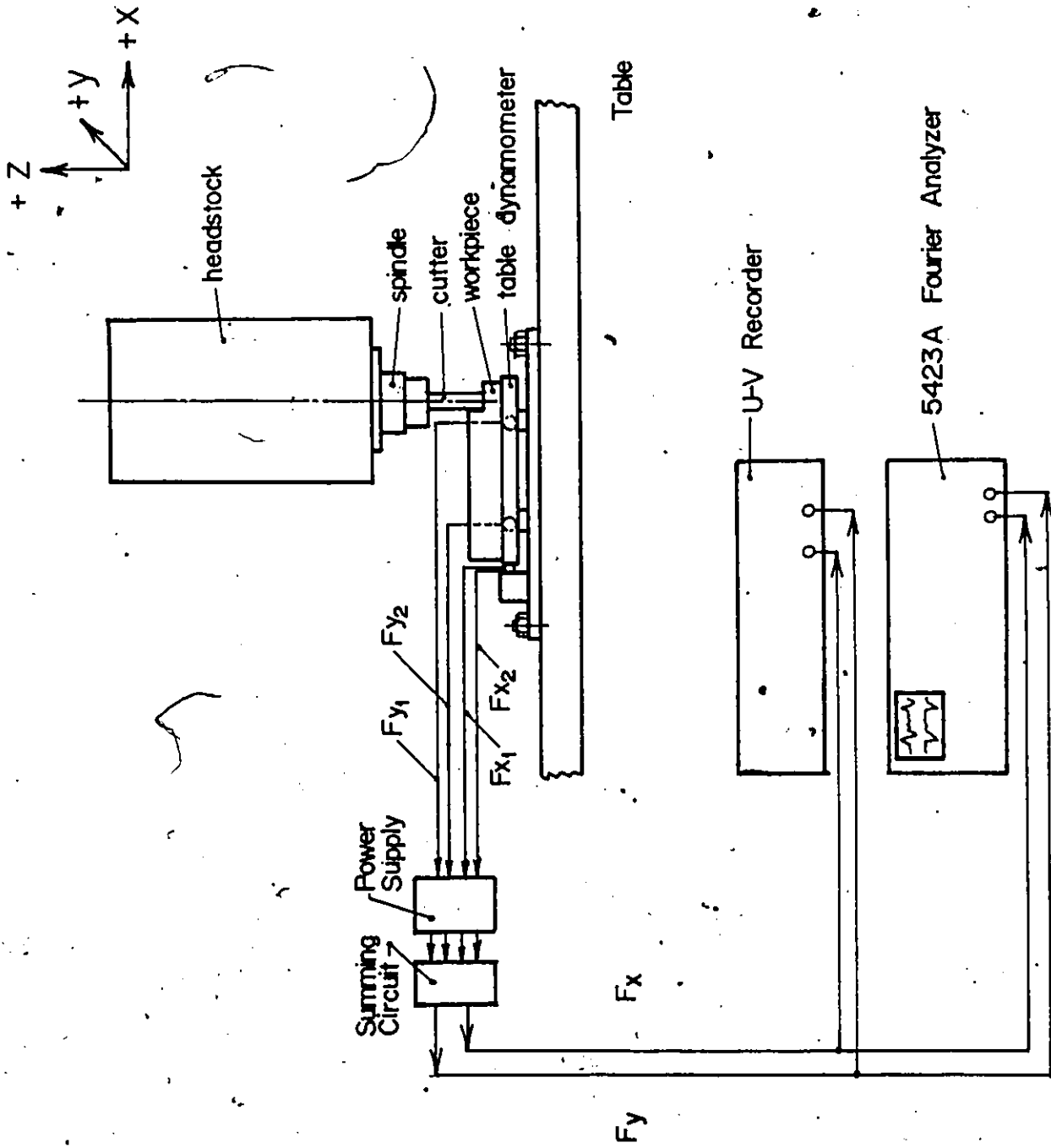
Figure 6.34 Experimental Set-Up for the Cutting Tests
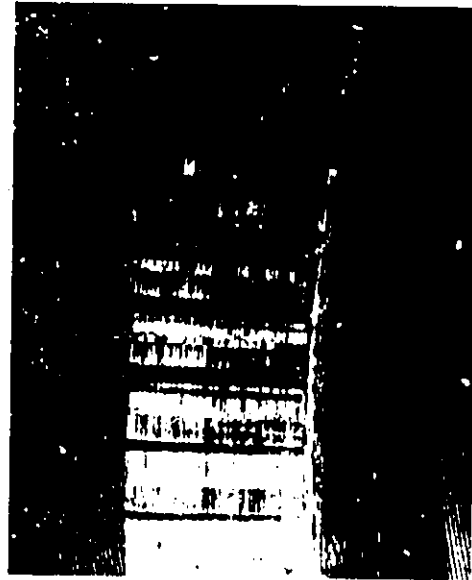
Carbide face milling of steel.
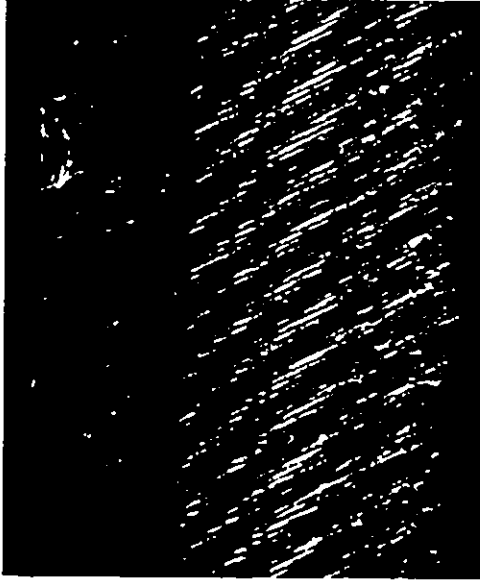
HSS end milling of Aluminum

Fig. 6.35   Chatter marks on machined surface.

Chips under chatter condition

Chips form in milling

Chips in stable cutting

Fig. 6.36   Chips form in milling
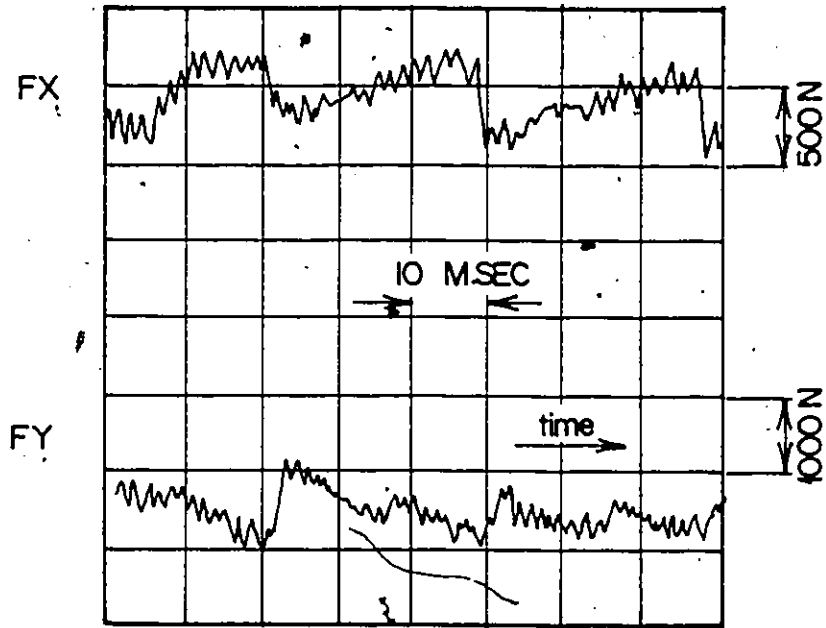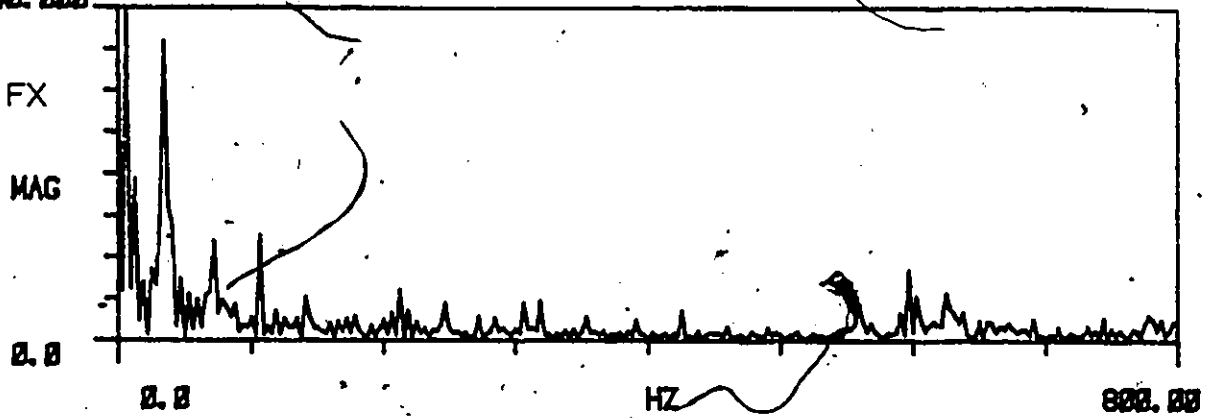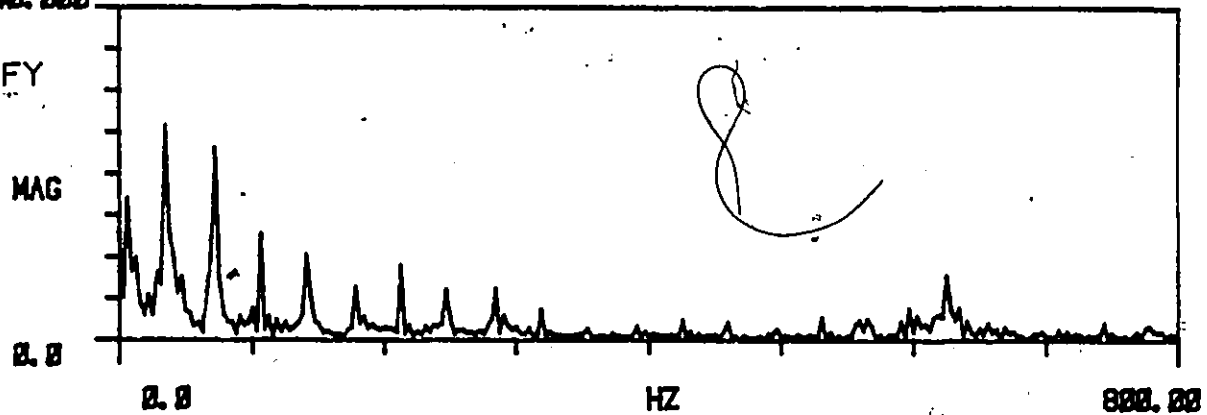
Figure 6.37 Measurements of Up-Milling in X, b = 5 mm
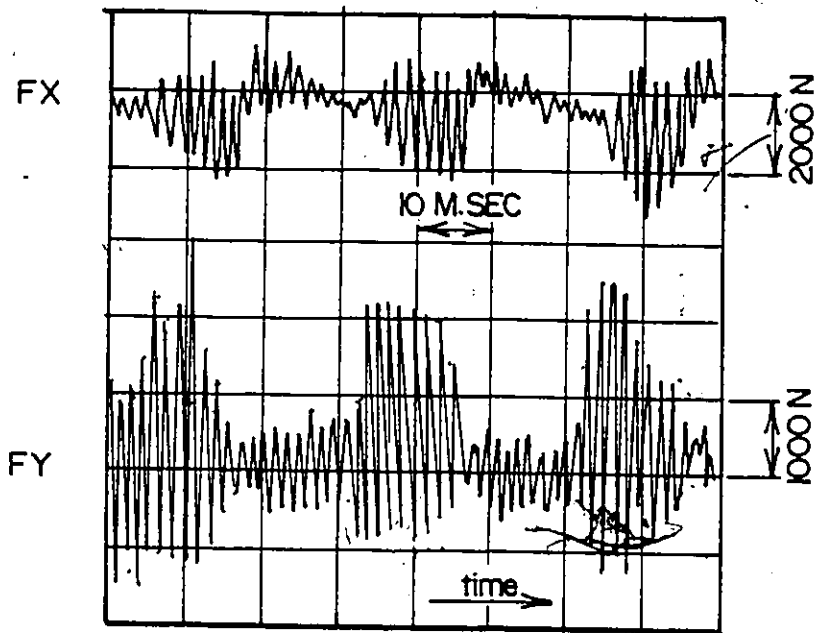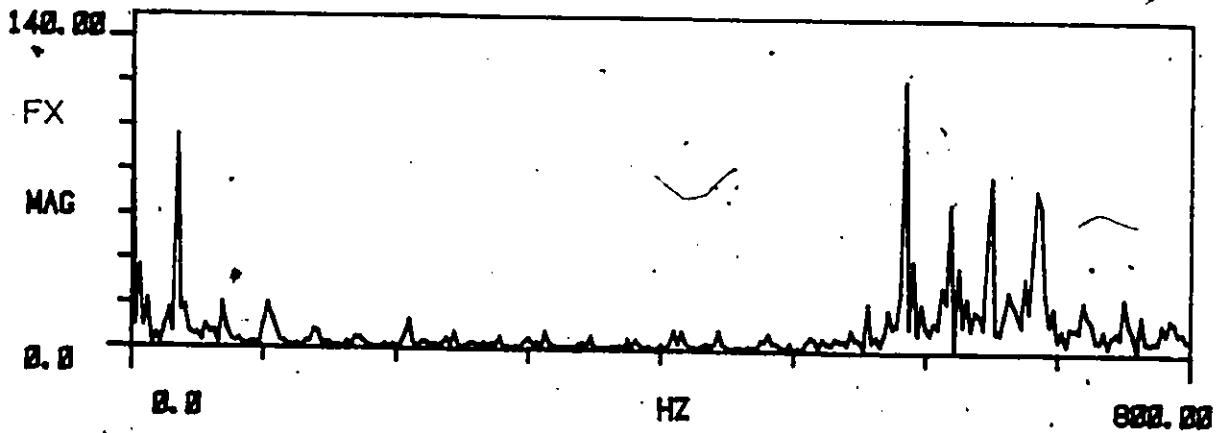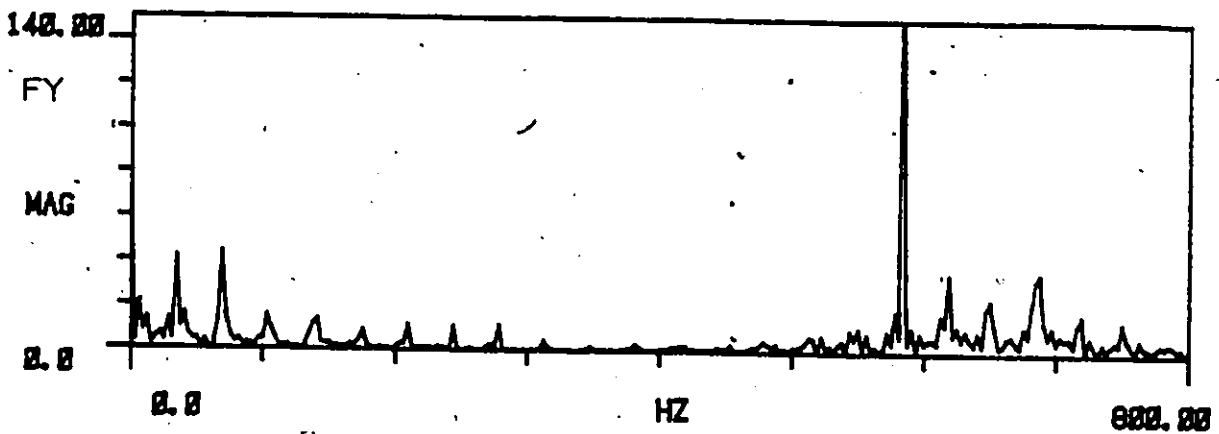
Figure 6.38 Measurements of Up-Milling in Y, b = 7 mm
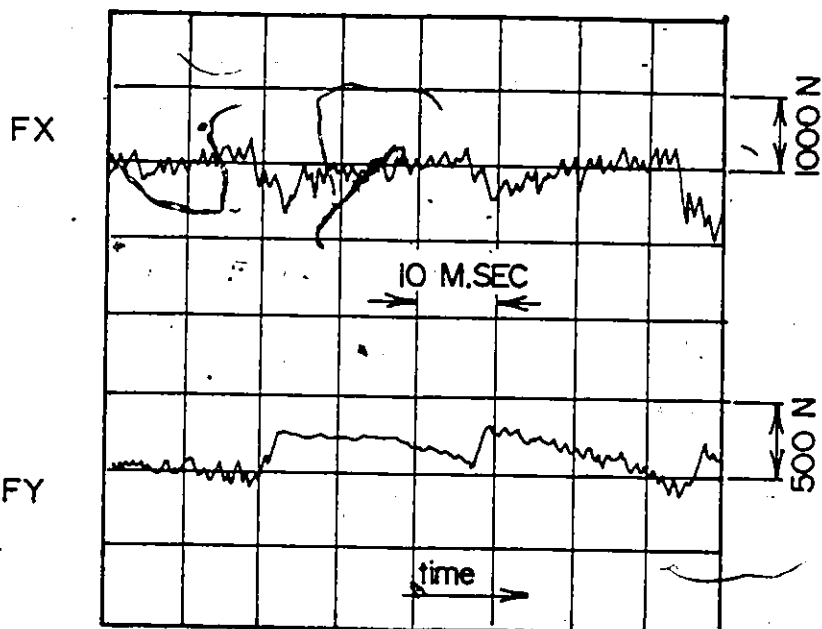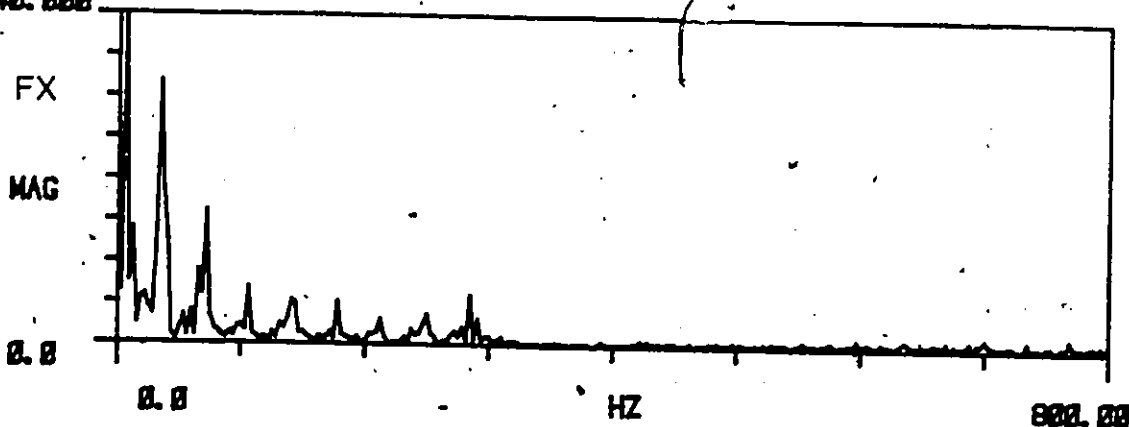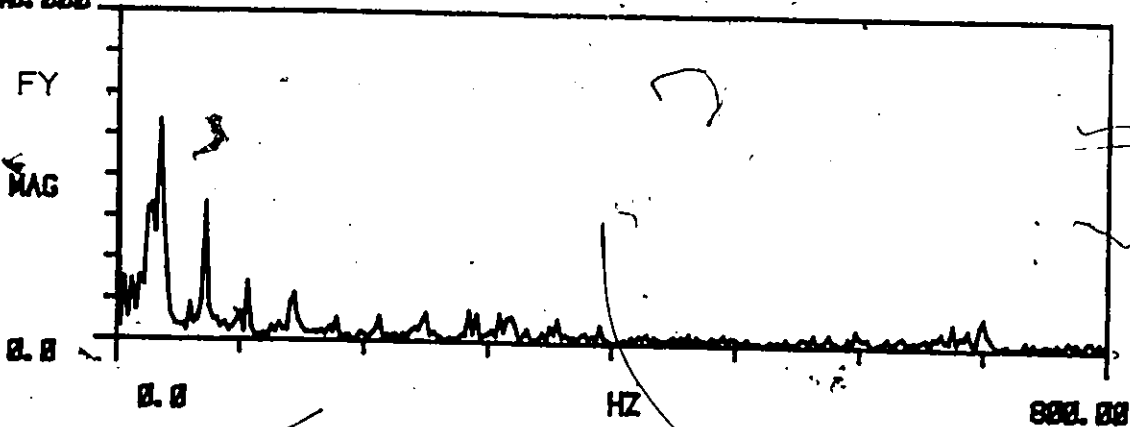
Figure 6.39   Measurements of Down-Milling in X, b = 5 mm
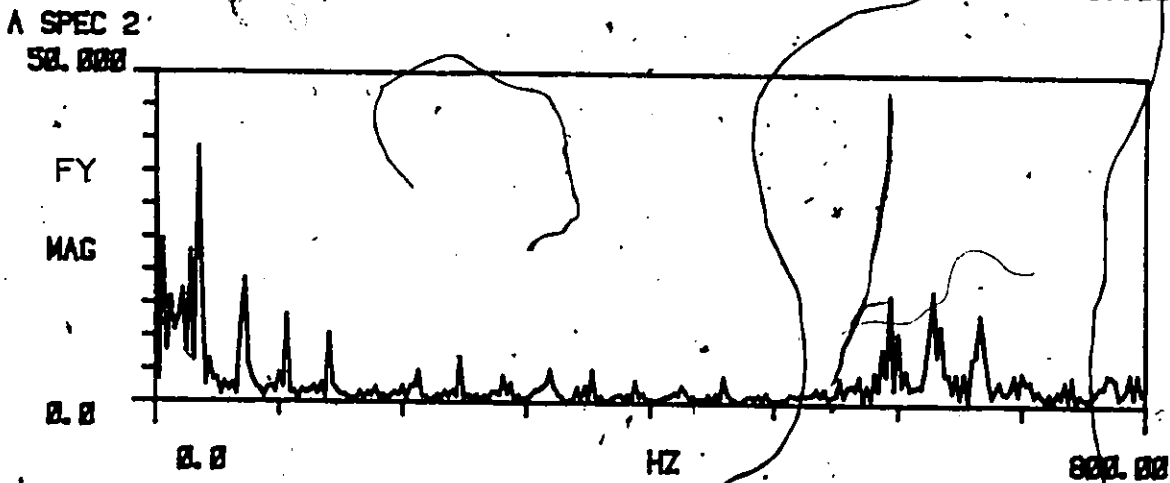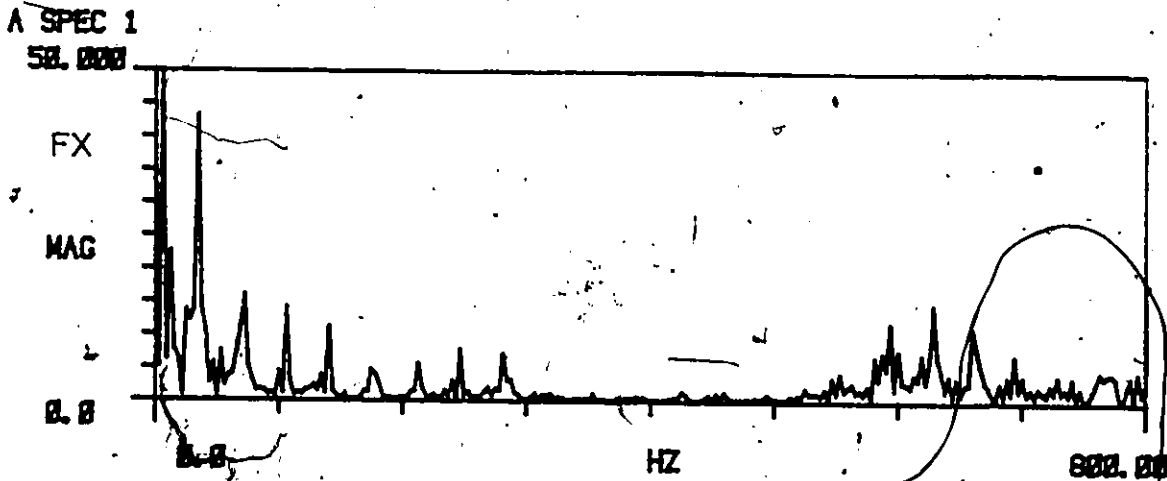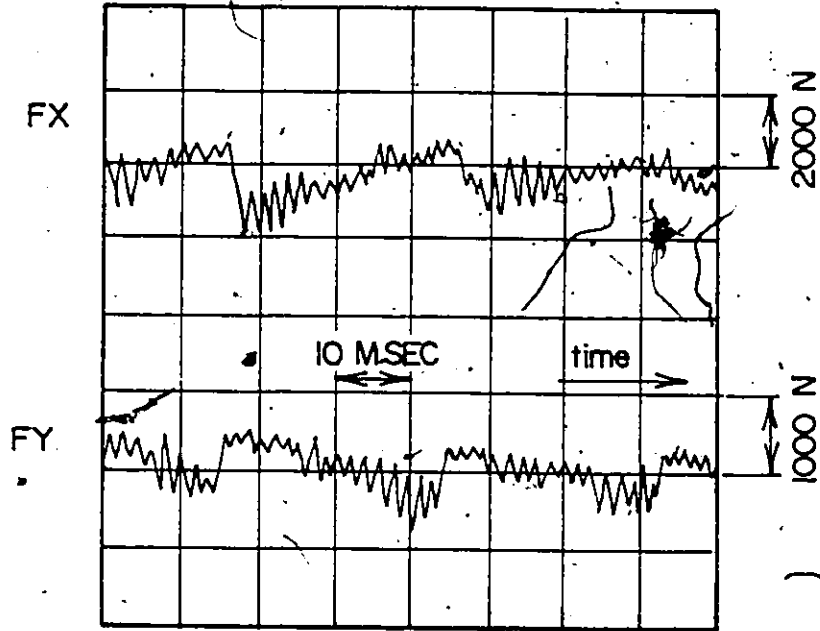
Figure 6.40   Measurements of Down-Milling in X, b = 15 mm
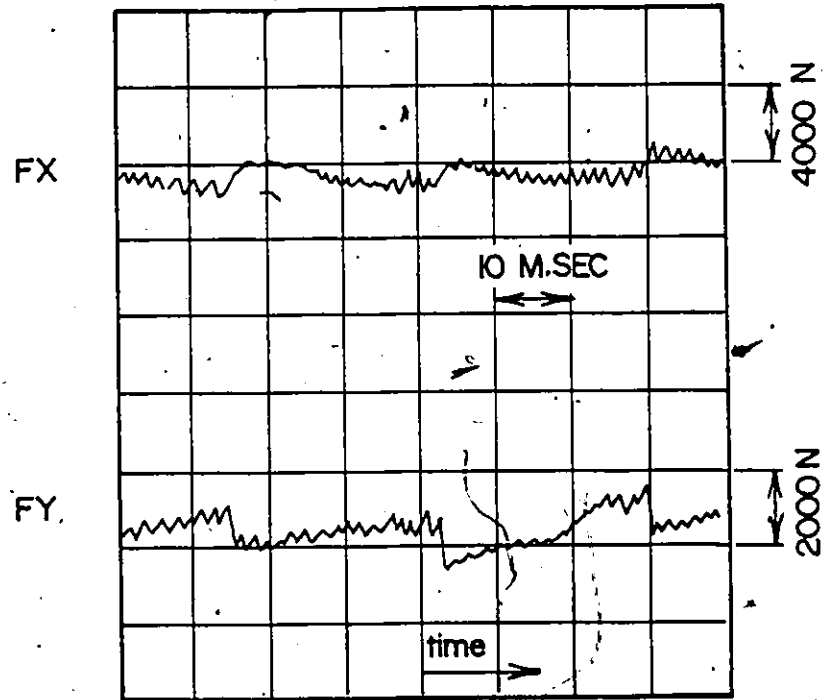
Figure 6.41   Measurements of Up-Milling
in Y, b = 15 mm

FX

1000 N

10 MSEC

500 N

time

FY

A SPEC 1
80.000

FX

MAG

0.0

0.0   HZ   800.00

A SPEC 2
80.000

FY

MAG

0.0
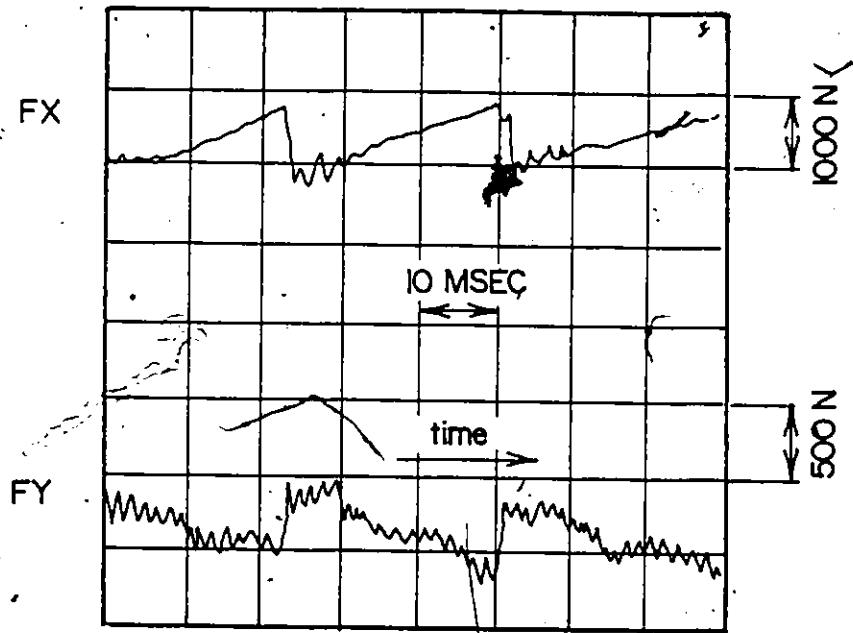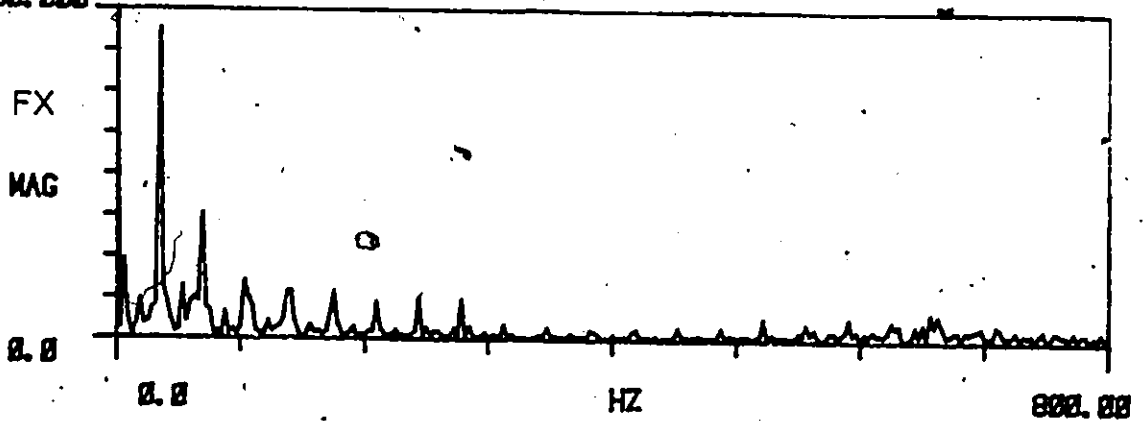
0.0   HZ   800.00
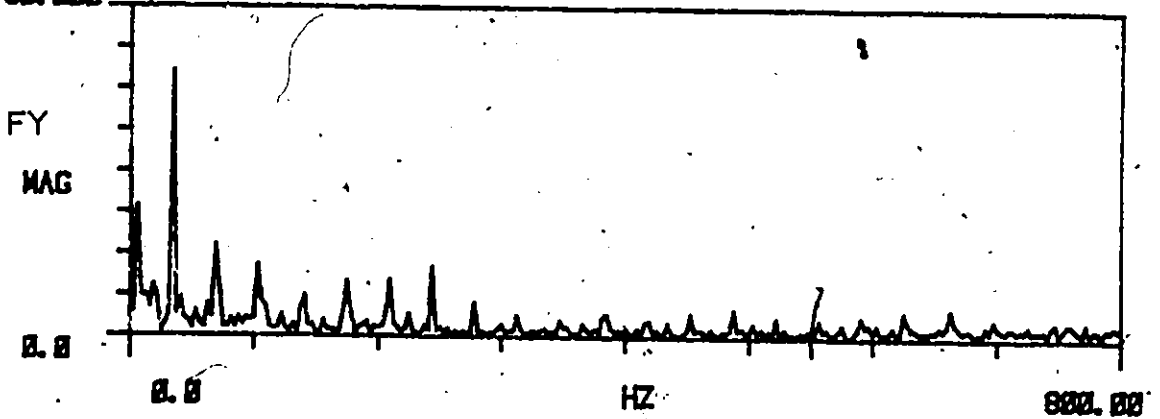
Figure 6.42   Measurements of Down-Milling in Y,
b = 5 mm
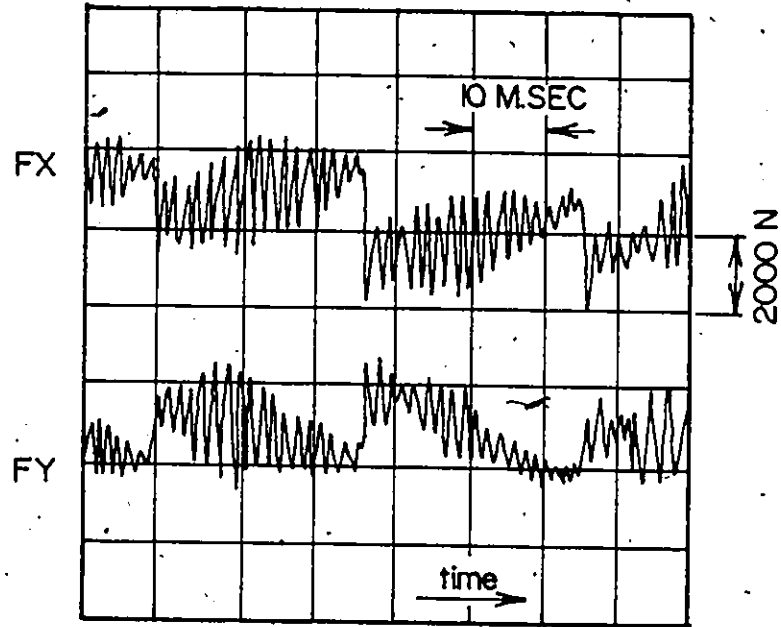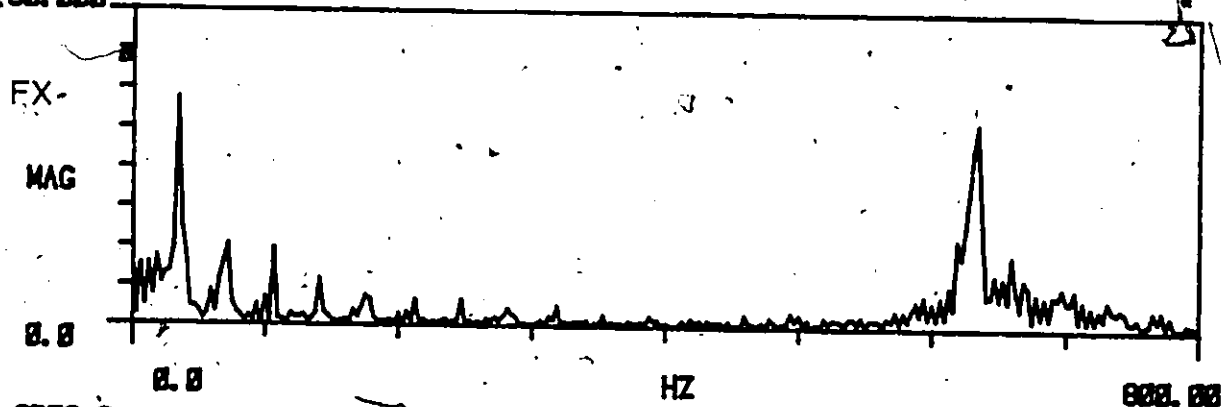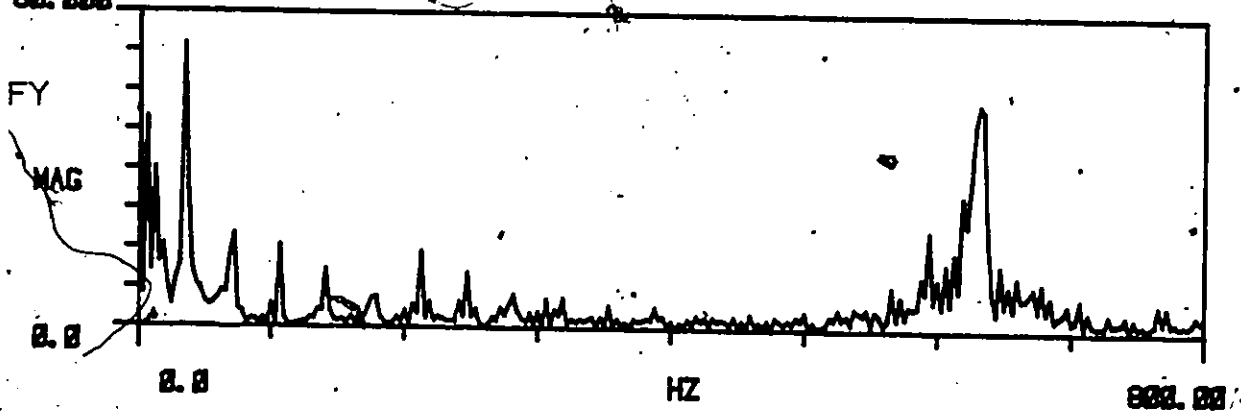
Figure 6.43 Measurements of Down-Milling in Y, Б = 10 mm
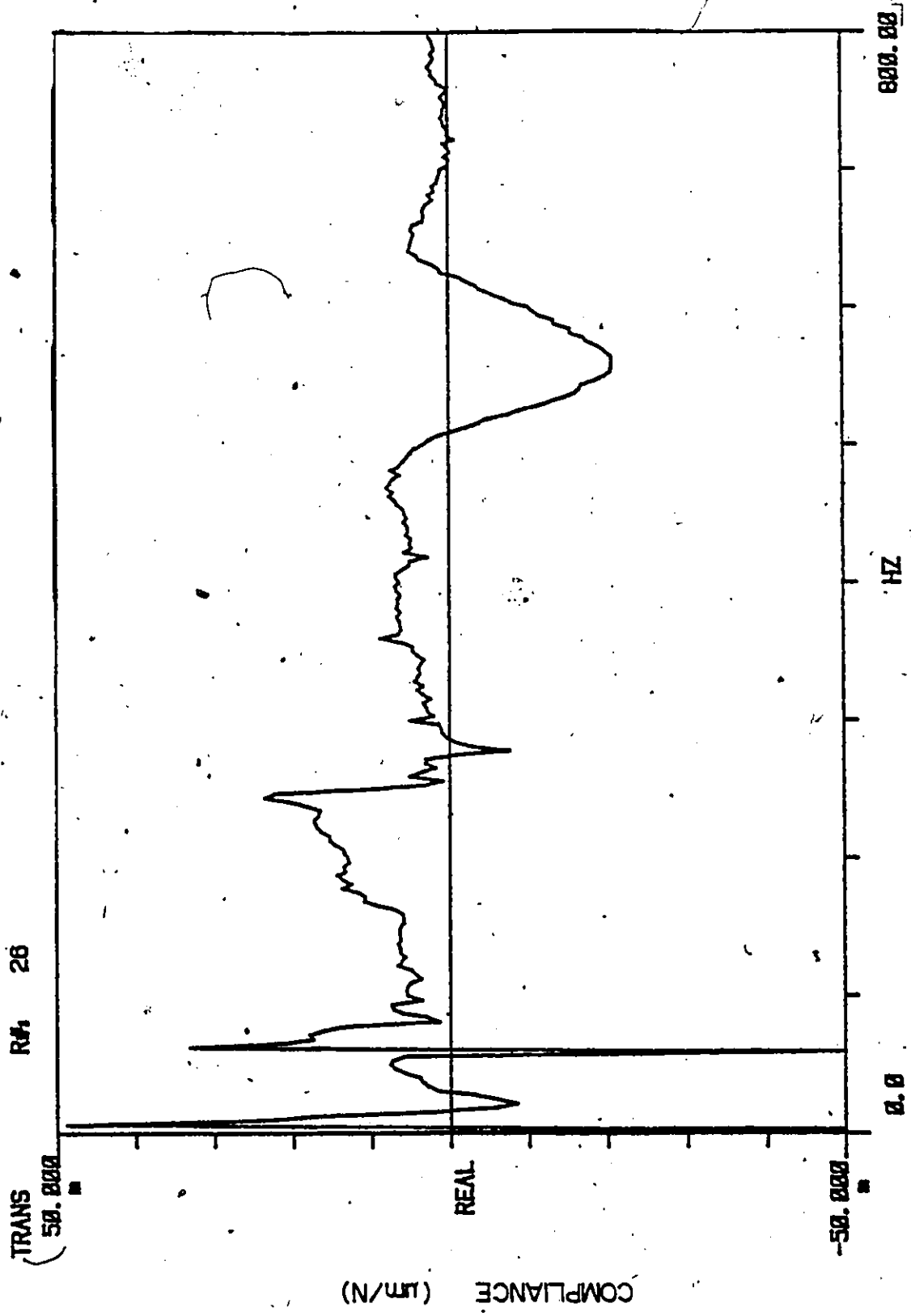
Figure 6.44 Oriented Transfer Function for Up-Milling in X and
Down-Milling in Y
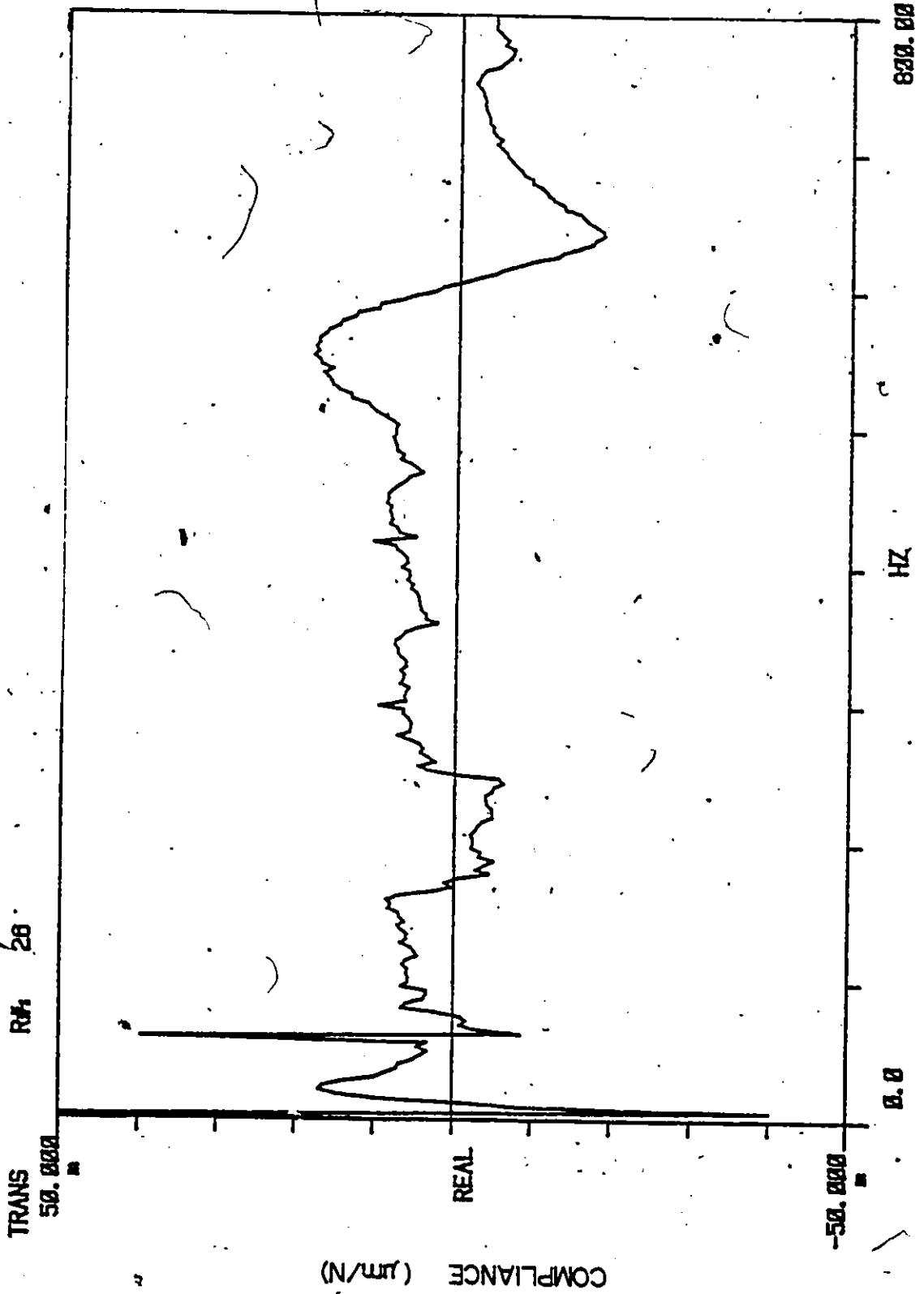
Figure 6.45 Oriented Transfer Function for Down-Milling in X and Up-Milling in Y
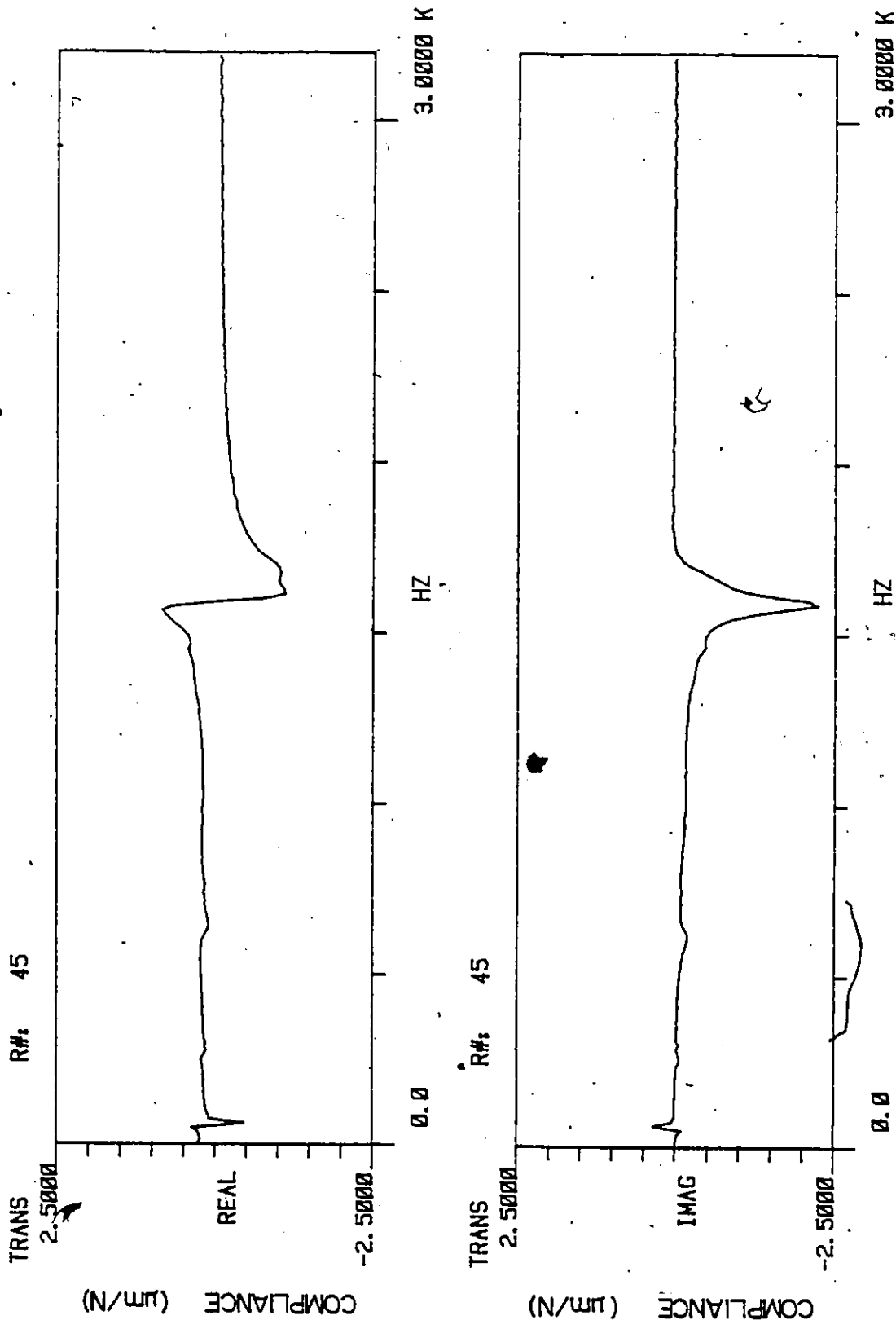
Figure 6.46   Relative Transfer Function for the End Mill in X
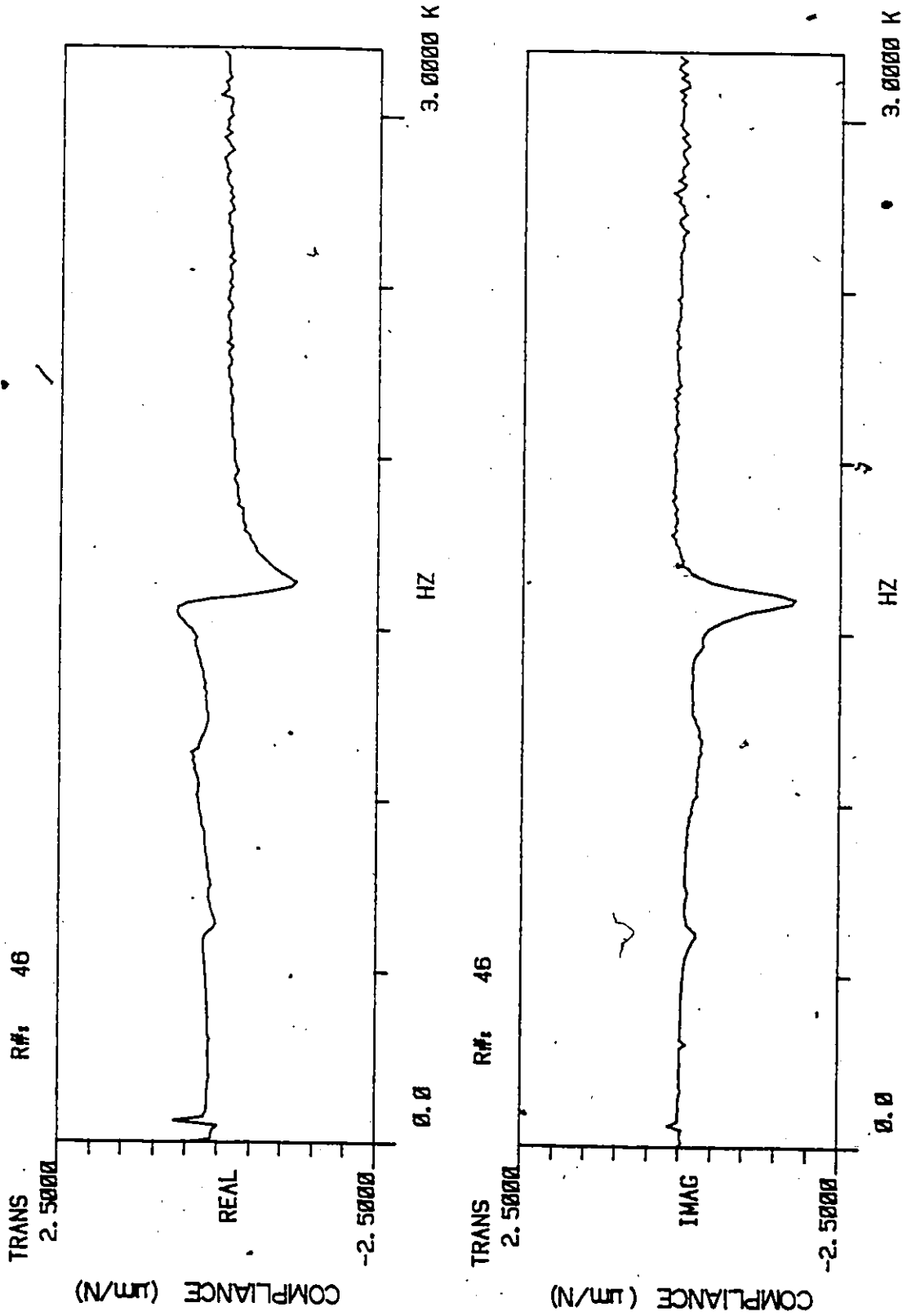
Figure 6.47 Relative Transfer Function for the End Mill in Y
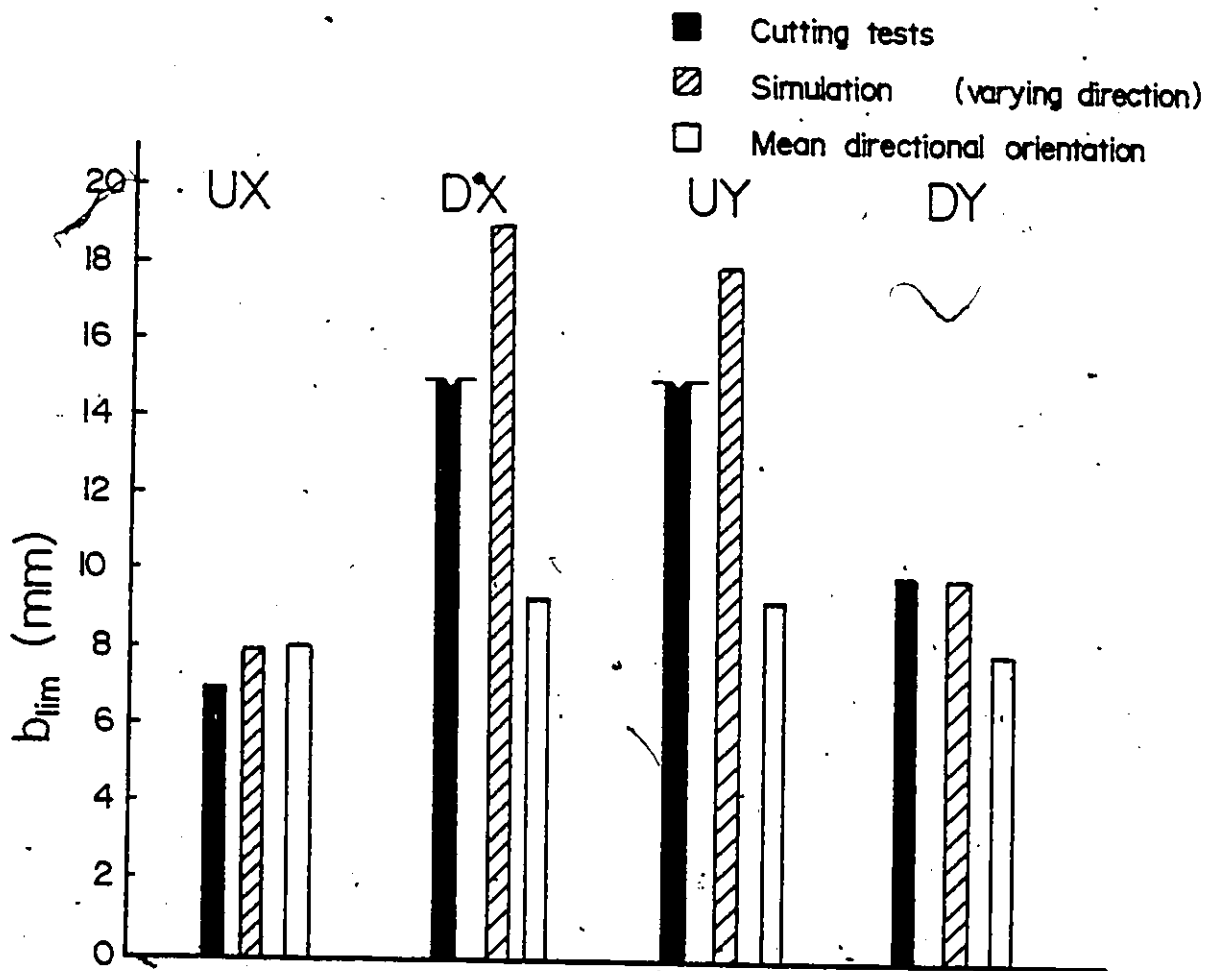
Figure 6.48   Comparison of Limits of Stability Obtained
Using; Cutting Tests, Simulation and Mean
Directional Factors
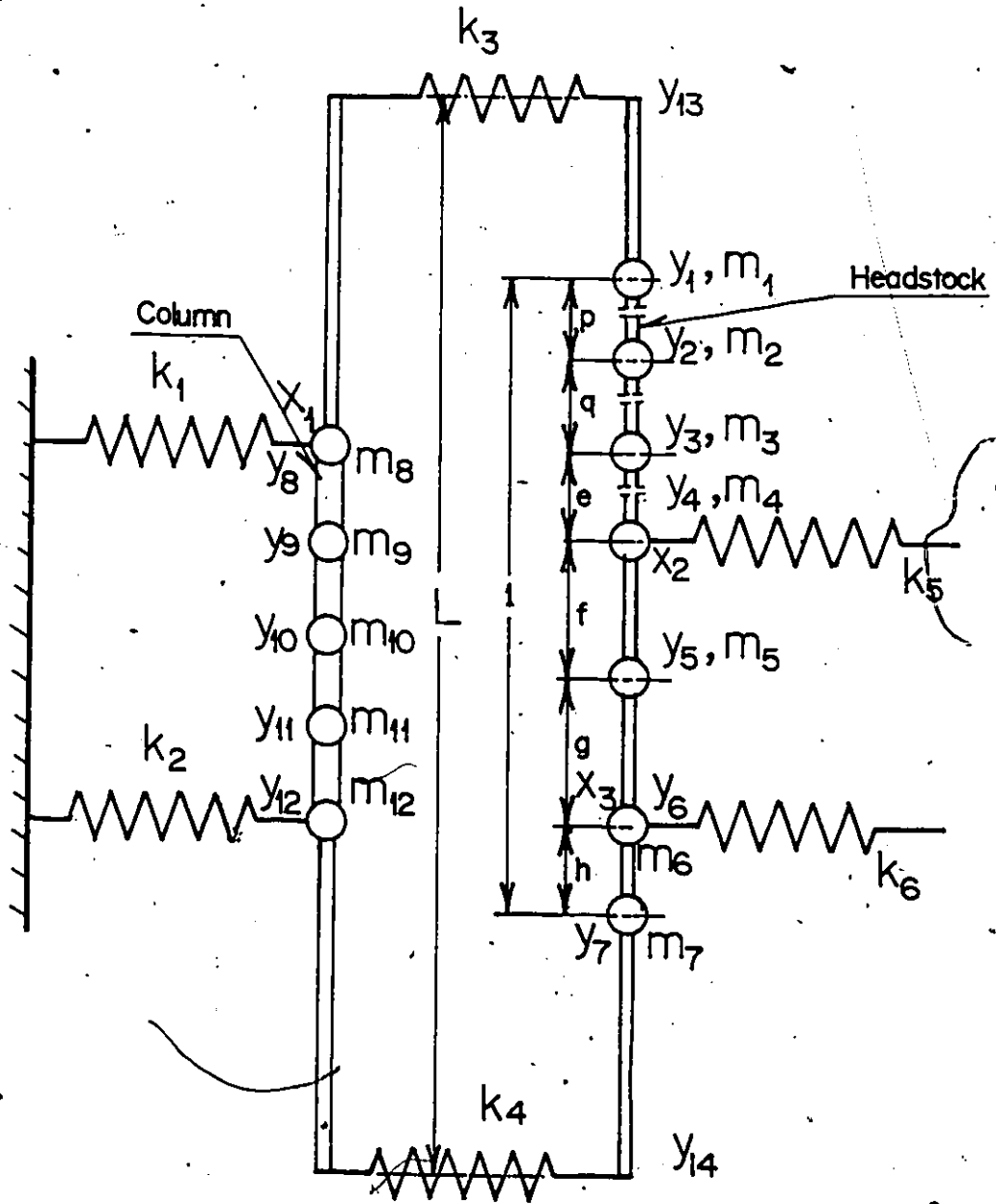
Figure II.1 Substructure 1 of Milling Machine
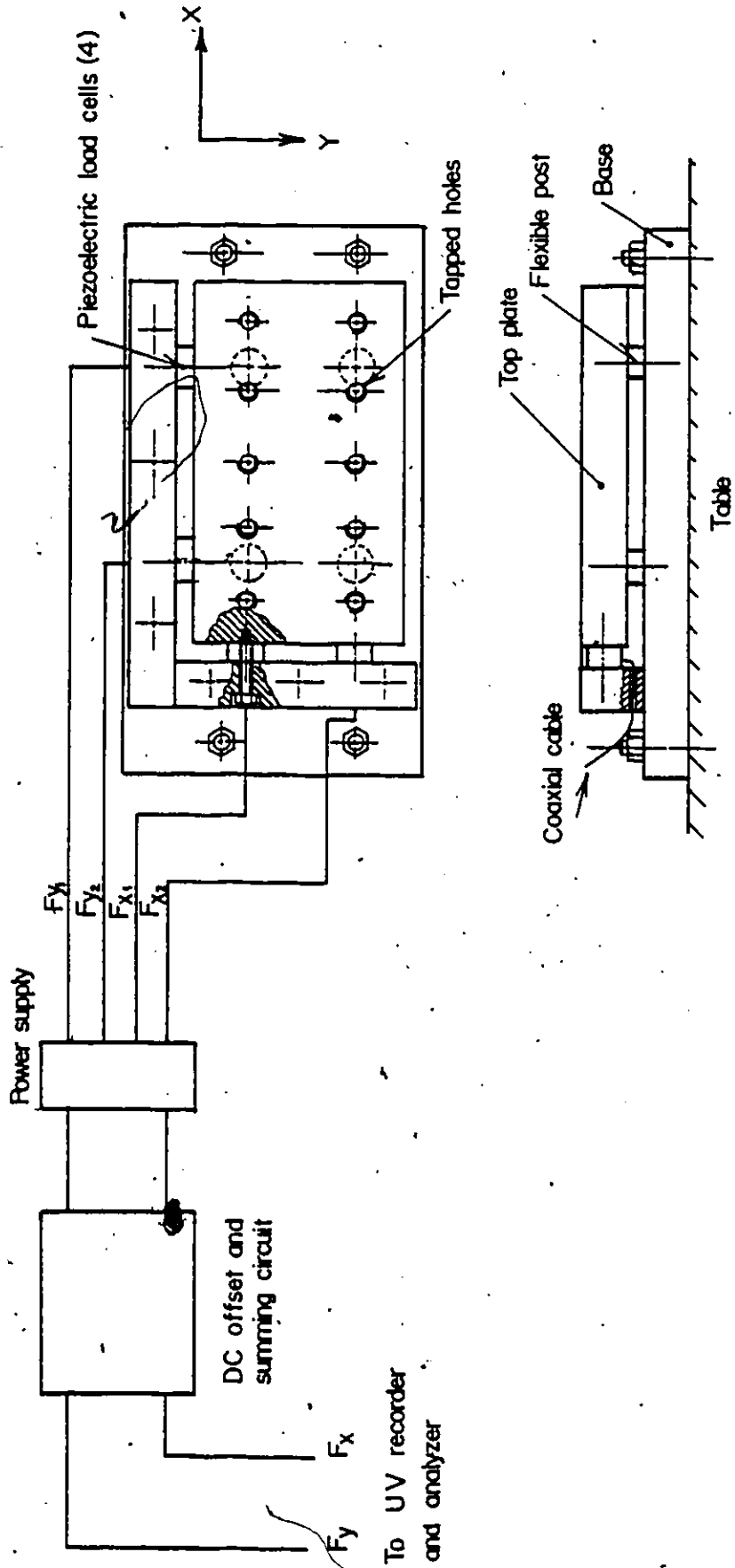
Figure VI.1   Schematic of Table Dynamometer
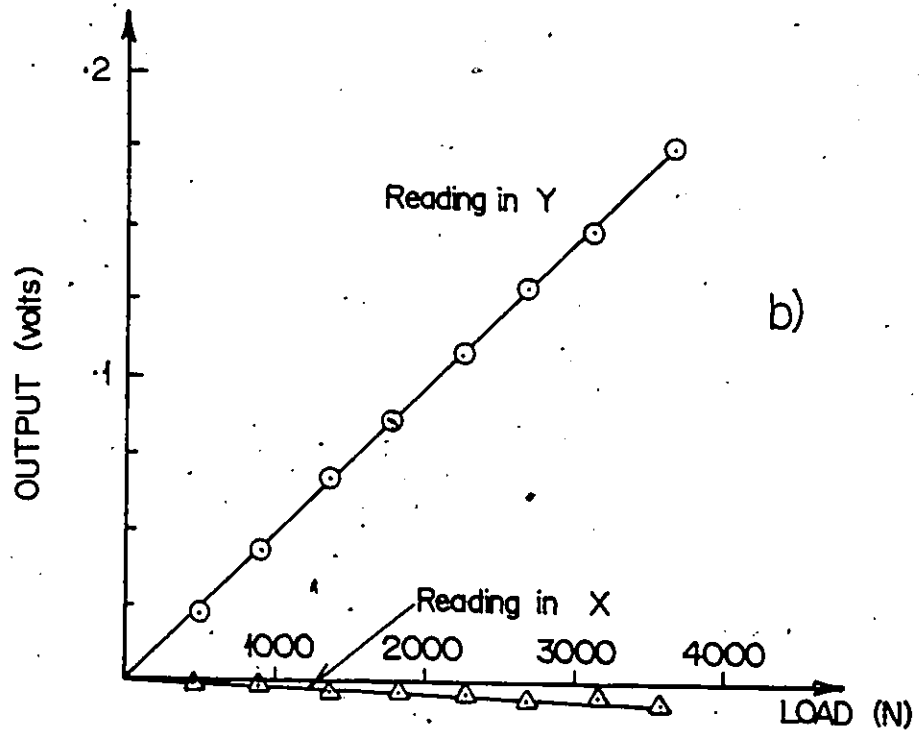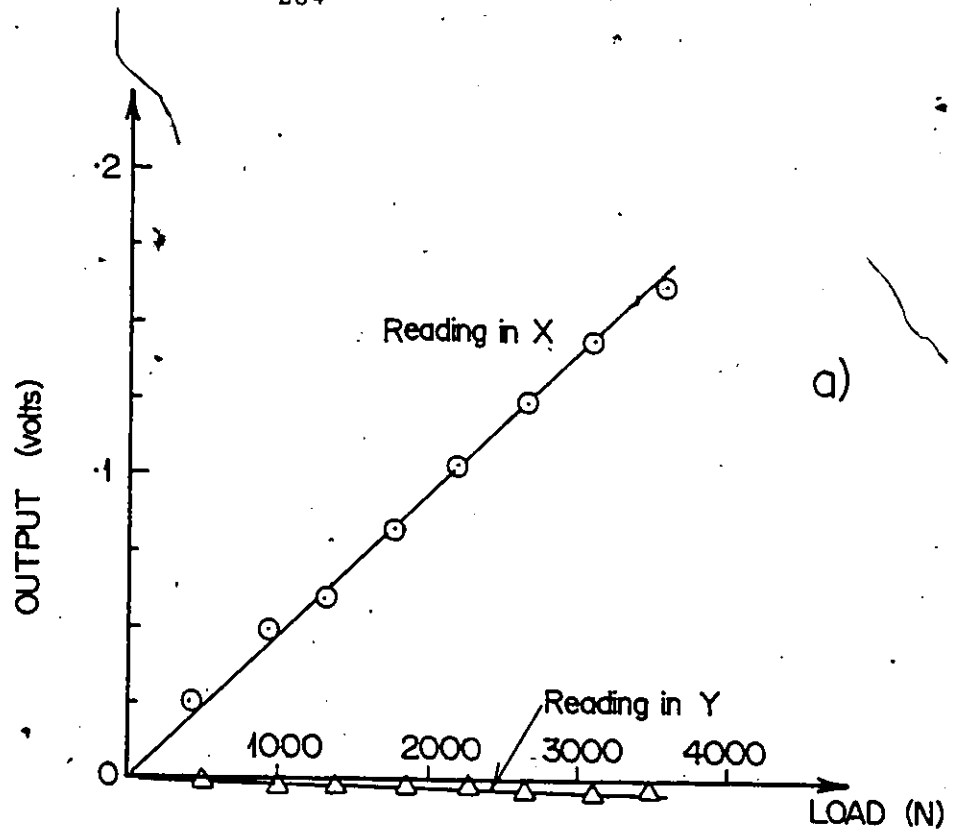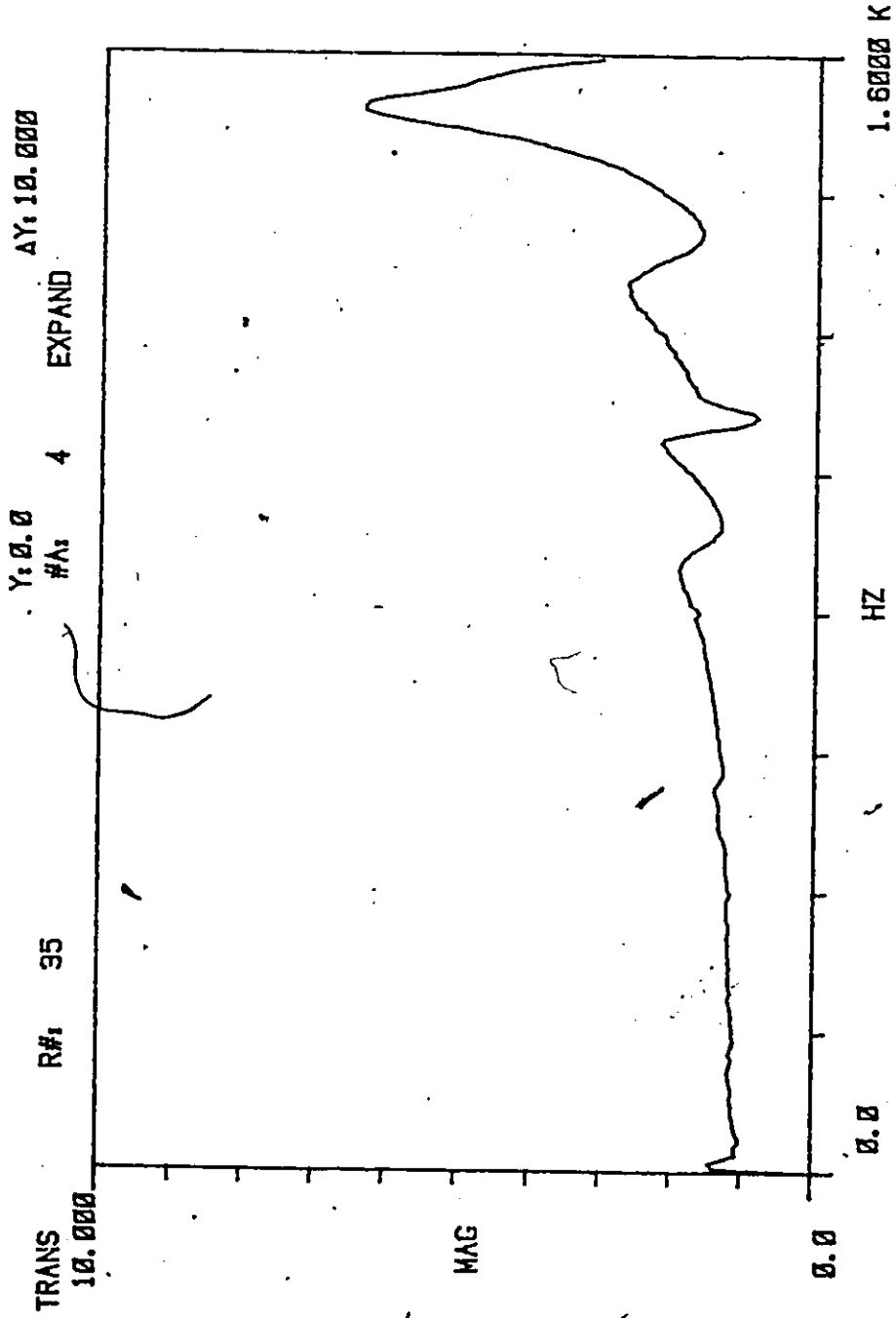
Figure VI.2   Static Calibration Curves of
Table Dynamometer

Figure VI.3   Frequency Characteristics of Table Dynamometer
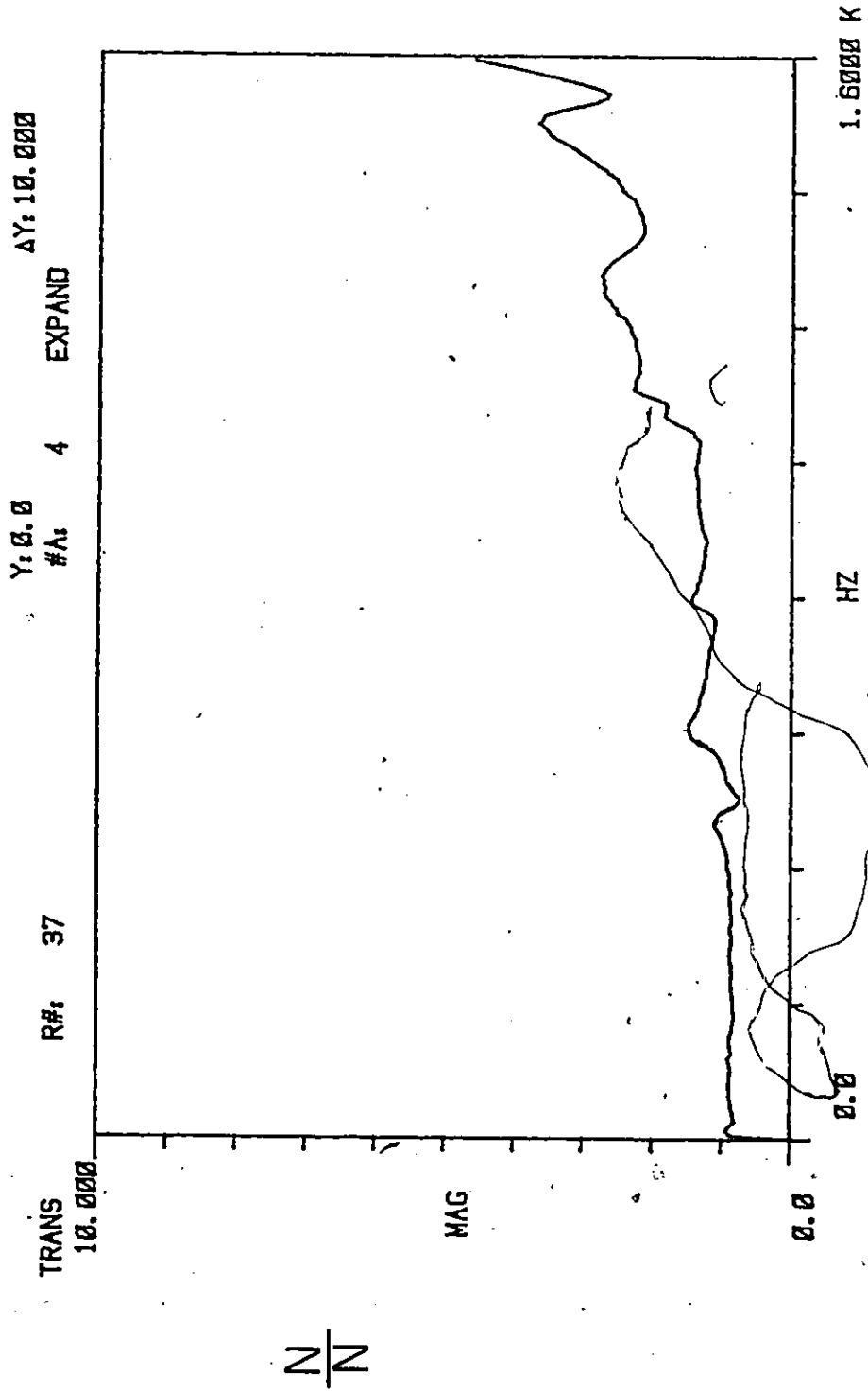in the X Direction

Figure VI.4 Frequency Characteristic of Table Dynamometer
in the Y Direction